A UNITED STATES DEPARTMENT OF **COMMERCE** PUBLICATION

NBS TECHNICAL NOTE 610

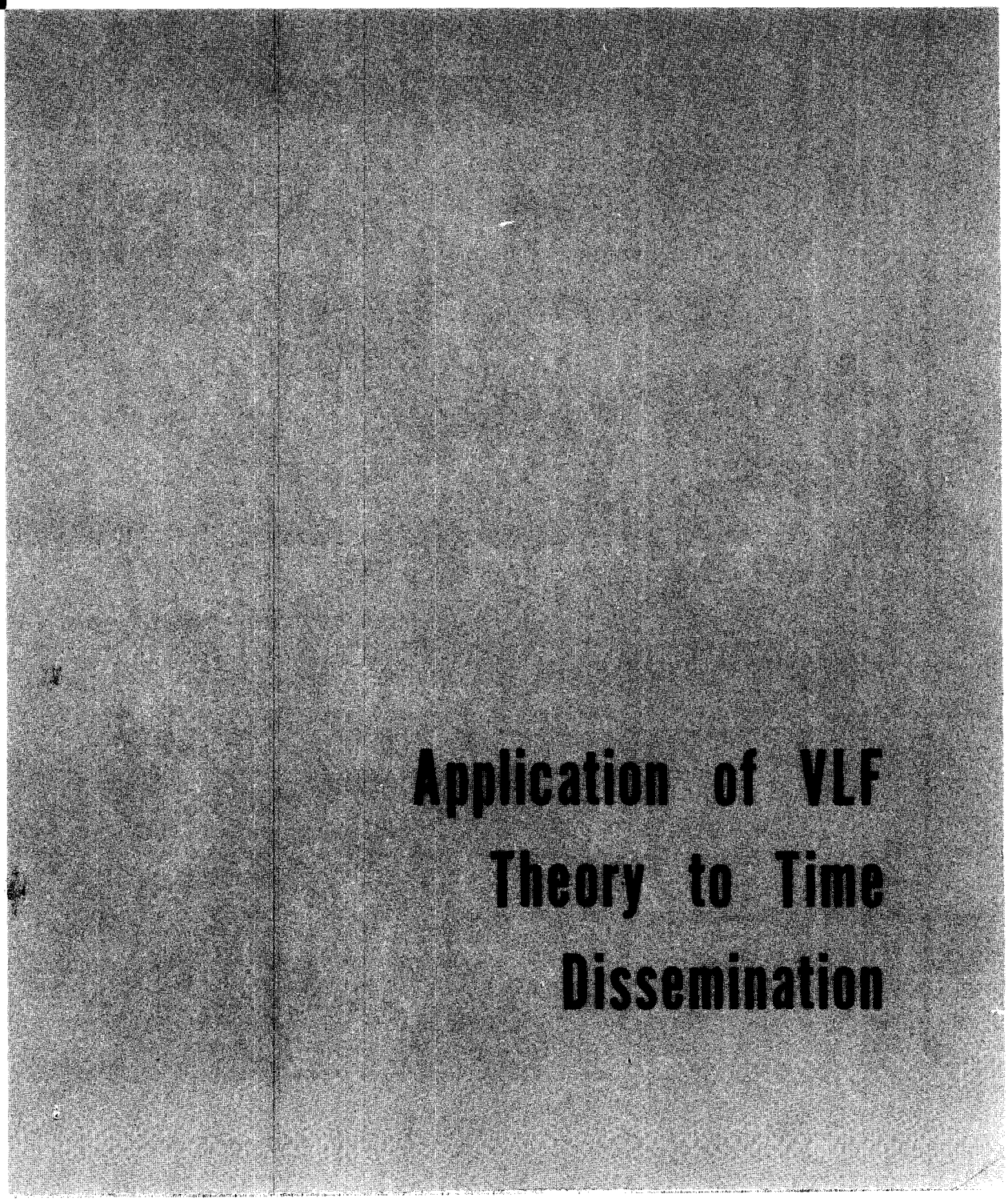

Application of VLF Theory to Time Dissemination

U. S. DEPARTMENT OF COMMERCE
National Bureau of Standards

NATIONAL BUREAU OF STANDARDS

The National Bureau of Standards[1] was established by an act of Congress March 3, 1901. The Bureau's overall goal is to strengthen and advance the Nation's science and technology and facilitate their effective application for public benefit. To this end, the Bureau conducts research and provides: (1) a basis for the Nation's physical measurement system, (2) scientific and technological services for industry and government, (3) a technical basis for equity in trade, and (4) technical services to promote public safety. The Bureau consists of the Institute for Basic Standards, the Institute for Materials Research, the Institute for Applied Technology, the Center for Computer Sciences and Technology, and the Office for Information Programs.

THE INSTITUTE FOR BASIC STANDARDS provides the central basis within the United States of a complete and consistent system of physical measurement; coordinates that system with measurement systems of other nations; and furnishes essential services leading to accurate and uniform physical measurements throughout the Nation's scientific community, industry, and commerce. The Institute consists of a Center for Radiation Research, an Office of Measurement Services and the following divisions:

Applied Mathematics—Electricity—Heat—Mechanics—Optical Physics—Linac Radiation[2]—Nuclear Radiation[2]—Applied Radiation[2]—Quantum Electronics[3]—Electromagnetics[3]—Time and Frequency[3]—Laboratory Astrophysics[3]—Cryogenics[3].

THE INSTITUTE FOR MATERIALS RESEARCH conducts materials research leading to improved methods of measurement, standards, and data on the properties of well-characterized materials needed by industry, commerce, educational institutions, and Government; provides advisory and research services to other Government agencies; and develops, produces, and distributes standard reference materials. The Institute consists of the Office of Standard Reference Materials and the following divisions:

Analytical Chemistry—Polymers—Metallurgy—Inorganic Materials—Reactor Radiation—Physical Chemistry.

THE INSTITUTE FOR APPLIED TECHNOLOGY provides technical services to promote the use of available technology and to facilitate technological innovation in industry and Government; cooperates with public and private organizations leading to the development of technological standards (including mandatory safety standards), codes and methods of test; and provides technical advice and services to Government agencies upon request. The Institute also monitors NBS engineering standards activities and provides liaison between NBS and national and international engineering standards bodies. The Institute consists of the following technical divisions and offices:

Engineering Standards Services—Weights and Measures—Flammable Fabrics—Invention and Innovation—Vehicle Systems Research—Product Evaluation Technology—Building Research—Electronic Technology—Technical Analysis—Measurement Engineering.

THE CENTER FOR COMPUTER SCIENCES AND TECHNOLOGY conducts research and provides technical services designed to aid Government agencies in improving cost effectiveness in the conduct of their programs through the selection, acquisition, and effective utilization of automatic data processing equipment; and serves as the principal focus within the executive branch for the development of Federal standards for automatic data processing equipment, techniques, and computer languages. The Center consists of the following offices and divisions:

Information Processing Standards—Computer Information—Computer Services—Systems Development—Information Processing Technology.

THE OFFICE FOR INFORMATION PROGRAMS promotes optimum dissemination and accessibility of scientific information generated within NBS and other agencies of the Federal Government; promotes the development of the National Standard Reference Data System and a system of information analysis centers dealing with the broader aspects of the National Measurement System; provides appropriate services to ensure that the NBS staff has optimum accessibility to the scientific information of the world, and directs the public information activities of the Bureau. The Office consists of the following organizational units:

Office of Standard Reference Data—Office of Technical Information and Publications—Library—Office of Public Information—Office of International Relations.

---

[1] Headquarters and Laboratories at Gaithersburg, Maryland, unless otherwise noted; mailing address Washington, D.C. 20234.
[2] Part of the Center for Radiation Research.
[3] Located at Boulder, Colorado 80302.

UNITED STATES DEPARTMENT OF COMMERCE
Maurice H. Stans, Secretary
NATIONAL BUREAU OF STANDARDS ● Lewis M. Branscomb, Director

TECHNICAL NOTE 610

ISSUED NOVEMBER 1971

Nat. Bur. Stand. (U.S.), Tech. Note 610, 170 pages (Nov. 1971)
CODEN: NBTNA

Application of VLF Theory to Time Dissemination

W. F. Hamilton and J. L. Jespersen

Frequency-Time Dissemination Research Section
Time and Frequency Division
Institute for Basic Standards
National Bureau of Standards
Boulder, Colorado 80302

Final Report Prepared for
National Aeronautics and Space Administration
under Contract No. 51740A-G

For sale by the Superintendent of Documents, U.S. Government Printing Office, Washington, D.C. 20402
(Order by SD Catalog No. C13.46:610), Price $1.50

Contents

List of Tables

List of Figures

APPLICATION OF VLF THEORY TO TIME DISSEMINATION

W. F. Hamilton and J. L. Jespersen

The characteristics of time dissemination systems are discussed. Particular emphasis is placed on the advantages and problems of very low frequency (VLF) timing systems. The parameters affecting VLF propagation along with causes of variations in these parameters, are discussed. Three methods of computing VLF propagation delays--mode theory, geometric-optics, and zonal harmonics--are compared. The method of zonal harmonics, used for the calculations in this paper, is discussed in more detail. A method of calculating reflection coefficients for a continuously varying ionosphere is described. The theoretical values are compared with experimental measurements. Graphical results of the calculations are included.

Key Words: Diurnal phase; Omega; time; time dissemination; VLF propagation; zonal harmonics.

1. Introduction

There are a number of existing or proposed time dissemination systems which operate in the VLF region of the radio spectrum. OMEGA is one of the most widely known such systems operating in the 10.0 to 14.0 kHz range. Although the system is conceived primarily for worldwide navigation, it has considerable potential for time dissemination. It is this potential which motivates the present report. Briefly, OMEGA is attractive for time dissemination for the following reasons:

a. OMEGA could provide the basis for a unified worldwide time dissemination system which does not presently exist.

b. A timing signal would be available reliably and continuously at any location on the earth's surface.

c. The time accuracy available to the user would be commensurate with his equipment investment.

In the following sections we discuss:

a. Characteristics of time dissemination systems,

b. Details of those characteristics which are particularly important for the calculations presented in this report,

c. Descriptions of the theory and method of calculation,

d. Graphical presentation of the results of the calculations,

e. Brief summary of the conclusions which may be drawn from calculations.

2. Time Dissemination Systems

There are a number of common elements which characterize most time dissemination systems. Among the more important are: accuracy, repeatability, coverage, and ambiguity. The accuracy of a system is usually limited by ones knowledge of the propagation delay, whereas repeatability is usually related to short-term variations in the characteristics of the propagation path. We can illustrate ambiguity by considering the following simple time dissemination system. Suppose the system consists of a sine wave which is a repetitive waveform. We can't tell by looking at the signal which one of the zero crossings is the one that is on time so the system is ambiguous. If we want to use it to improve our knowledge of the time we must somehow pick out the correct cycle and then measure its arrival time with respect to our local clock. To pick the correct cycle, however, we must already know the time from some other source to an accuracy equal to the period of our sine wave (100 microseconds in the case of a 10 kHz sine wave). Many users won't know the time to 100 microseconds and in addition, they would prefer to use the same system from beginning to end. To reduce

the ambiguity it is usual to transmit another coherent frequency say at 10.1 kHz and then inspect the 100 Hz difference frequency. To pick out the on-time cycle of the 100 Hz difference frequency, we need only know the time to 10 milliseconds (the period of a 100 Hz sine wave). We see that by adding more signals at different frequencies, we can reduce the ambiguity of the system to any desired level. However, as we reduce the ambiguity, we must at the same time increase the amount of frequency spectrum which the system occupies. For very low frequency systems, we can't very well put on modulations which require large bandwidths. That is, you can't put a signal which occupies 50 kHz on a 10 kHz carrier. In many cases, the usefulness of the system may be increased by averaging many measurements.

3. Path Delay

Path delay predictions, and thus, the accuracy of the system are limited by knowledge of the geometry of the transmitter and user locations and by the availability of information concerning the propagation medium. At VLF, at great distances from the transmitter, the signal velocity has a nearly constant value, whereas near the transmitter the average velocity between the user and the transmitter changes in an irregular way as a function of distance. In general, the transition from regular to irregular occurs at a distance of about 10,000 kilometers from the transmitter. In this report, the irregular region is of most interest. It is important to consider this near region because here the signal-to-noise ratio is greatest and receivers' costs, in principle, should be at a minimum. To consider in more detail the problem of path delay, we must introduce the ideas of phase velocity, V_p, and group velocity, V_g, as they apply to VLF.

Let us consider a simple two-frequency timing system. Suppose we have two closely spaced cw signals at frequencies f1 and f2 where f2 - f1 = Δf. In this system, the beat frequency Δf is used as a coarse time marker to identify a specific cycle of either carrier frequency. This removes ambiguities and a more precise time of arrival measurement is made at the higher carrier frequency. The difference frequency signal will travel from transmitter to receiver with a group velocity which depends upon the phase velocity versus frequency characteristic of the propagation medium. Specifically, the group velocity is related to phase velocity V_p by the following expression:

$$V_g = 1/\left[\frac{d}{d\omega}(\omega/V_p)\right] \tag{1}$$

where ω is the angular frequency. We see that the concept of group velocity breaks down if the derivative $\frac{d}{d\omega}(\omega/V_p)$ is not well behaved. In a dispersive medium, such as we are considering at VLF, Vp is a function of ω so that the group delay, t_d over a path r is given by the following expression:

$$t_d = \left(\frac{r}{V_p}\right)\left(1 - \frac{\omega}{V_p}\frac{dV_p}{d\omega}\right) \tag{2}$$

At very low frequencies the phase velocity versus frequency dependence cannot be expressed as a simple function of the properties of the propagation medium, except perhaps at great distances from the transmitter. The most accurate results are obtained from numerical solutions of Maxwell's equations, i.e., full wave solutions, with some realistic model of the ionosphere, the approach taken in this paper. Since the difference frequency may travel with a group velocity that is different than the phase velocity of either one of the two carrier frequencies, the

difference frequency signal may slip in phase with respect to either one of the carrier frequencies as a function of distance from the transmitter. This could lead to incorrect cycle identification of the carrier frequency unless the difference in velocities is known. At great distances, one can correctly identify a cycle by using different group and phase velocities. Unfortunately, the concept of group velocity applies only at great distances from the transmitter, where the phase velocity versus frequency characteristics are well behaved, i.e., $\frac{d}{d\omega}(\omega/V_p)$ is well behaved. Near the transmitter, a different approach must be used. To help illustrate what is happening near the transmitter we will consider first how a VLF pulse would propagate in this region.

There are two distinct effects which one must consider. First, the average propagation velocity of the pulse (group velocity) may be equal to or less than the velocity of light. Second, the pulse may be changing its shape as it propagates through the medium. If a particular point on the pulse has been tagged as the time reference point, at the transmitter, it is necessary to determine how this "tag" point is mapped into its new position as the pulse distorts during its propagation away from the transmitter. If this is not known, it will not be clear to the user which point on the received pulse represents the reference point as transmitted. In addition, having correctly identified the tagged point, one must also consider the fact that the average pulse velocity may be less than the velocity of light. A multifrequency VLF system is somewhat similar to the propagation of a pulse in the following sense: A short pulse of length - consists of a spectrum of frequencies, i.e., a number of Fourier components which occupy a spectral region approximately equal to 1/-. In a dispersive medium, such as the ionosphere, each one of these Fourier components will travel with a different phase velocity. In a sense then, when we use a VLF tone system, we are

sending one Fourier component at a time and the user, if he desired, could by storing the received tones add them together to produce something looking like a pulse. This composite waveform would have some well defined shape as it left the transmitter. Because of the dispersive properties of the propagation medium this composite waveform will change its shape as a function of distance from the transmitter until it has propagated out to the region where the phase velocity is well behaved. Beyond this point, the composite waveform would maintain essentially the same shape as a function of distance although it would not be the same as transmitted. To use the time system for accurate transferral, it is necessary to know in detail the structure of this composite waveform as a function of distance from the transmitter.

Similarly, use of the VLF multitone system for accurate time transferral requires detailed knowledge of the phase versus frequency and distance characteristics of the signals. We will turn to the details of theoretical calculations of VLF phase velocity in Sections 4 and 5.

4. Important Parameters for VLF Calculations

The phase velocity versus frequency characteristics at VLF are particularly sensitive to the propagation medium. The propagation medium is characterized by the conductivity of the ground, the electrical properties of the ionosphere,the direction of propagation with respect to the earth's magnetic field,and the strength of the magnetic field.

The most important electrical properties of the ionosphere for VLF calculations are:

a. The electron density vs height.

b. The proton density vs height.

c. The collision frequency between charged and neutral particles vs height.

The composition of the ionosphere is not static. Many different types of events, for example solar flares, can cause short-term variations in the ionization. The theoretical calculations in this report do not take these short-term variations into account but are based on the average properties of the ionosphere as it might appear at noon and at midnight of the summer solstice at midlatitudes.

There is considerable experimental evidence that the propagation delay of a VLF signal from one day to the next at the same time of day is repetitive to a few microseconds, so that consideration of the average properties of the ionosphere should be sufficient for many applications. This is an attractive feature of VLF signals for time dissemination. We list here briefly some physical processes responsible for these average properties. The most important factors are as follows:

a. Solar X-rays ($\simeq$ 10 A) above 85 km at sunspot minimum and above 70 km at sunspot maximum;

b. The ionization of NO by solar Lyman -α in the 70 to 90 km range;

c. Primary cosmic rays below 70 km with the flux increasing by a factor of about 4 from sunspot maximum to minimum. However, this subject is very volatile and recent work indicates that water vapor and metastable states of O_2 are important.

d. Various reactions between free electrons, ions and neutral particles; and

e. Mechanical and electrodynamical forces which redistribute the ionization.

Although, as stated previously, the calculations in this report are based upon the average properties of the ionosphere, it is important to realize that there are short-term variations in the medium. The short-term phase variations are one of the most noticeable features of a VLF

record. These fluctuations are much shorter (of the order of 30 minutes) than one would expect from solar controlled phenomena and are undoubtedly at times related to the motions in the neutral atmosphere.

There is not much information on the turbulent structure of the mesosphere (the region of the neutral atmosphere which overlaps the D Region) because this is a region that is too high for balloon soundings and too low for satellites. However, there is some information on the irregular structure in this region based upon rocket and meteor trail investigations. For example, sodium cloud measurements by Blamont and Jager[1] indicated the existence of irregularities below 100 km which they explained by a combination of turbulent mixing and molecular diffusion. About 10 years ago, Greenhow and Neufeld[2] suggested the presence of large scale irregularities in the 80-90 km region based upon radar observations of meteor trails. However, there is some controversy about these observations since later measurements by Manring, et al.,[3] via rocket sodium cloud measurements suggested that the turbulence explanation may be spurious and in fact may be due to the rocket. An alternative explanation has been made by Charney and Drazin[4] who suggest that the irregularities are produced by the propagation of gravity waves into the upper atmosphere.

In any case, phase fluctuations of VLF signals are in some fashion related to the irregular structure of the mesosphere.

As discussed earlier, realistic calculations of VLF radio fields are obtained from full wave solutions and for the present these solutions have only been obtained for plane stratified ionospheric models. Thus, the possibility of using this approach to obtain wavefields for a more complicated irregular ionosphere does not seem particularly practical at the present time and it appears necessary to resort to simpler more approximate methods.

As an example of one such possible approach, suppose that one is several thousand kilometers from a VLF transmitter. At such a distance, the phase velocity of the radio signal is nearly constant (this corresponds to the situation in a waveguide where mode 1 is dominant) and is given approximately by

$$V_p = c/\sqrt{1 - \lambda^2/16h_o^2} \tag{3}$$

where λ is the radio wavelength, h_o the height of the ionospheric reflecting layer, and c the velocity of light. To a first approximation, we might consider that the effect of a large irregularity would be to change the height of the reflecting layer by an amount Δh, which would in turn alter the phase velocity. Thus from the equation above, we obtain

$$\frac{\Delta v}{V_p} \simeq \frac{\lambda^2}{16h_o^2}\frac{\Delta h}{h_o} \tag{4}$$

since $\lambda << h_o$.

This change in phase velocity would produce a change in the phase of the received signal which could be interpreted in a straight forward manner for this situation. However, the situation becomes more complicated when the irregularities are small compared to the path length or to the radio wave length. Crombie[5] has attempted this problem theoretically. He has taken the work by Rice[6] which was developed specifically for VHF forward scatter problems and has attempted to adapt it for the interpretation of VLF phase measurements. Although this work appears to be far from exact, it does give some interesting results. Specifically, Crombie considers the two cases when VLF phase measurements are made on a distant transmitter using two VLF receiving sites. In the first case (longitudinal case) the two receiving sites are in line with the transmitter, and in the second case (transverse case) occurs when the line joining the two receivers is

perpendicular to the line between one of the receivers and the transmitter. He then takes some experimental data of Hargreaves[7] which apply to the transverse case and concludes that the average size of the irregularities is about 65 km and that the horizontal drift velocity is about 35 m/sec. Crombie compares these values with some results from Hines[8], (which appear to apply to the region in question) which predict a horizontal velocity of about 100 m/sec. for internal gravity waves with horizontal components of 65 km. Although the predicted value is higher than that deduced by Crombie, the values agree within an order of magnitude.

5. Theory of Calculations

Three approaches to theoretical VLF calculations have seen wide usage: (1) Wave guide mode theory,[9] (2) geometric optics, and (3) zonal harmonics. Mode theory has the advantage that at large distances only one mode need normally be considered. As the distance between the transmitter and receiver decreases, more modes are necessary. Some disadvantages are that physical interpretation of modes is difficult and the introduction of varying propagation parameters along the path becomes very complicated. It is possible that significant modes may be overlooked. In addition, unless a Fourier transform into the time domain is employed, mode theory does not account for the observed difference in arrival time between the ground wave and the various sky waves.

Geometric optics, on the other hand, lends itself well to clear physical interpretation. Various "hops" arrive later than the ground wave. The accuracies of geometric optics are greatest near the transmitter, just the opposite of mode theory. The approximations made by this theory become more valid with increasing frequency, but are in general not valid at VLF except very near the transmitter. Geometric

optics is not a rigorous theory for electromagnetic wave propagation in the VLF region.

The mathematical derivation of the zonal harmonic and geometric series representations for electromagnetic wave propagation is well documented by Johler[10,11,12,13,14,15]. The approach used here will be primarily nonmathematical in an attempt to give physical insight to this method.

The use of zonal harmonics in propagation formulae was introduced early in the 20th century by Debye[16] (for electromagnetic waves) and Lord Rayleigh[17] (for sound). It was not, however, until recently that practical application of this theory could be accomplished. The high speed digital computer allows summation of the large number of terms that are required for convergence of the series. (Here convergence is used to mean that additional terms do not significantly effect the result.) In addition, new theoretical advances have greatly reduced the number of terms required for convergence.

Zonal harmonics allow the introduction of rigorous analysis while maintaining the clear physical interpretation of geometric optics. The term in the classical zonal harmonic series containing both the ground and ionospheric reflection coefficients can be represented as a geometric series. Inverting the order of summation--summing the zonal harmonic series before the geometric series--yields a series, each term of which is analogous to the geometric optic series. The zeroth order term of the geometric series is the ground wave and the jth term represents a wave which has suffered j reflections from the ionosphere.

The large number of terms ordinarily required for convergence of the zonal harmonic series is found to be necessary only because the ground wave is included in the calculations. The higher order terms converge with approximately one-fifteenth the number of terms. Since the ground wave may be computed more effectively by other means[18], the remaining terms of the geometric series can be rapidly computed.

Very few terms are required for convergence of the geometric series at VLF. Under normal conditions, 10 terms (i.e., hops) have been found sufficient for convergence to distances of 8,000 to 10,000 kilometers. Greater distances may require a few more terms.

Each term of the geometric series may be thought of as a set of "n-waves" (the n terms of the zonal harmonic series). Each of the n-waves is incident on the ionosphere and the ground at an angle which is an approximate function of n. (The rigorous theory uses complex angles of incidence which are given exactly by functions of n. Little difference has been noticed between using real and complex angles of incidence since normally the imaginary portion is quite small.) This function of n is the determining factor for the number of terms required for convergence. The series converges abruptly as the angle of incidence approaches 90 degrees. The contribution of terms where the angle of incidence is less than approximately 30 degrees is negligible. Consequently, even fewer terms are required.

Because of lateral displacement at both the ionosphere and the ground, no specific angle of incidence is required for a wave to reach a particular distance. Lateral displacement as used here means that a wave may be trapped and propagate radially within the ionosphere or ground for some distance before emerging again to continue normal propagation (see figs. 12 through 15, pp. 45-48, Johler and Mellecker, 1970--Ref. 15). Most of the reflection does, however, take place near the angle predicted by geometric optics.

Each n-wave contains a factor which may be called the effective reflection coefficient. In essence this factor is the sum of all possible reflection coefficients for ordinary and extraordinary reflection from the ground and ionosphere. For the case of vertical electric polarization of both the transmitter and receiver antennae, for example, only

ordinary reflection can effect the field for the first hop so the effective reflection coefficient is T_{ee}. Both ordinary and extraordinary reflection can affect the second hop field and the effective coefficient is $T_{em}R_{m}T_{me} + T_{ee}R_{e}T_{ee}$. Higher order coefficients become very complicated. Here T stands for the ionospheric reflection coefficient with the first subscript denoting the incident polarization and the second the reflected polarization (e is vertical electric and m is vertical magnetic). The ground reflection coefficient, R, needs only one subscript since no abnormal component is generated during ground reflections.

Since most of the reflection for a given "hop" takes place within a region, local reflection coefficients may be introduced. For example, a land sea boundary changes the reflection coefficient of the ground and may be incorporated. Similarly, if part of the path is in sunlight while the rest is in darkness (i.e., the "terminator" occurs along the propagation path) this fact may be used in the analysis.

The ionospheric reflection coefficients which are most readily available are plane Fresnel coefficients. These may be used as an approximation to the true coefficients. The approximation becomes quite good if the coefficients are multiplied by a convergence-divergence factor. The best method, however, is to allow complex angles of incidence. It has been stated earlier that the contribution of the imaginary term will normally be small, but it may not be mathematically negligible.

Since the only distance related portion of each n-wave is the Legendre function, the field at many distances can be calculated simultaneously. Upwards of 200 distances may be calculated with only minimal increase in computation time.

It is necessary to compute the reflection coefficients for each n. This is no difficulty for the ground reflections since this calculation

is relatively straightforward and does not consume much computer time. The ionospheric reflection coefficients, however, are computationally quite complicated and can consume as much as 2 minutes of computer time for each set of coefficients required. Because the reflection coefficients are a smooth function of angle of incidence (of n), it is practical to set up a table of reflection coefficients and to interpolate on this table to obtain the desired coefficient. The table should be made in such a way that no extrapolation is necessary.

The electrical qualities of the ionosphere may be characterized by electron and ion density profiles, and a collision frequency model. To facilitate calculation of the reflection coefficients, the ionosphere is divided into layers. Each layer is assumed to have uniform densities. By increasing the number of layers, this representation can be made as close as desired to the continuous distribution.

Maxwell's equations and the equation of motion of the electron are solved yielding transmitted and reflected portions of the incident wave for each of the layers. By keeping track of these upgoing and downgoing waves and solving for continuity at the boundaries between each of the layers, the reflection coefficients are obtained.

Coupling of the vertical electric and vertical magnetic polarizations within the ionosphere causes the generation of an abnormal component and necessitates calculation of two reflection coefficients for the vertical electric incident polarization. Also, since ground reflections do not change the polarization of the incident wave (i. e., there is no coupling at the ground), it is necessary to compute reflection coefficients for normal and abnormal ionospheric reflection of vertical magnetic incident polarization. To summarize, four reflection coefficients must be computed for each angle of incidence; (1) vertical electric polarization of the incident and reflected wave (T_{ee}), (2) vertical electric

polarization of the incident wave with abnormal or vertical magnetic polarization of the reflected wave (T_{em}), (3) vertical magnetic polarization of the incident and reflected wave (T_{mm}), and (4) vertical magnetic polarization of the incident wave and vertical electric polarization of the reflected wave (T_{me}).

NOTE: Vertical electric polarization is in quadrature (at 90 degrees) to vertical magnetic polarization and may also be called horizontal magnetic polarization. Similarly, vertical magnetic polarization may be called horizontal electric polarization.

Each reflection coefficient gives the phase and amplitude of the reflected wave. The phase is normally referenced to the bottom of the ionosphere. This causes the phase to vary rapidly with angle of incidence. Interpolation on this wildly varying phase can be very inaccurate. The problem is solved by re-referencing the phase to a height where the phase is slowly varying with angle of incidence. This height is sometimes referred to as the effective reflection height.

6. The Calculations

Table 1 lists the calculations that are reported in this paper. Throughout these calculations a magnetic dip of 70 degrees and a magnetic field strength of 40 ampere-turns/meter have been employed. These values are a good approximation of the magnetic field vector experienced in the United States. All of the phase and group delay graphs are relative to a medium where the index of refraction is 1.0001.

Two ionospheric profiles (electron density as a function of height above the surface of the earth) designated normal day (fig. 1) and normal night (fig. 2), have been used for the majority of the calculations with six other profiles used to demonstrate the types of fluctuations one might expect under certain conditions. The normal day and normal night profiles were raised and lowered 2.5 km. While this is admittedly

an artificial alteration of the ionosphere, it was felt that calculations made by using such profiles would indicate the variations to be expected during ionospherically active periods. The Deeks 1200[19] profile (fig. 3) and the Bain and May[20] profile (fig. 4) represent sunspot maximum and sunspot minimum conditions as experienced over Great Britain.

The variable most comprehensively treated herein is magnetic azimuth. The majority of the calculations were repeated with at least three changes in azimuth. For purposes of interpolation, propagation towards the magnetic north (0 degrees) has been assumed to be reciprocal to propagation towards the magnetic south (180 degrees).

The surface reflection coefficients were computed on the basis of a conductivity of .005 mhos per centimeter and a ground dielectric constant of 15 for land, and a conductivity of 5 mhos per centimeter and dielectric of 80 for sea. Unless the graphs are otherwise marked, the values for land were used for the computations.

Table 2 gives a comparison of the theory and experimental data. These data are in the form of diurnal phase shift measurements. Diurnal phase shift refers to the phase difference between day and night, resulting from increased ionization of the upper atmosphere caused by the sun's rays. This phase difference was computed as the night phase at a given geodetic distance minus the daytime phase at that same distance. A few group delay comparisons have been made in table 3.

Table 4 lists the predicted daytime phase delay and the diurnal variation for various sites. Table 5 gives the associated group delays for these same sites. The values given for Canberra, Australia represent an extrapolation from the graphs.

Figure 5 gives a comparison of theoretical and experimental diurnal phase shifts measured by NBS on the 20.0 kHz transmissions from WWVL. Figure 6 compares theoretical and experimental relative phase values for the same transmissions.

Figures 8 through 69 give a phase correction in radians for various frequencies and magnetic azimuths under normal day and normal night conditions. This phase correction is that value which must be added to the phase delay of a hypothetical wave traveling at the speed of light in a medium where the index of refraction is 1.0001. Consequently, these figures are labeled "Relative Phase."

Figures 70 through 128 give the amplitude in volts per meter, referenced to unity dipole current, for the various frequencies and azimuths under normal day and normal night conditions.

Figures 129 through 204 give the group delay correction in microseconds for various frequencies and azimuths under normal night conditions. Again, because this correction is obtained as the difference between the absolute group delay and the delay of a wave traveling at the speed of light and an index of refraction of 1.0001, the figures are labeled "Relative Group Delay." The actual method of calculation of this group delay has been developed by Fey and Looney[21] and is analogous to the method presented earlier in the text.

Figures 205 through 233, "Diurnal Phase," give the phase shift to be expected between night and day using the normal day and normal night profiles.

Figures 234 through 254 are special cases of the previous calculations in that either the profile or ground conditions are changed from previous figures for the same frequency and azimuth.

7. Discussion and Conclusions

The analysis of the theoretical data presented here is aimed at timing implications. It should be noted during the analysis of these

graphs that the calculations have a tendency to deteriorate with distance. This does not affect many of the graphs, but at the point where the trend towards linearity with increasing distance breaks down, the graph should be disregarded or, conversely, the linearity may be extrapolated to obtain the desired results. The cause of the degeneracy is a need for more terms (hops) in the geometric series summation.

The fluctuations in the amplitude of the sum of the various hops is highly correlated to the points at which the amplitudes of two of the hops are equal (see fig. 78--Amplitude, 12.5 kHz, 150°, Normal Day). These amplitude fluctuations are also well correlated to fluctuations in phase. Unfortunately, it is precisely these points of equal amplitude that are most likely to be displaced most by small changes in the ionosphere. Therefore, there are certain critical distances at which the phase is likely to be unstable. Since there are more fluctuations in both phase and amplitude under nighttime conditions, this may account for the large phase deviations normally experienced at night. An interesting presentation of this idea is given in figure 7. Here phase and amplitude are combined on one graph for 13.6 kHz, 90°, Normal Night. (r is a logarithamic scale giving amplitude in volts/meter and ϕ is relative phase in degrees.) The points on the curve are at 500 km increments.

It is interesting to note that the gross features of the nighttime phase and amplitude graphs at the Omega frequencies are very similar to the daytime features near 20 kHz. This points out the dependence of the field upon the ratio of wave length to ionospheric height. One implication of this dependence is that the Omega frequencies may be nearly as reliable for time synchronization at night as are the WWVL transmissions during the day. The graphs of the theoretical group delay indicate that, with a few exceptions, this may indeed be the case. The smoothness of the night phase from several of the Omega stations monitored at the National Bureau of Standards again points towards reliable time transfer

during the night at these frequencies. Near 20 kHz, however, it is apparent that synchronization cannot be accomplished with any degree of reliability during the night.

During the day, synchronization at the Omega frequencies should be very reliable. The small fluctuations in the group delay graphs are dissipated in nearly all cases by approximately 2,000 km. From this point on the group delay becomes nearly linear and very predictable.

One is able to arrive at an estimate of the maximum timing error to be expected using a given pair of frequencies, by examining the group delay plots. In the majority of cases these plots have fluctuations which are similar to damped sine waves. The amplitude of these waves is then the maximum expected error. Neglecting the first 500 to 1000 kilometers, the following estimates of maximum timing error are given:

a. for the Omega frequencies during the day the expected error is approximately ± 20 μsec;

b. for the frequencies near 20 kHz during the day, approximately ± 50 μsec;

c. for the Omega frequencies at night, approximately ± 70 μsec;

d. for the frequencies near 20 kHz during the night, approximately ± 120 μsec.

Because of the similarity of the relative phase graphs with changes in azimuth it appears that linear interpolation may be used for both azimuth and distance from the transmitter during the day. The night phase, though, is not nearly so well behaved. In fact, the night phase at 270° is very dissimilar to the 90° and the 180° phases (which are rather alike). A possible area for further study would be to determine whether these changes take place linearly with azimuth.

The fluctuations (high frequency Fourier component) in group delay are very much correlated to the frequency separation. Wide frequency separations have fewer and smaller fluctuations than do narrow frequency separations. At some point then, one must choose between the high resolution and subsequently large ambiguities of wide separations, and the low resolution but small ambiguity of small separations.

The Omega navigation system, with its proposed worldwide coverage, has great potential as a time synchronization tool. The variety of frequencies and frequency separation, coupled with the possibility of 24-hour utilization, available at each of the eight stations in the network offer medium to high resolution time synchronization to almost all locales.

8. References

[1] Blamont, J. E., and de Jager, C., "Upper-atmospheric turbulence determined by means of rockets," J. Geophys. Res., 67, No. 8, pp. 3113-3119, July 1962.

[2] Greenhow, J. S., and Neufeld, E. L., "Large scale irregularities in high altitude winds," Proc. Phys. Soc., 75, pp. 228-234, 1960.

[3] Manring, E., Bedinger, J. F., and Knaflich, H., "Measurements of winds in the upper atmosphere during April 1961," J. Geophys. Res., 67, No. 10, pp. 3923-3925, September 1962.

[4] Charney, J. G., and Drazin, P. G., "Propagation of planetary-scale disturbances from the lower into the upper atmosphere," J. Geophys. Res., 66, No. 1, pp. 83-109, January 1961.

[5] Crombie, D. D., "Effects of normal ionospheric fluctuations on propagation of VLF signals to great distances," Phase and Frequency Instability in Electromagnetic Wave Propagation (AGARD-EWP Sym., Ankara, Turkey, October 4-12, 1967), AGARD Conf. Proc. No. 33, K. Davies (Ed.), pp. 35-43 (Technivision Services, Slough, England, July 1970).

[6] Rice, S. O., "Statistical fluctuations of radio field strength far beyond the horizon," Proc. IRE, 41, No. 2, pp. 274-281, February 1953.

[7] Hargreaves, J. K., "Random fluctuations in VLF signals reflected obliquely from the ionosphere," J. Atmos. Terr. Phys., 20, pp. 155-166, 1961.

[8] Hines, C. O., "Internal gravity waves at ionospheric heights," Can. J. Phys., 38, No. 11, pp. 1441-1481, November 1960.

[9] Wait, J. R., and Spies, K. P., "Characteristics of the earth-ionosphere waveguide for VLF radio waves," Nat. Bur. Stand. (U.S.) Tech. Note 300, 1964. 1st Suppl., February 1965; 2nd Suppl., March 1965.

[10] Johler, J. R., "On the analysis of LF ionospheric radio propagation phenomena," J. Res., 65D, No. 5, pp. 507-529, September-October 1961.

[11] Johler, J. R., and Berry, L. A., "Propagation of terrestrial radio waves of long wavelength--theory of zonal harmonics with improved summation techniques," J. Res., 66D, No. 6, pp. 737-773, November-December 1962.

[12] Johler, J. R., "Concerning limitations and further corrections to geometric-optical theory for LF, VLF propagation between the ionosphere and the ground," Radio Sci. J. Res., NBS/USNC-URSI, 68D, No. 1, pp. 67-78, January 1964.

[13] Johler, J. R., "Zonal harmonics in low frequency terrestrial radio wave propagation," Nat. Bur. Stand. (U.S.) Tech. Note 335, April 13, 1966.

[14] Johler, J. R., "Theory of propagation of low frequency terrestrial radio waves--mathematical interpretation of D-region propagation studies," ESSA Tech. Report IER48-ITSA 47, August 1967.

[15] Johler, J. R., and Mellecker, C., "Theoretical LF, VLF field calculations with spherical wave functions of integer order," ESSA Tech. Report, ERL165-ITS 106, April 1970.

[16] Debye, P., "Der lichtdruck auf kugeln von beleibigem material," (English translation: "The pressure of light on spheres made of any material."), Ann. Physik (Leipzig), 30, pp. 57-136, 1909.

[17] Lord Rayleigh, "On the acoustic shadow of a sphere," with Appendix giving the values of Legendre's functions from P_0 to P_{20} at intervals of 5 degrees by Prof. A. Lodge, Phil. Trans. Roy. Soc., London, A203, pp. 87-110, 1904.

[18] Johler, J. R., "Ground wave propagation in a normal and an ionized atmosphere," ESSA Tech. Report, ERL121-ITS 85, 1969a.

[19] Deeks, D. G., "D-region electron distributions in middle latitudes deduced from the reflexion of long radio waves," Proc. Roy. Soc., A291, pp. 413-437, 1966.

[20] Bain, W. C., and May, B. R., "D-region electron-density distributions from propagation data," Proc. IEE, 114, No. 11, pp. 1593-1597, November 1967.

[21] Fey, L., and Looney, C. H., Jr., "A dual frequency VLF timing system," IEEE Trans. Instrum. and Meas., IM-15, No. 4, pp. 190-195, December 1966.

APPENDIX

In a series of papers, Johler has combined the zonal harmonic series with the geometric series and by extracting the ground wave from the total field, greatly reduced the number of terms required for convergence of the series. The material presented in this Appendix is an attempt to condense this theory.

To gain insight into this application of zonal harmonics we will first consider the case of a sharply bounded isotropic ionosphere and then generalize to an anisotropic ionosphere with a continuously varying electrical makeup.

For the isotropic case, and particularly for vertical electric polarization, the zonal harmonic representation is

$$E_r = \frac{I_0 \ell}{k_1^2 a^4} \frac{\mu_0 c}{4\pi} \sum_{n=0}^{\infty} n(n+1)\,(2n+1)\,P_n(\cos\theta)\,\zeta_{1a}^{(2)}\,\Psi_{1a}$$

$$\times \left\{ 1 + R_n \frac{-\zeta_{1a}^{(2)}}{\Psi_{1a}} \right\} \left\{ 1 + T_n \frac{-\Psi_{1a}}{\zeta_{1a}^{(2)}} \right\} \left\{ 1 - RnTn \right\}^{-1} \qquad (1)$$

$I_0 \ell$ is the intensity of the electrical source, a point dipole, which for convenience may be taken to be 1. μ_0 is the permeability of space ($4\pi \times 10^{-7}$ henry/meter) and c is the speed of light (2.997925×10^8 m/s). a is the radius of the earth and k_1 is the wave number of air. $P_n(z)$ is the solution of Legendre's differential equation. R_n and T_n are the ground and ionospheric reflection coefficients respectively (the subscript denotes that the reflection coefficients must be recomputed for each n). $\zeta_{1a}^{(1,2)}$ is the spherical wave function and $\Psi_{1a} = \frac{1}{2}\left[\zeta_{1a}^{(1)} + \zeta_{1a}^{(2)}\right]$.

The geometric series may be introduced by noting that the denominator of eq (1) can be expressed as a geometric series.

$$\left[1-R_n T_n\right]^{-1} = 1+\sum_{j=1}^{\infty} \left[R_n T_n\right]^j \tag{2}$$

Substituting into (1) and interchanging the order of summation yields

$$E_r = E_{r,o} + \sum_{j=1}^{\infty} E_{r,j} \tag{3}$$

where

$$E_{r,o} = \frac{\mu_o c}{8\pi} \frac{I_o \ell}{k_1^2 a^4} \sum_{n=0}^{\infty} F(n)\, \zeta_{1a}^{(2)}\, \zeta_{1a}^{(1)}\, (1+R_n) \tag{4}$$

and

$$E_{r,j} = \frac{\mu_o c}{8\pi} \frac{I_o \ell}{k_1^2 a^4} \sum_{n=0}^{\infty} F(n)\, \zeta_{1a}^{(2)}\, \zeta_{1a}^{(1)}\, (1+R_n)^2 \begin{Bmatrix} \zeta_{1a}^{(1)} & \zeta_{1g}^{(2)} \\ \zeta_{1a}^{(2)} & \zeta_{1g}^{(1)} \end{Bmatrix} [R_n]^{j-1}\, [T_n]^j \tag{5}$$

and $F(n) = n(n+1)(2n+1)\, P_n(\cos\theta)$.

At this point an analogy may be drawn with geometric optics. $E_{r,o}$ is the ground wave and $E_{r,j}$ is a wave which has been reflected from the ionosphere j times. Because of lateral displacement at the ionosphere, and also at the ground, the wave is not reflected from a point but rather from a region. The largest portion of the reflection does occur at or near the point predicted by geometric optics. The actual angle of incidence at the ground, τ_i, or at the ionosphere, φ_i,

for each of the n waves is given by

$$\sin \tau_i \sim \frac{\sqrt{n(n+1)}}{k_1 a} \qquad \text{and} \quad \sin \varphi_i \sim \frac{\sqrt{n(n+1)}}{k_1 g} \tag{6}$$

with the convention that the sine = 1 when $\frac{\sqrt{n(n+1)}}{k_1 a}$ or $\frac{\sqrt{n(n+1)}}{k_1 g}$ is greater than one.

The spherical wave functions may easily be evaluated from the recurrence relation given ($z = k_1 a$) and $\zeta_{1a}^{(1,2)} = \zeta_n^{(1,2)}(z)$

$$\zeta_{n+1}^{(1,2)}(z) = \frac{2n+1}{z} \zeta_n^{(1,2)}(z) - \zeta_{n-1}^{(1,2)}(z) \tag{7}$$

where,

$$\zeta_0^{(1,2)}(z) = \mp i \exp[\pm iz] \tag{8}$$

and

$$\zeta_{-1}^{(1,2)}(z) = \exp[\pm iz]. \tag{9}$$

Similarly the Legendre function can be found for integral n from the recurrence relation

$$P_n(z) = \frac{(2n-1)z}{n} P_{n-1}(z) - \frac{n-1}{n} P_{n-2}(z) \tag{10}$$

where

$$P_0(z) = 1$$

and

$$P_1(z) = z.$$

Note: With $z = \cos\theta$, θ is the central angle of the sphere subtended by a given distance.

For the case of an anisotropic ionosphere, eq (5) must be modified to read,

$$E_{r,j} = \frac{\mu_0 c}{8\pi} \frac{I_0 \ell}{k_1^2 a^4} \sum_{n=0}^{\infty} F(n)\, \zeta_{1a}^{(2)} \zeta_{1a}^{(1)} (1+R_{e1n})^2 \left\{ \frac{\zeta_{1a}^{(1)}}{\zeta_{1a}^{(2)}} \cdot \frac{\zeta_{1g}^{(2)}}{\zeta_{1g}^{(1)}} \right\} C_j \quad (11)$$

where C_j is the "effective reflection coefficient." C_j can be graphically evaluated by analogy with geometric optics,

$$\begin{aligned} C_1 &= T_{ee} \\ C_2 &= R_e T_{ee}^2 + R_m T_{em} T_{me} \\ C_3 &= 2 R_e R_m T_{ee} T_{em} T_{me} + R_e^2 T_{ee}^3 + R_m^2 T_{mm} T_{em} T_{me} \qquad (12) \\ &\cdots \end{aligned}$$

or from

$$C_j = \frac{1}{j! R_e} \frac{d^j}{dx^j} \left[\frac{1+A_1 x}{1-A_2 x - A_3 x^2} \right] x = 0 \qquad (13)$$

where

$$A_1 = R_m T_{mm}$$

$$A_2 = R_e T_{ee} + R_m T_{mm}$$

$$A_3 = R_e R_m \left[- T_{ee} T_{mm} + T_{me} T_{em} \right].$$

The ground reflection coefficients are defined by,

$$R_{m,n} = \frac{\dfrac{\zeta_{1a}^{(1)'}}{\zeta_{1a}^{(1)}} - \dfrac{k_2}{k_1} \dfrac{\Psi_{2a}'}{\Psi_{2a}}}{\dfrac{-\zeta_{1a}^{(2)'}}{\zeta_{1a}^{(2)}} + \dfrac{k}{k_1} \dfrac{\Psi_{2a}'}{\Psi_{2a}}} \tag{14}$$

and,

$$R_{e,n} = \frac{\dfrac{\zeta_{1a}^{(1)'}}{\zeta_{1a}^{(1)}} - \dfrac{k_1}{k_2} \dfrac{\Psi_{2a}'}{\Psi_{2a}}}{\dfrac{-\zeta_{1a}^{(2)'}}{\zeta_{1a}^{(2)}} + \dfrac{k_1}{k_2} \dfrac{\Psi_{2a}'}{\Psi_{2a}}} \tag{15}$$

where

$$\frac{\zeta_o^{(1,2)'}(z)}{\zeta_o^{(1,2)}(z)} = \pm i.$$

Note that

$$\frac{\zeta_n^{(1)'}(z)}{\zeta_n^{(1)}(z)} \sim \frac{\Psi_n'(z)}{\Psi_n(z)}.$$

Since most of the reflection takes place near the points predicted by geometric optics the concept of local reflection coefficients may be introduced in the expression for C_j. That is, changes in ionospheric or ground parameters along the propagation path may be included in the field equation.

The convergence of the zonal harmonic series (1) is notoriously slow primarily because of the inclusion of the groundwave in this expression. Equation (3), however, separates the groundwave, $E_{r,0}$, from the skywaves. By using other methods of calculation for the groundwave, the number of terms required for convergence may be reduced by a factor of approximately 15. That is, convergence of the skywave series occurs rapidly as n approaches $k_1 a$ ($\sin \varphi_i \rightarrow 1$), whereas for the groundwave $15\, k_1 a$ terms are required. Furthermore, the contribution of terms with small angles of incidence, $\varphi_i < 30^\circ$, are nearly negligible so that for frequencies up to 20 kHz, only a few hundred terms may be required for convergence.

TABLE 1

LIST OF CALCULATIONS

Frequency (kHz)	Magnetic Azimuth (Degrees)	Profile Identification
10.20	90	Normal Day
10.20	90	Normal Night
10.20	180	Normal Day
10.20	180	Normal Night
10.20	270	Normal Day
10.20	270	Normal Night
12.20	90	Normal Day
12.20	90	Normal Night
12.25	90	Normal Day
12.25	90	Normal Night
12.30	90	Normal Day
12.30	90	Normal Night
12.50	90	Normal Day
12.50	90	Normal Night
12.50	135	Normal Day
12.50	135	Normal Night
12.50	150	Normal Day
12.50	180	Normal Day
12.50	180	Normal Night
12.50	225	Normal Day
12.50	270	Normal Day
12.50	270	Normal Night
12.70	90	Normal Day
12.70	90	Normal Night
12.70	135	Normal Day
12.70	135	Normal Night
12.70	150	Normal Day
12.70	180	Normal Day
12.70	180	Normal Night
12.70	225	Normal Day
12.70	270	Normal Day
12.70	270	Normal Night

TABLE 1 (Continued)

Frequency (kHz)	Magnetic Azimuth (Degrees)	Profile Identification
13.60	90	Normal Day
13.60	90	Normal Night
13.60	180	Normal Day
13.60	180	Normal Night
13.60	270	Normal Day
13.60	270	Normal Night
19.90	90	Normal Day
19.90	90	Normal Night
19.90	180	Normal Day
19.90	180	Normal Night
19.90	270	Normal Day
19.90	270	Normal Night
20.00	90	Normal Day
20.00	90	Normal Night
20.00	180	Normal Day
20.00	180	Normal Night
20.00	270	Normal Day
20.00	270	Normal Night
20.50	90	Normal Day
20.50	90	Normal Night
20.50	180	Normal Day
20.50	180	Normal Night
20.50	270	Normal Day
20.50	270	Normal Night
20.90	90	Normal Day
20.90	90	Normal Night
20.90	180	Normal Day
20.90	180	Normal Night
20.90	270	Normal Day
20.90	270	Normal Night
10.20	90	Deeks 1200
12.50	90	Deeks 1200
12.70	90	Deeks 1200
20.00	90	Deeks 1200

TABLE 1 (Continued)

Frequency (kHz)	Magnetic Azimuth (Degrees)	Profile Identification
10.20	90	Bain & May
12.50	90	Bain & May
12.70	90	Bain & May
20.00	90	Bain & May
10.20	90	Normal Day (Sea Water)
12.50	90	Normal Day (Sea Water)
12.70	90	Normal Day (Sea Water)
20.00	90	Normal Day (Sea Water)
12.20	90	Normal Day (Raised 2.5 km)
12.20	90	Normal Day (Lowered 2.5 km)
12.20	90	Normal Night (Raised 2.5 km)
12.20	90	Normal Night (Lowered 2.5 km)
12.30	90	Normal Day (Raised 2.5 km)
12.30	90	Normal Day (Lowered 2.5 km)
12.30	90	Normal Night (Raised 2.5 km)
12.30	90	Normal Night (Lowered 2.5 km)

TABLE 2

COMPARISON OF EXPERIMENTAL AND THEORETICAL DIURNAL PHASE

Location	Transmitter	Frequency	Magnetic Azimuth (Degrees)	Geodetic Distance	Experimental Diurnal	Theoretical Diurnal	Reference
Carlsbad	WWVL	20.0	168.3	920.0	35	24	1
Tucson	WWVL	20.0	204.4	1074.0	27	16	1
San Diego	WWVL	20.0	227.8	1392.8	17-21	18	1
College	WWVL	20.0	322.2	3821.9	21	19	1
Maui	WWVL	20.0	254.6	5306.8	35	28	1
WWV Md.	WWVL	20.0	78.3	2411.0	10-15	4	2
Inubo	WWVL	20.0	304.8	9205.4	46-54	41	3
Koganei	WWVL	20.0	305.5	9325.6	42-45	41	3
Columbus	WWVL	20.0	79.6	1875.7	17	8	4
San Diego	WWVL	20.0	227.8	1392.8	17	18	4
Cairo	WWVL	20.0	30.3	10974.1	77	60	5
WWVH	WWVL	20.0	254.6	5306.8	29-32	28	2
JPL	WWVL	20.0	236.9	1191.4	24	17	6
USNOB	WWVL	20.0	78.8	2394.6	16±4	5	6
GSFC	WWVL	20.0	78.3	2411.0	62±5	54	7
Quito	WWVL	20.0	135.7	5266.7	50±5	30	7
Lima	WWVL	20.0	140.6	6516.5	40±5	34	7
Santiago	WWVL	20.0	144.6	8939.6	70±10	48	7
Rosman	WWVL	20.5	93.4	2035.7	63	55	7
Ft. Myers	WWVL	19.9/20.5	112.2	2648.0	61	41	7
Johannes-burg	WWVL	19.9/20.5	77.2	15438.7	117	88	7
Carlsbad	NSS	21.4	255.5	2606.4	16	8*	1
Tucson	NSS	21.4	260.3	3193.2	11	14*	1

*Values for diurnal phase extrapolated in the frequency domain.

TABLE 2 (Continued)

COMPARISON OF EXPERIMENTAL AND THEORETICAL DIURNAL PHASE

Location	Transmitter	Frequency	Magnetic Azimuth (Degrees)	Geodetic Distance	Experimental Diurnal	Theoretical Diurnal	Reference
San Diego	NSS	21.4	265.2	3710.2	43	22*	1
San Diego	NPM	19.8	57.0	4225.1	27-33.5	18*	1
College	NPM	19.8	359.6	4888.2	41	23*	1
Boulder	NPM	19.8	48.1	5379.3	58±7	31*	1
Inuba	NPM	19.8	292.4	6077.2	32	29*	1
Perth	NPM	19.8	232.0	10888.8	100-76	51*	1
GSFC	Ω/NY	12.5	211.4	516.0	58±2	40	7
GSFC	Ω/H	12.2	48.0	7789.4	72±2	60	7
San Diego	Ω/H	12.2	56.9	4195.8	38.5	33	1
GSFC	Ω/T	12.0	329.9	3479.0	38	31*	7
San Diego	Ω/H	10.2	56.9	4195.8	48.5	39	1
Boulder	Ω/H	10.2	48.1	5352.9	61	49	1
Forest-port	Ω/H	10.2	43.0	7834.6	87	72	1
College	Balboa	10.2	328.6	8079.7	93	79	1
Haiku	Balboa	10.2	283.0	8434.8	107	80	1
Forest-port	Balboa	10.2	358.9	3835.3	30	36	1

*Values for diurnal phase extrapolated in the frequency domain.

References for
Table 2

1. W. D. Westfall, "Diurnal Changes of Phase and Group Velocity of VLF Radio Waves," Radio Science, Vol. 2 (New Series), No. 1, January 1967.

2. B. E. Blair and A. H. Morgan, "Control of WWV and WWVH Standard Frequency Broadcasts by VLF and LF Signals," Radio Science J. of Res. NBS/USNC-URSI, Vol 69D, No. 7, July 1965.

3. Yoshiyuki Yasuda, private communication.

4. P. B. Rao and W. A. Teso, "An Investigation of Propagation Phase Changes at VLF," The Radio and Electronic Engineer, November 1966.

5. A. L. el Sayed, "Comparison of WWVL and the Local Standard," Proc. of the Mathematical and Physical Society, U.A.R., 1969.

6. Measurements made by NBSBL.

7. J. H. Roeder, unpublished report.

TABLE 3

COMPARISON OF EXPERIMENTAL AND THEORETICAL GROUP DELAY

Location	Transmitter	Frequency 1 (kHz)	Frequency 2 (kHz)	Experimental Delay	Theoretical Delay
USNOB	WWVL	20.0	20.5	8061	8057
WWVH	WWVL	20.0	20.5	17785	17797
JPL	WWVL	20.0	20.5	4014	4017
NBSBL	Ω/NY	12.5	12.7	8513	8554
NBSBL	Ω/T	12.0	13.6	17985	18084
GSFC	WWVL	19.9	20.0	8052	8109
Quito	WWVL	19.9	20.0	17942	17667
Lima	WWVL	19.9	20.0	21717	21861
Santiago	WWVL	19.9	20.0	29764	29997

TABLE 4

PREDICTED DIURNAL AND PHASE DELAY

Location	Frequency (kHz)	Transmitter	Magnetic Azimuth (Degrees)	Geodetic Distance (km)	Phase (μsec)	Diurnal (μsec)
Meritt Island	19.9	WWVL	106.8	2597.3	8622.9	47
	20.0				8623.7	51
	20.5				8626.3	52
	20.9				8627.9	51
	12.5	Ω/NY	212.9	1731.7	5761.6	15
	12.7				5762.2	14
Madrid	19.9	WWVL	45.0	7992.7	26656.8	40
	20.0				26657.5	41
	20.5				26660.5	41
	20.9				26663.8	43
Bahama	19.9	WWVL	107.0	2916.4	9690.2	23
	20.0				9690.6	24
	20.5				9692.1	25
	20.9				9693.7	29
	12.5	Ω/NY	203.9	1886.8	6279.0	17
	12.7				6279.3	17
Canberra	19.9	WWVL	242.6	13701.3	45736.8	53
	20.0				45738.2	53
	20.5				45743.7	54
	20.9				45746.8	57
Bermuda	19.9	WWVL	84.5	3700.1	12309.8	20
	20.0				12310.2	20
	20.5				12313.4	21
	20.9				12315.6	22
	12.5	Ω/NY	154.2	1533.3	5098.4	10
	12.7				5099.3	7

TABLE 4 (Continued)

PREDICTED DIURNAL AND PHASE DELAY

Location	Frequency (kHz)	Transmitter	Magnetic Azimuth (Degrees)	Geodetic Distance (km)	Phase (usec)	Diurnal (usec)
Mojave	19.9	WWVL	237.1	1194.0	3933.6	15
	20.0				3934.2	16
	20.5				3936.2	16
	20.9				3938.3	17
	12.5	Ω/NY	263.3	3669.5	12219.8	27
	12.7				12221.3	23
Rosman	19.9	WWVL	93.4	2035.7	6750.2	55
	20.0				6750.8	55
	20.5				6752.2	55
	20.9				6753.3	54
	12.5	Ω/NY	233.0	1134.6	3771.6	6
	12.7				3773.1	6
Ft. Myers	19.9	WWVL	112.2	2648.0	8792.4	41
	20.0				8792.7	43
	20.5				8795.7	48
	20.9				8797.2	50
	12.5	Ω/NY	214.5	1972.2	6563.3	16
	12.7				6564.8	17
GSFC	19.9	WWVL	78.3	2411.0	8001.4	54
	20.0				8001.3	54
	20.5				8005.0	54
	20.9				8006.7	54
	12.5	Ω/NY	211.4	516.0	1714.7	40
	12.7				1715.8	43

TABLE 5

PREDICTED GROUP DELAY

Location	Transmitter	Frequency 1 (kHz)	Frequency 2 (kHz)	Magnetic Azimuth (Degrees)	Geodetic Distance (km)	Group Delay (μsec)
Meritt Island	WWVL	19.9	20.0	106.8	2597.3	8733
		19.9	20.5			8731
		19.9	20.9			8732
		20.0	20.5			8732
		20.0	20.9			8732
		20.5	20.9			8734
	Ω/NY	12.5	12.7	212.9	1731.7	5814
Madrid	WWVL	19.9	20.0	45.0	7992.7	26820
		19.9	20.5			26813
		19.9	20.9			26812
		20.0	20.5			26813
		20.0	20.9			26810
		20.5	20.9			26811
Bahama	WWVL	19.9	20.0	107.0	2916.4	9757
		19.9	20.5			9762
		19.9	20.9			9765
		20.0	20.5			9764
		20.0	20.9			9766
		20.5	20.9			9771
	Ω/NY	12.5	12.7	203.9	1886.8	6334
Canberra	WWVL	19.9	20.0	242.6	13701.3	45971
		19.9	20.5			45956
		19.9	20.9			45962
		20.0	20.5			45963
		20.0	20.9			45964
		20.5	20.9			45958

TABLE 5 (Continued)

PREDICTED GROUP DELAY

Location	Transmitter	Frequency 1 (kHz)	Frequency 2 (kHz)	Magnetic Azimuth (Degrees)	Geodetic Distance (km)	Group Delay (μsec)
Bermuda	WWVL	19.9	20.0	84.5	3700.1	12424
		19.9	20.5			12428
		19.9	20.9			12428
		20.0	20.5			12429
		20.0	20.9			12429
		20.5	20.9			12427
	Ω/NY	12.5	12.7	154.2	1533.3	5163
Mojave	WWVL	19.9	20.0	237.1	1194.0	4025
		19.9	20.5			4029
		19.9	20.9			4029
		20.0	20.5			4028
		20.0	20.9			4029
		20.5	20.9			4031
	Ω/NY	12.5	12.7	263.3	3669.5	12336
Rosman	WWVL	19.9	20.0	93.4	2035.7	6837
		19.9	20.5			6822
		19.9	20.9			6815
		20.0	20.5			6820
		20.0	20.9			6813
		20.5	20.9			6804
	Ω/NY	12.5	12.7	233.0	1134.6	3803
Ft. Myers	WWVL	19.9	20.0	112.2	2648.0	8900
		19.9	20.5			8897
		19.9	20.9			8900
		20.0	20.5			8896

TABLE 5 (Continued)

PREDICTED GROUP DELAY

Location	Transmitter	Frequency 1 (kHz)	Frequency 2 (kHz)	Magnetic Azimuth (Degrees)	Geodetic Distance (km)	Group Delay (μsec)
		20.0	20.9			8900
		20.5	20.9			8903
	Ω/NY	12.5	12.7	214.5	1972.2	6640
GSFC	WWVL	19.9	20.0	78.3	2411.0	8109
		19.9	20.5			8111
		19.9	20.9			8110
		20.0	20.5			8111
		20.0	20.9			8111
		20.5	20.9			8110
	Ω/NY	12.5	12.7	211.4	516.0	1746

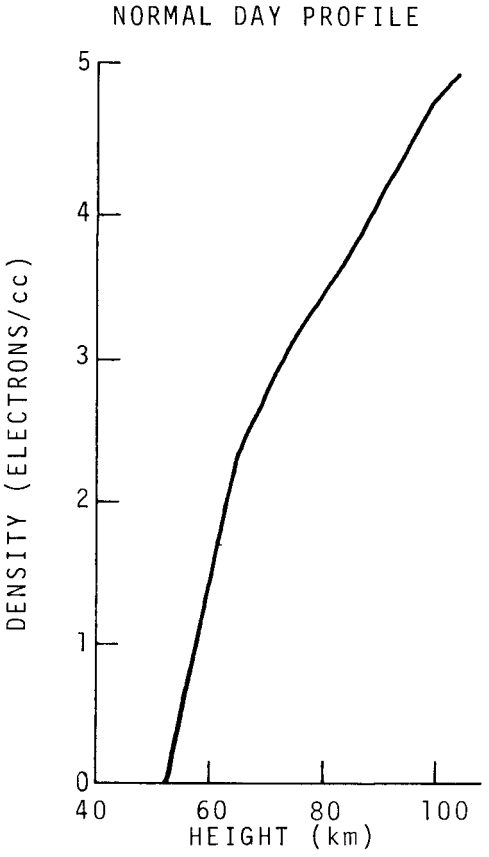

Figure 1.

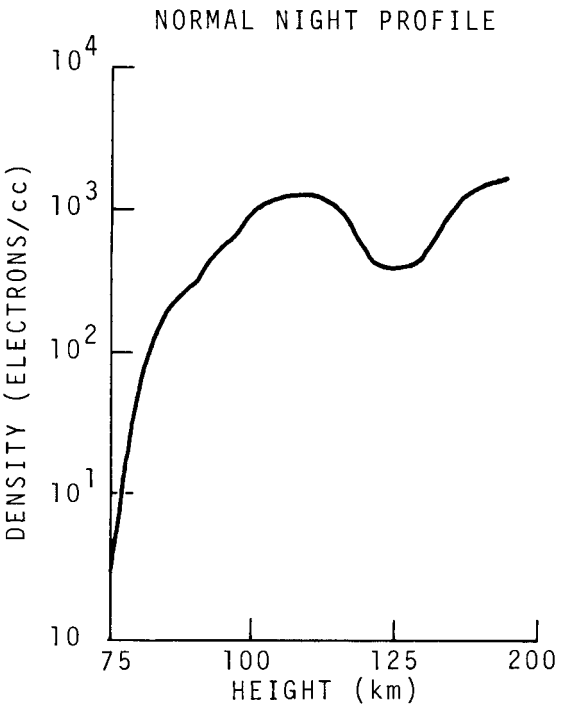

Figure 2.

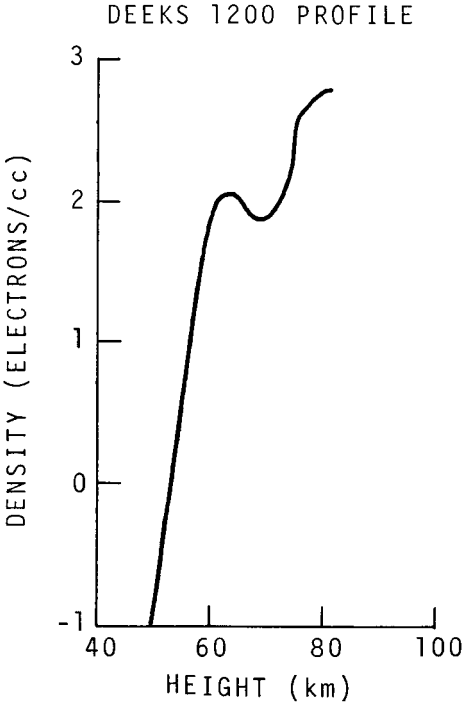

Figure 3.

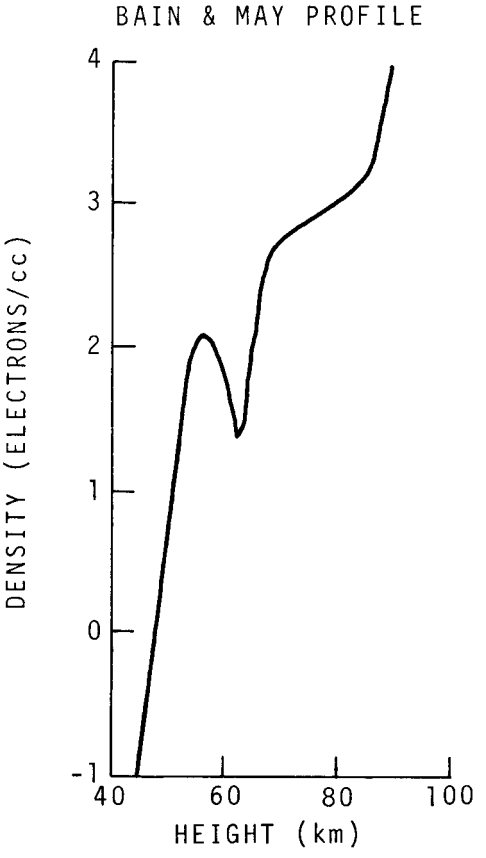

Figure 4.

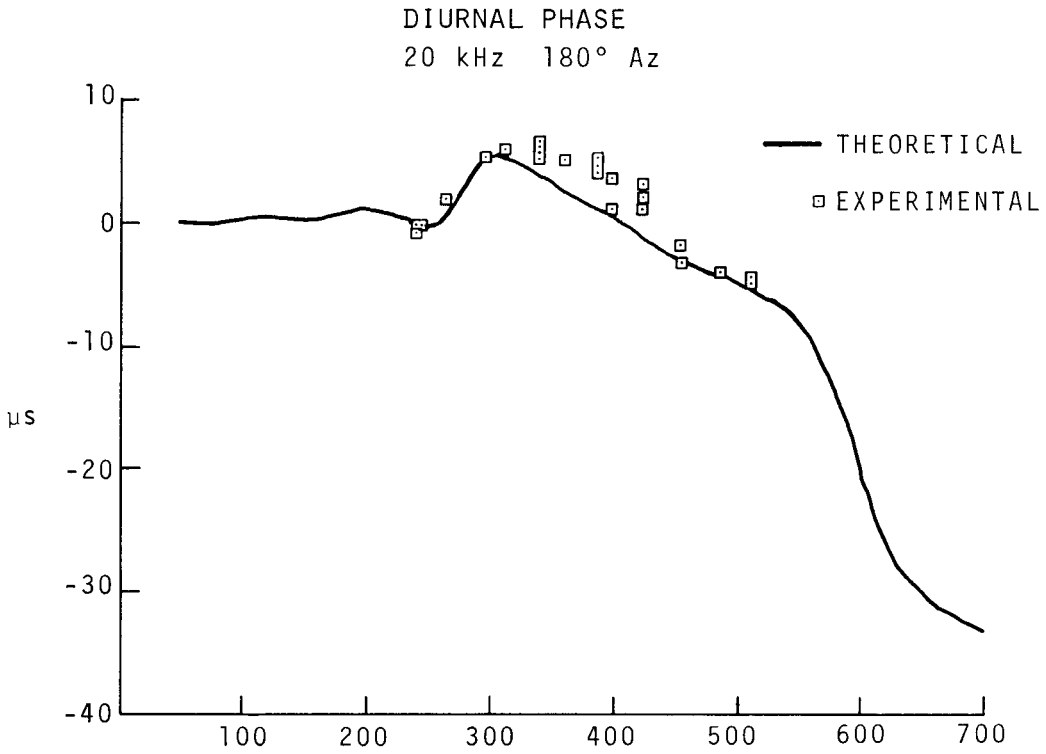

Figure 5.

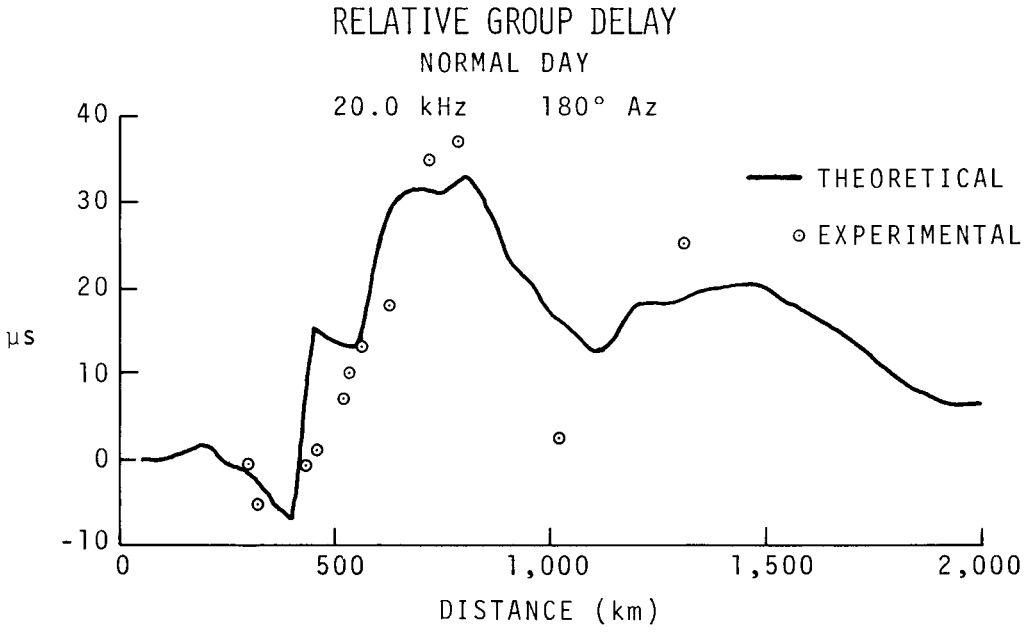

Figure 6.

NORMAL NIGHT

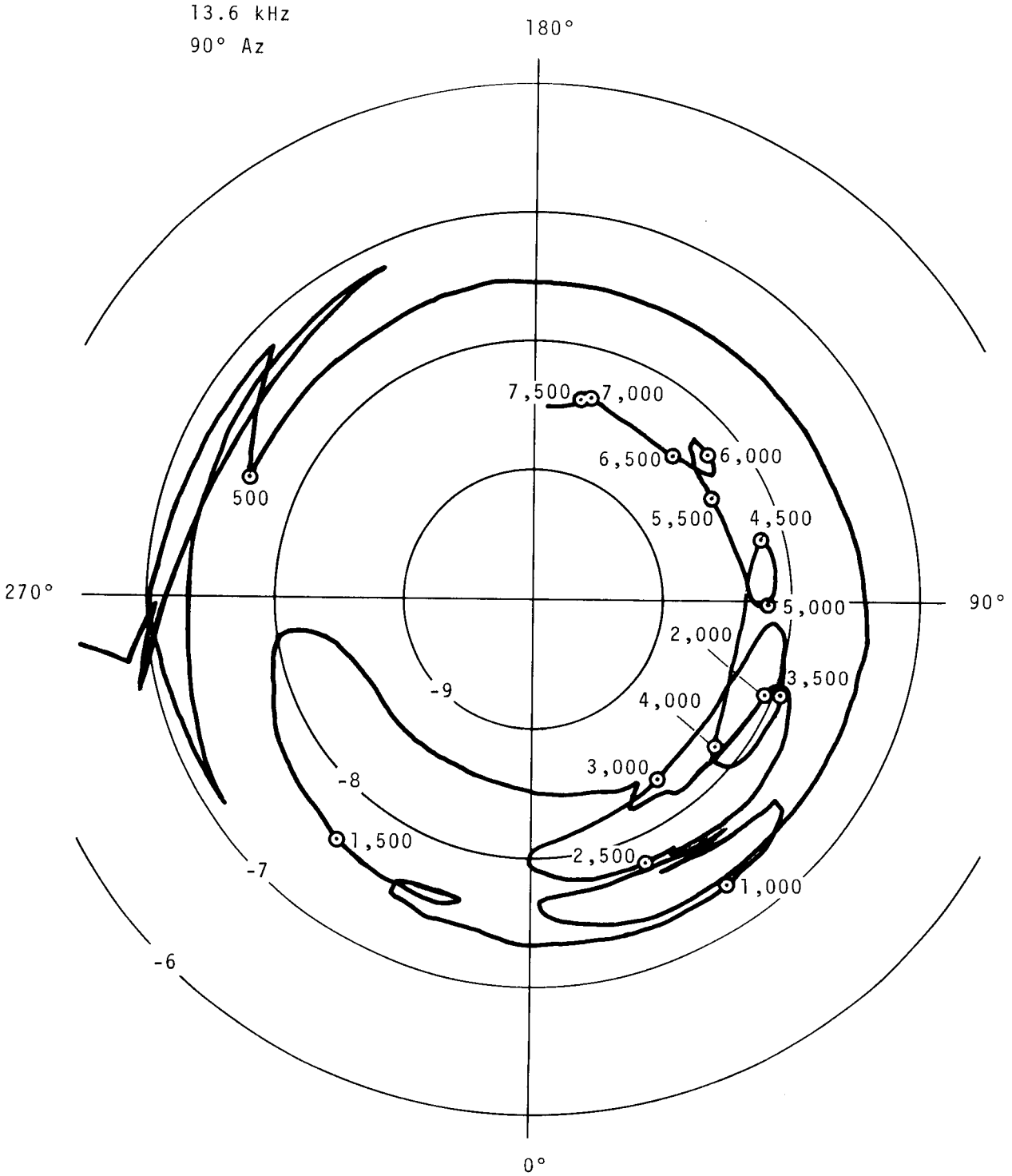

Figure 7.

RELATIVE PHASE
NORMAL DAY

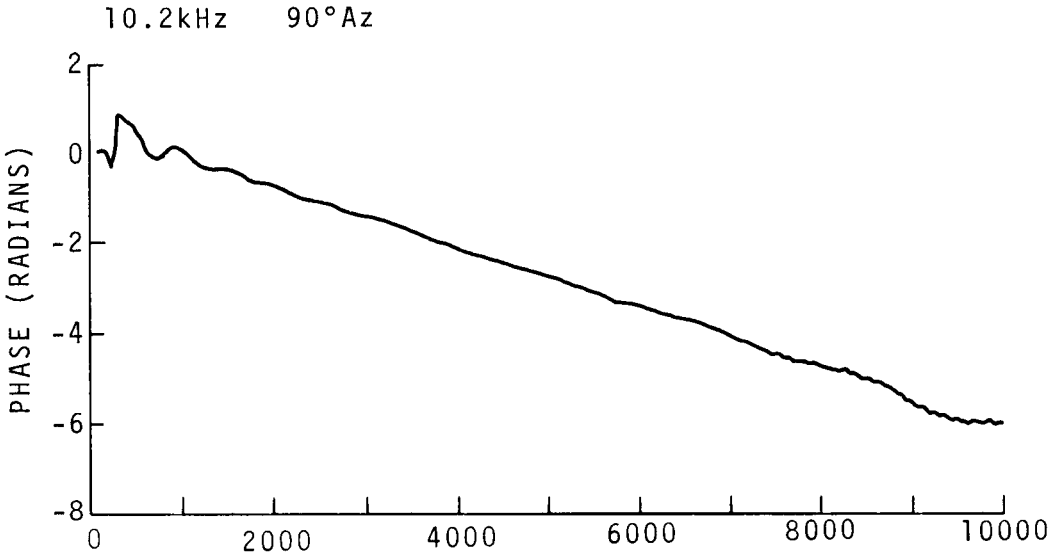

Figure 8.

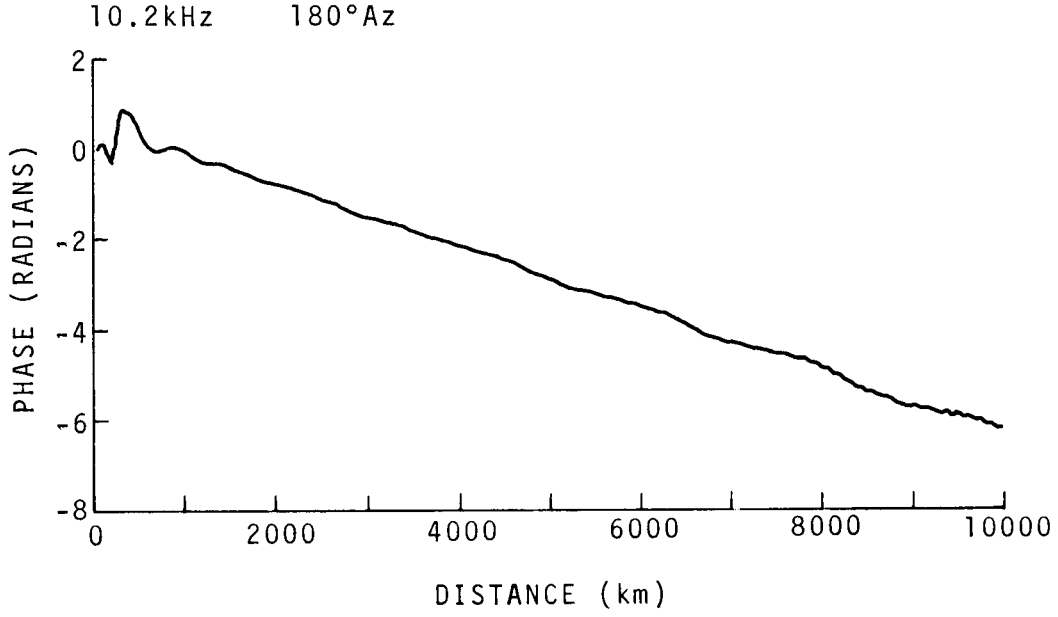

Figure 9.

RELATIVE PHASE
NORMAL DAY

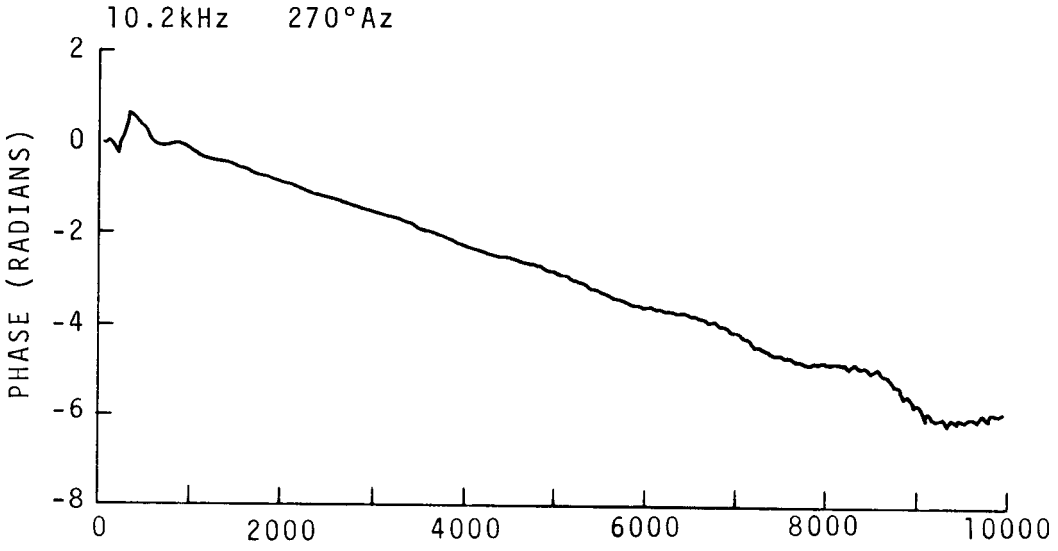

Figure 10.

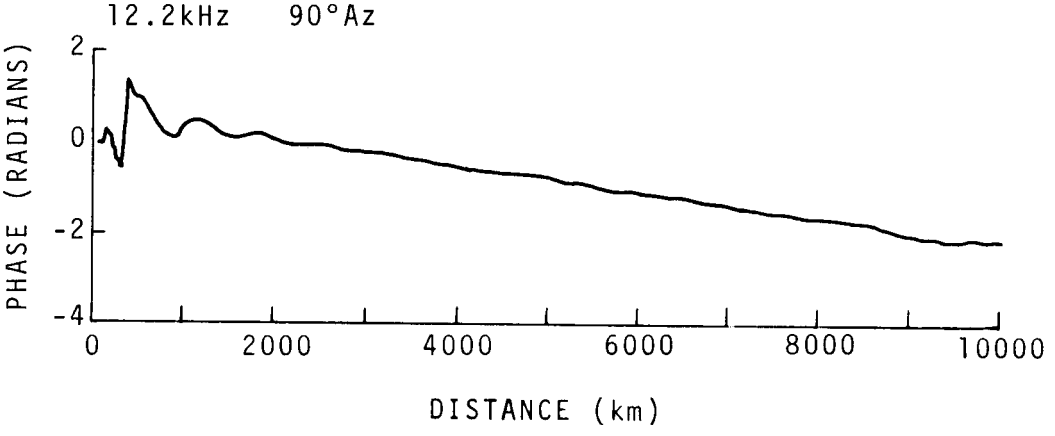

Figure 11.

RELATIVE PHASE
NORMAL DAY

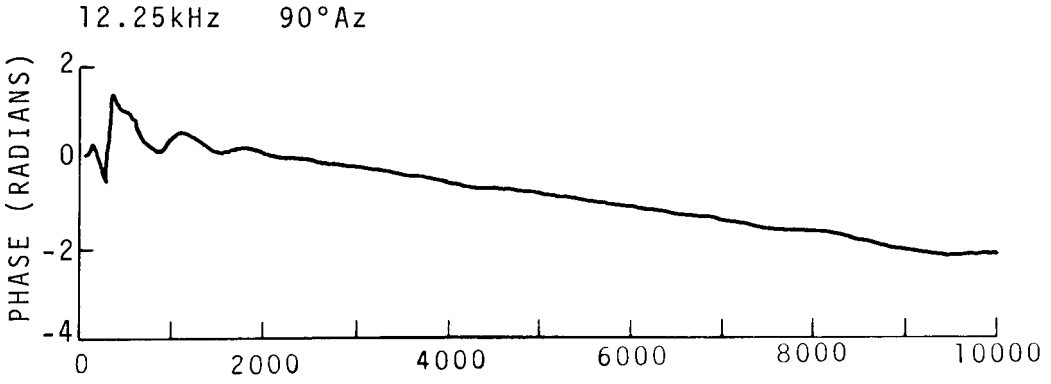

Figure 12.

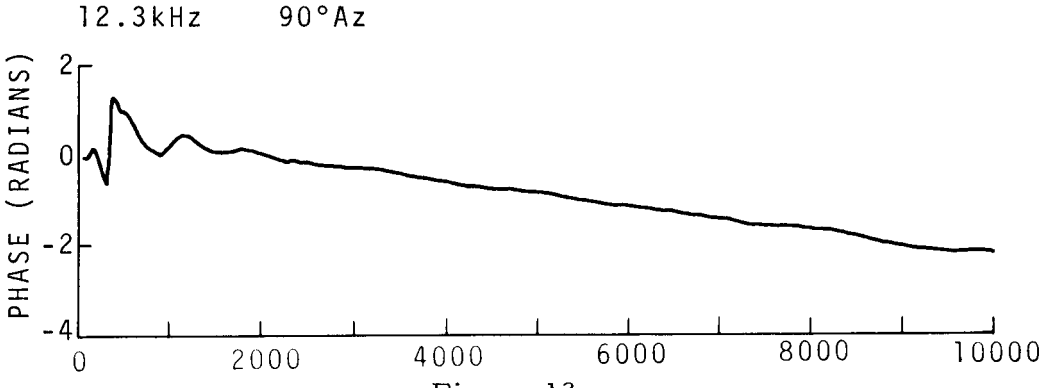

Figure 13.

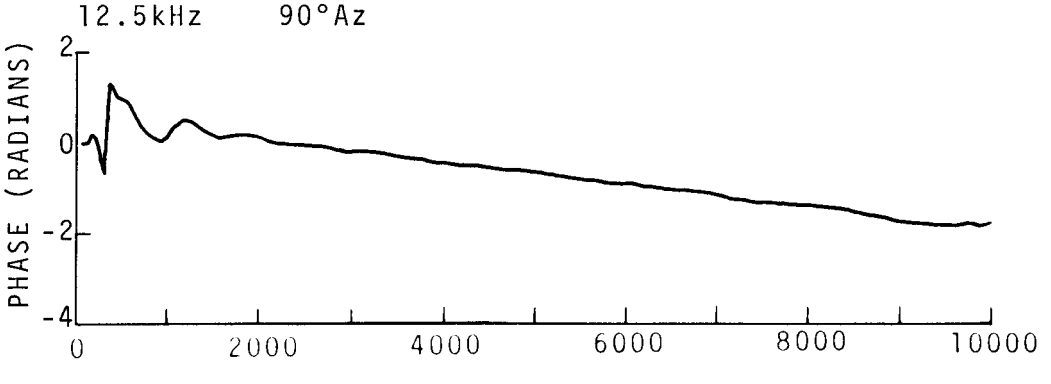

Figure 14.

RELATIVE PHASE
NORMAL DAY

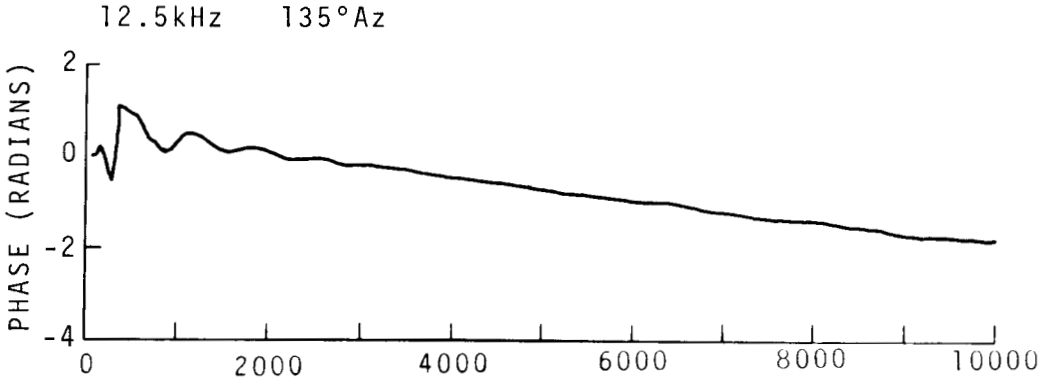

Figure 15.

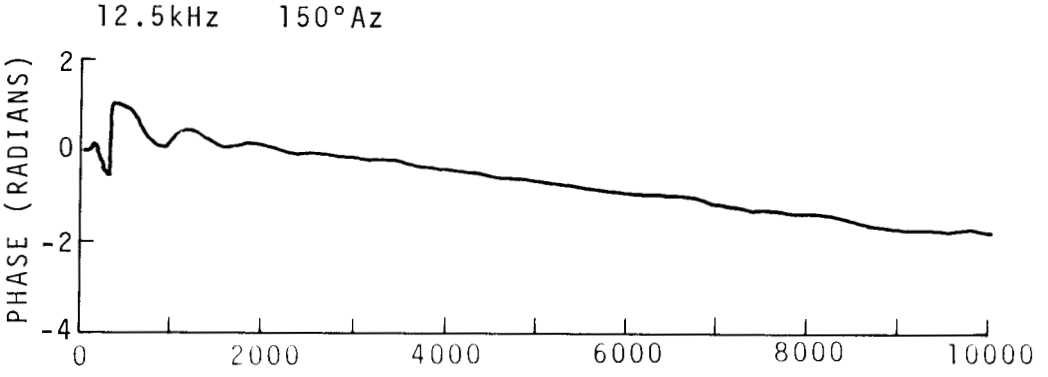

Figure 16.

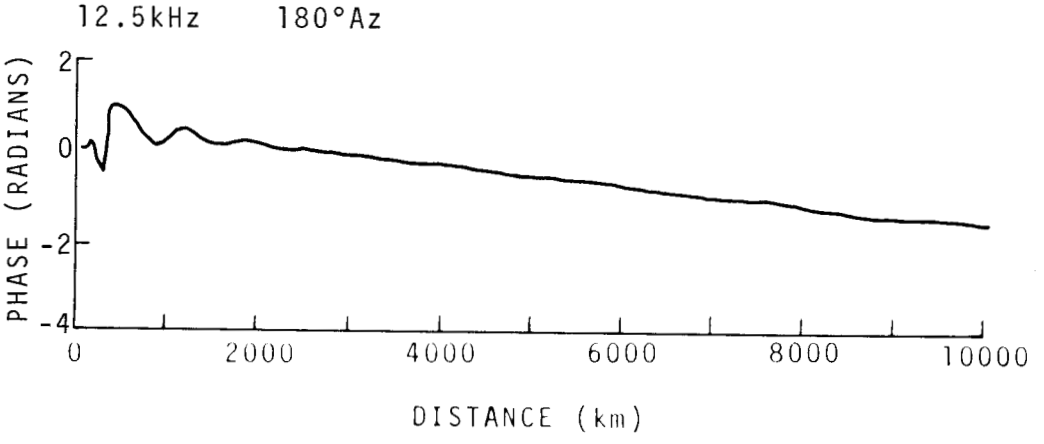

Figure 17.

RELATIVE PHASE
NORMAL DAY

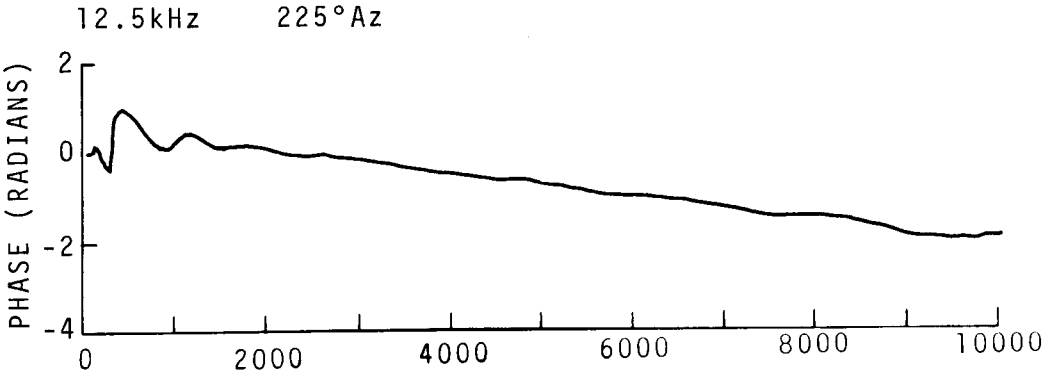

Figure 18.

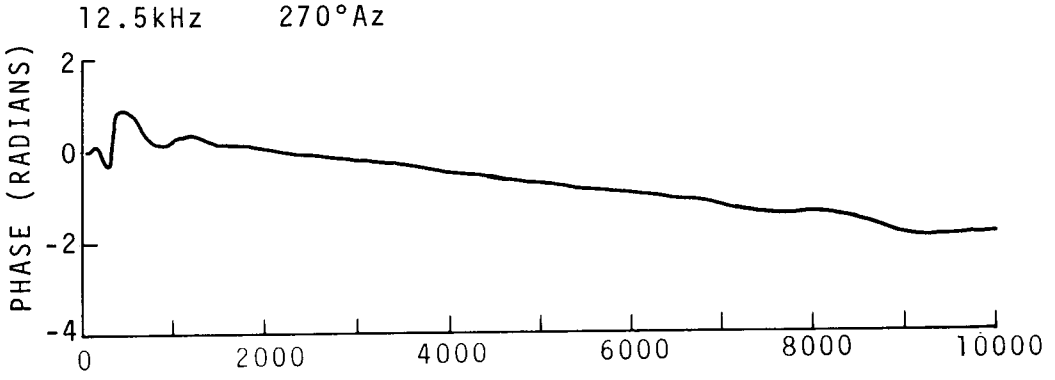

Figure 19.

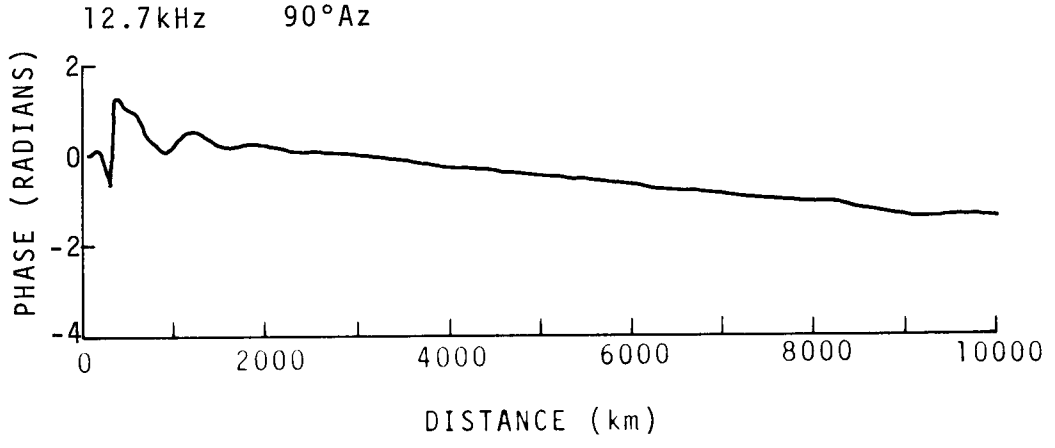

Figure 20.

RELATIVE PHASE
NORMAL DAY

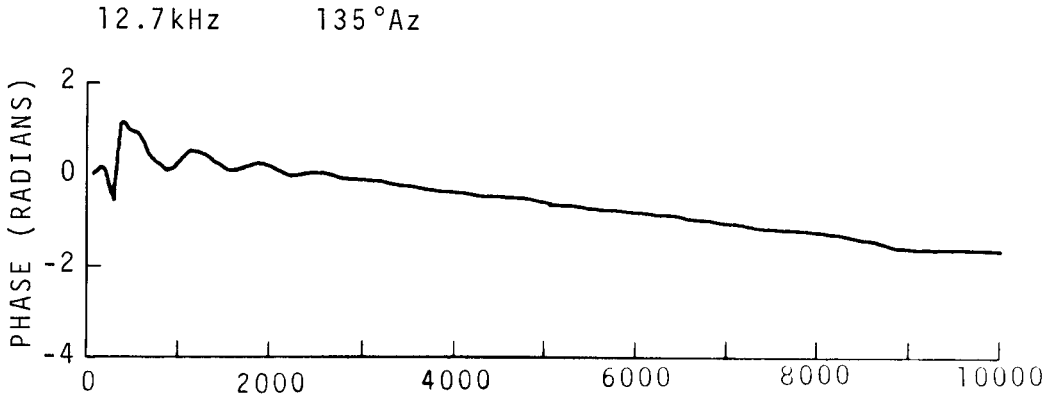

Figure 21.

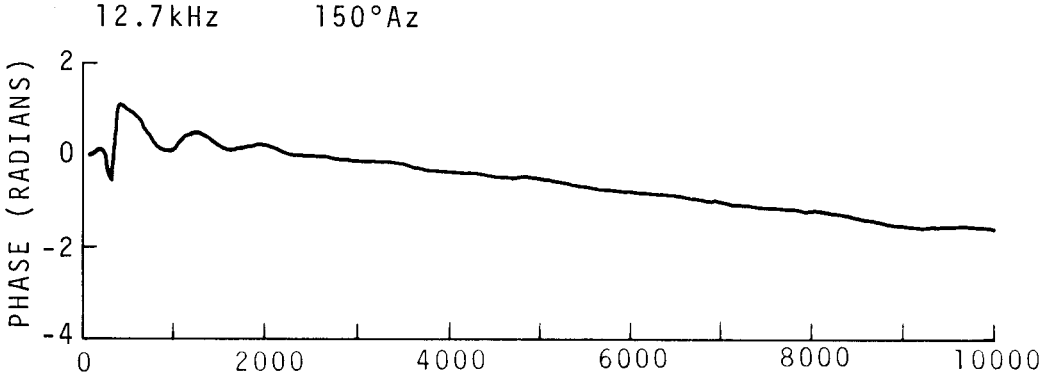

Figure 22.

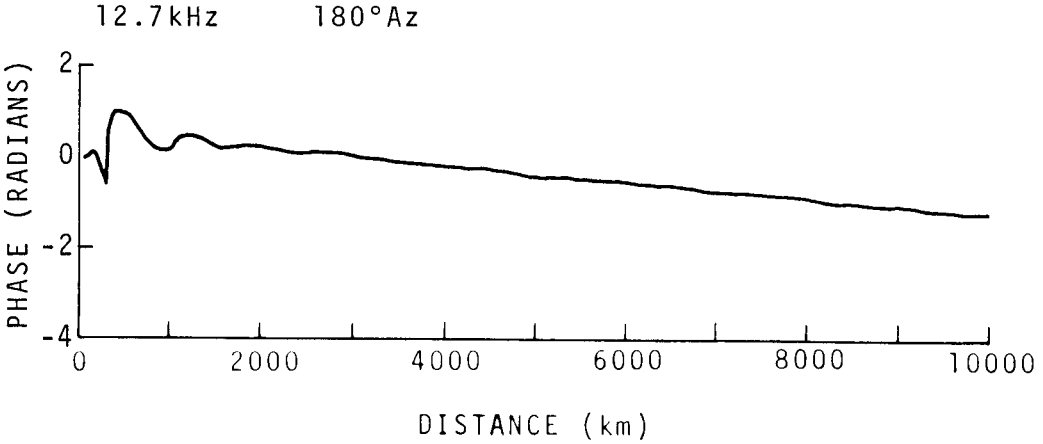

Figure 23.

RELATIVE PHASE
NORMAL DAY

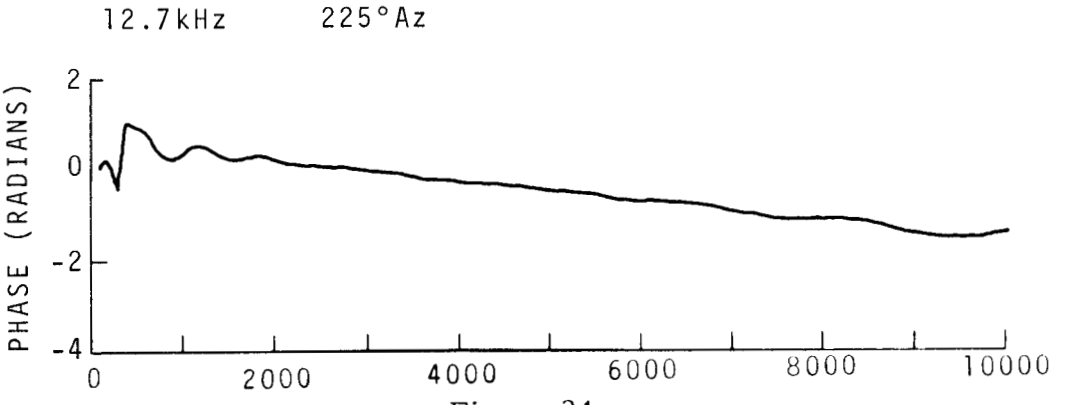

Figure 24.

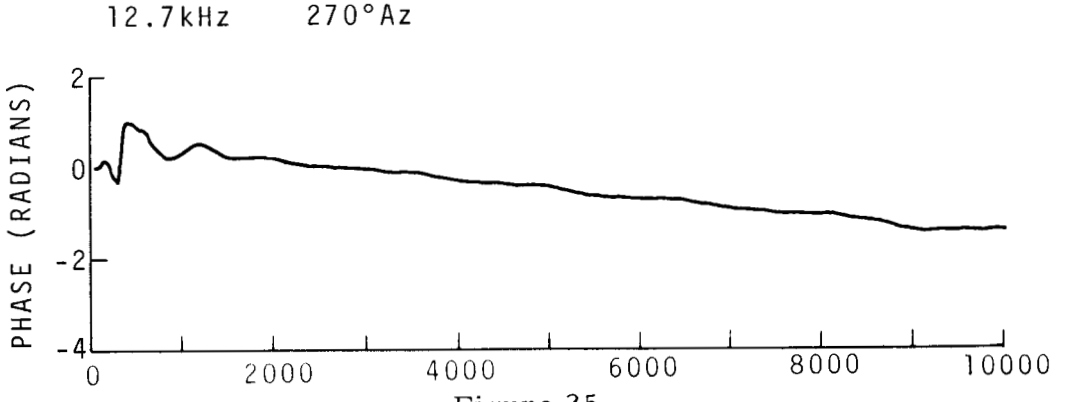

Figure 25.

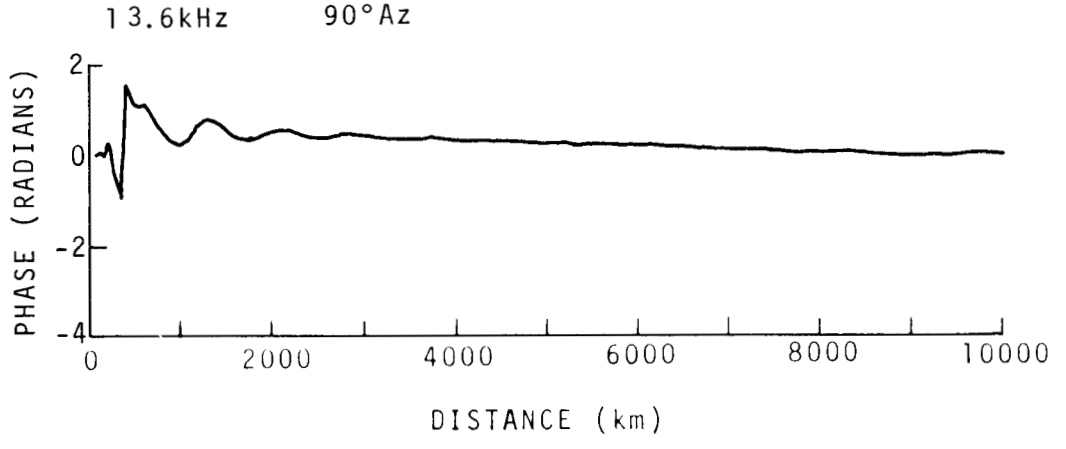

Figure 26.

RELATIVE PHASE
NORMAL DAY

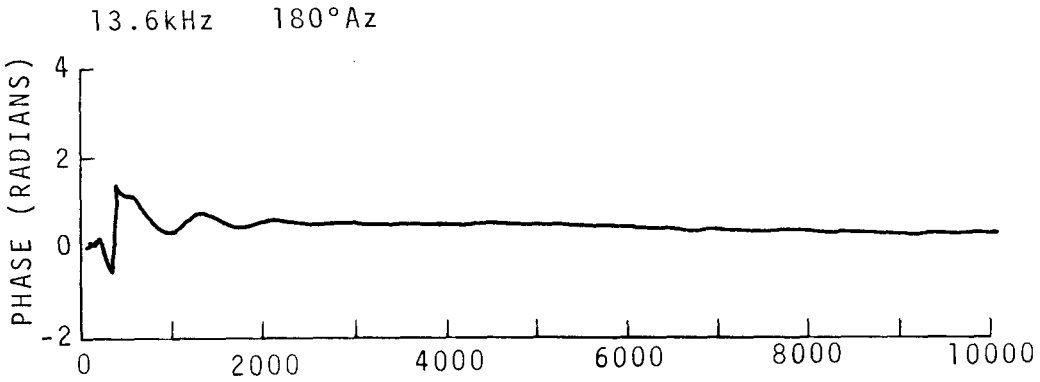

Figure 27.

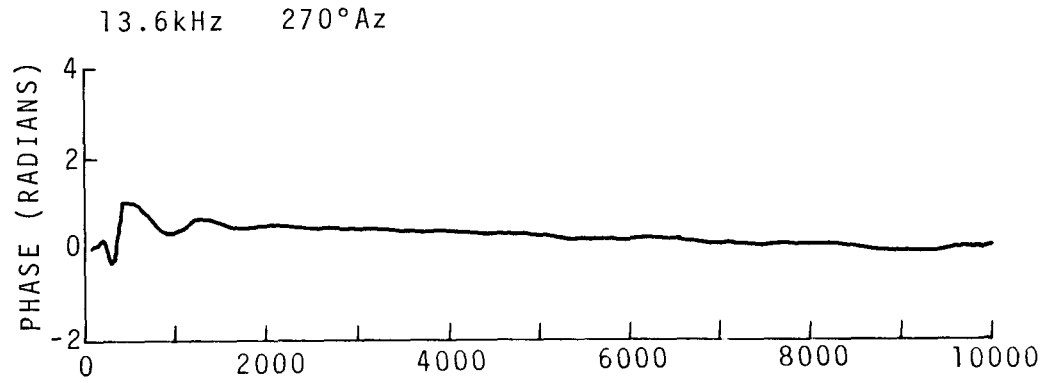

Figure 28.

RELATIVE PHASE
NORMAL DAY

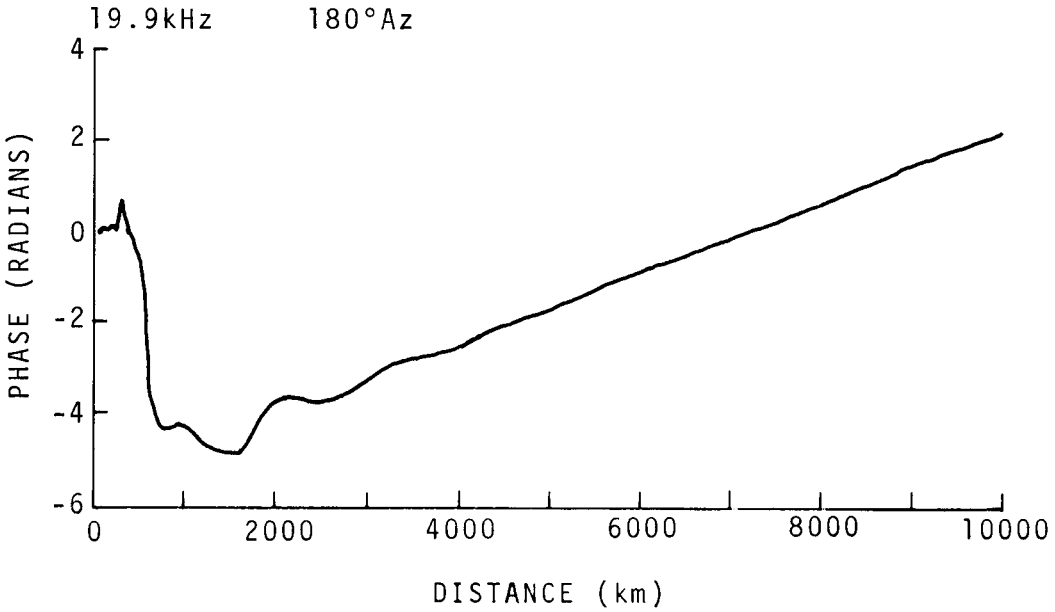

Figure 29.

RELATIVE PHASE
NORMAL DAY

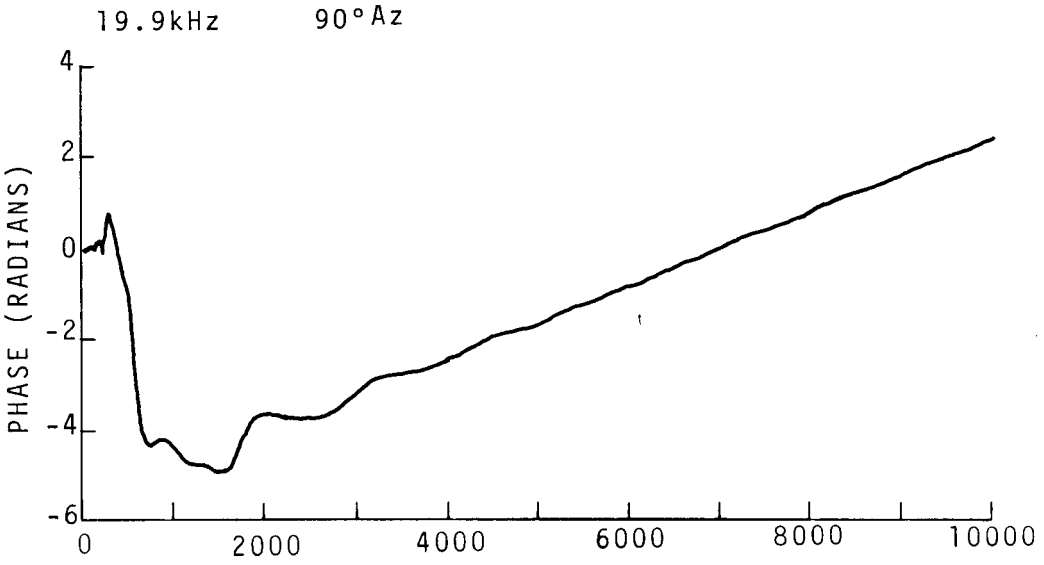

Figure 30.

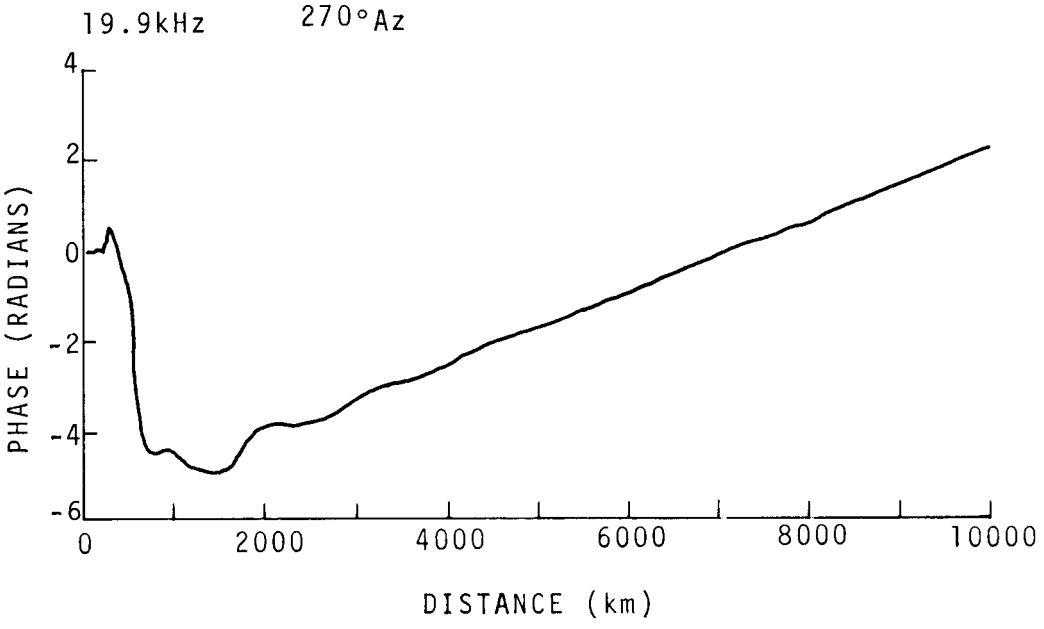

Figure 31.

RELATIVE PHASE
NORMAL DAY

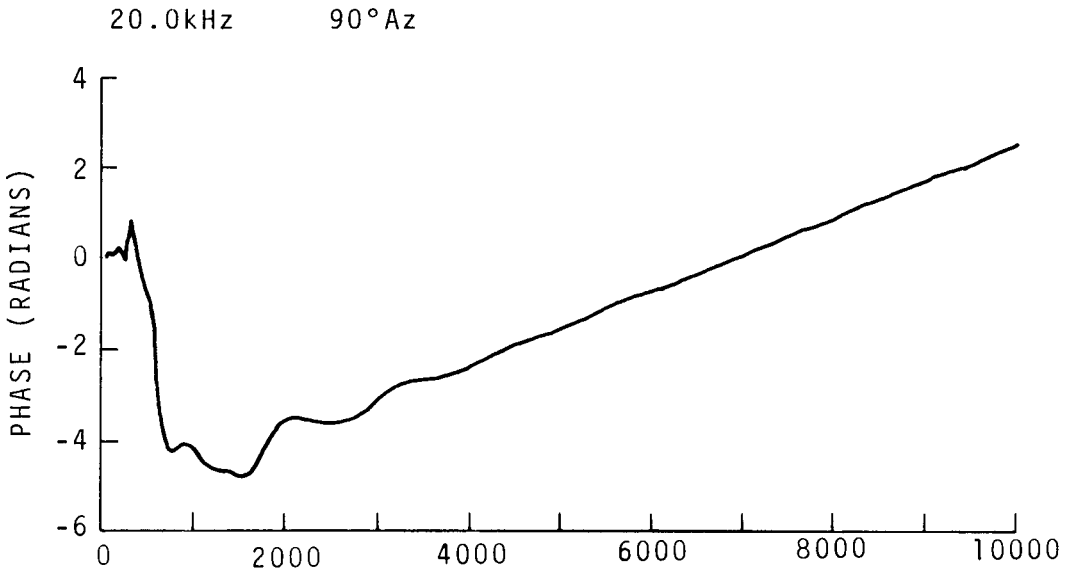

Figure 32.

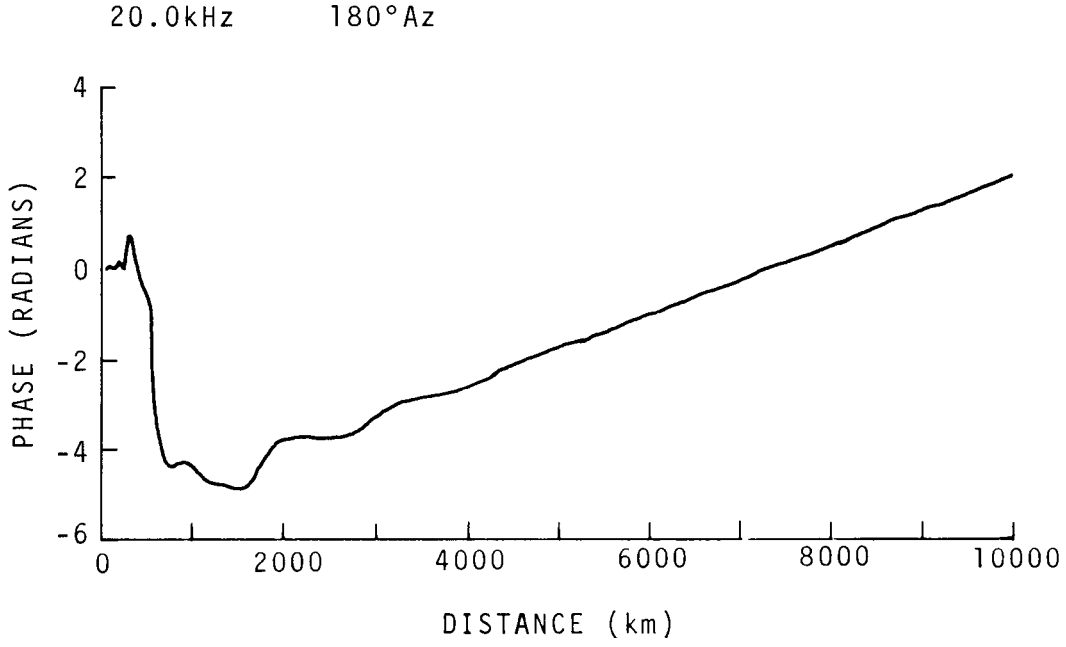

Figure 33.

RELATIVE PHASE
NORMAL DAY

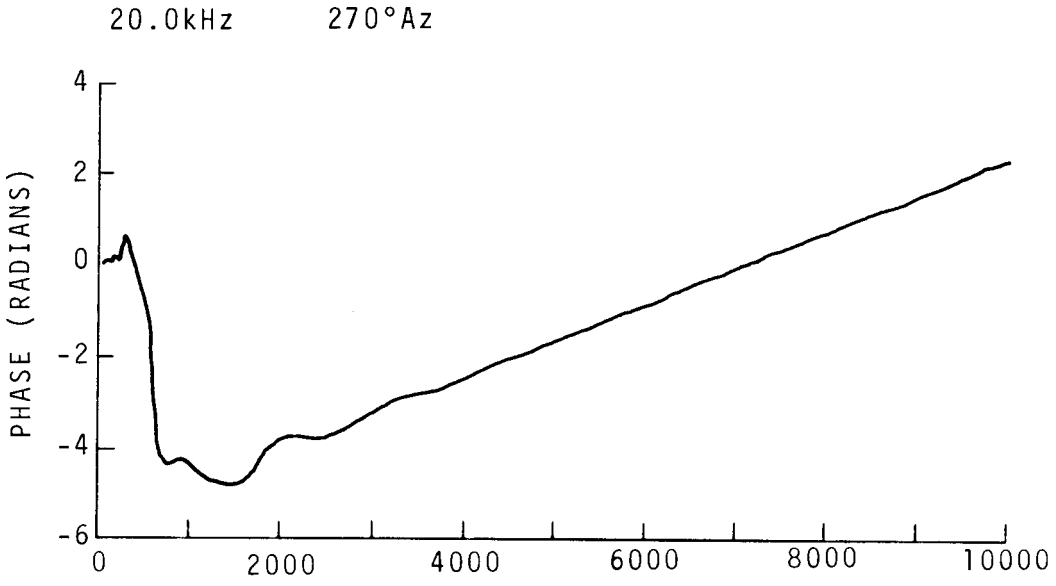

Figure 34.

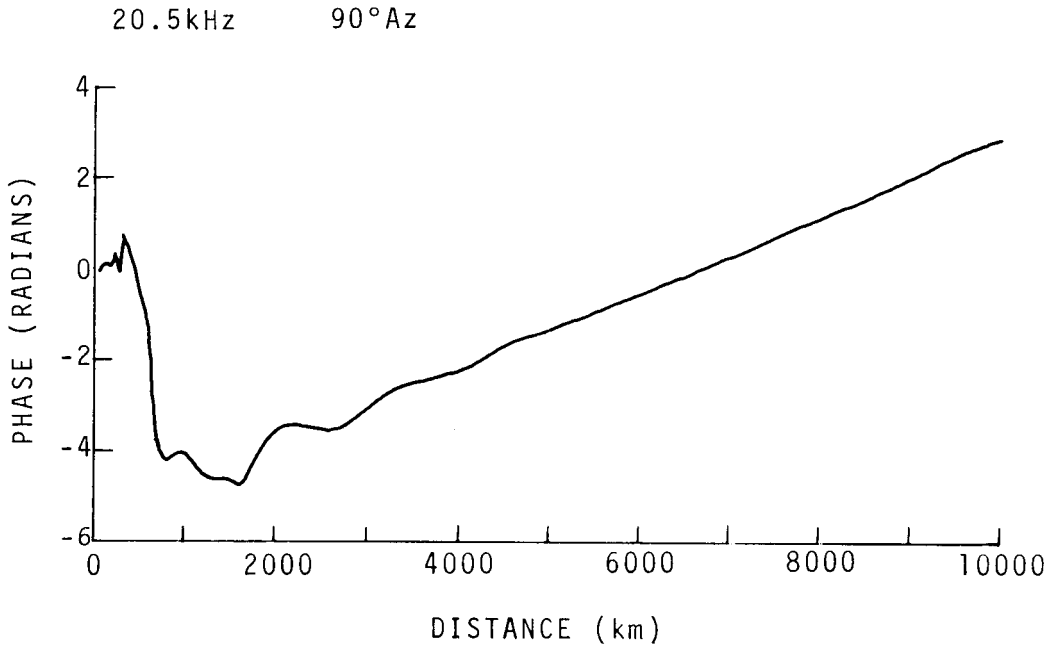

Figure 35.

RELATIVE PHASE
NORMAL DAY

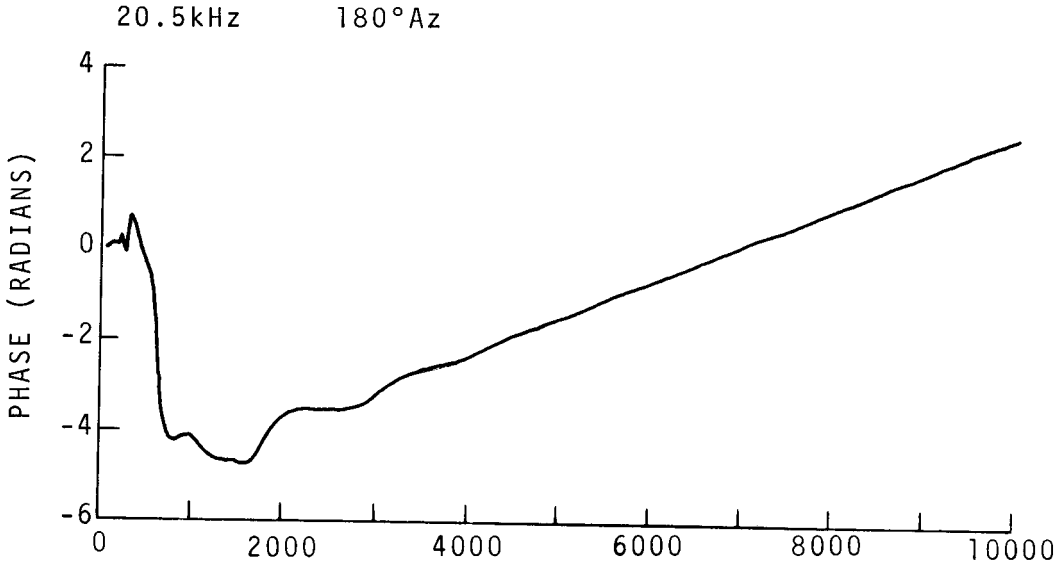

Figure 36.

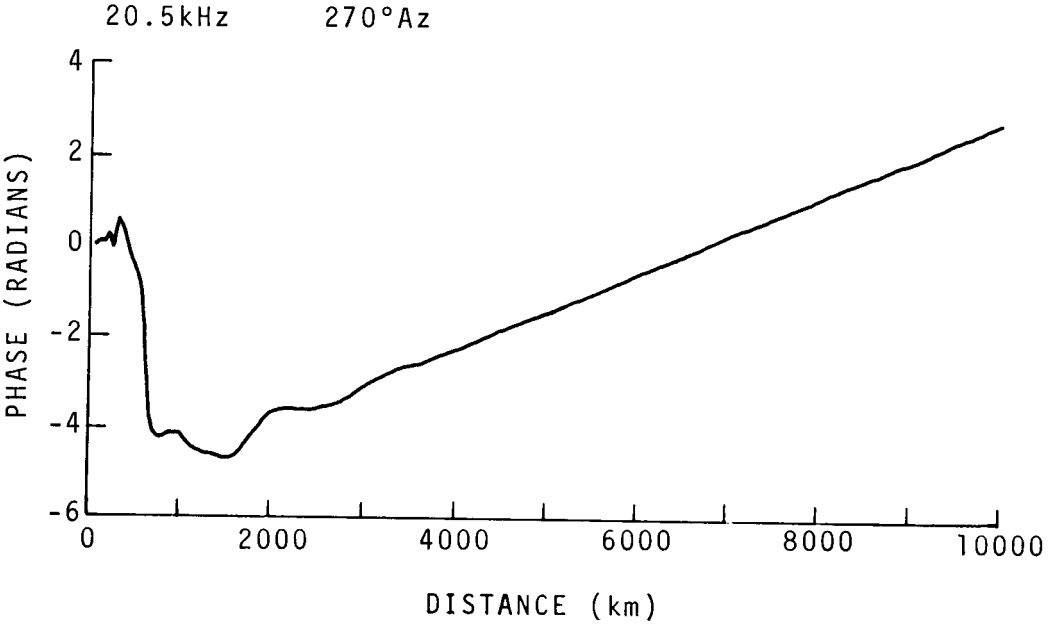

Figure 37.

RELATIVE PHASE
NORMAL DAY

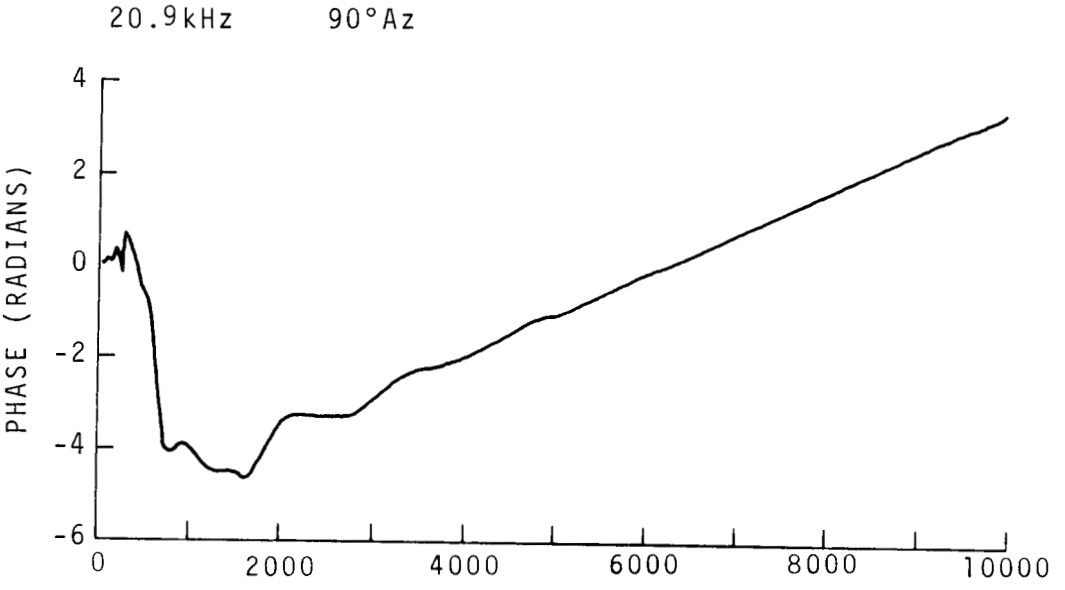

Figure 38.

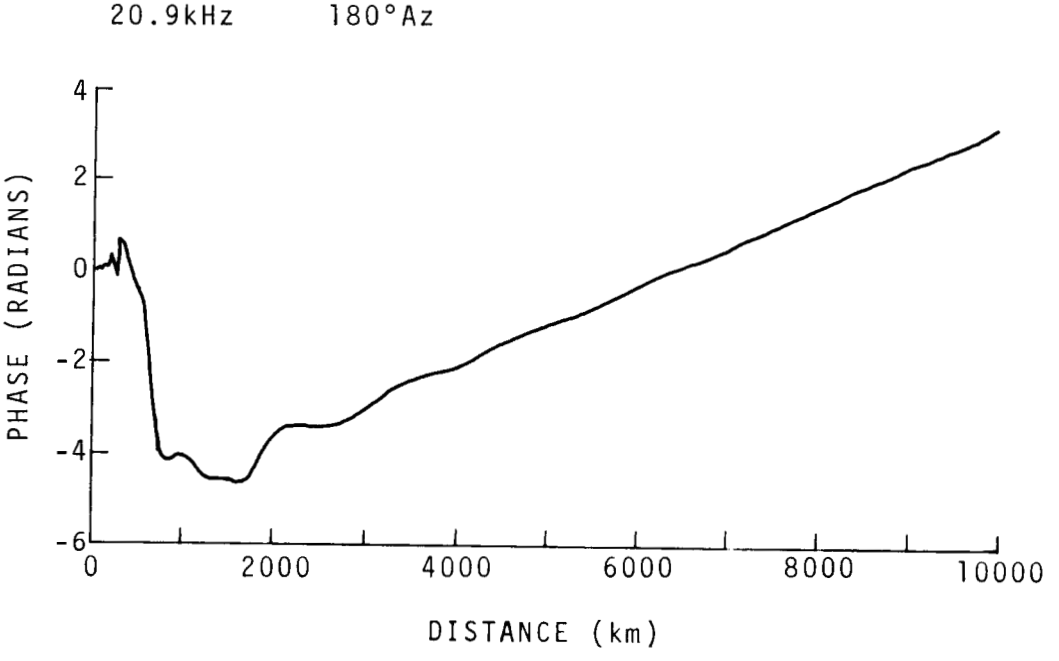

Figure 39.

RELATIVE PHASE
NORMAL DAY

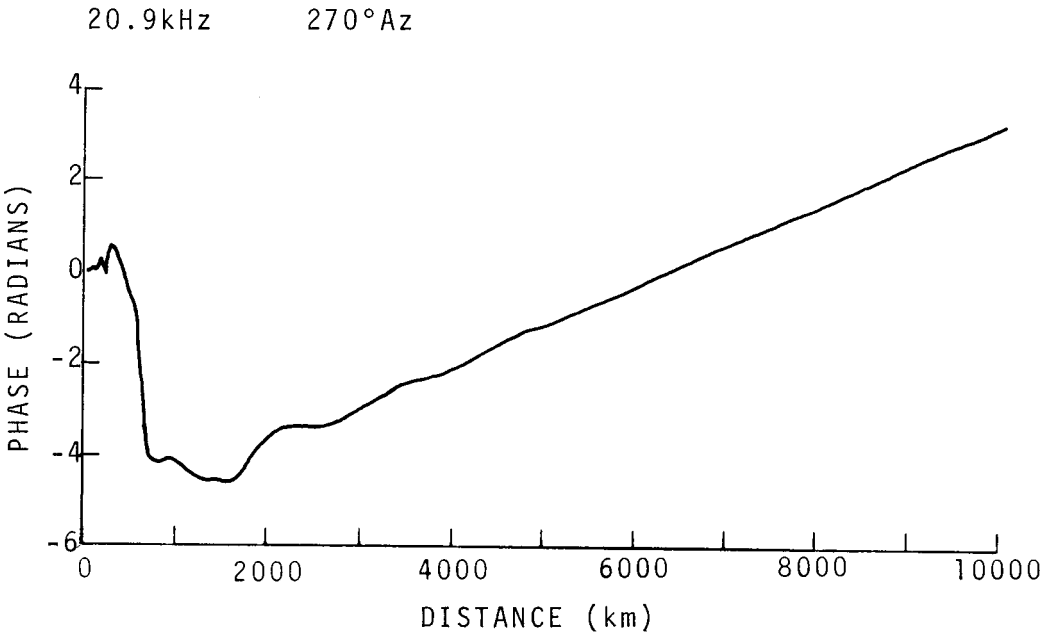

Figure 40.

RELATIVE PHASE
NORMAL NIGHT

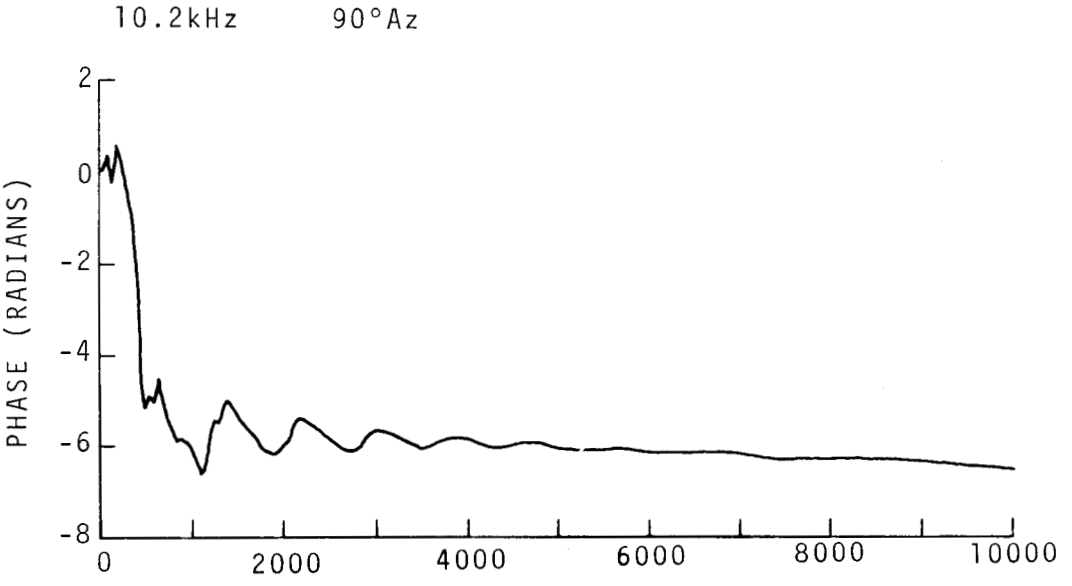

Figure 41.

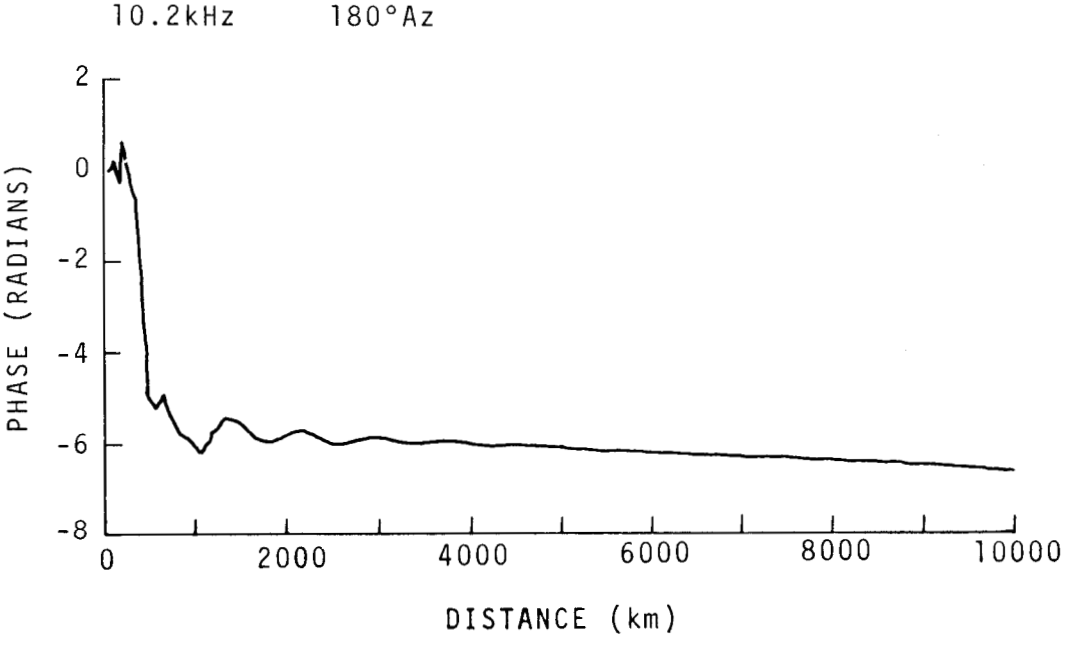

Figure 42.

RELATIVE PHASE
NORMAL NIGHT

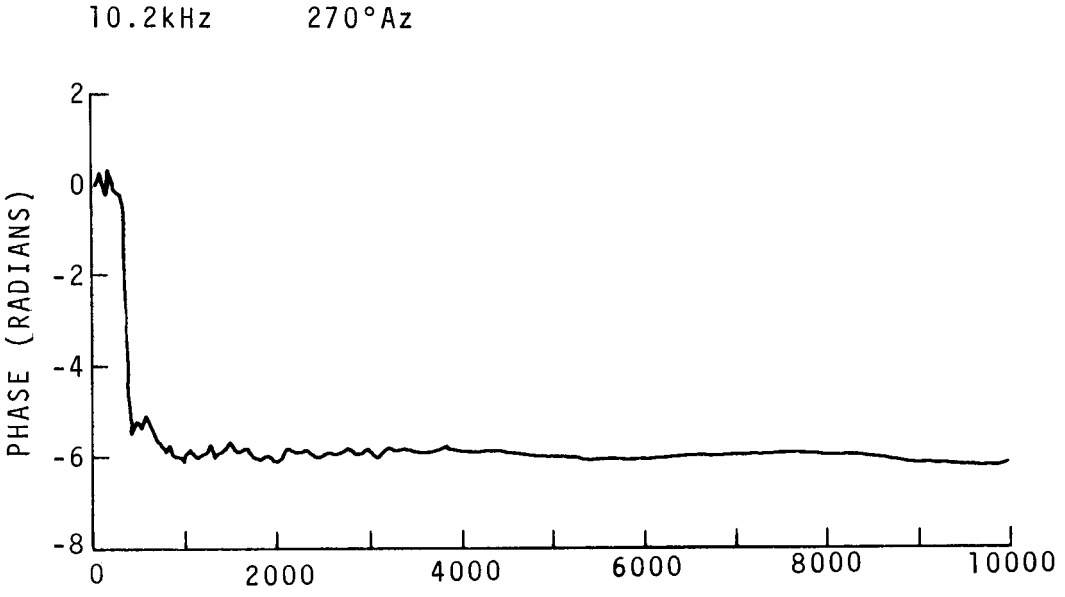

Figure 43.

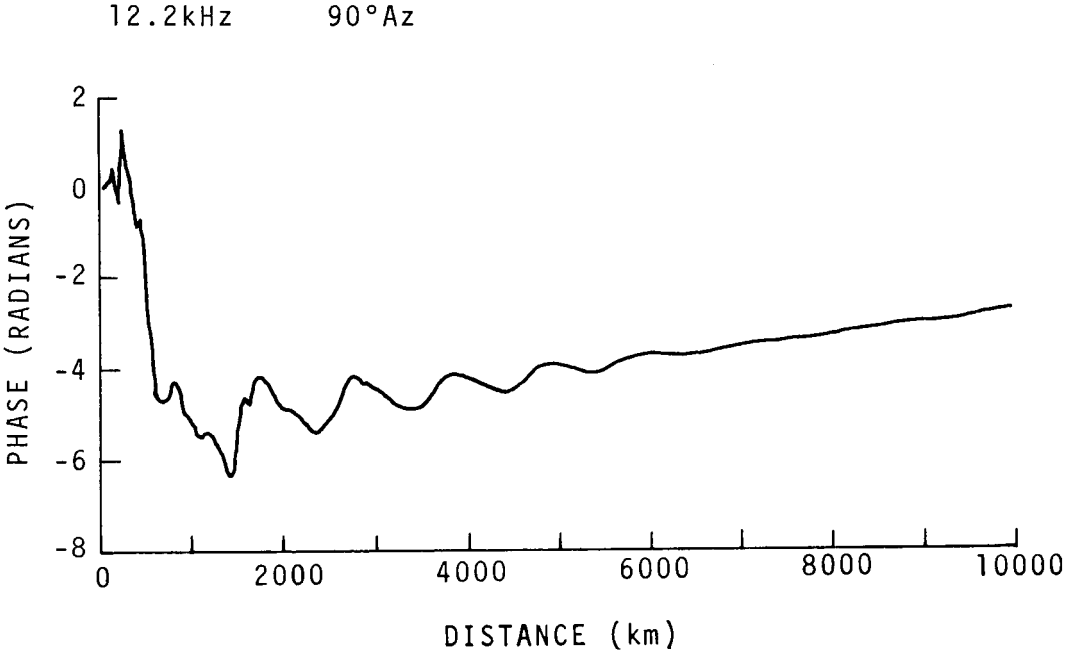

Figure 44.

RELATIVE PHASE
NORMAL NIGHT

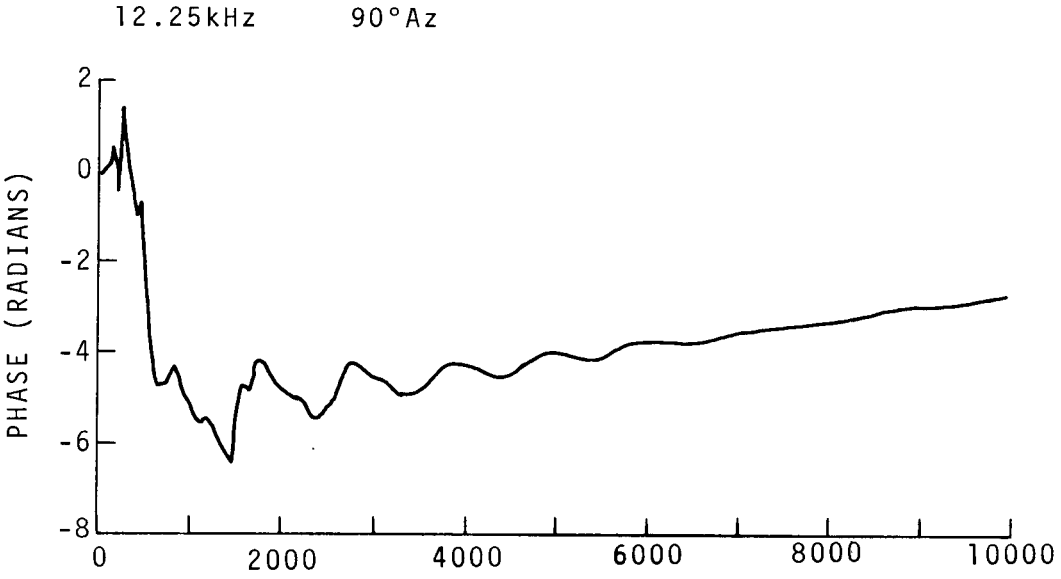

Figure 45.

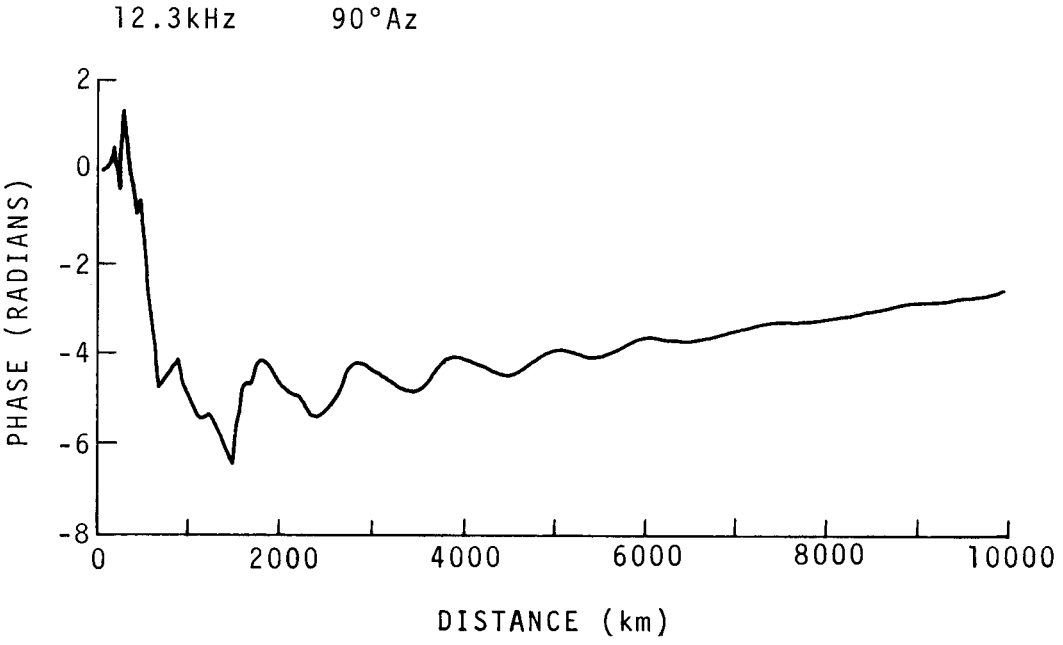

Figure 46.

RELATIVE PHASE
NORMAL NIGHT

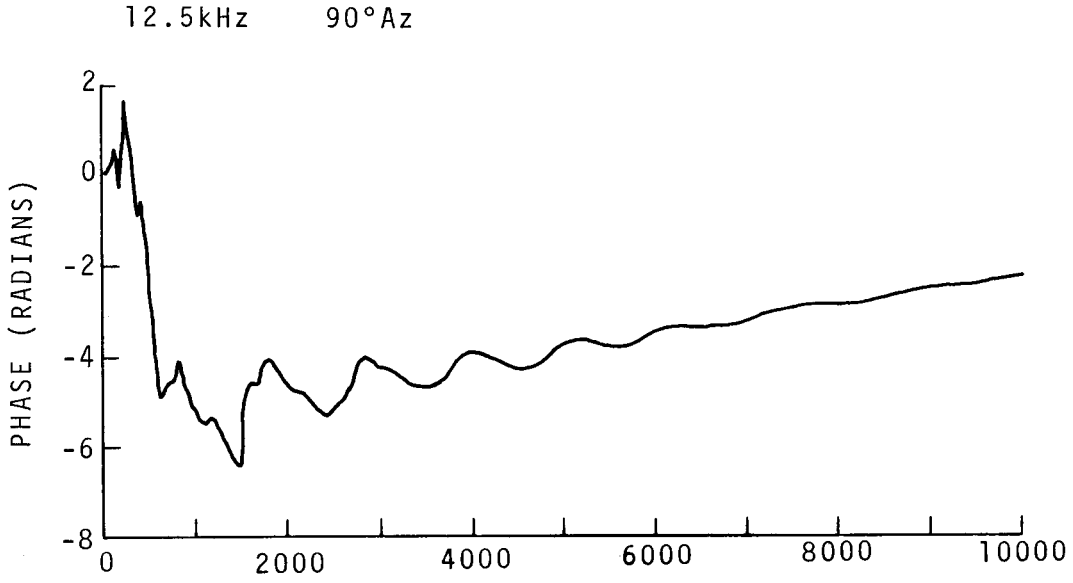

Figure 47.

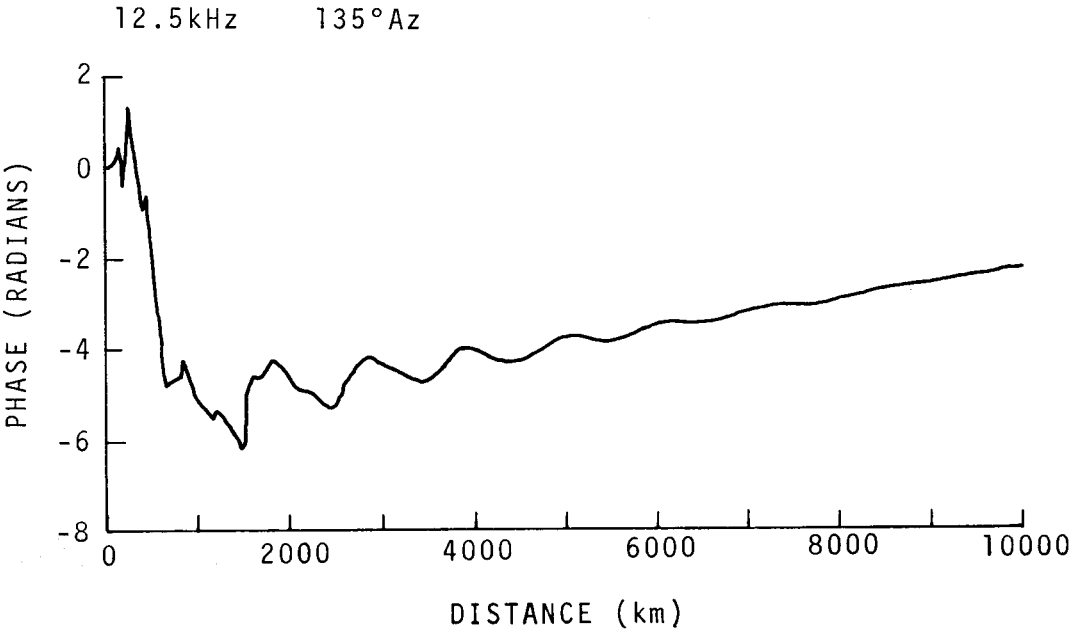

Figure 48.

RELATIVE PHASE
NORMAL NIGHT

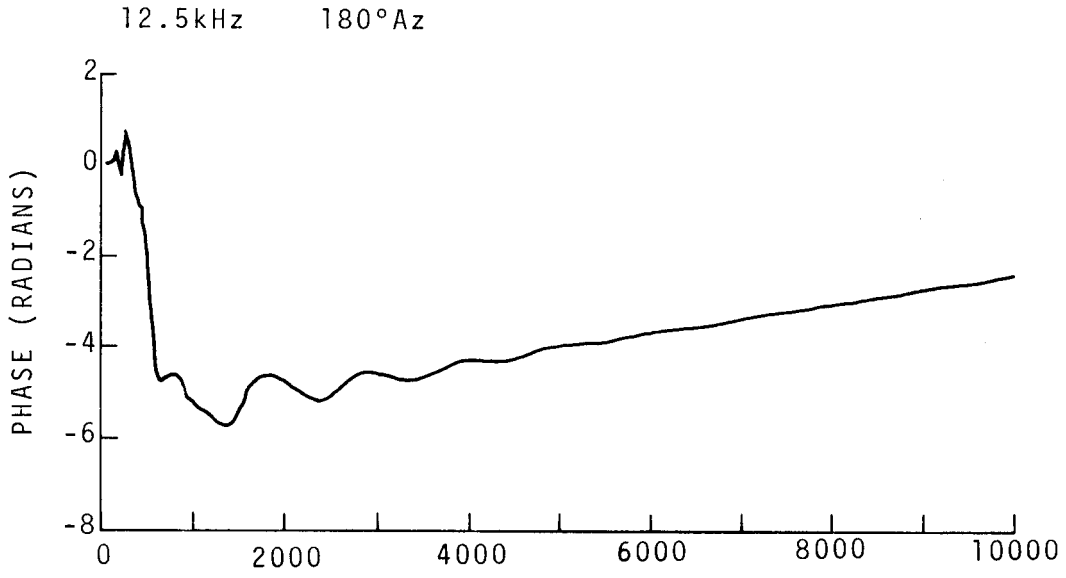

Figure 49.

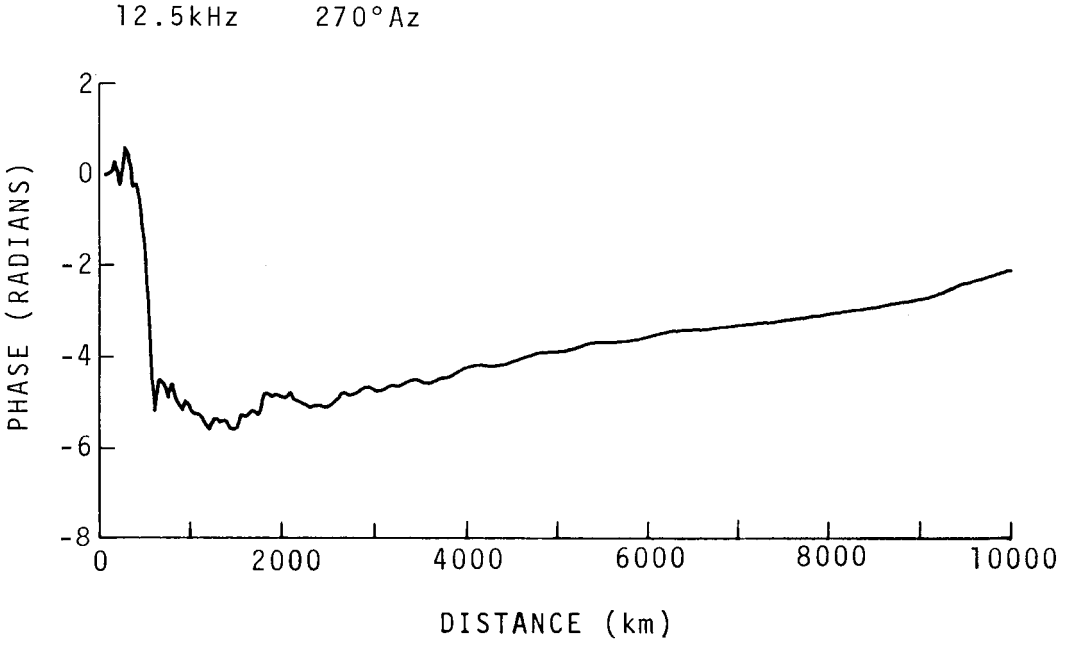

Figure 50.

RELATIVE PHASE
NORMAL NIGHT

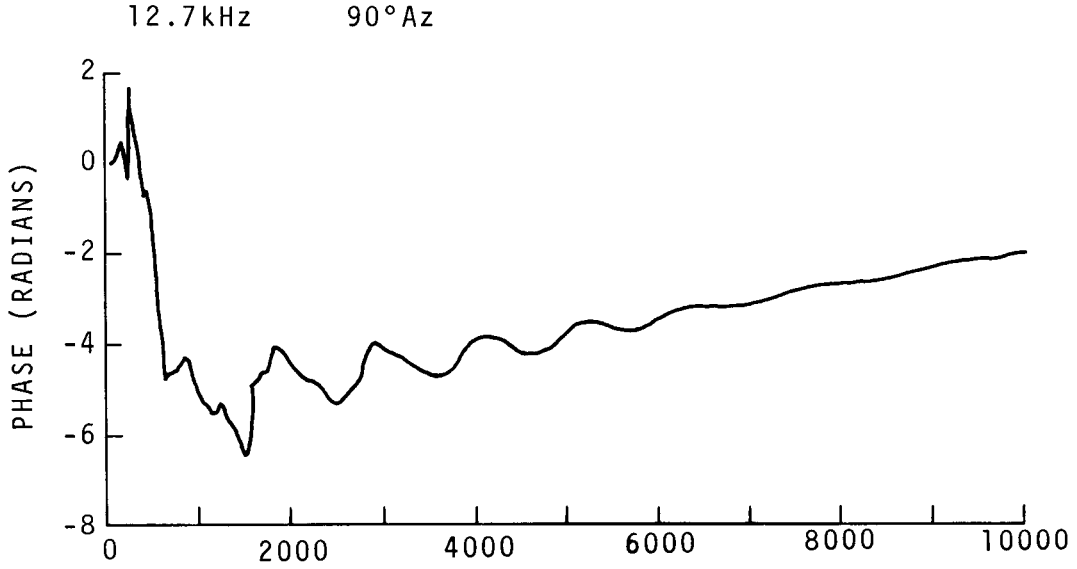

Figure 51.

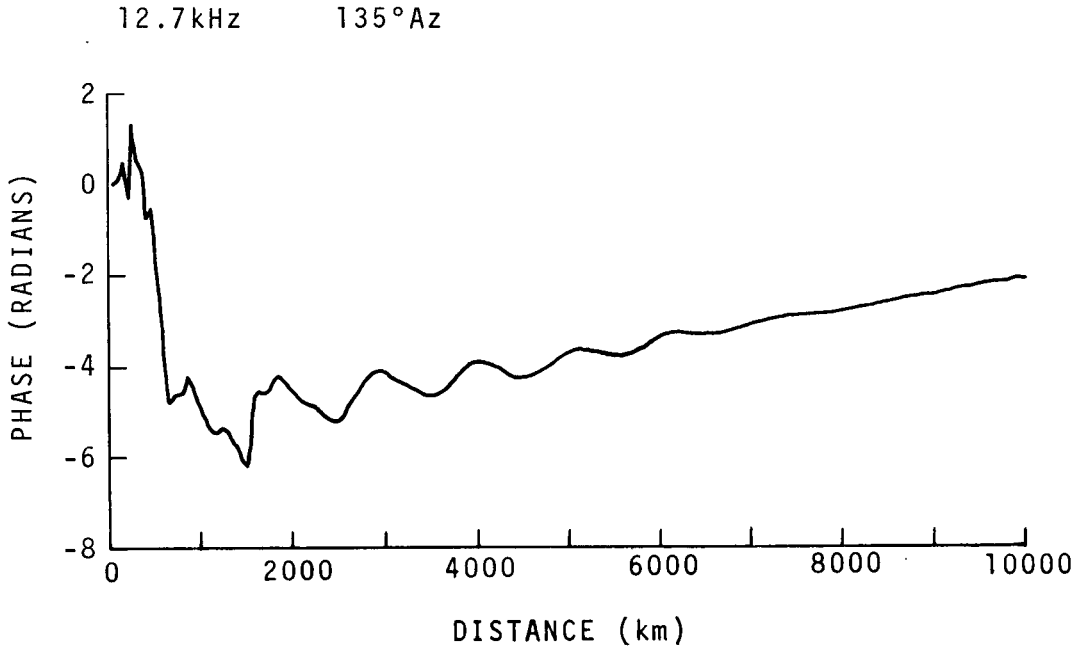

Figure 52.

RELATIVE PHASE
NORMAL NIGHT

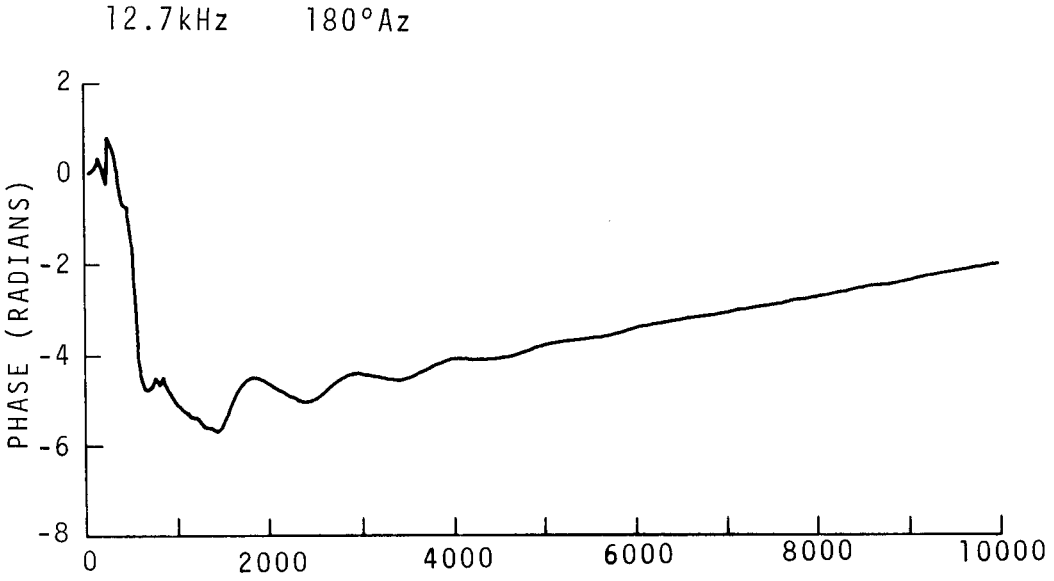

Figure 53.

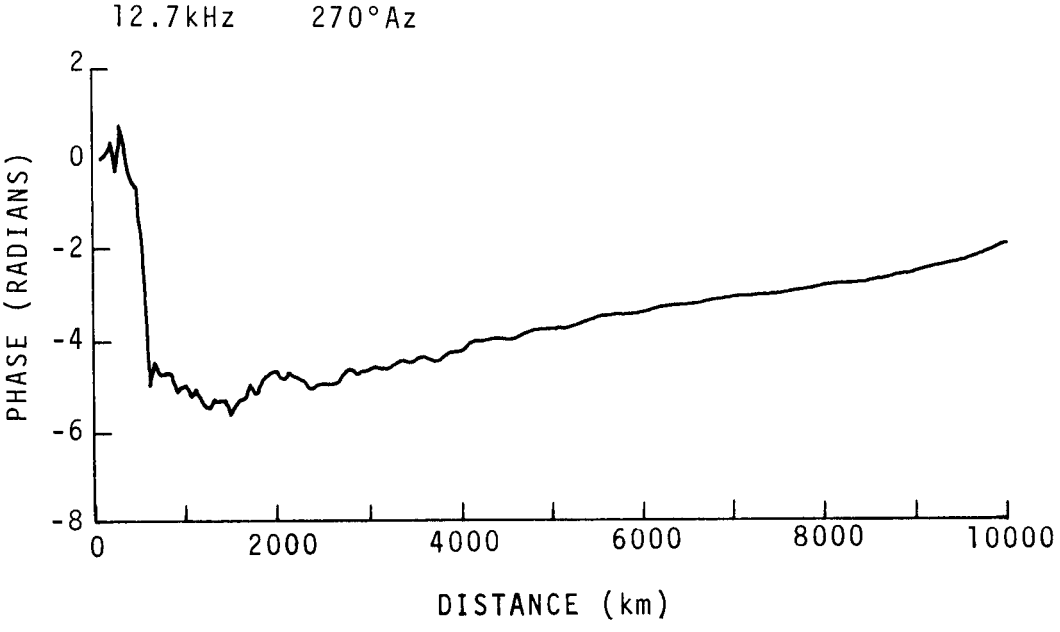

Figure 54.

RELATIVE PHASE
NORMAL NIGHT

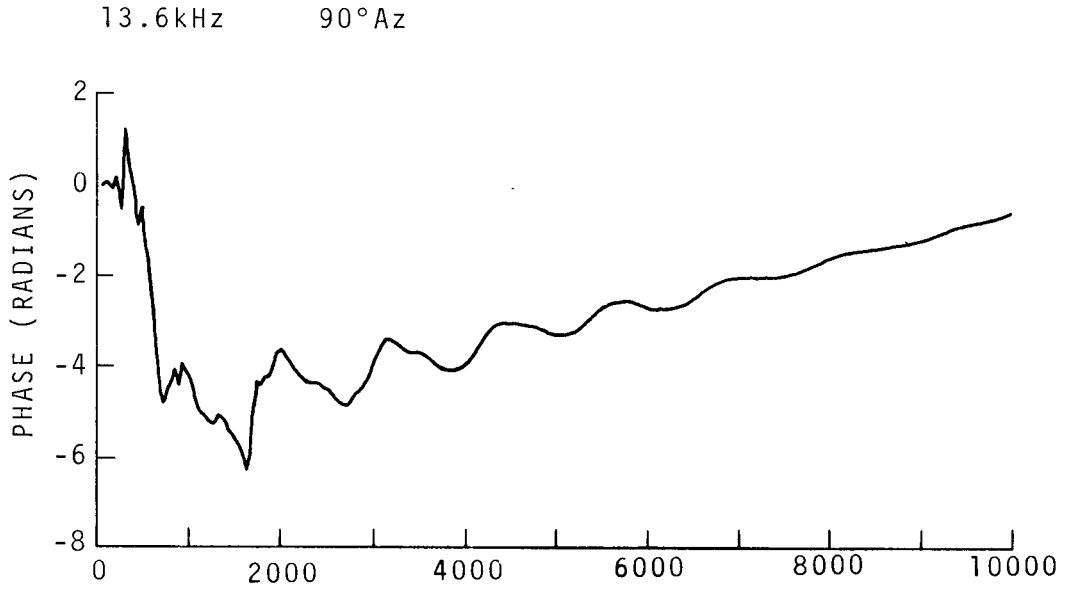

Figure 55.

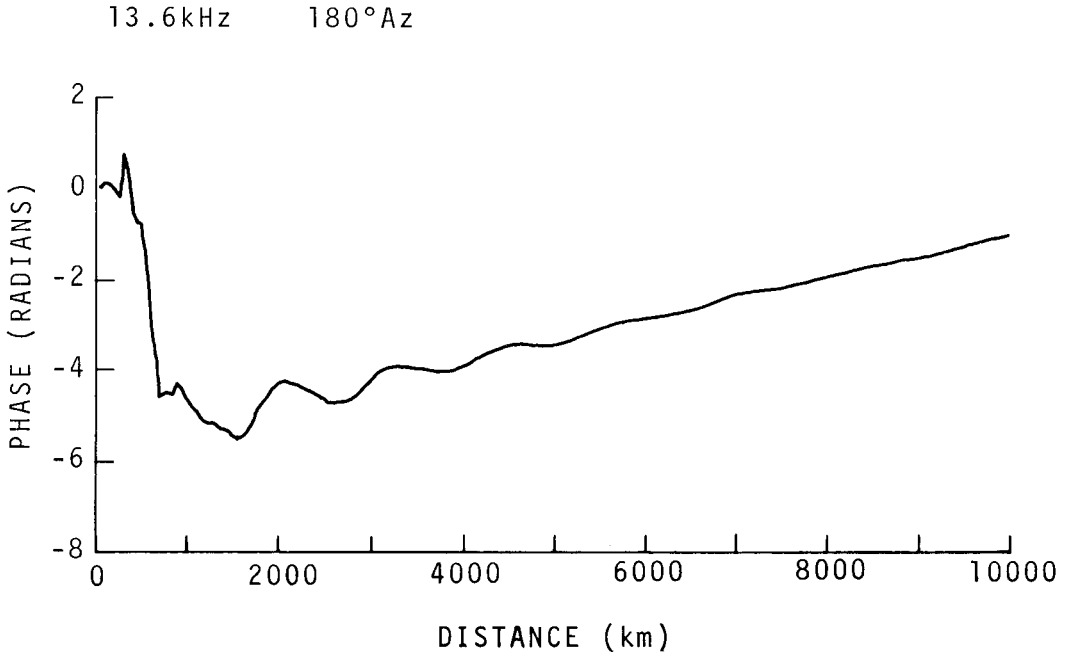

Figure 56.

RELATIVE PHASE
NORMAL NIGHT

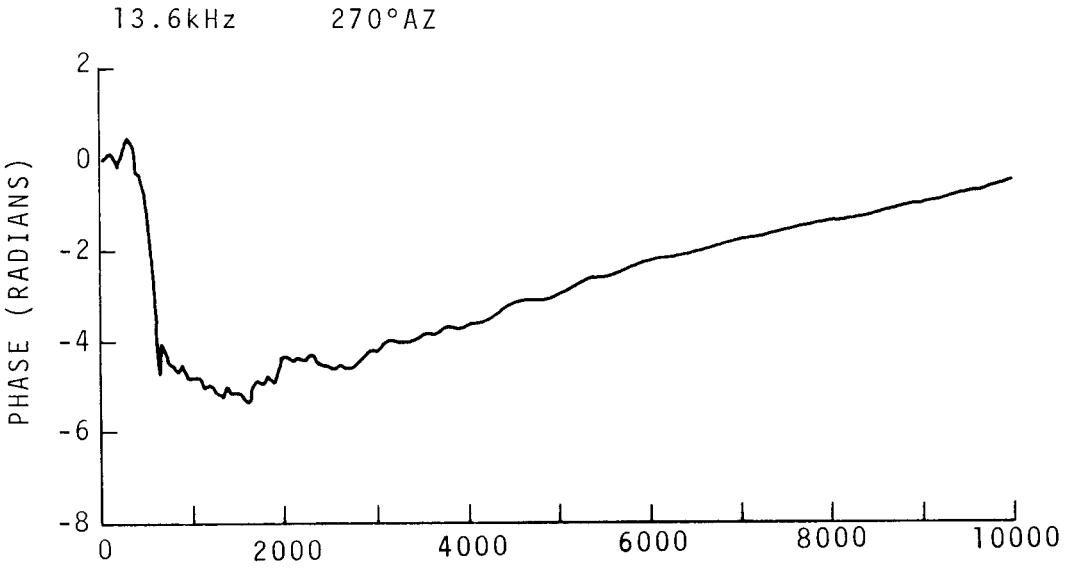

Figure 57.

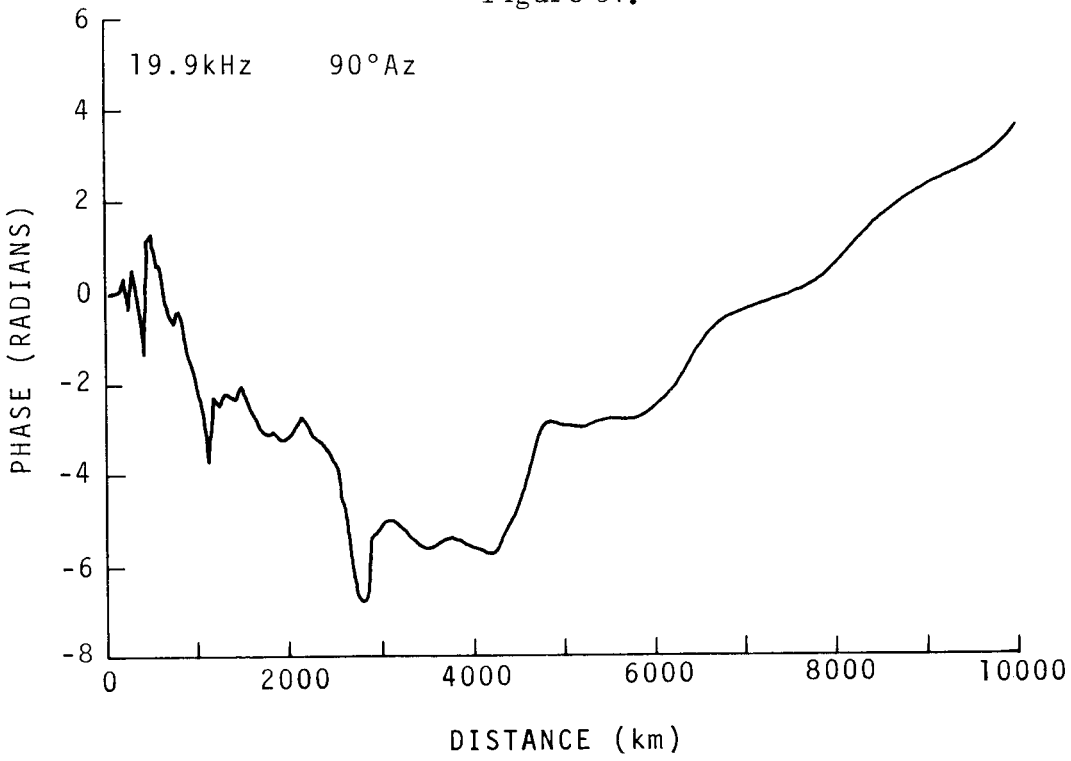

Figure 58.

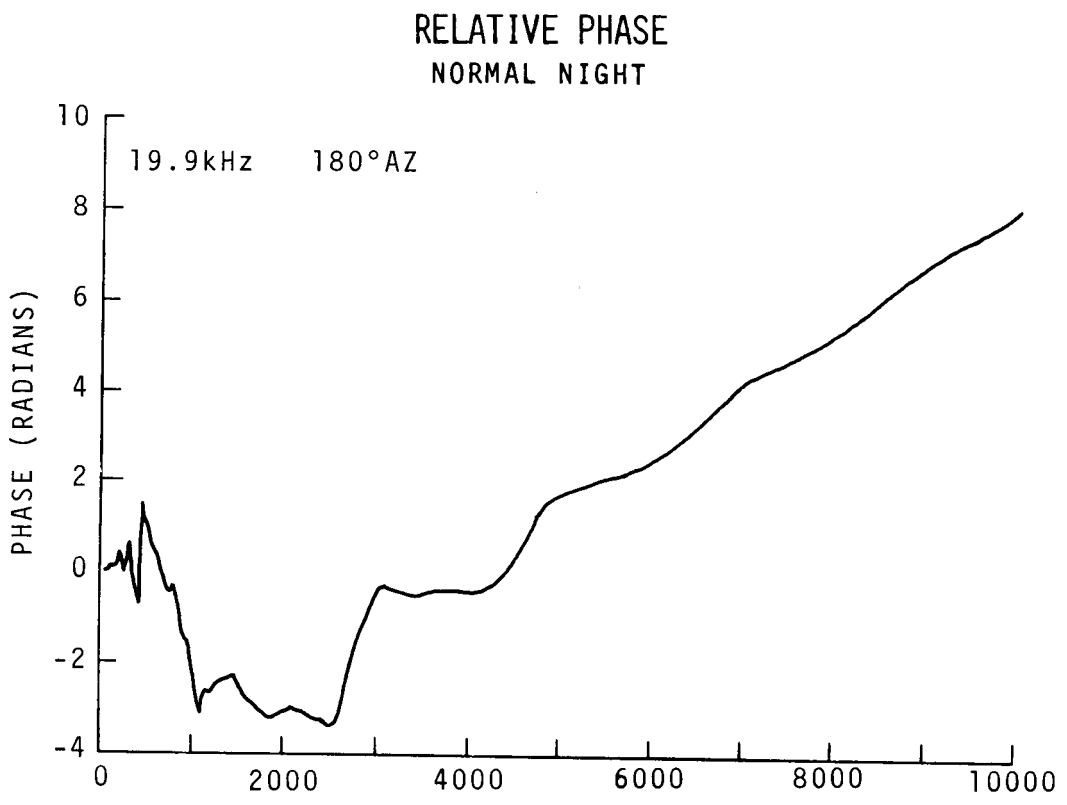

Figure 59.

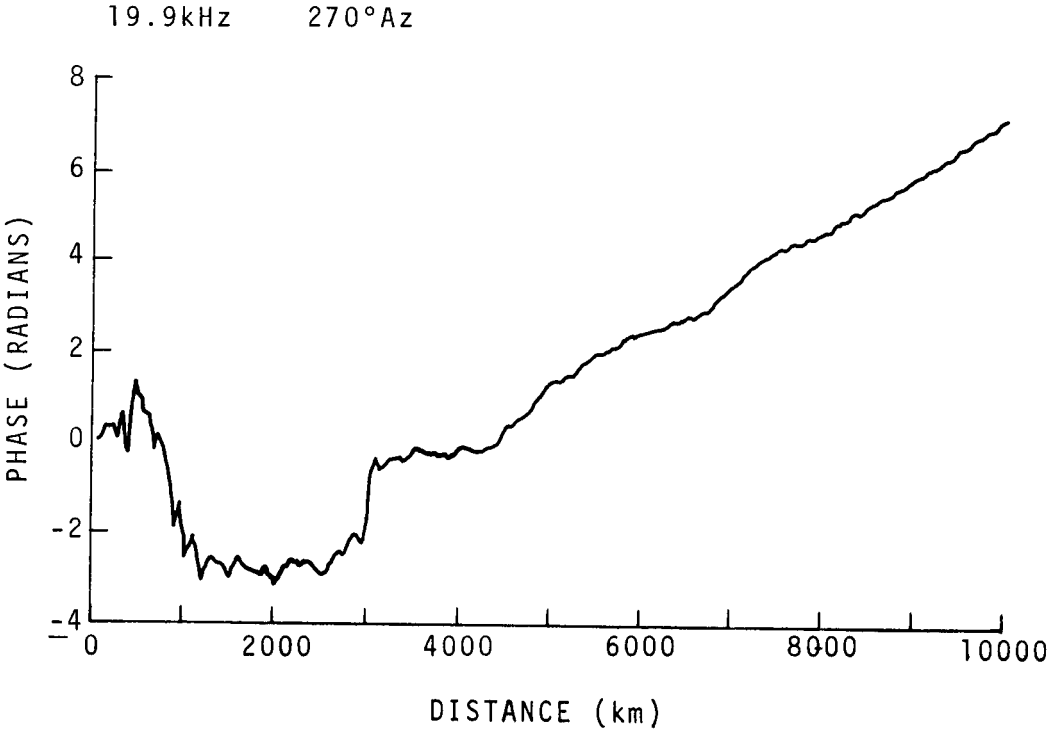

Figure 60.

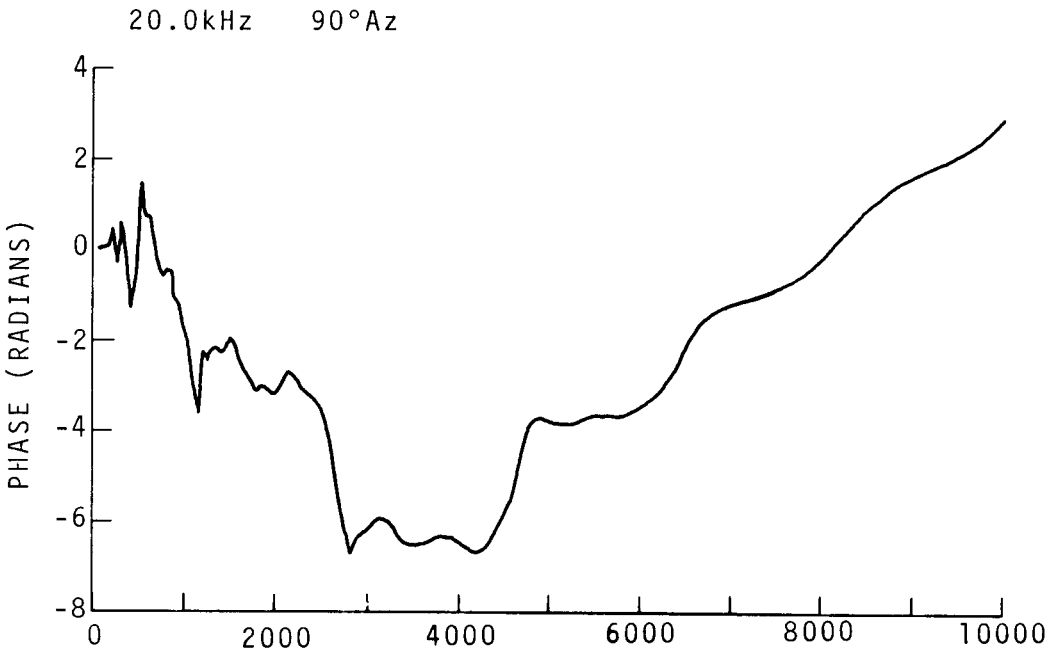

Figure 61.

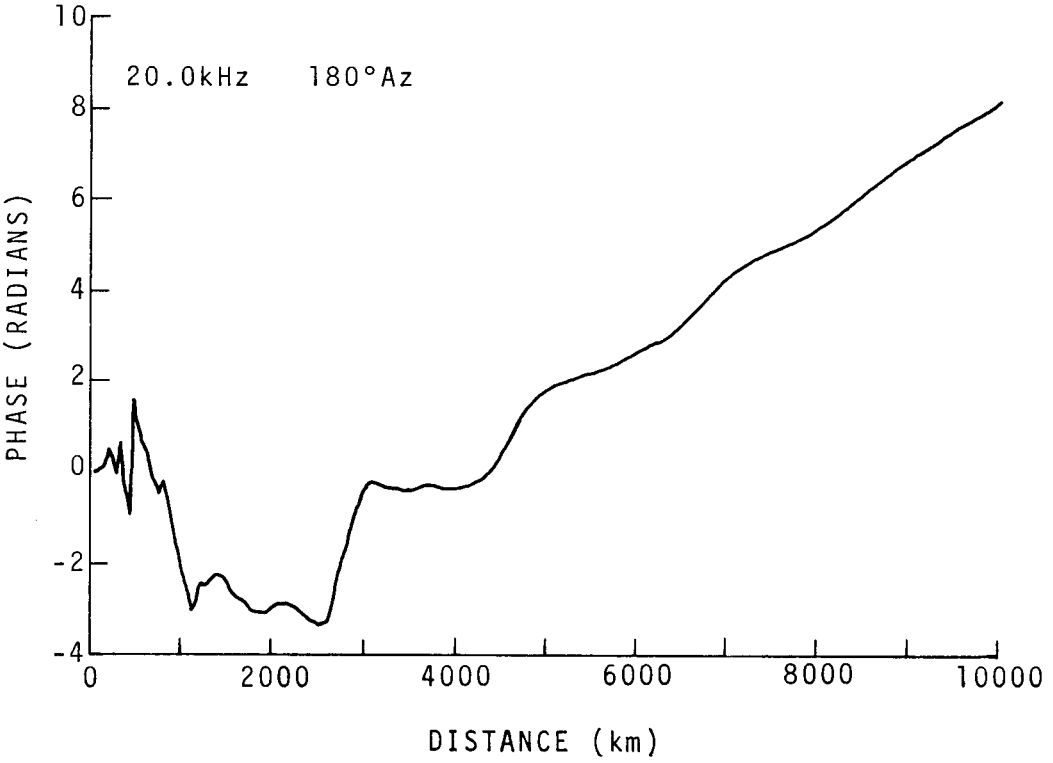

Figure 62.

RELATIVE PHASE
NORMAL NIGHT

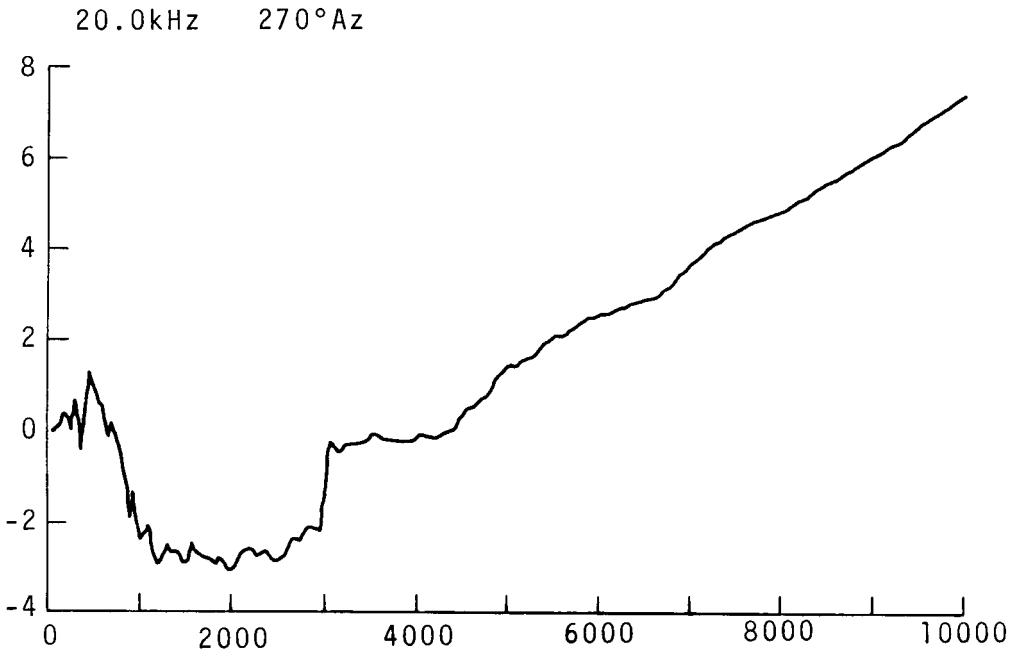

Figure 63.

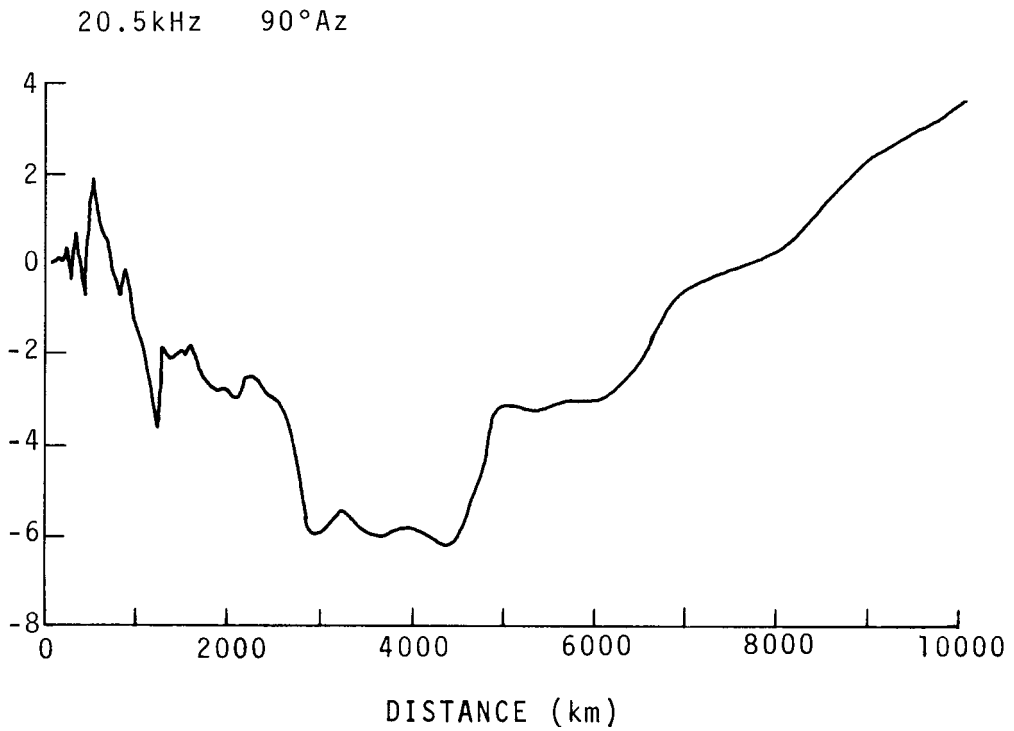

Figure 64.

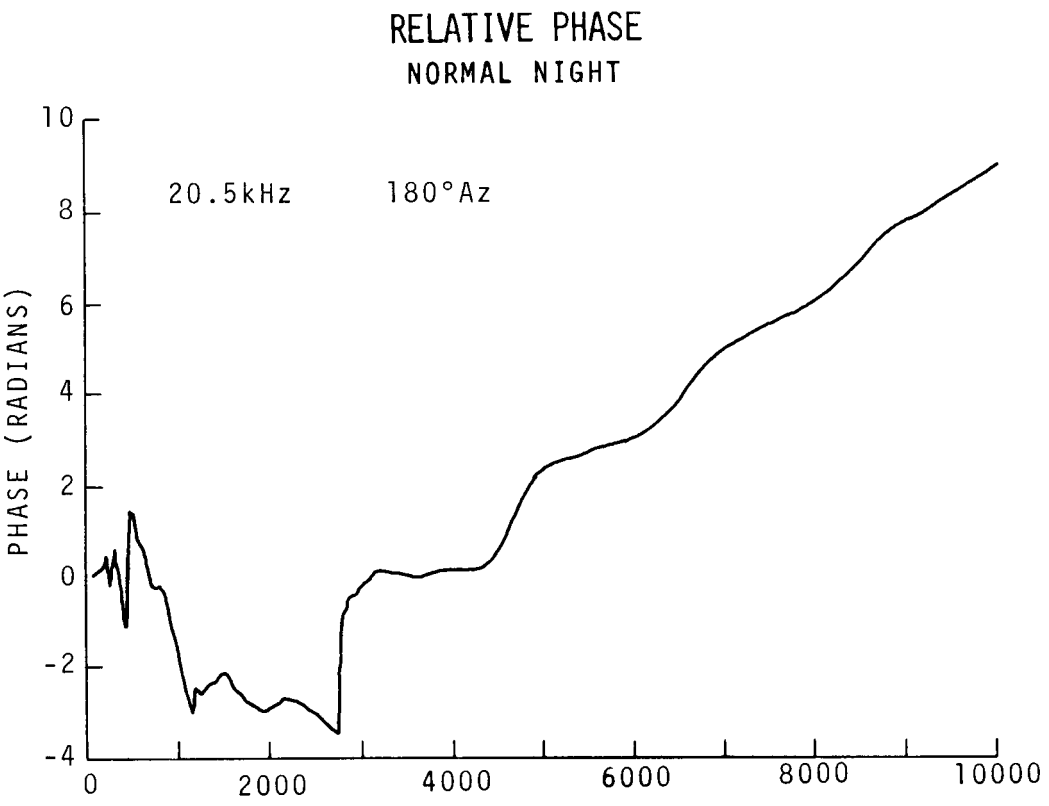

Figure 65.

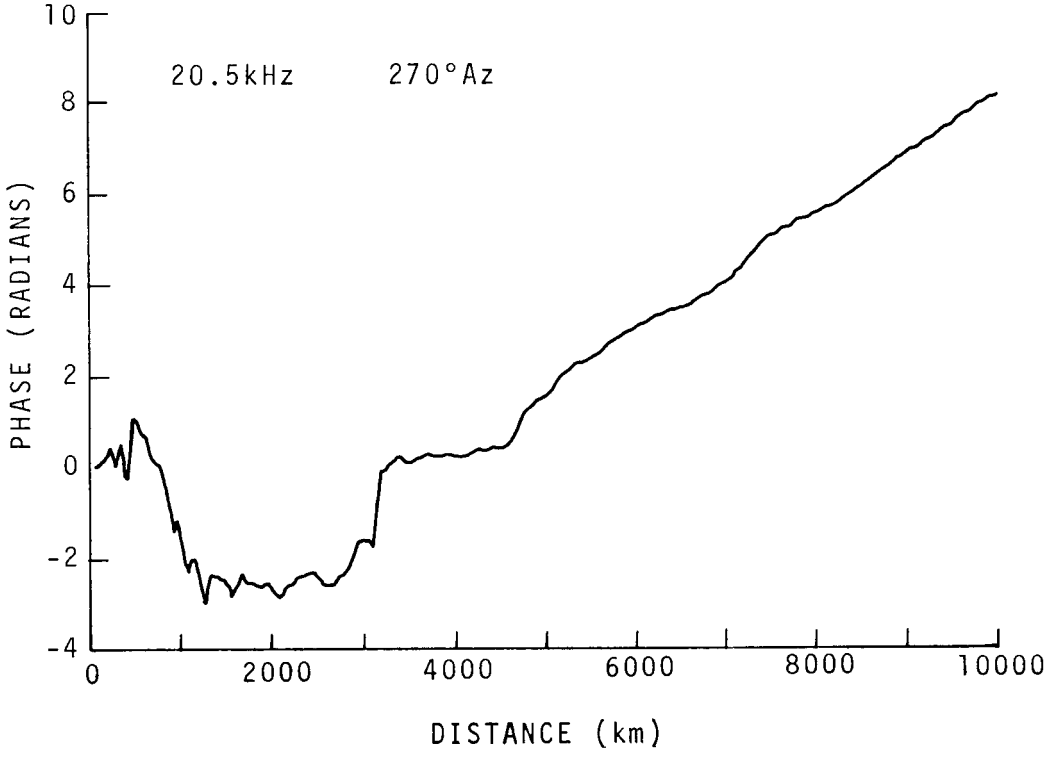

Figure 66.

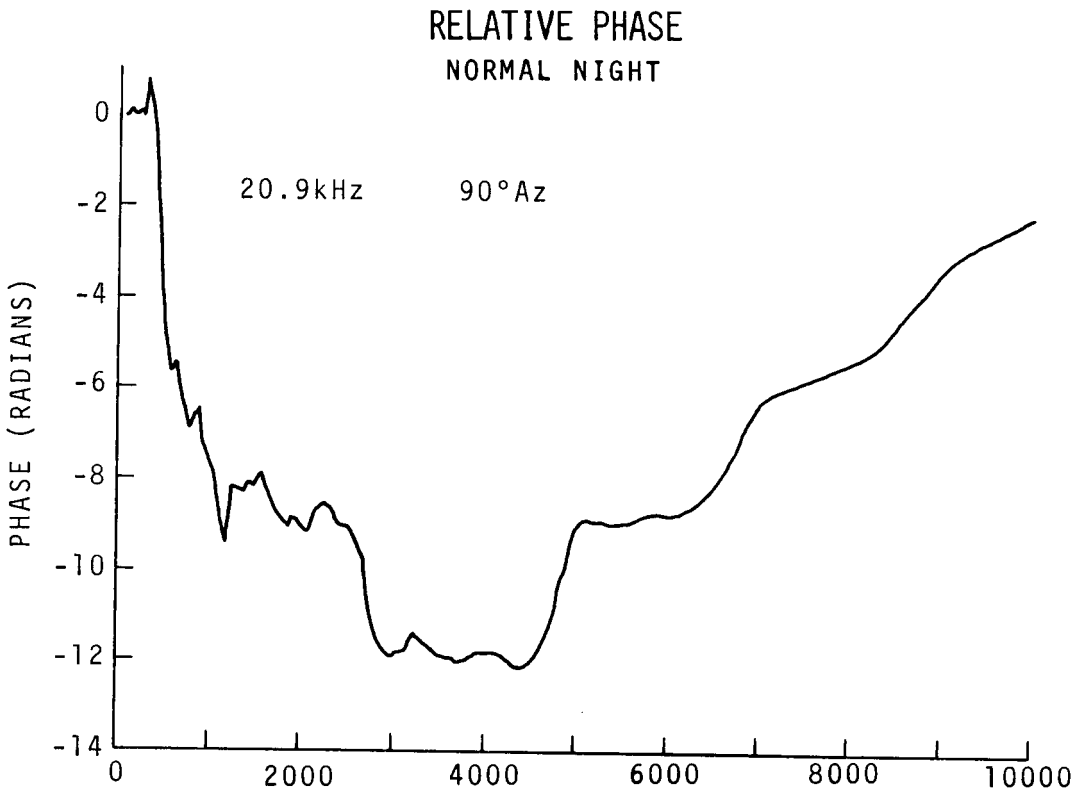

Figure 67.

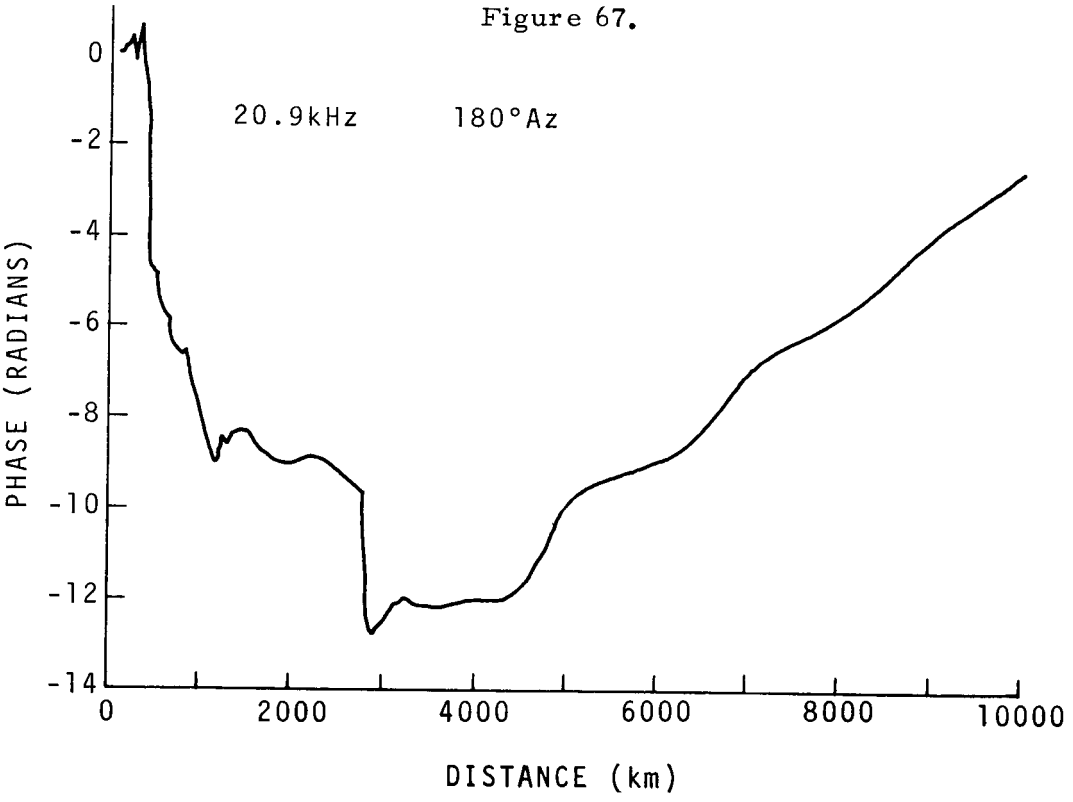

Figure 68.

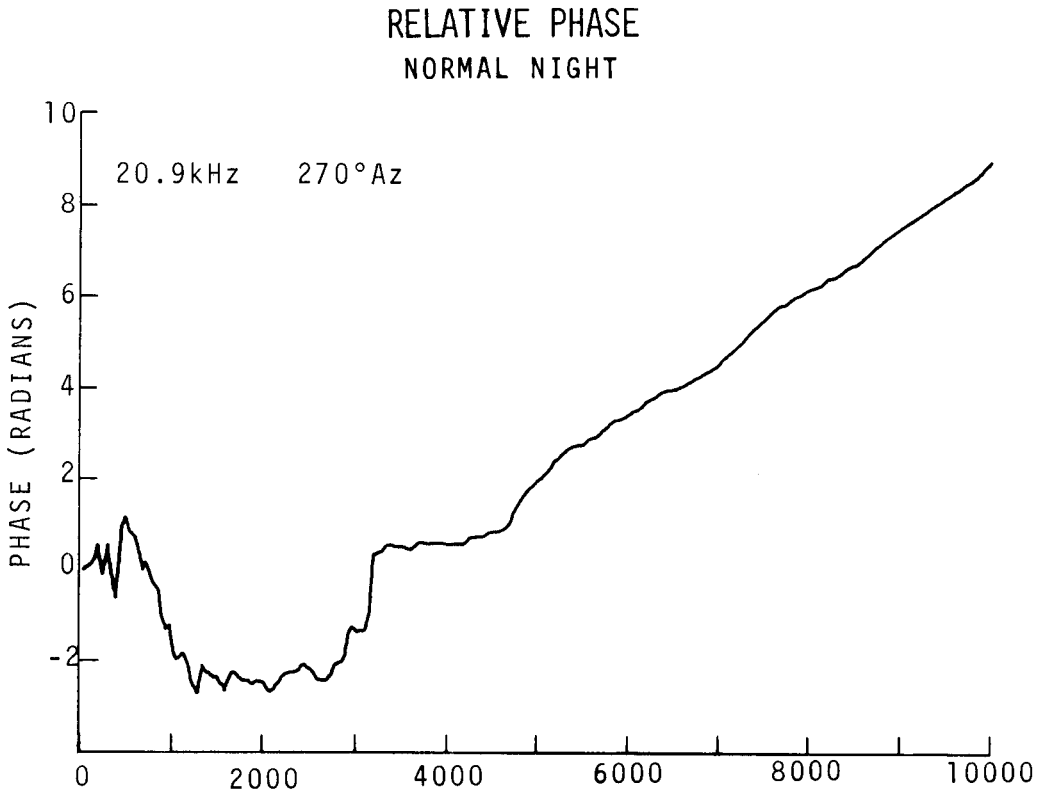
RELATIVE PHASE
NORMAL NIGHT
20.9kHz 270°Az
PHASE (RADIANS)
10
8
6
4
2
0
-2
0
2000
4000
6000
8000
10000

Figure 69.

AMPLITUDE
NORMAL DAY

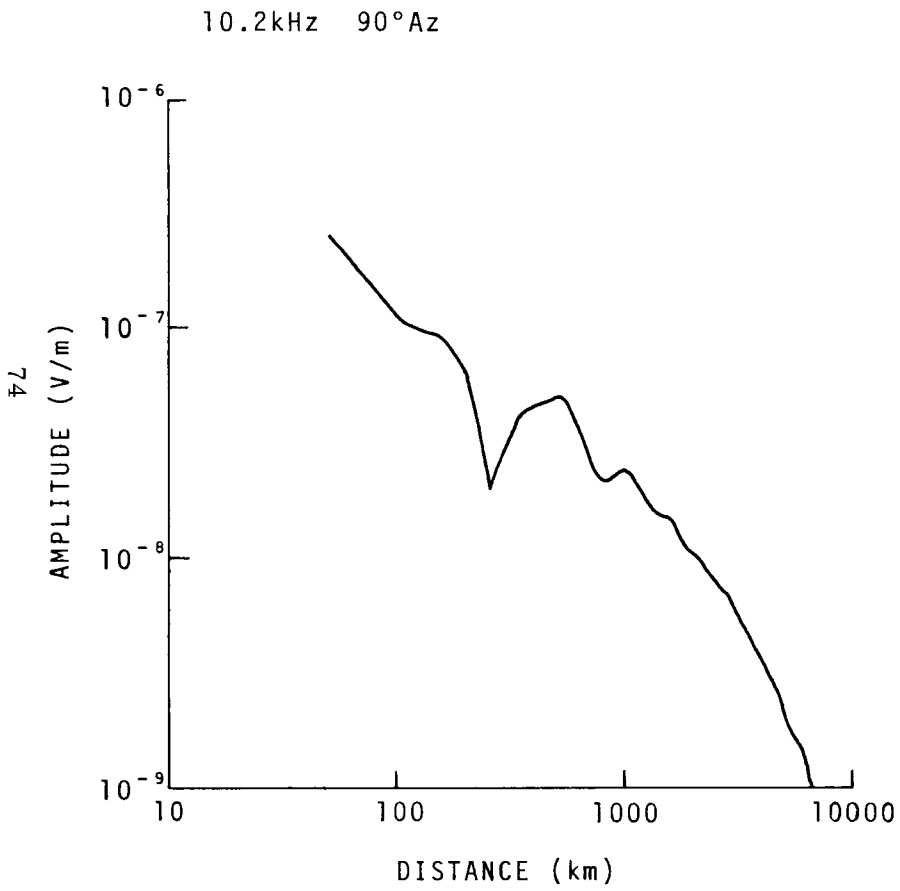

Figure 70.

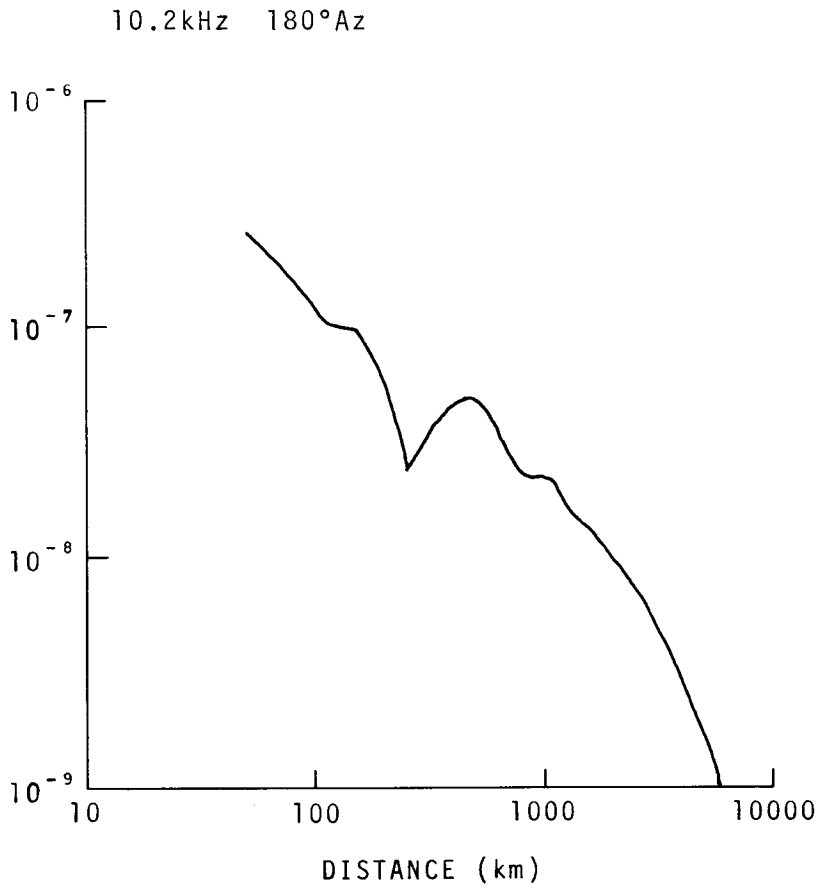

Figure 71.

AMPLITUDE
NORMAL DAY

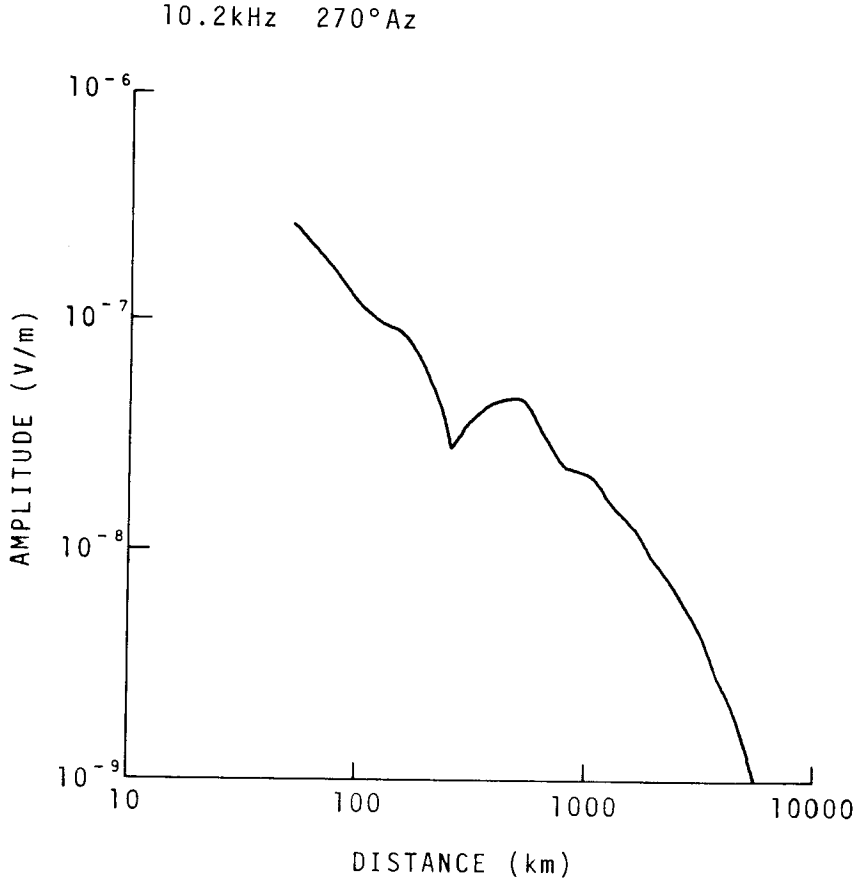

Figure 72.

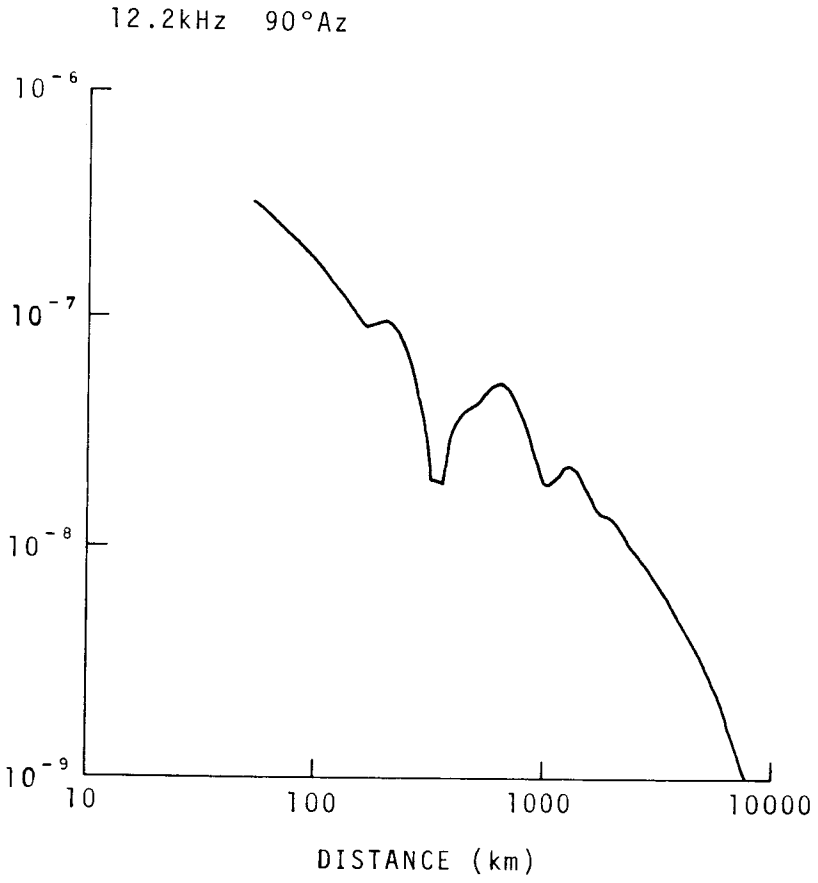

Figure 73.

AMPLITUDE
NORMAL DAY

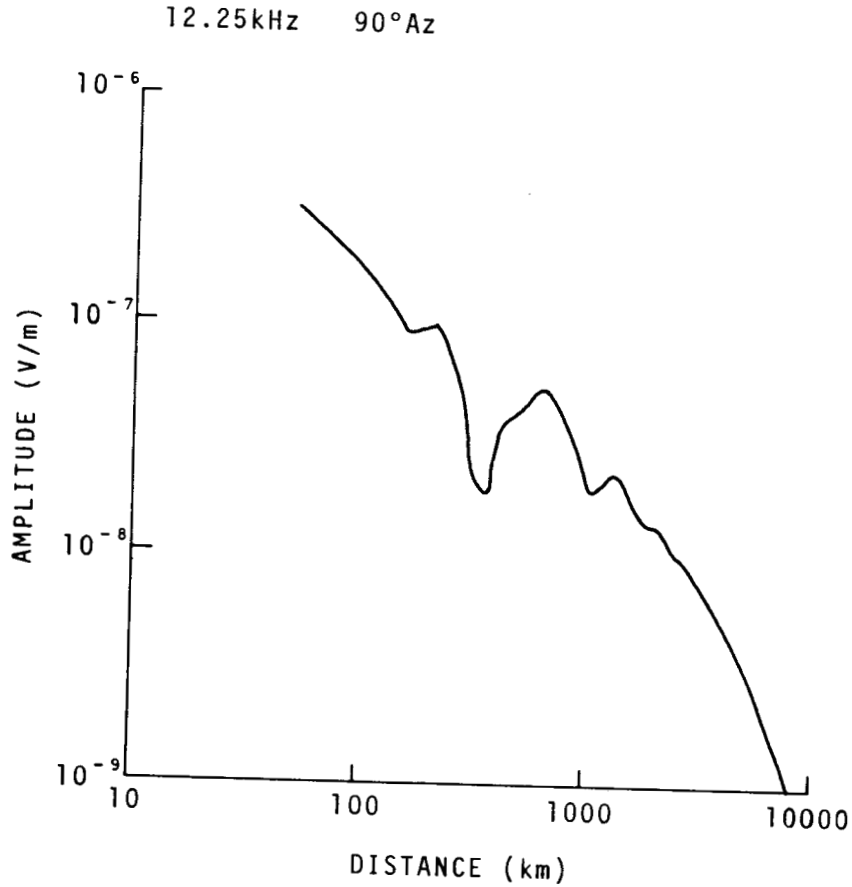

Figure 74.

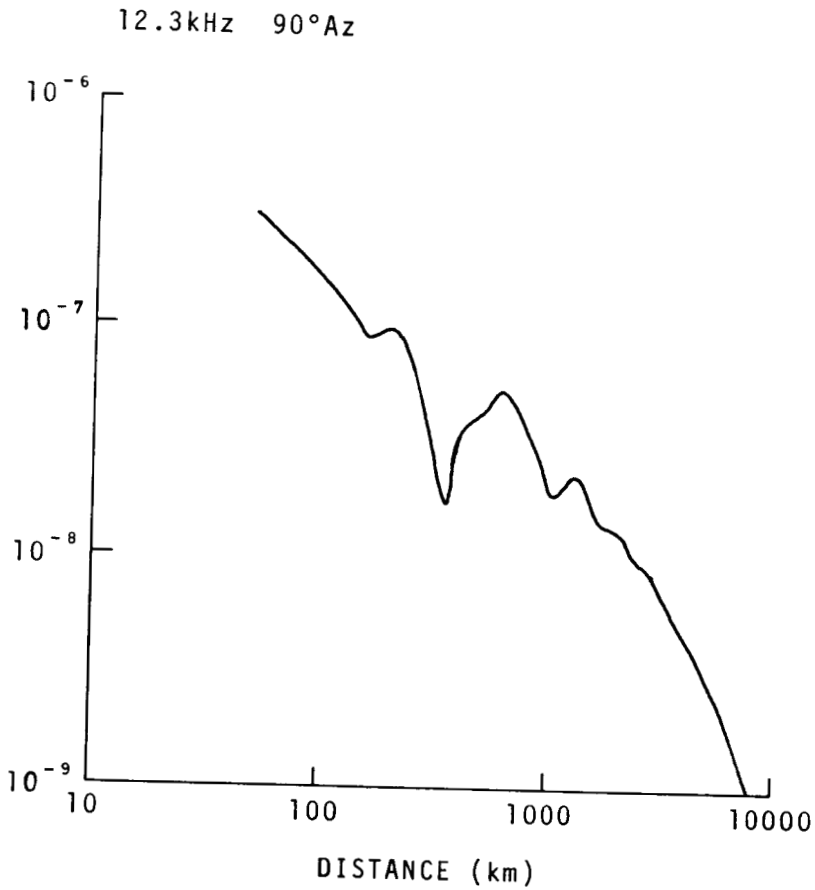

Figure 75.

AMPLITUDE
NORMAL DAY

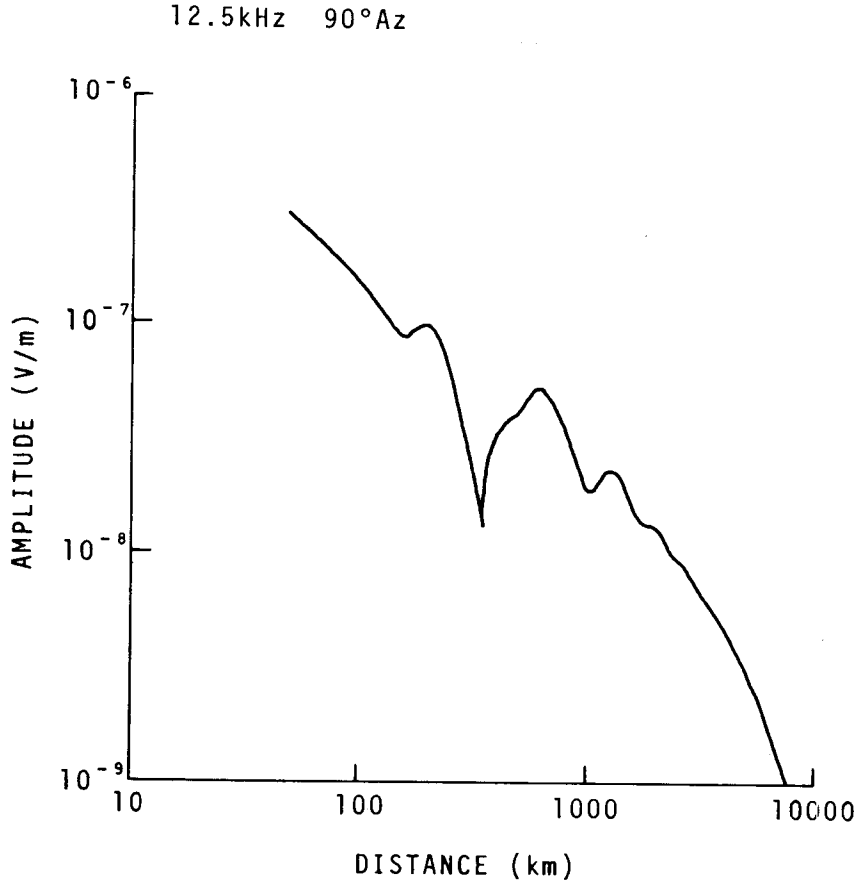

Figure 76.

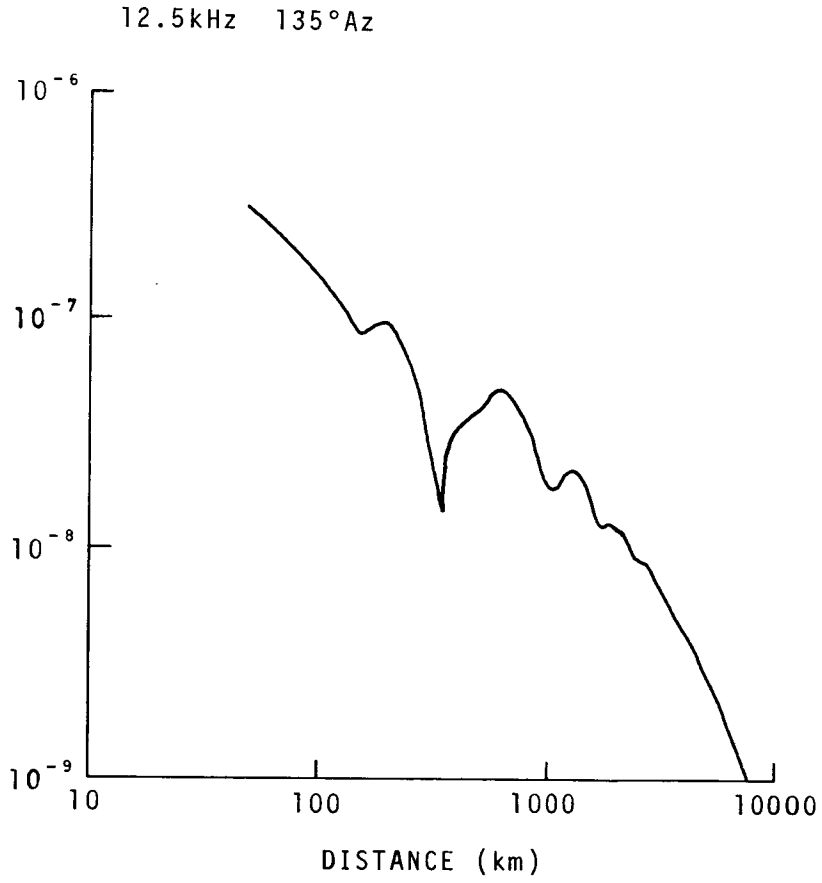

Figure 77.

AMPLITUDE
NORMAL DAY

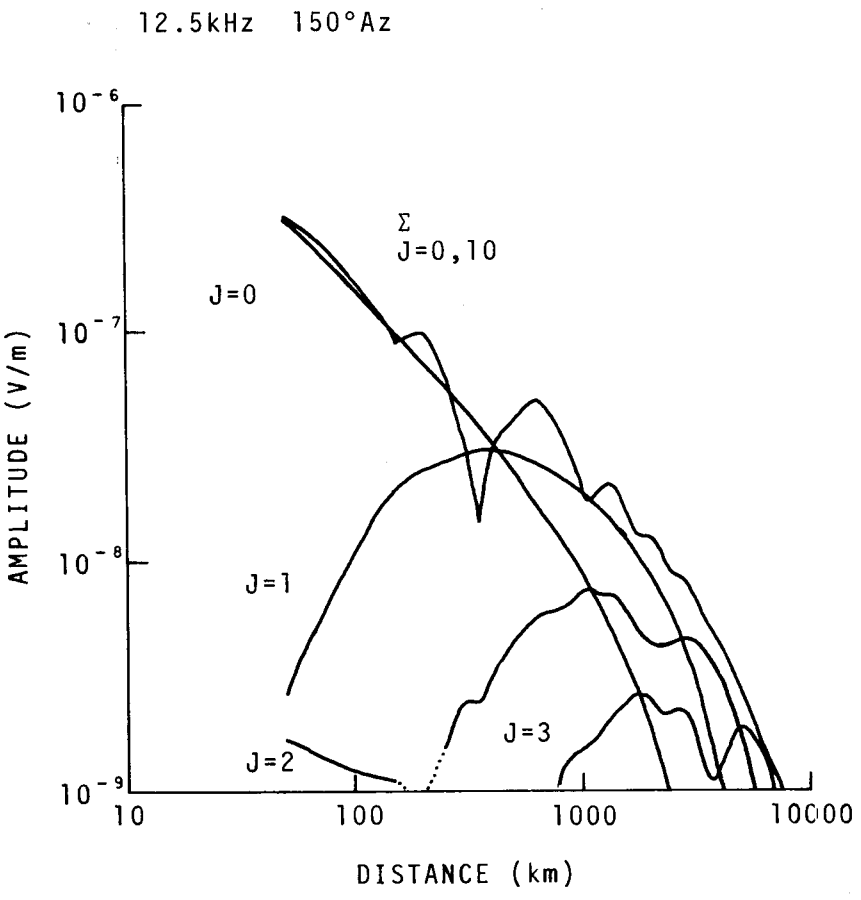

Figure 78.

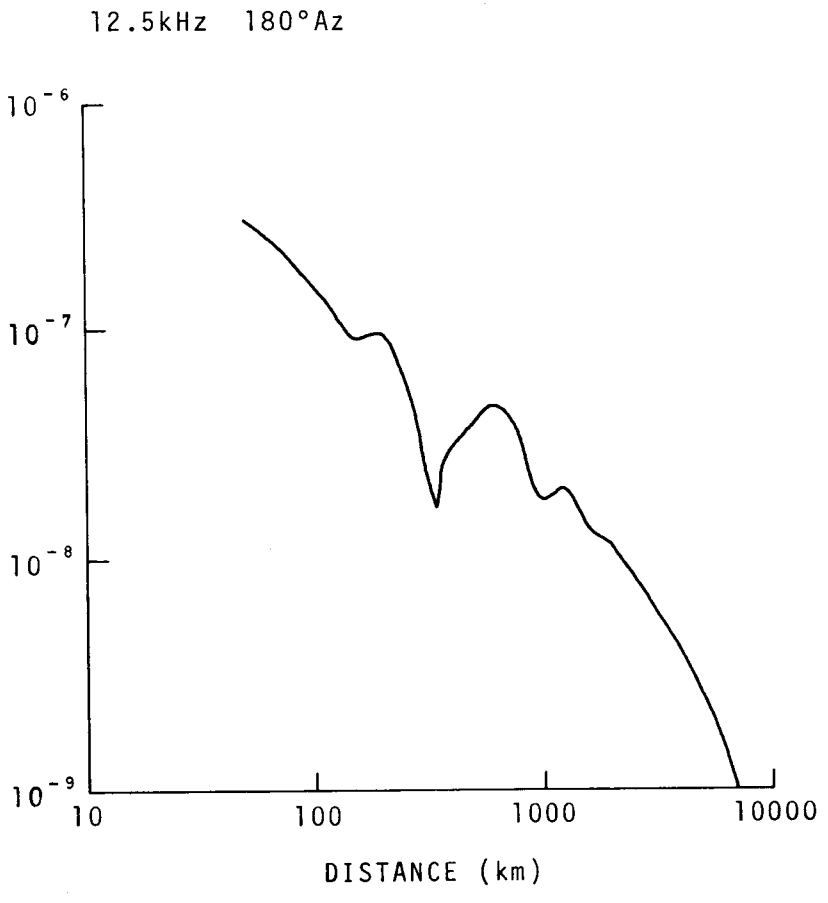

Figure 79.

AMPLITUDE
NORMAL DAY

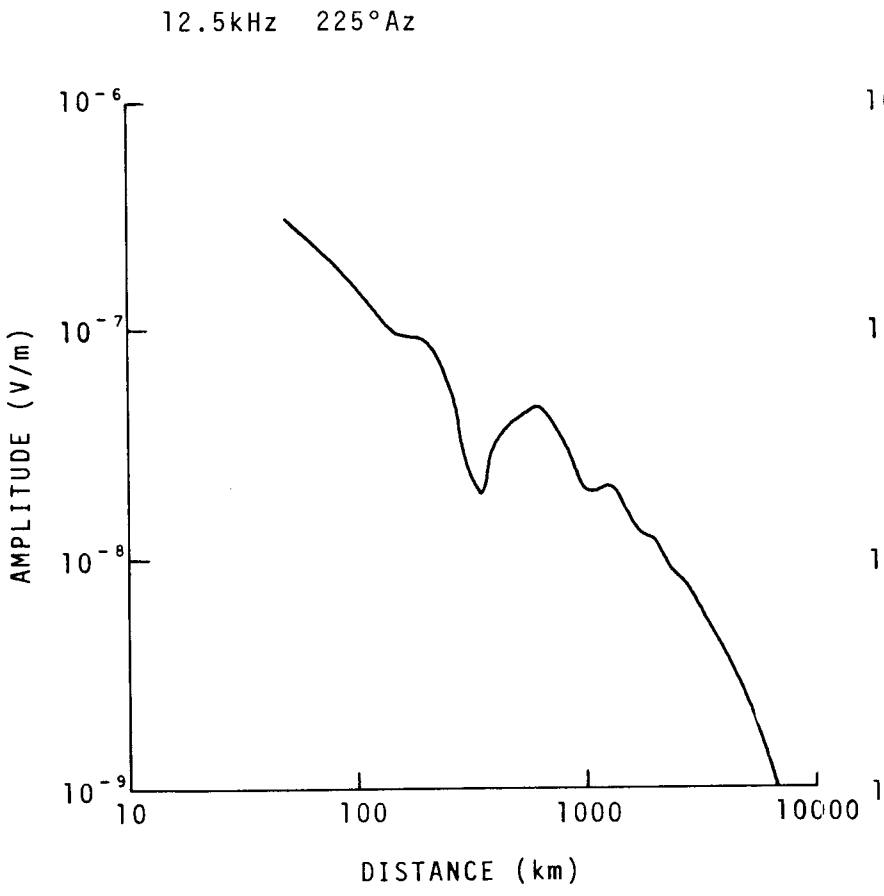

Figure 80.

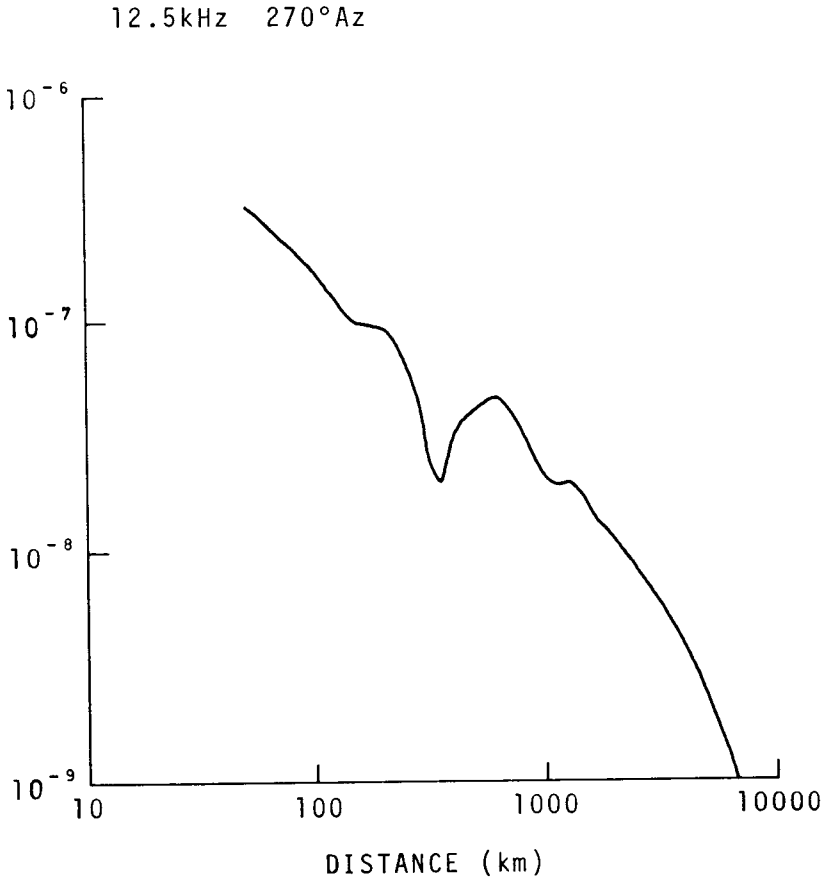

Figure 81.

AMPLITUDE
NORMAL DAY

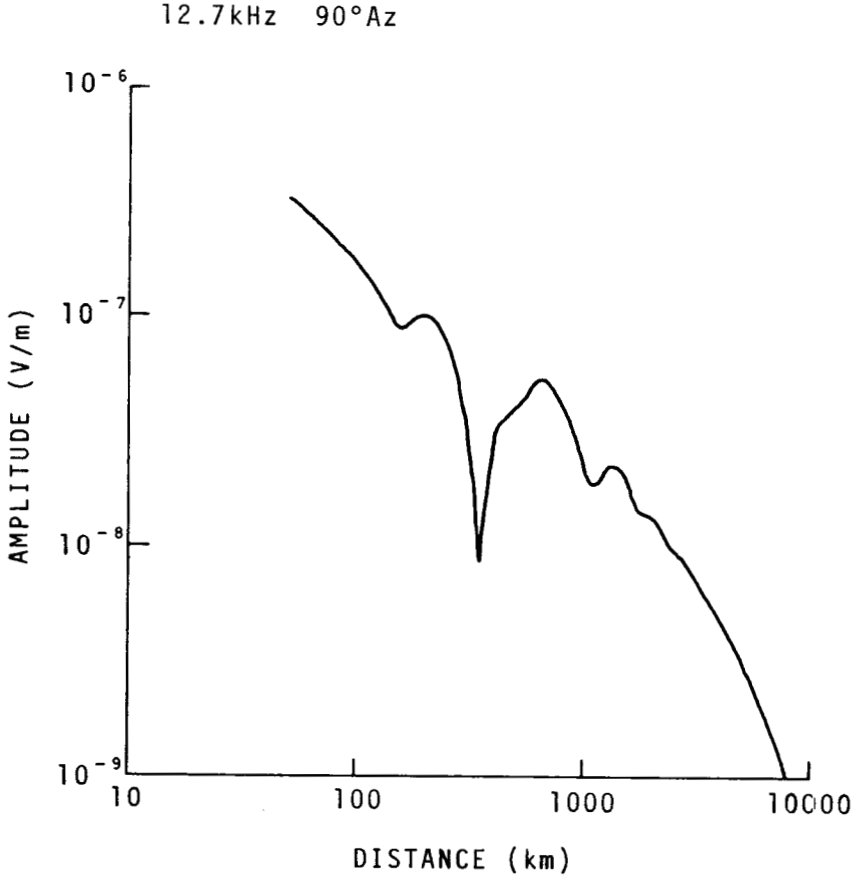

Figure 82.

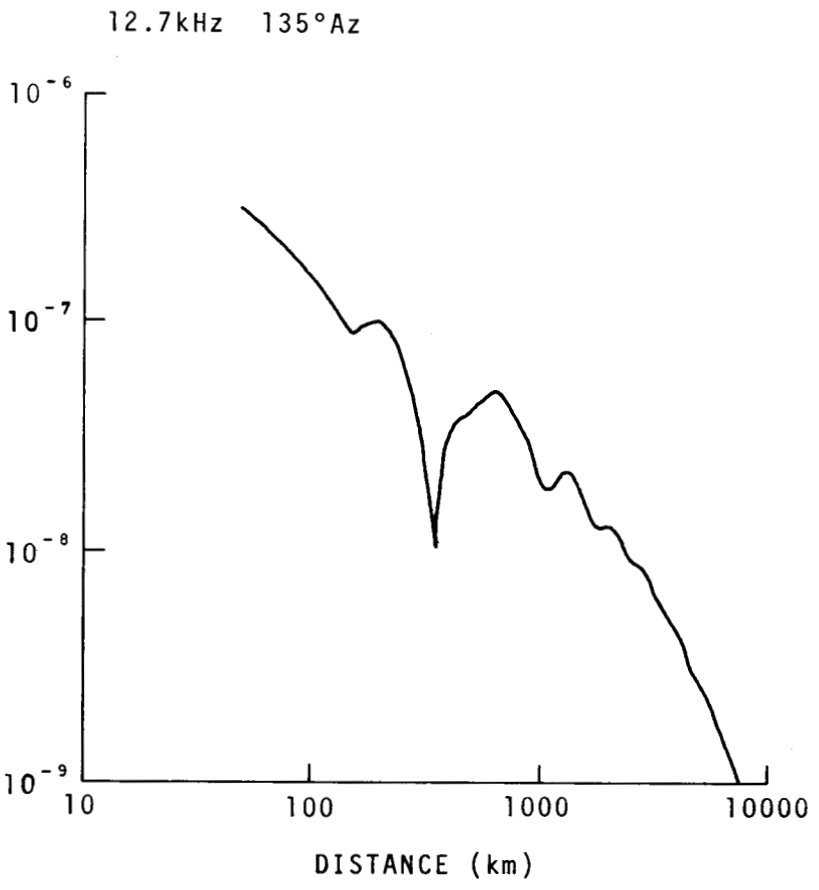

Figure 83.

AMPLITUDE
NORMAL DAY

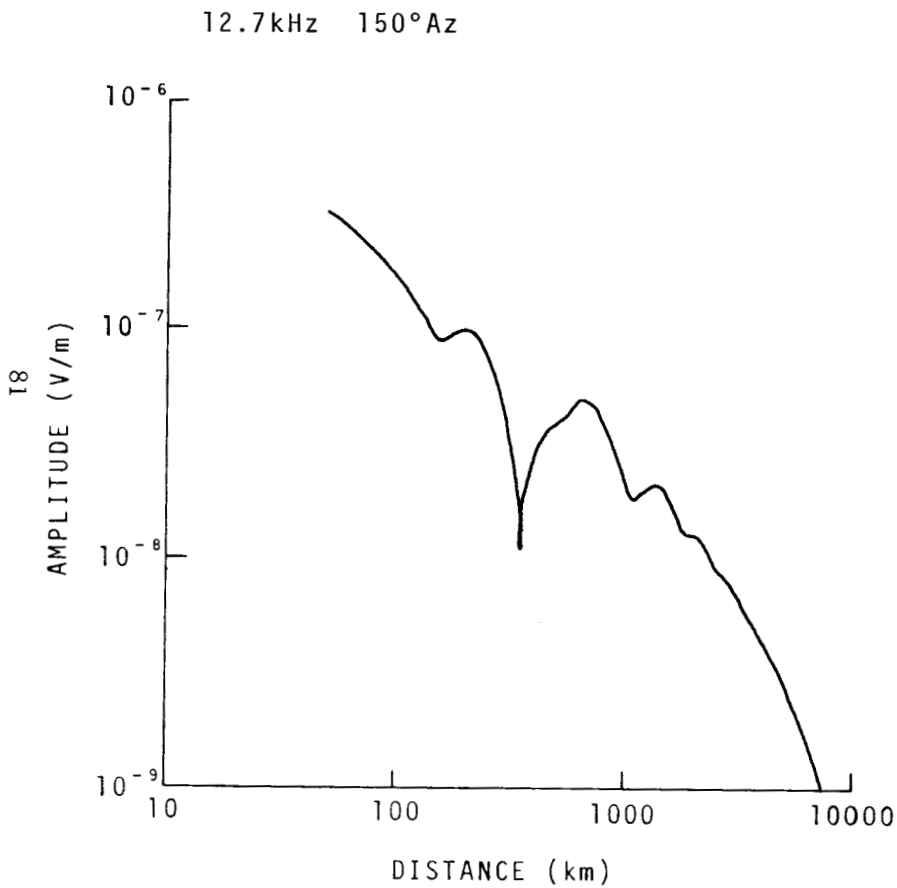

Figure 84.

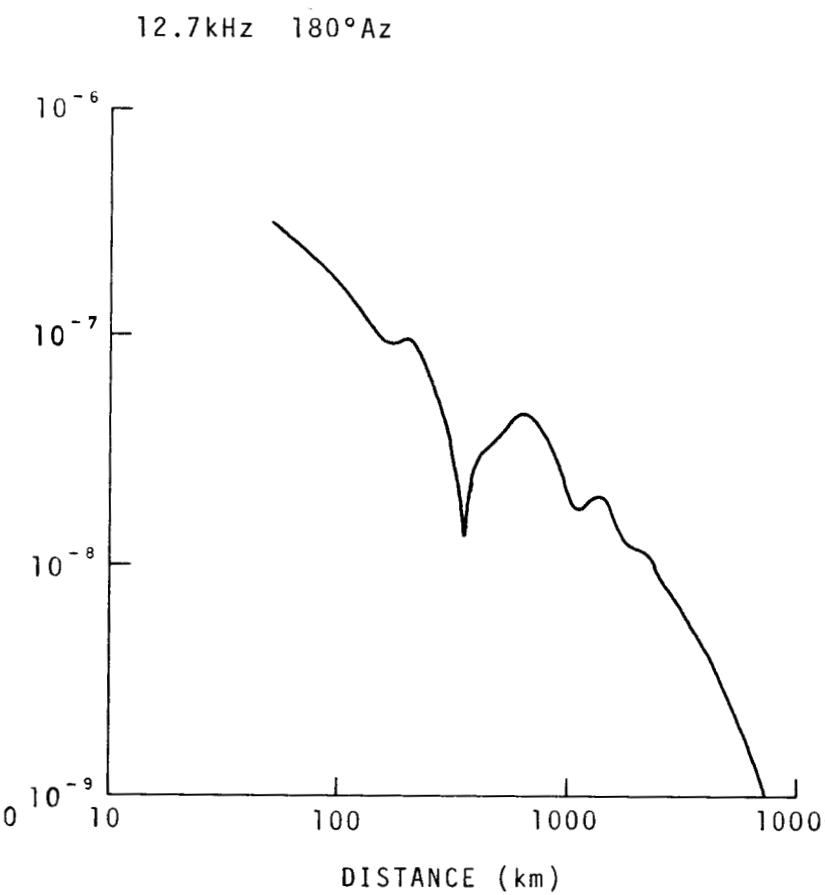

Figure 85.

AMPLITUDE
NORMAL DAY

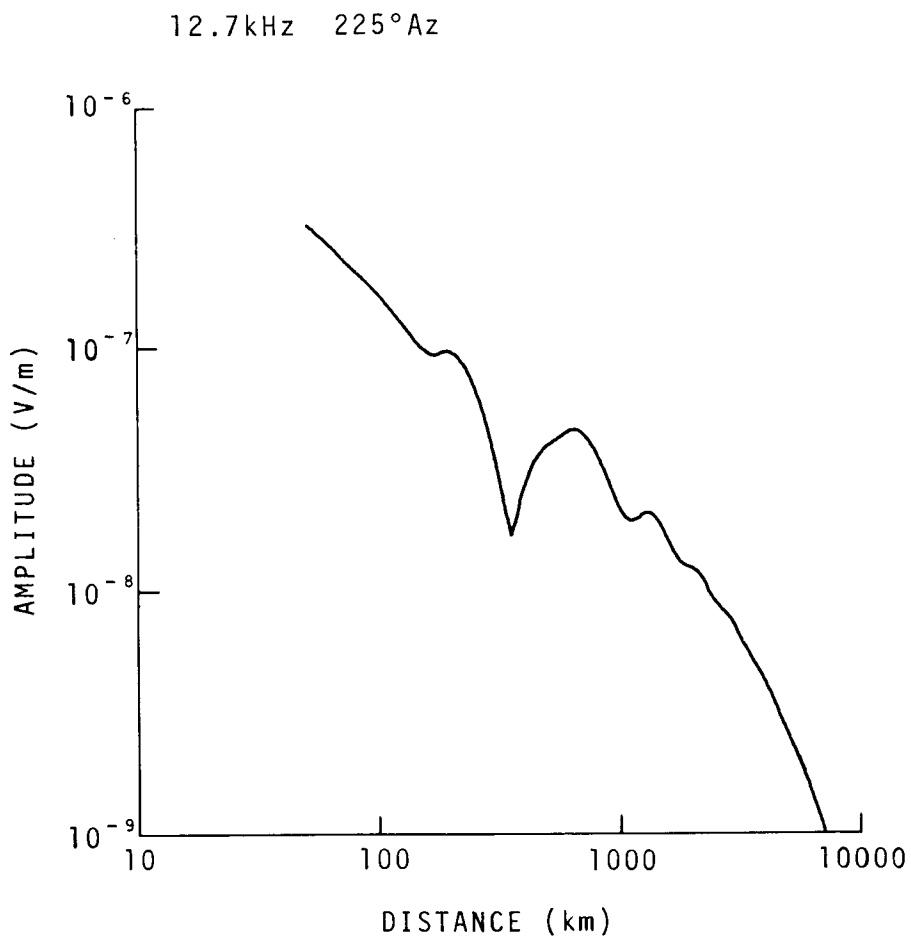

Figure 86.

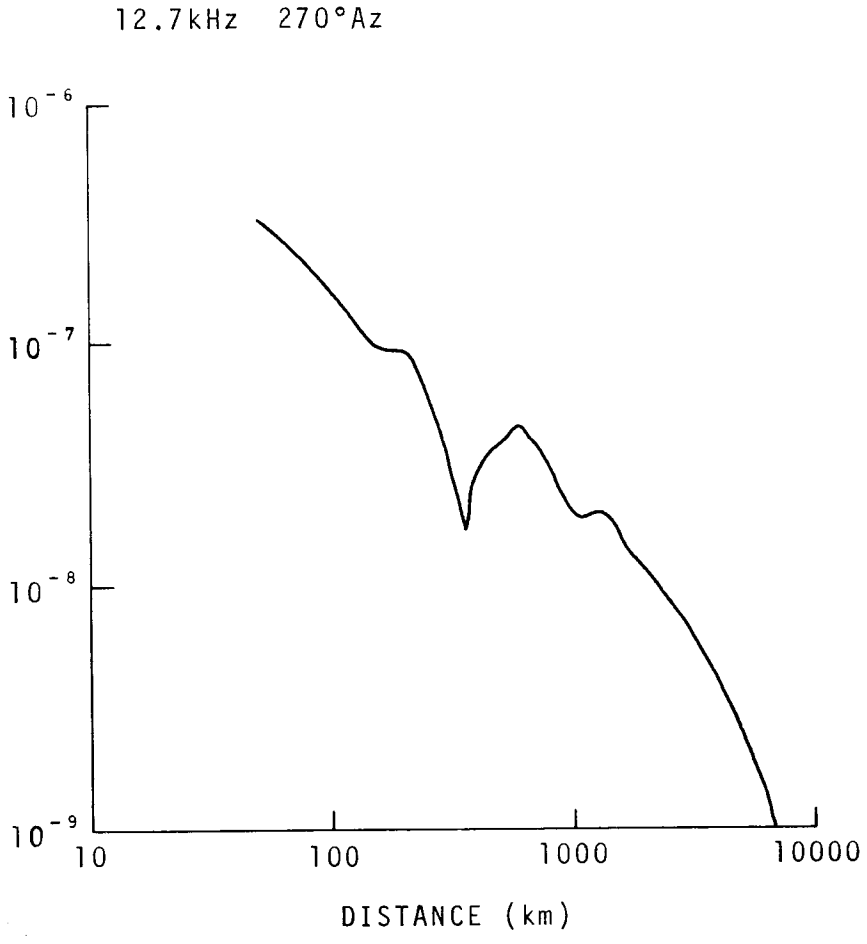

Figure 87.

AMPLITUDE
NORMAL DAY

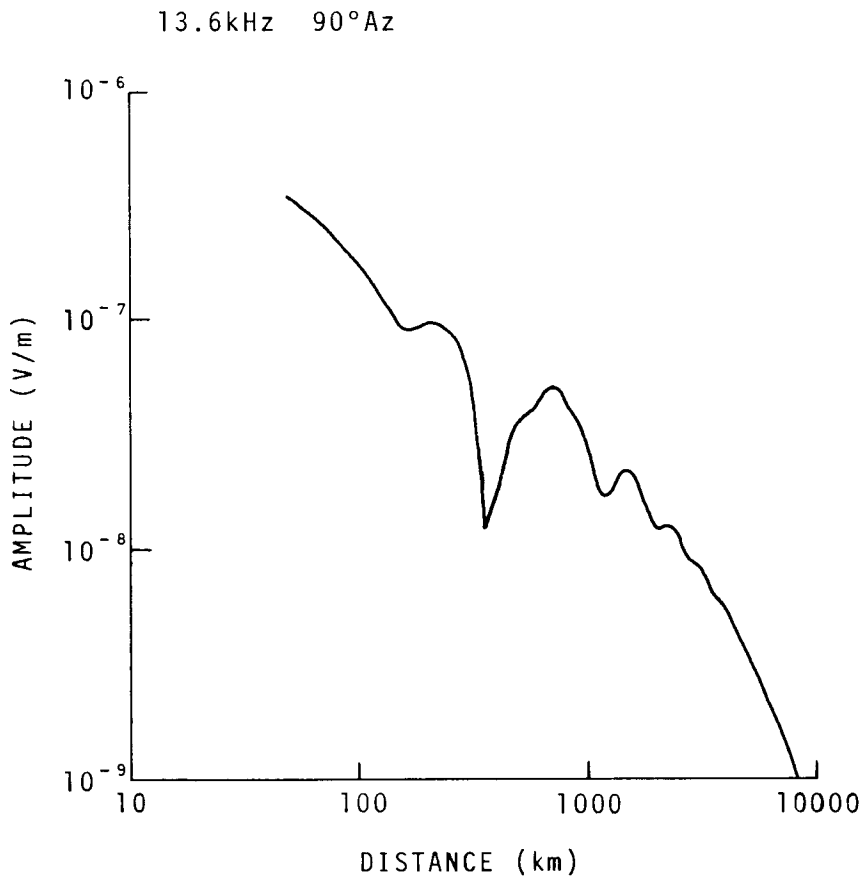

Figure 88.

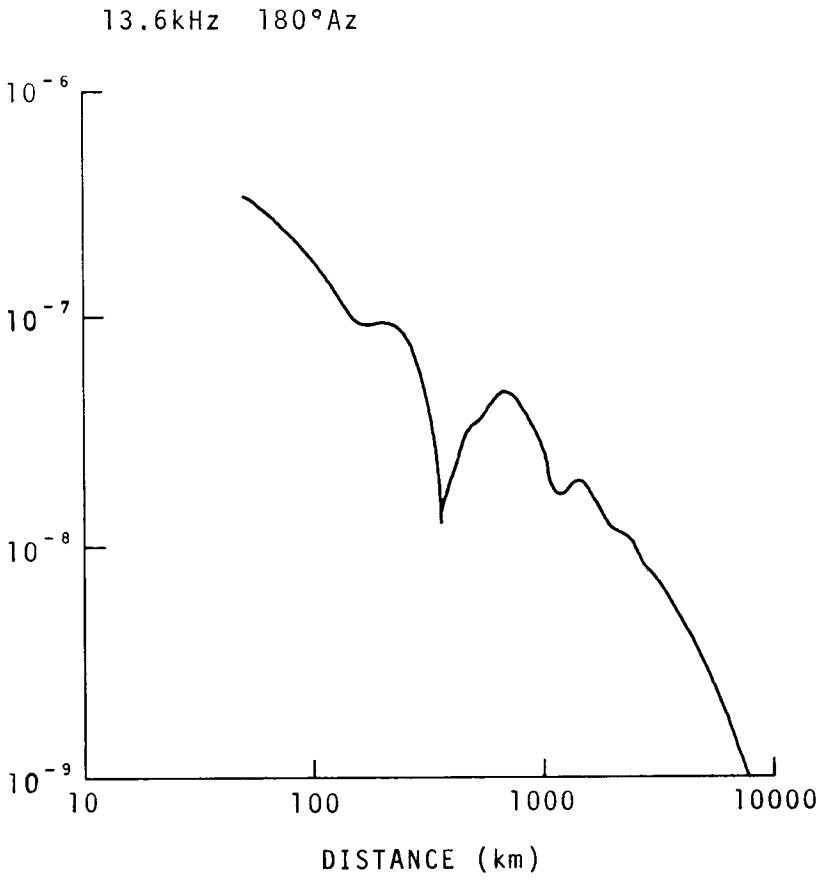

Figure 89.

AMPLITUDE
NORMAL DAY

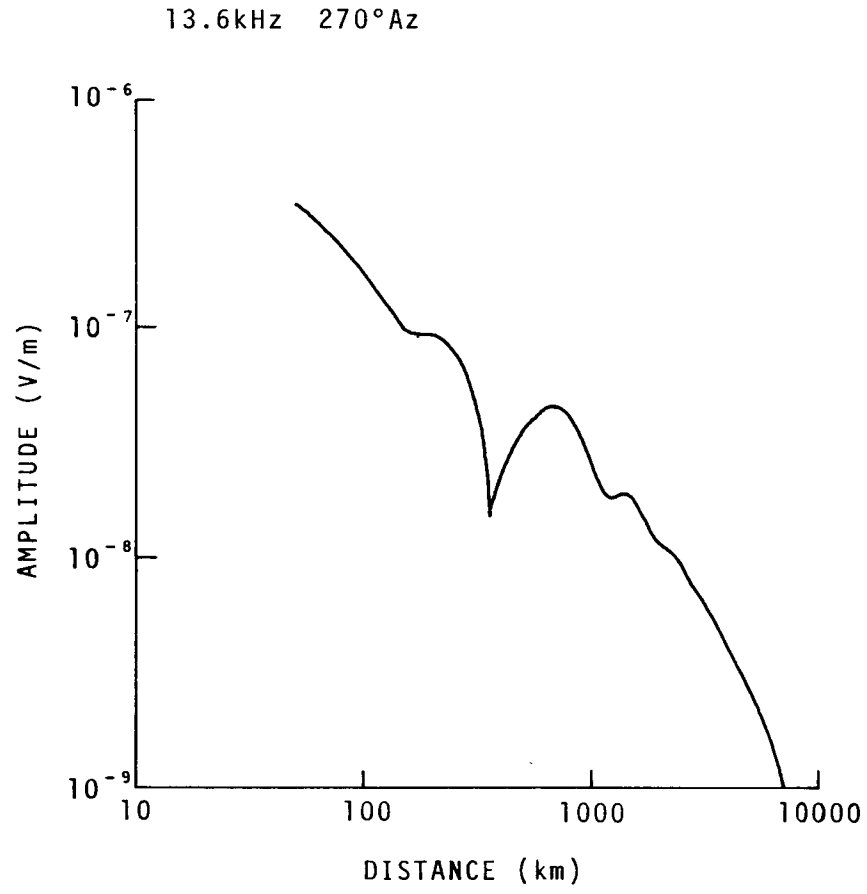

Figure 90.

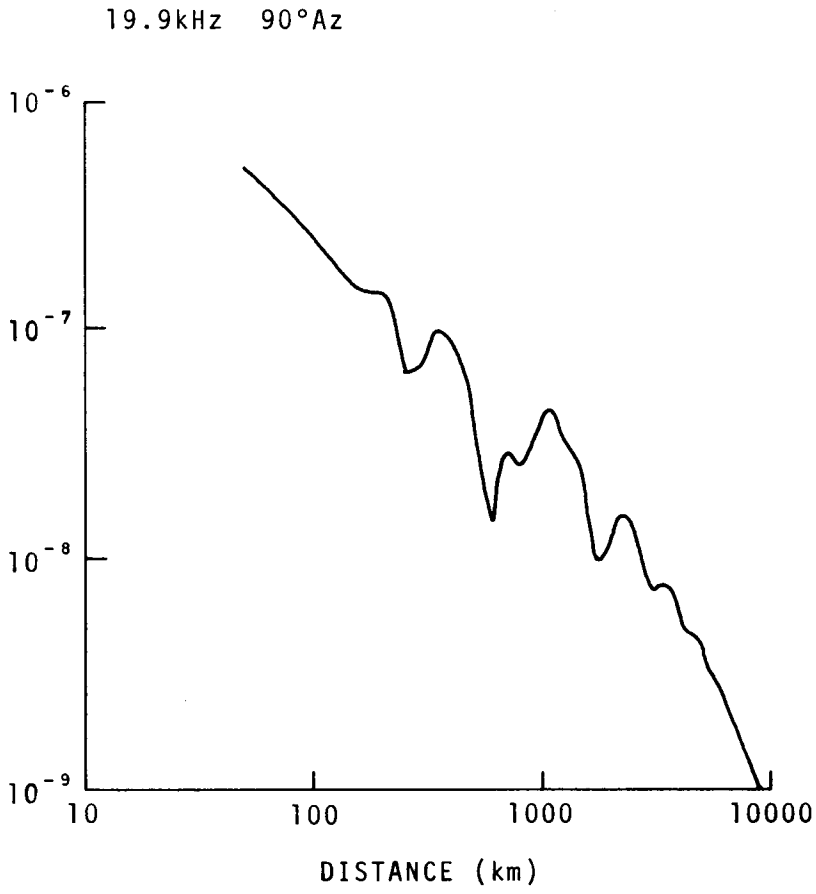

Figure 91.

AMPLITUDE
NORMAL DAY

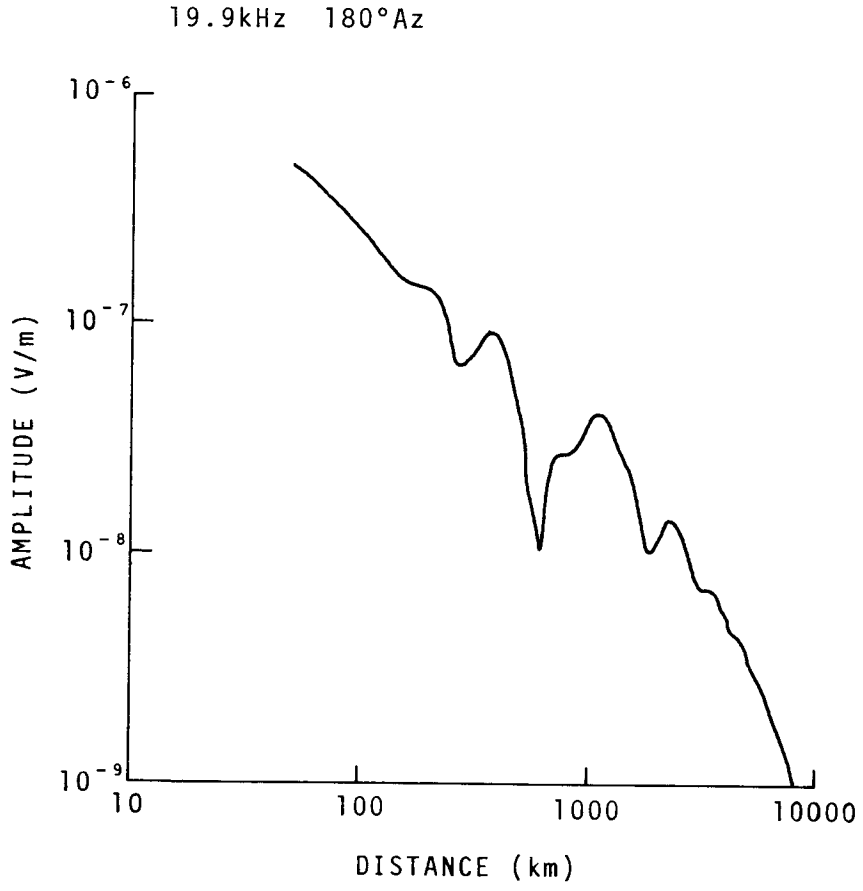

Figure 92.

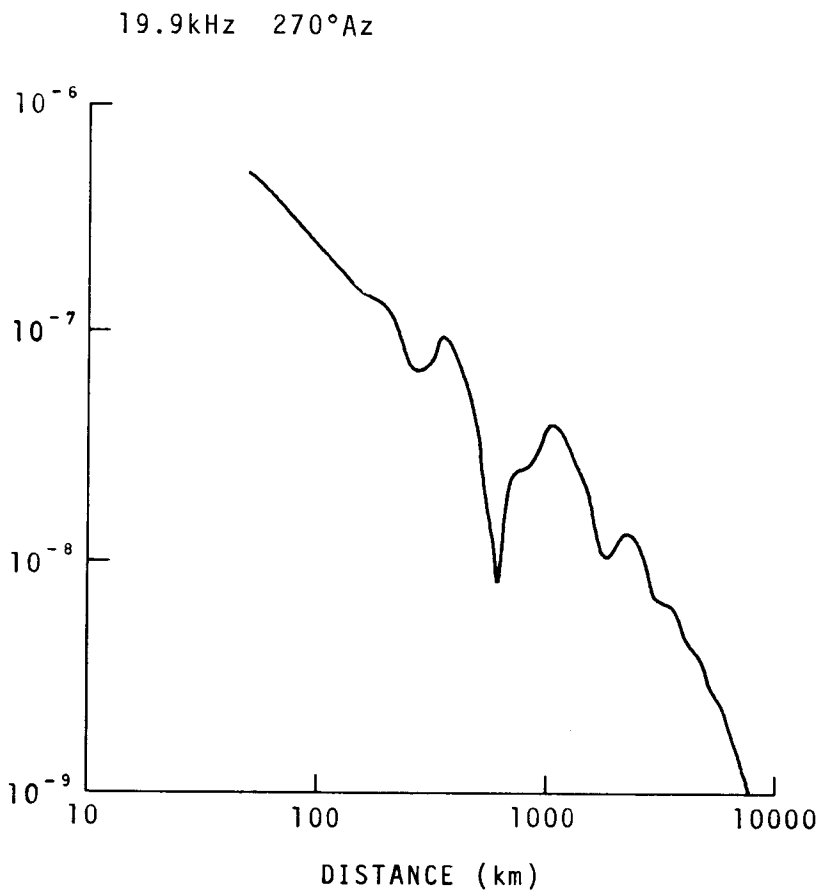

Figure 93.

AMPLITUDE
NORMAL DAY

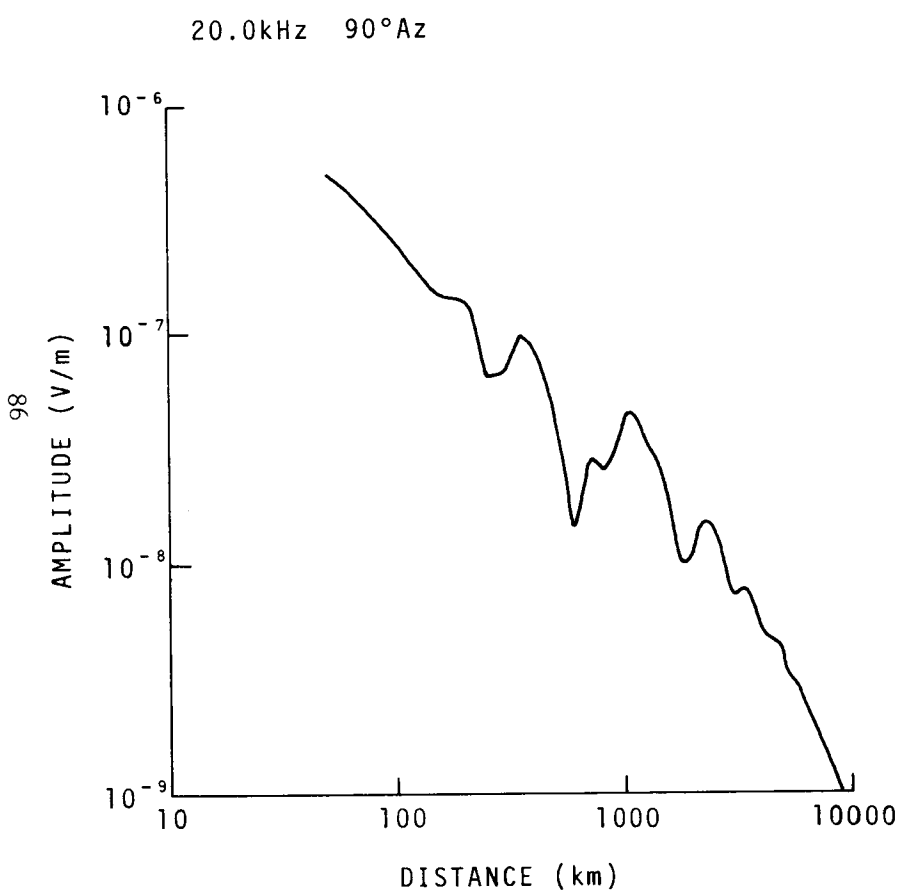

Figure 94.

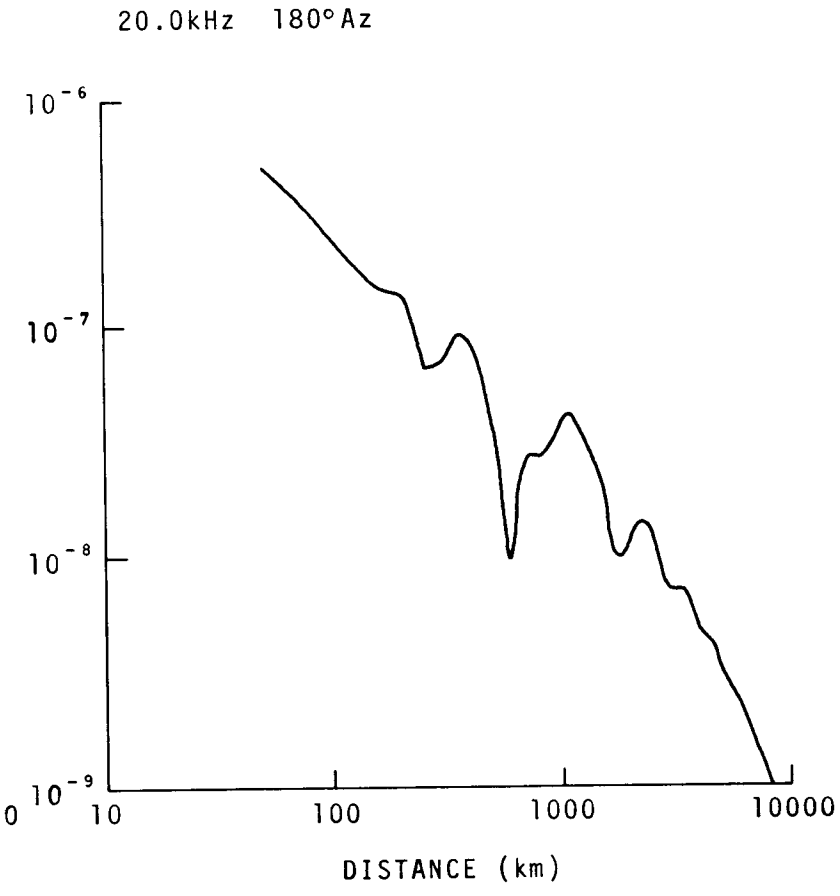

Figure 95.

AMPLITUDE
NORMAL DAY

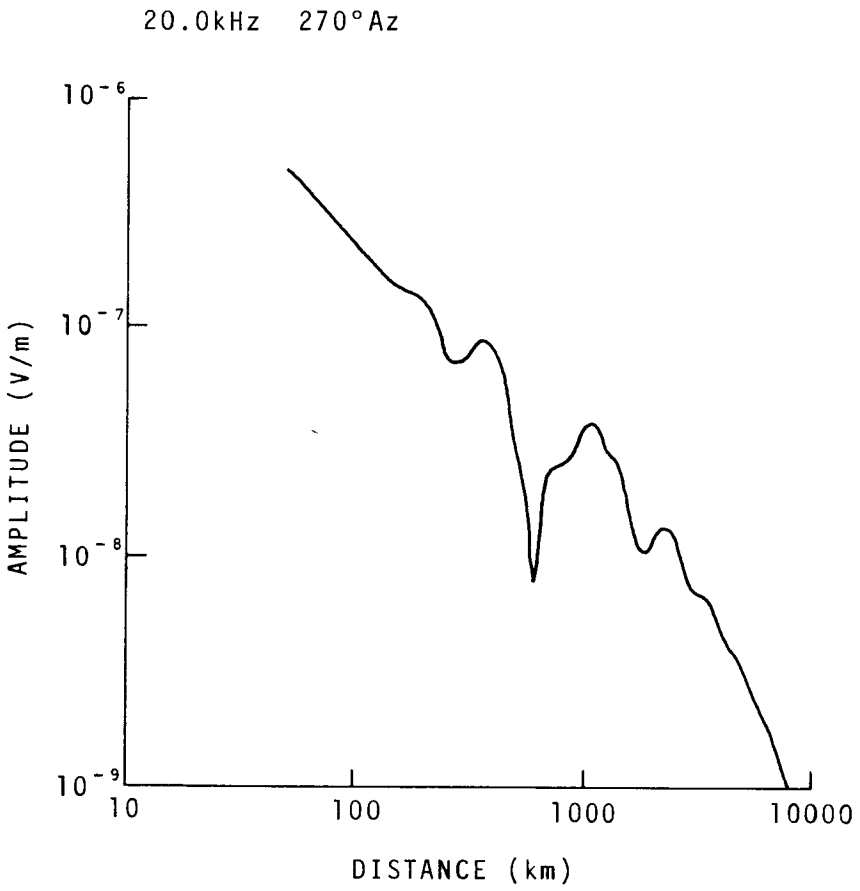

Figure 96.

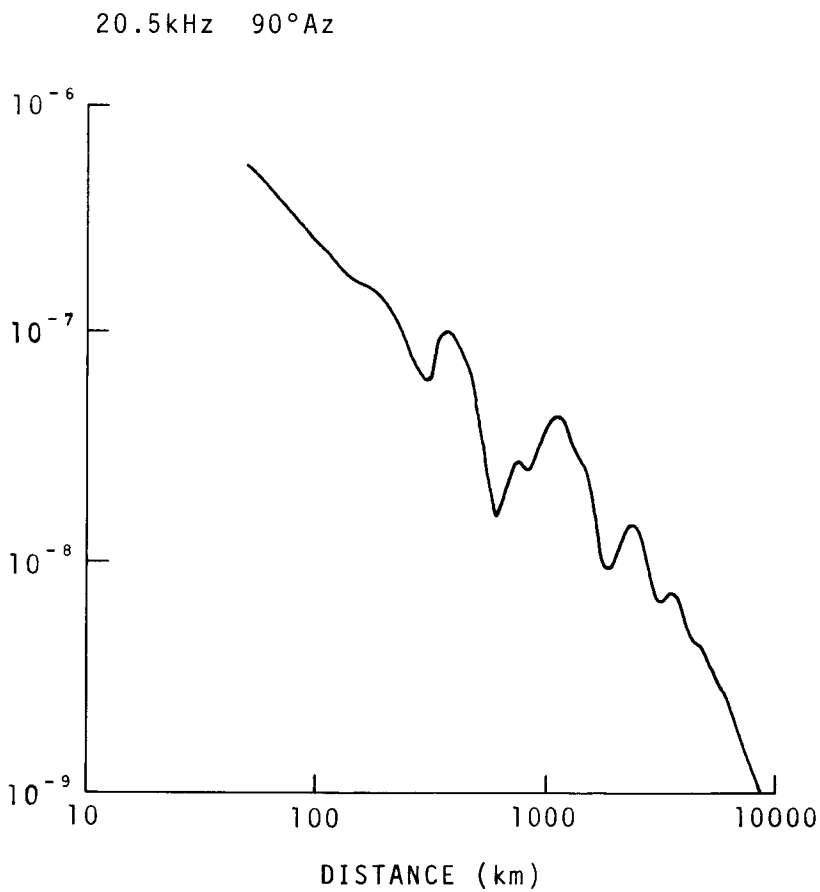

Figure 97.

AMPLITUDE
NORMAL DAY

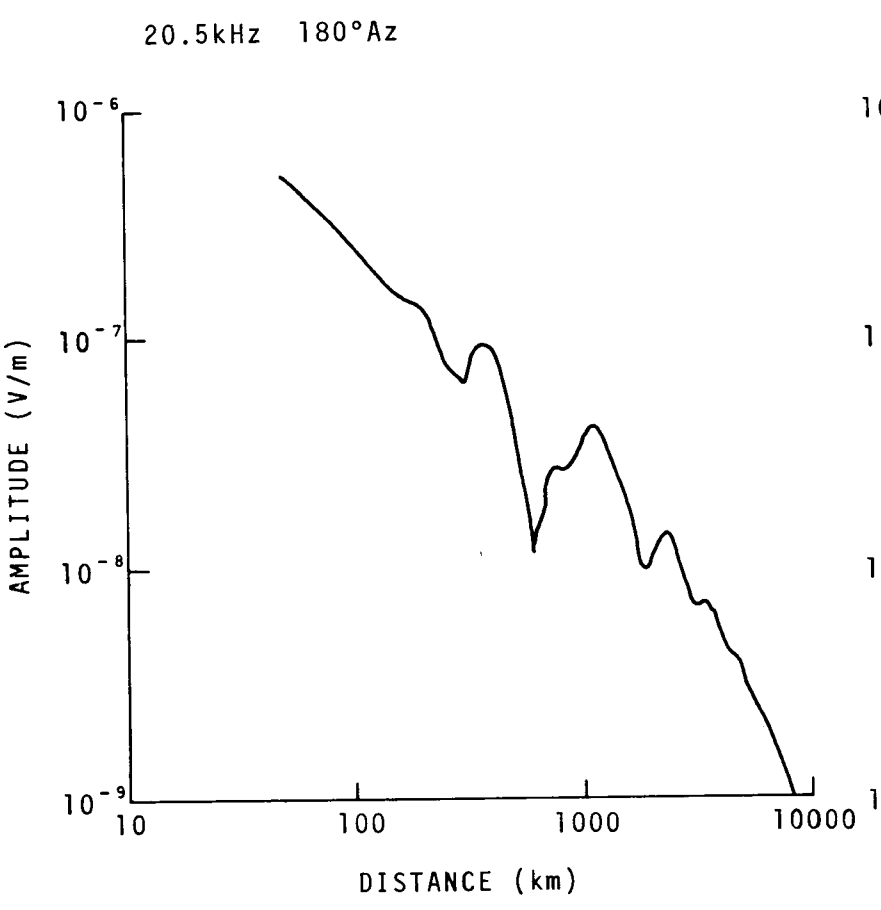

Figure 98.

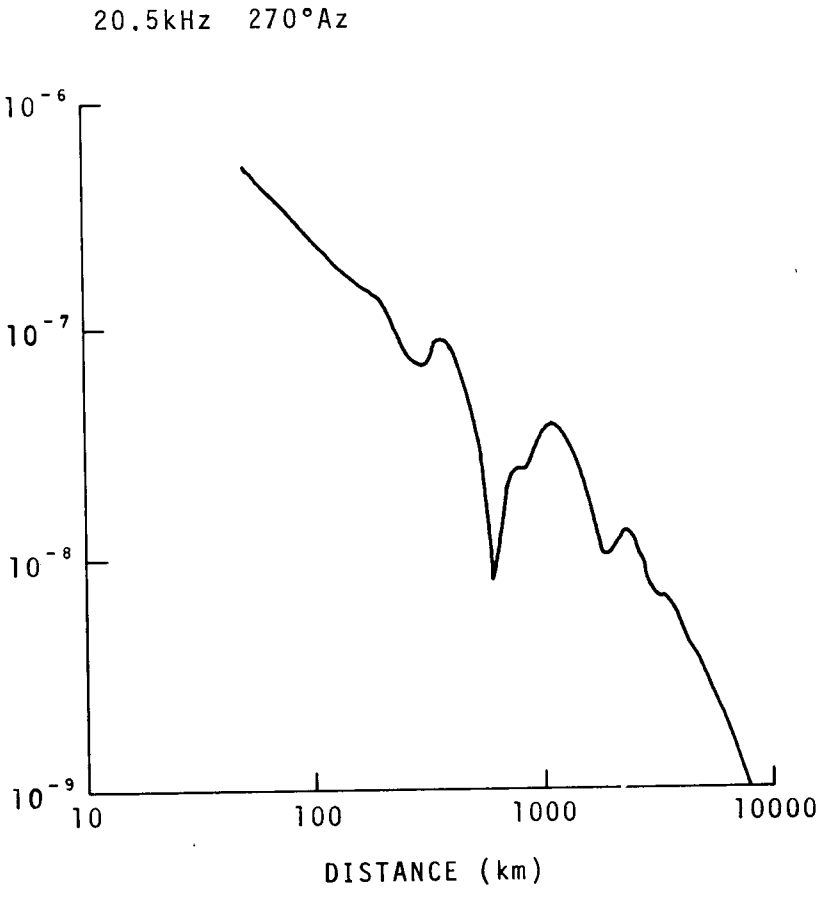

Figure 99.

AMPLITUDE
NORMAL DAY

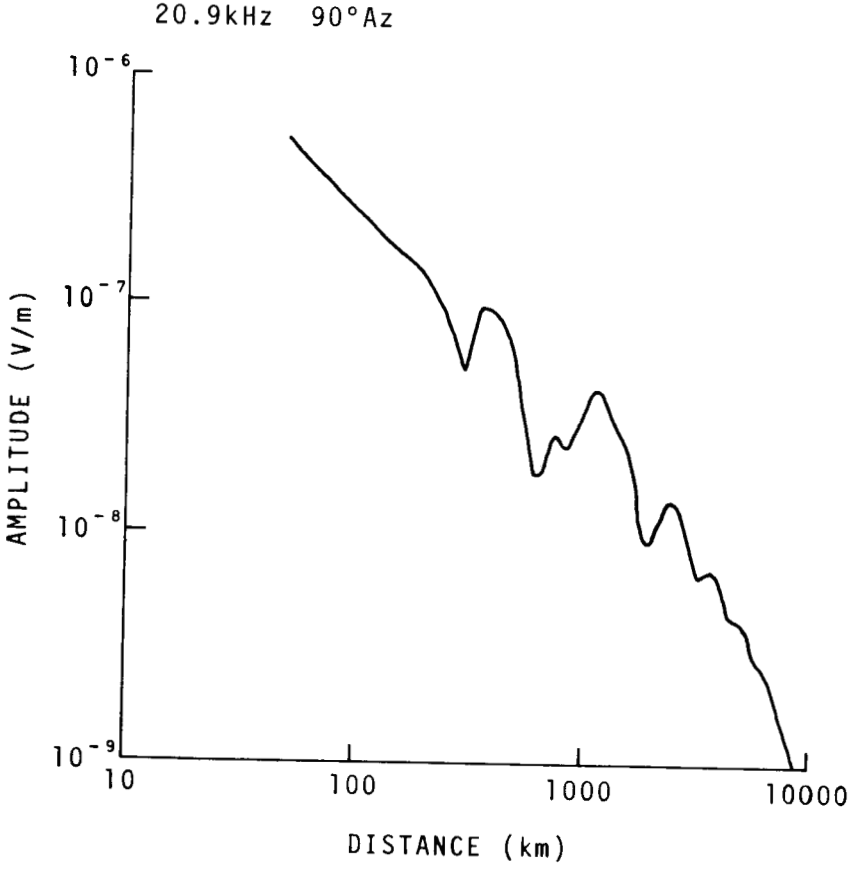

Figure 100.

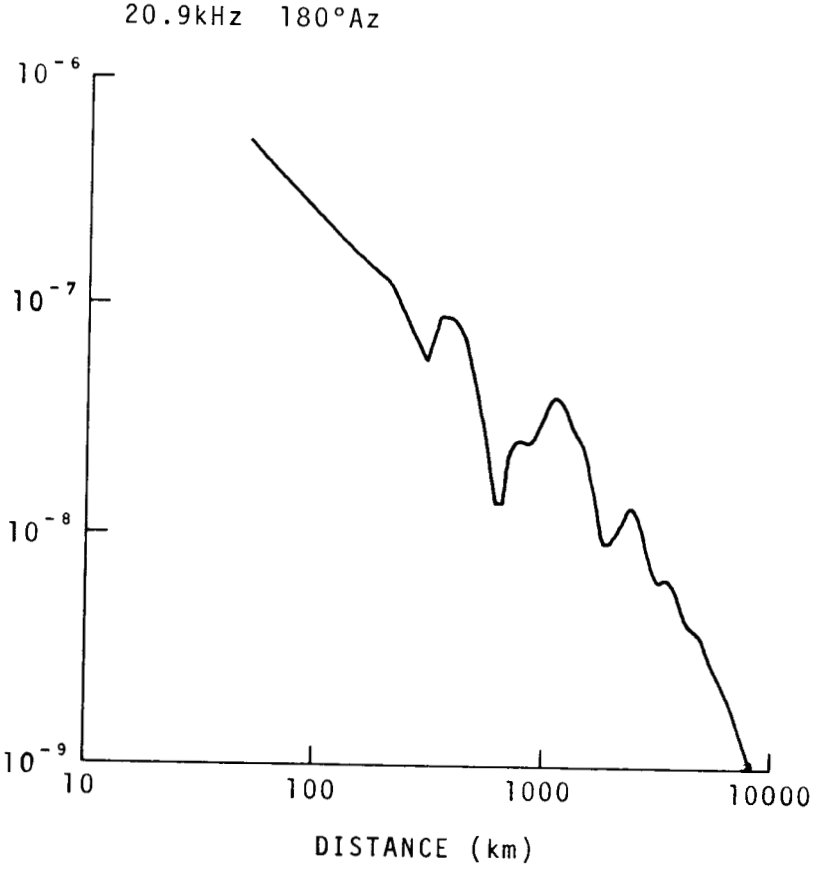

Figure 101.

AMPLITUDE
NORMAL DAY

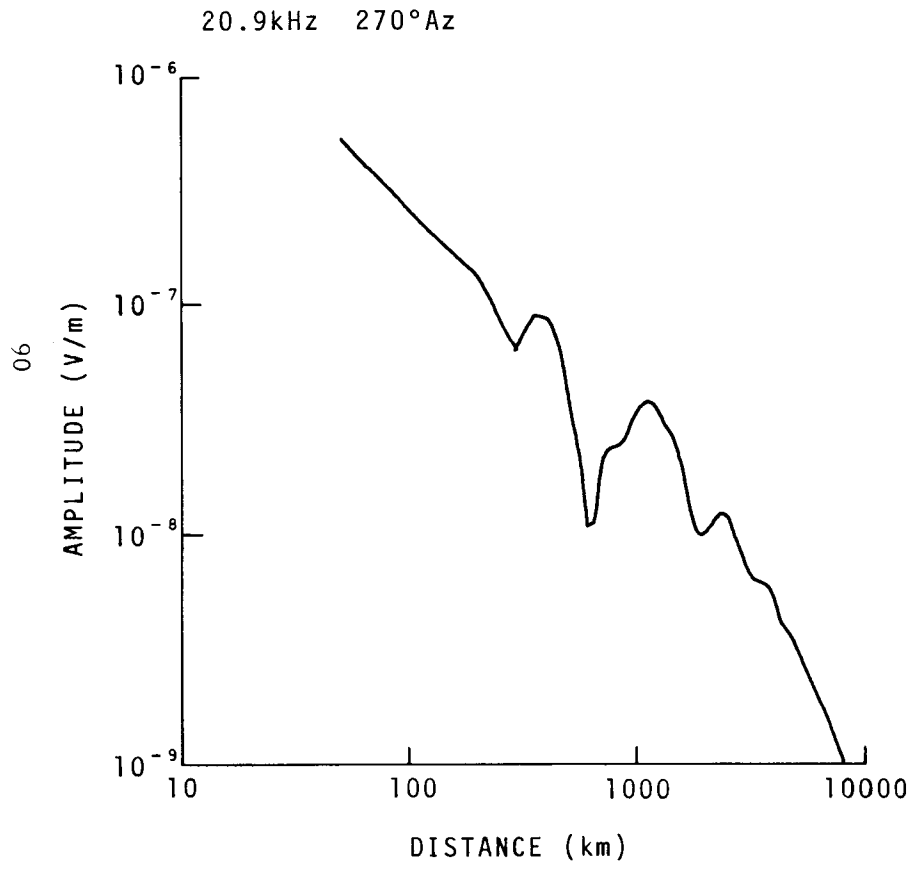

Figure 102.

AMPLITUDE
NORMAL NIGHT

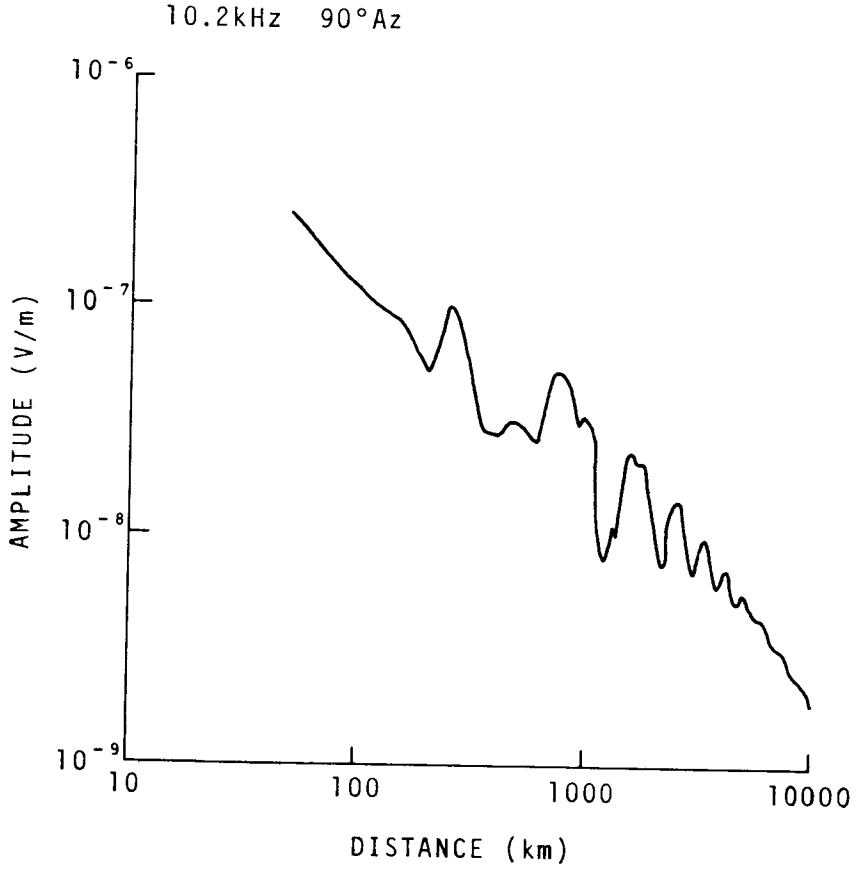

Figure 103.

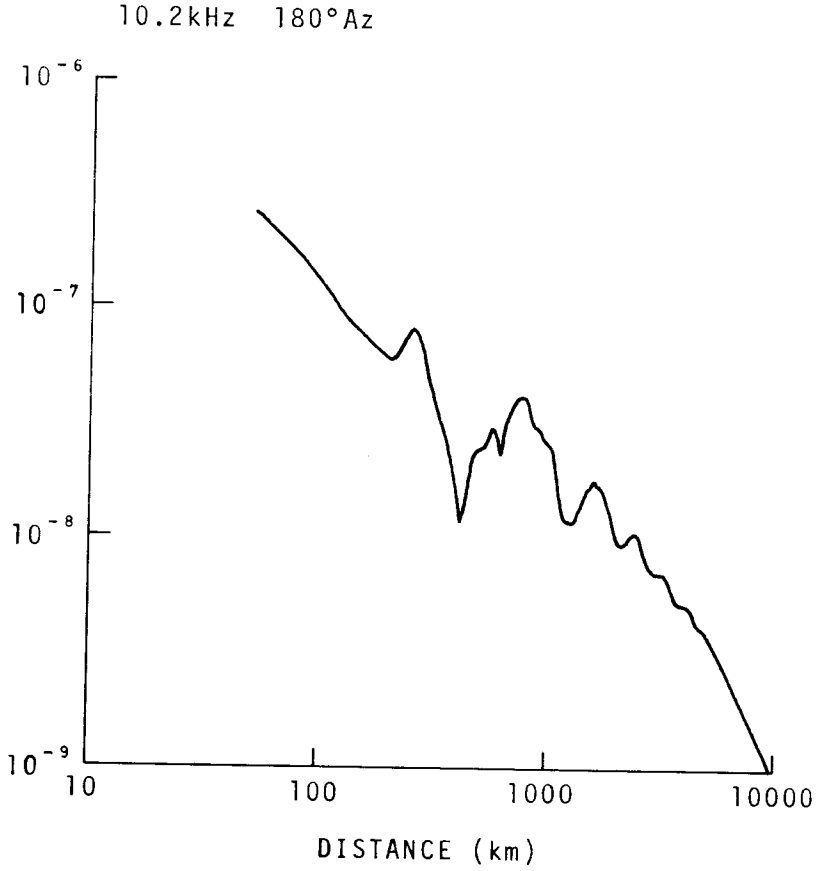

Figure 104.

AMPLITUDE
NORMAL NIGHT

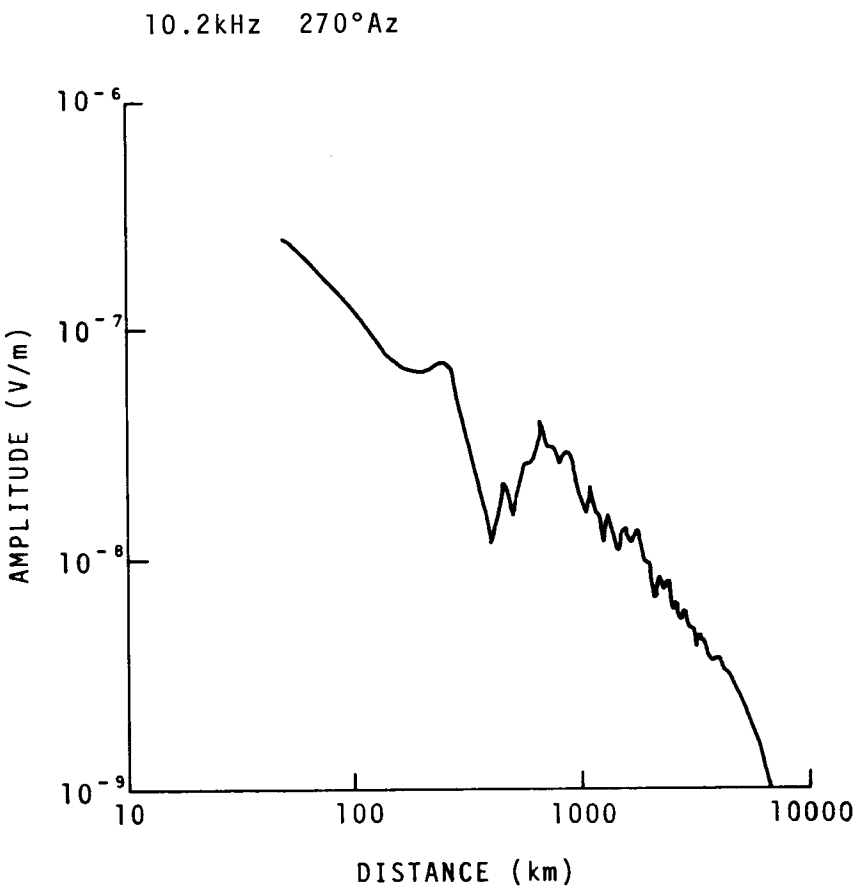

Figure 105.

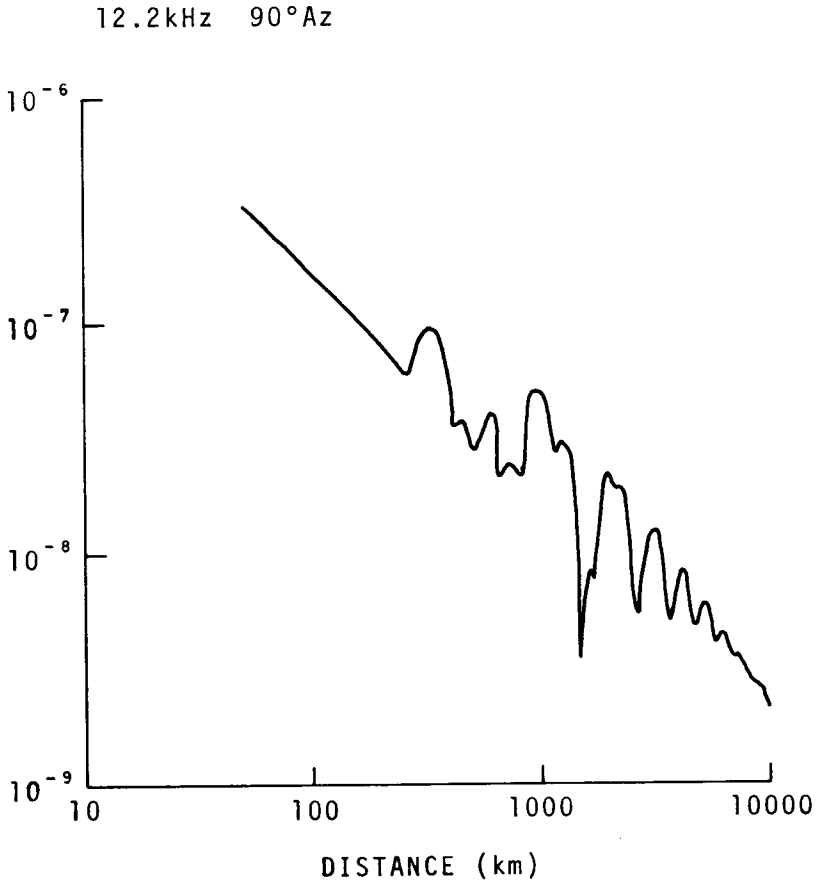

Figure 106.

AMPLITUDE
NORMAL NIGHT

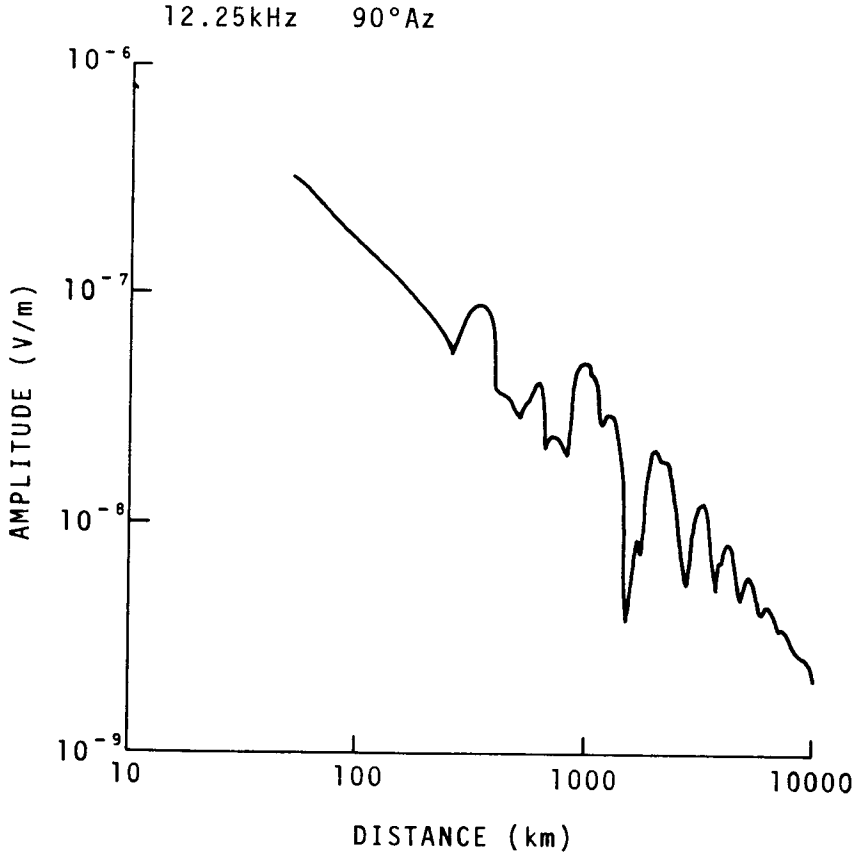

Figure 107.

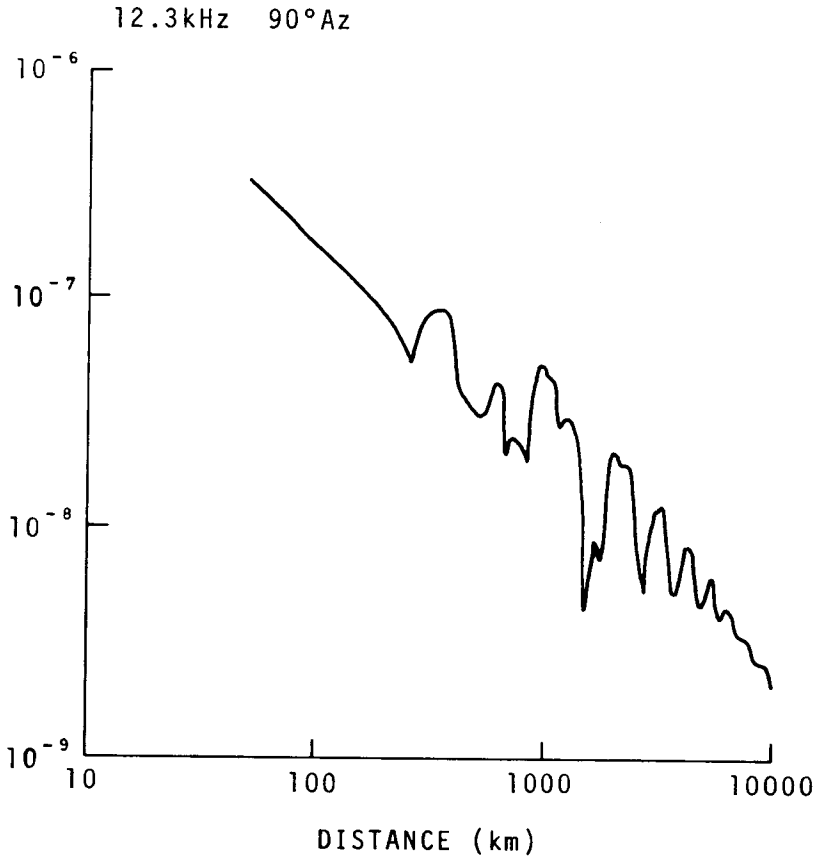

Figure 108.

AMPLITUDE
NORMAL NIGHT

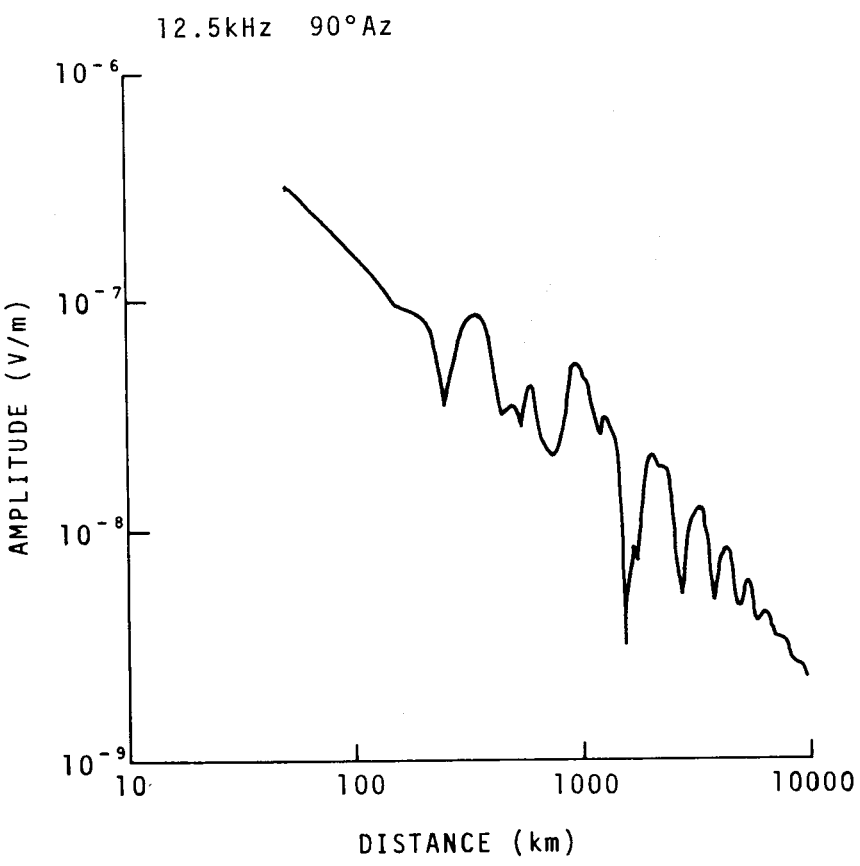

Figure 109.

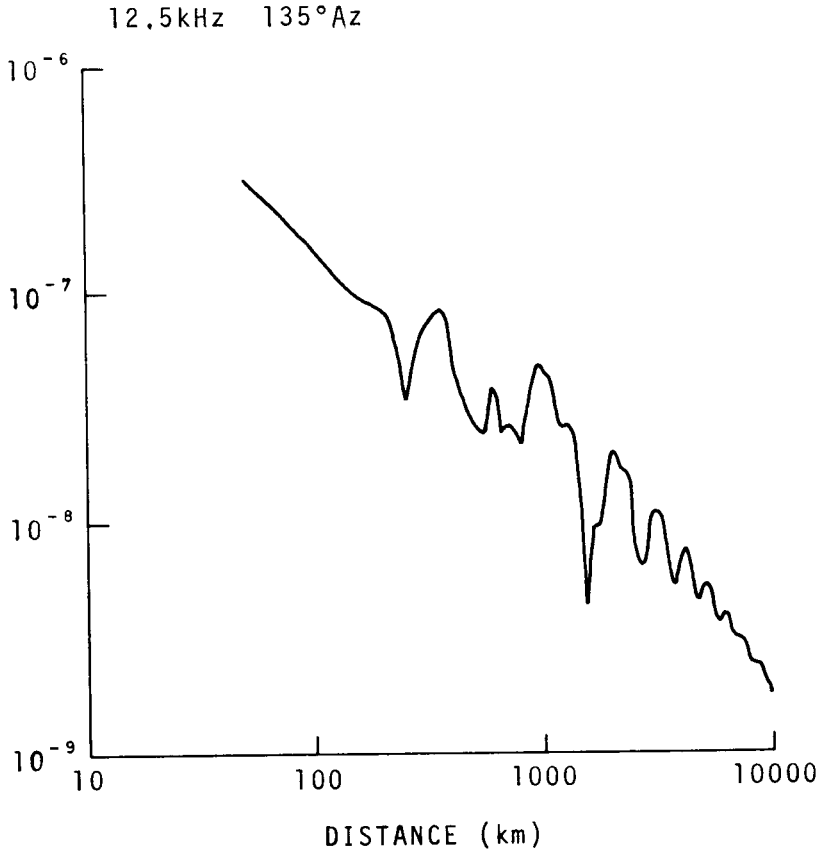

Figure 110.

AMPLITUDE
NORMAL NIGHT

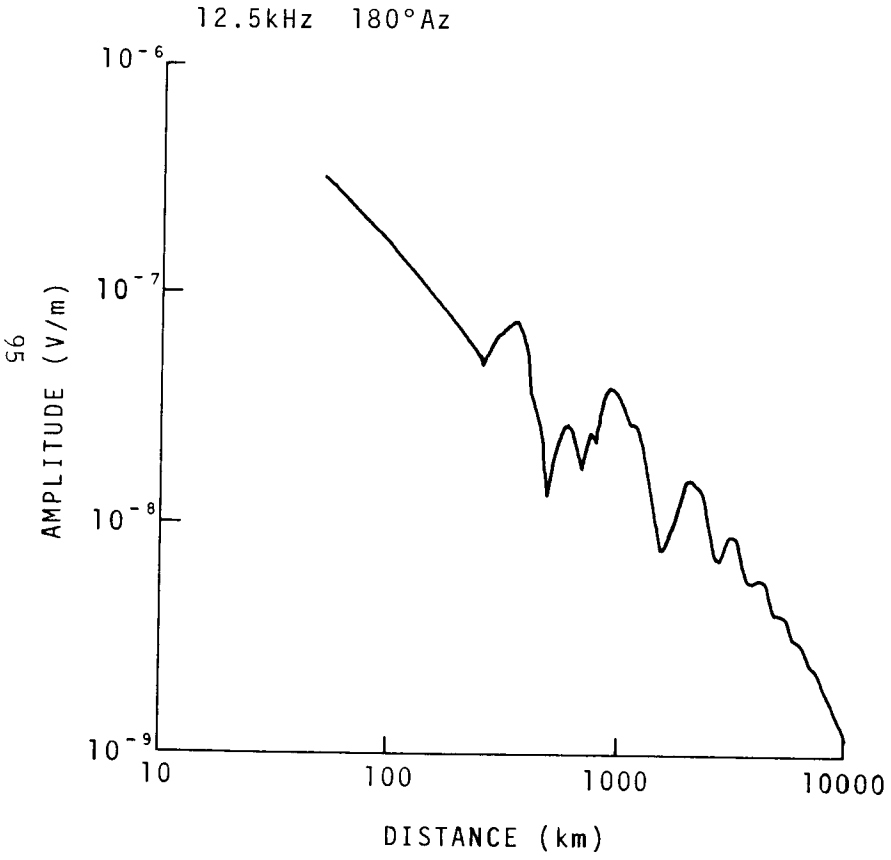

Figure 111.

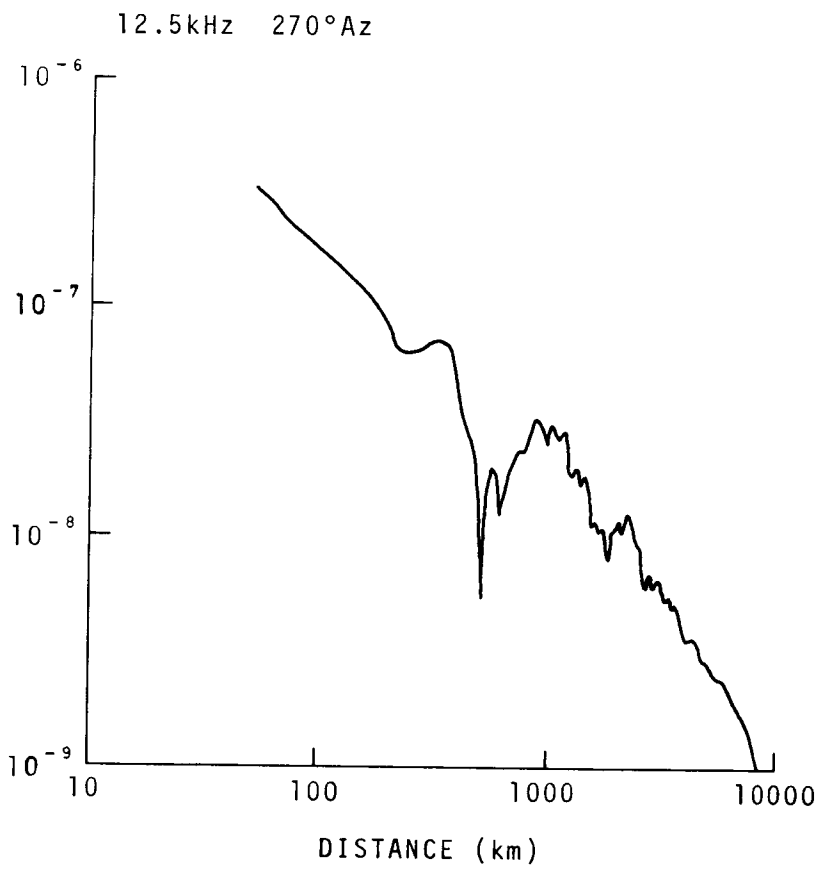

Figure 112.

AMPLITUDE
NORMAL NIGHT

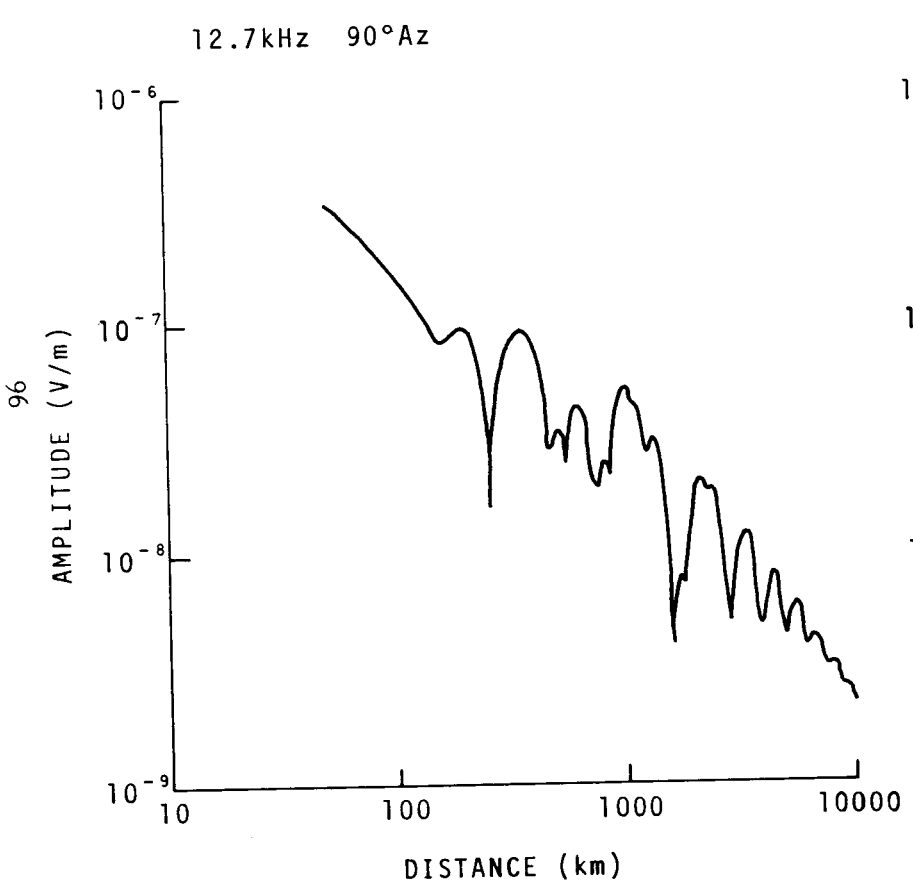

Figure 113.

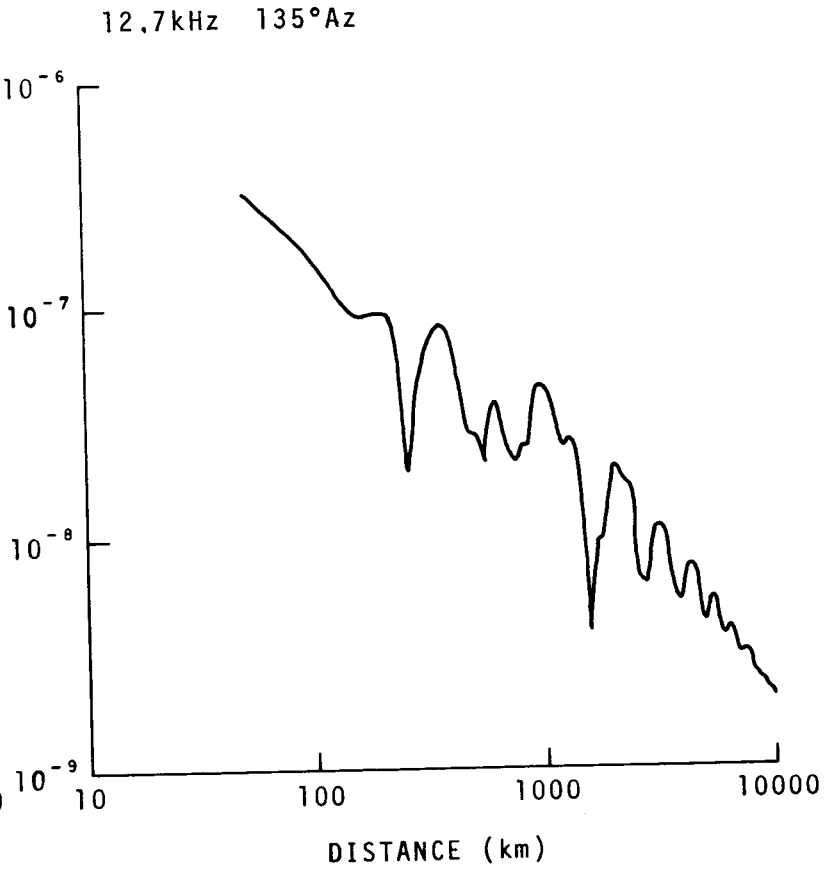

Figure 114.

AMPLITUDE
NORMAL NIGHT

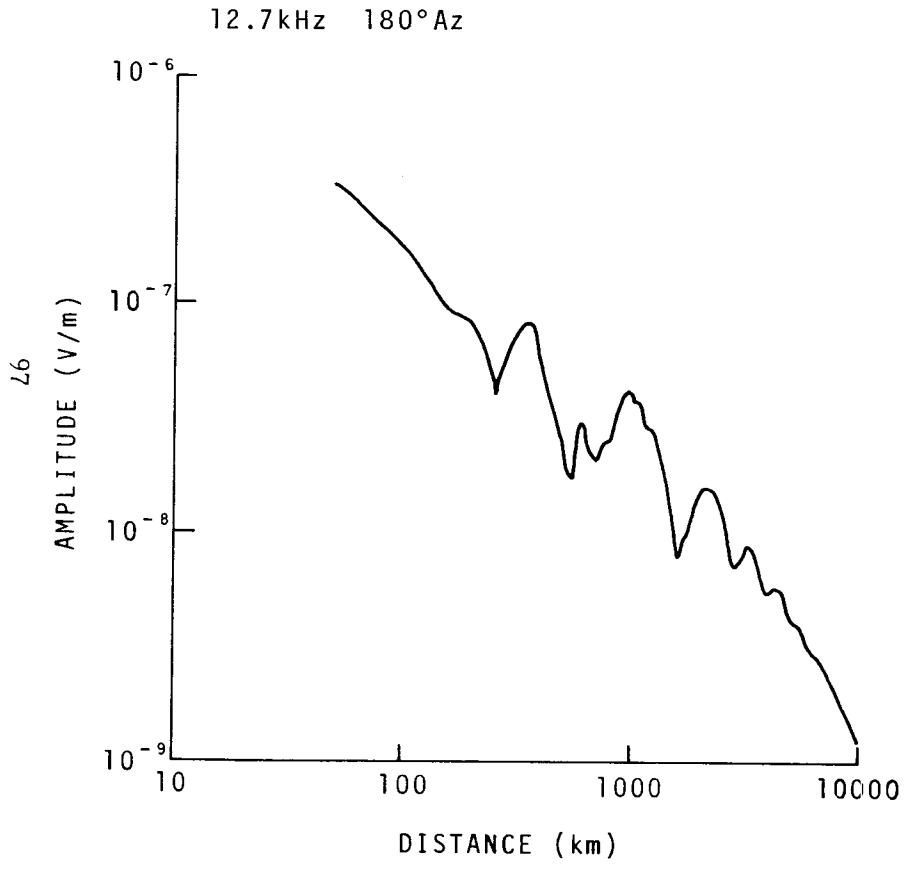

Figure 115.

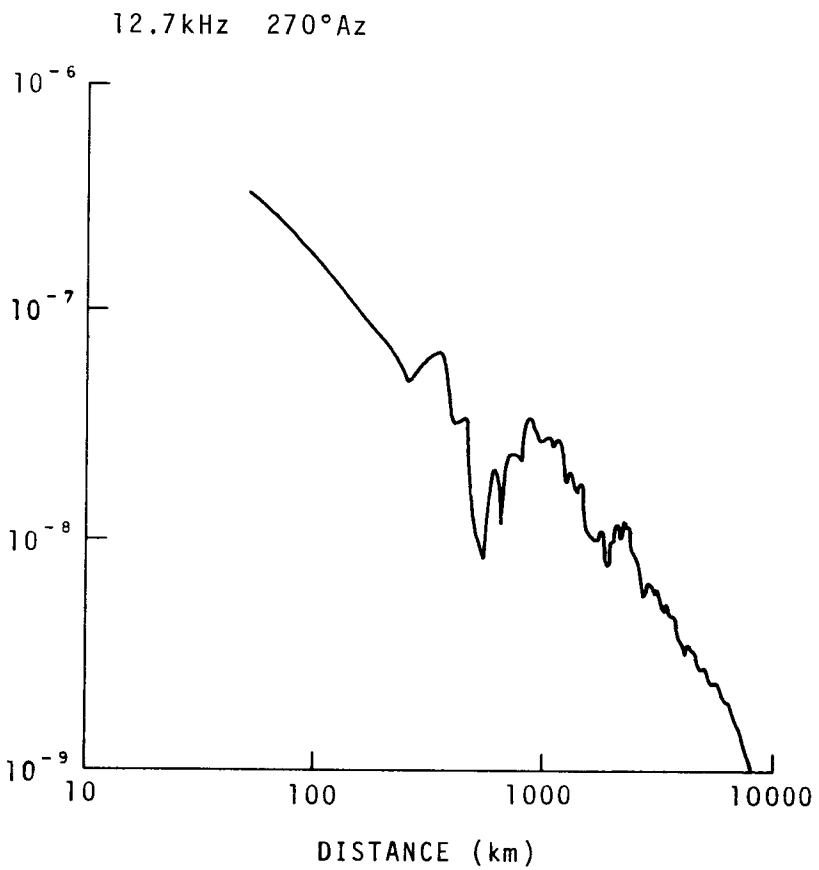

Figure 116.

AMPLITUDE
NORMAL NIGHT

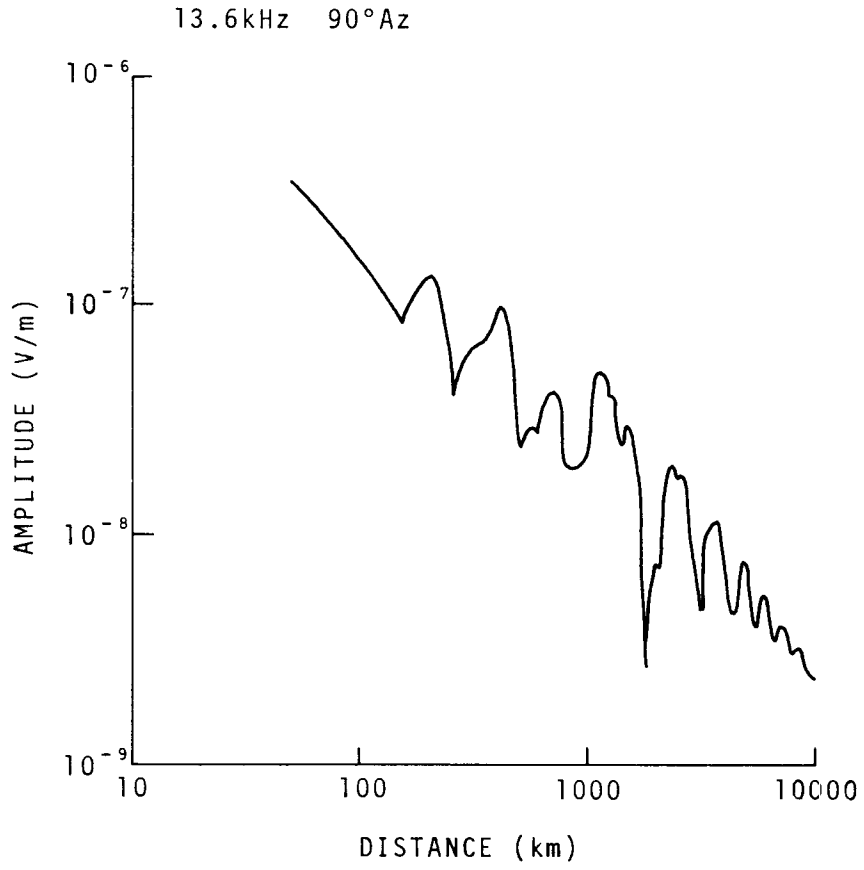

Figure 117.

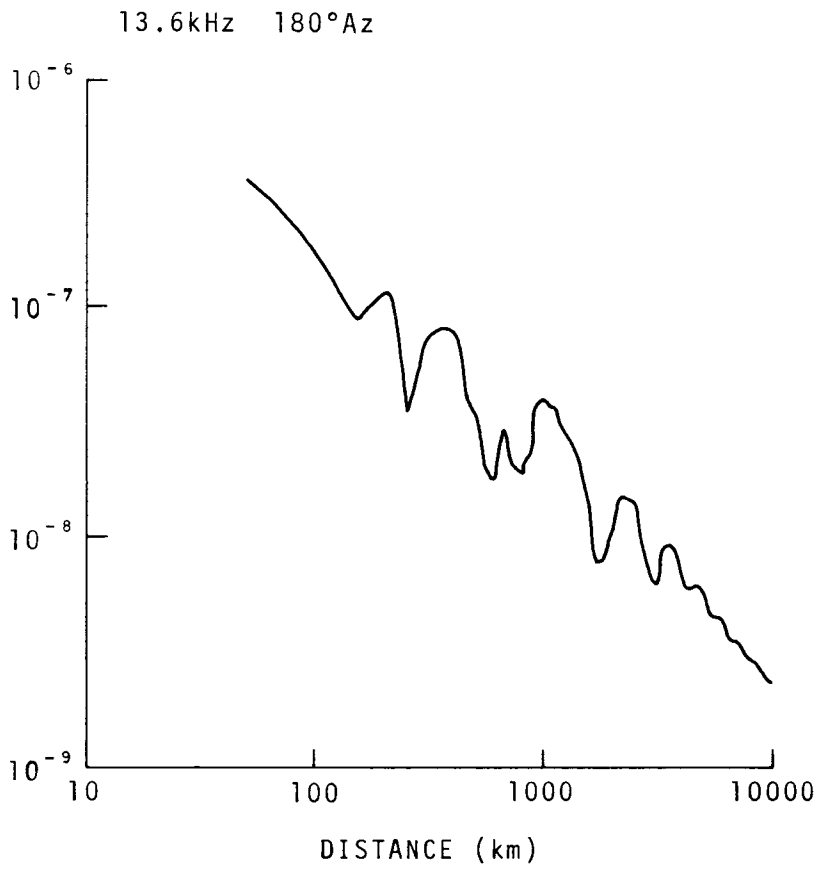

Figure 118.

AMPLITUDE
NORMAL NIGHT

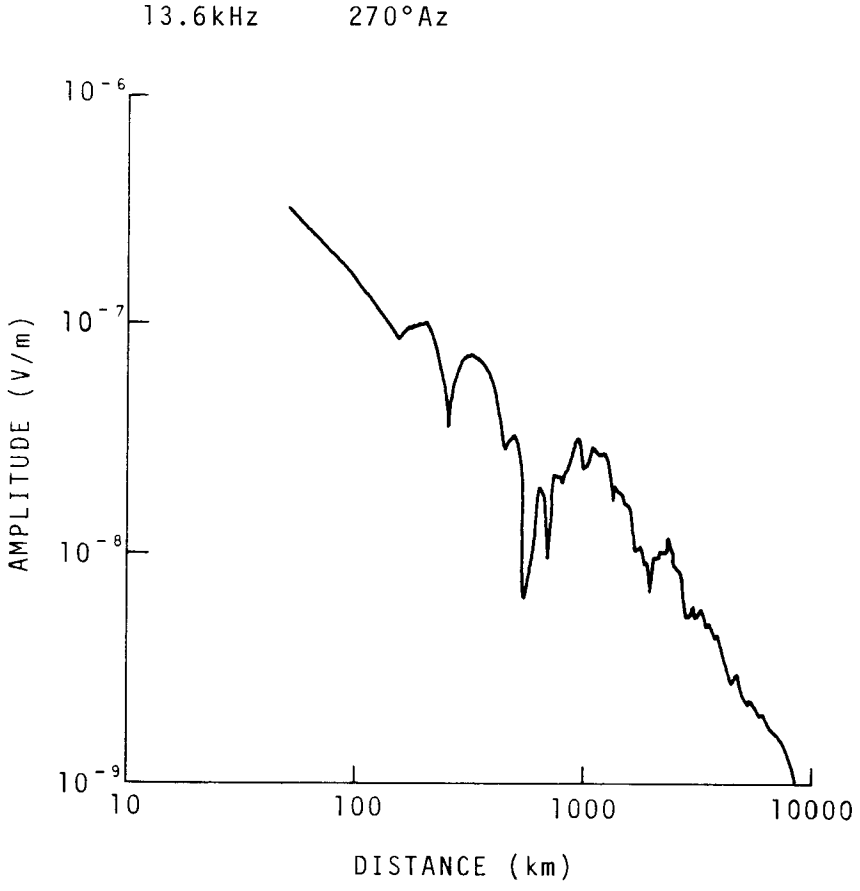

Figure 119.

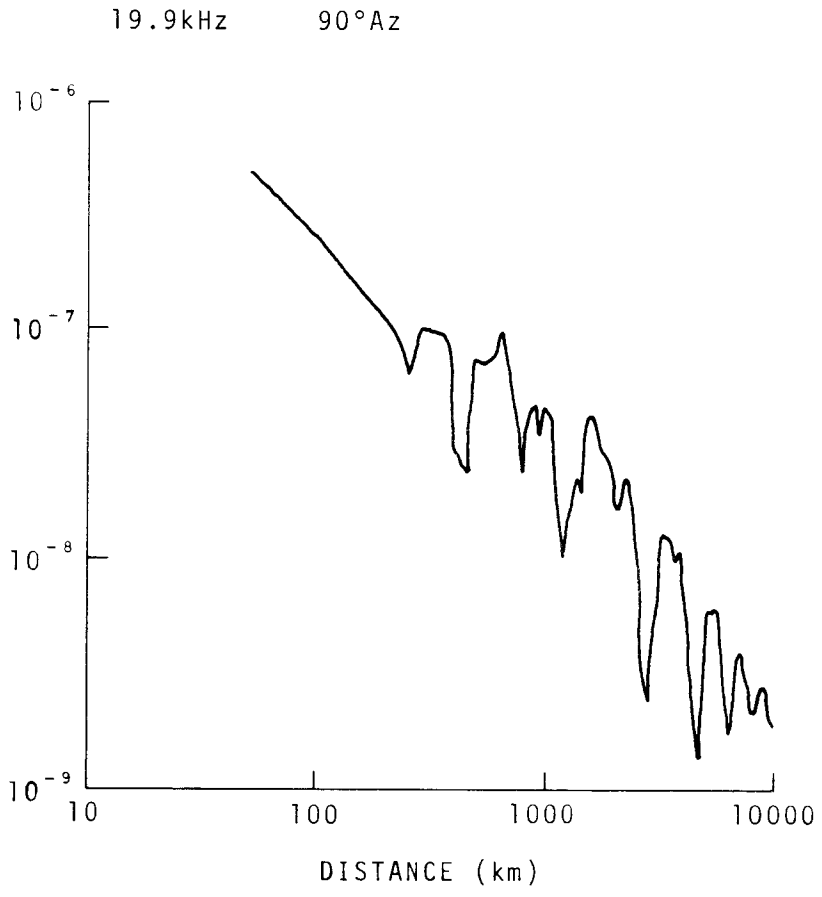

Figure 120.

AMPLITUDE
NORMAL NIGHT

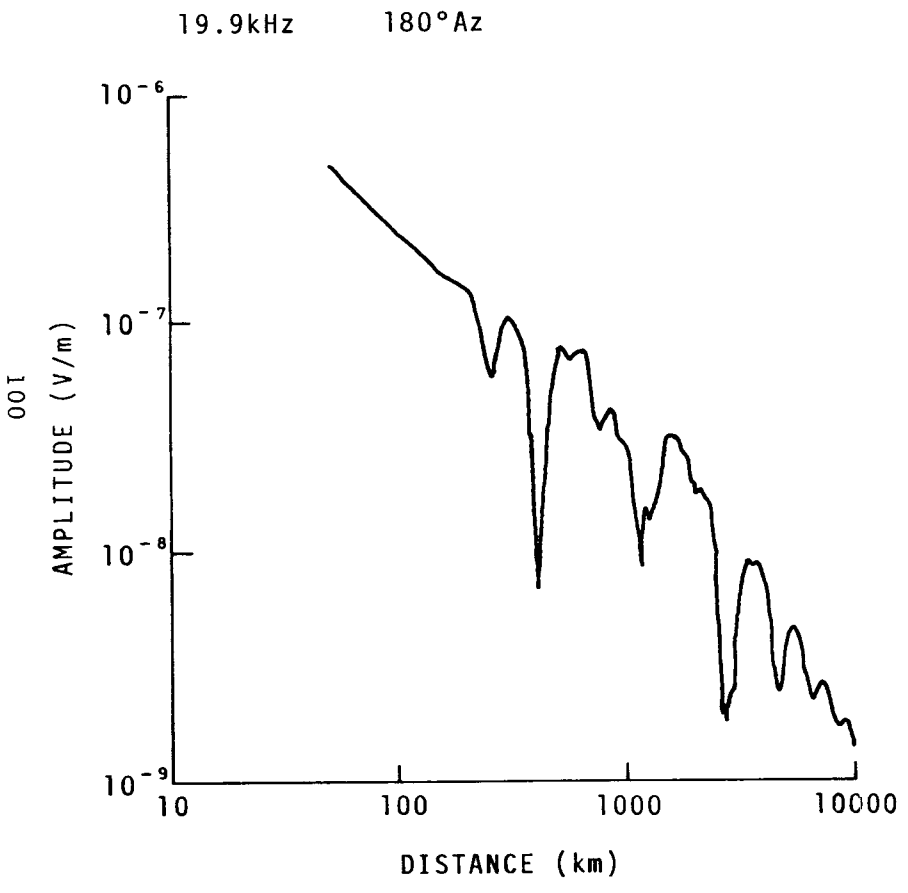

Figure 121.

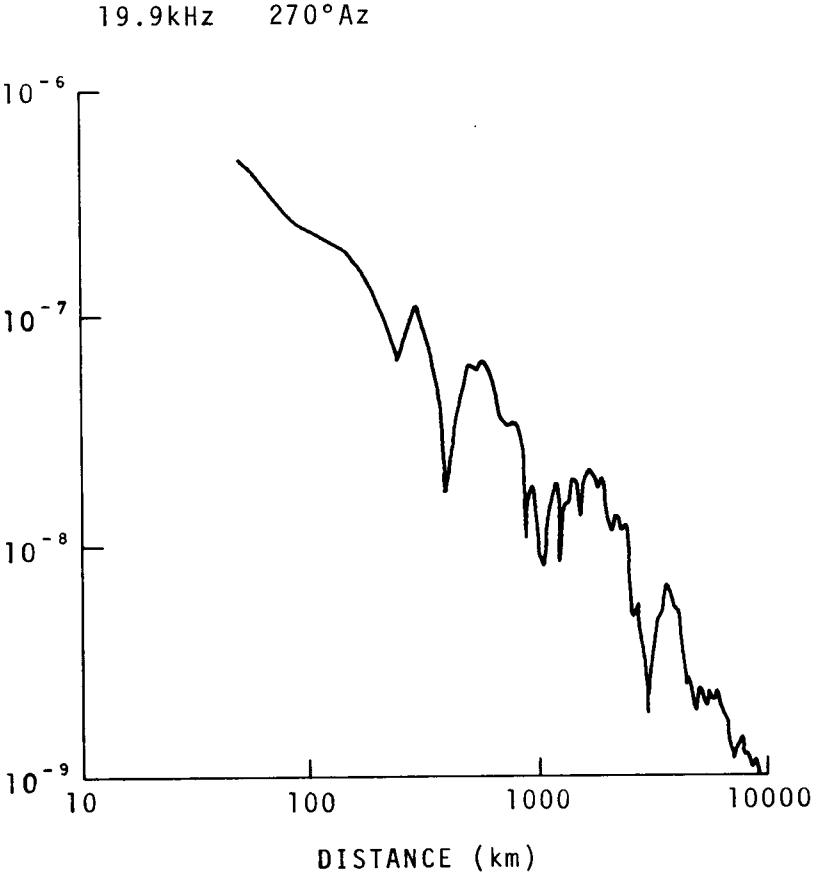

Figure 122.

AMPLITUDE
NORMAL NIGHT

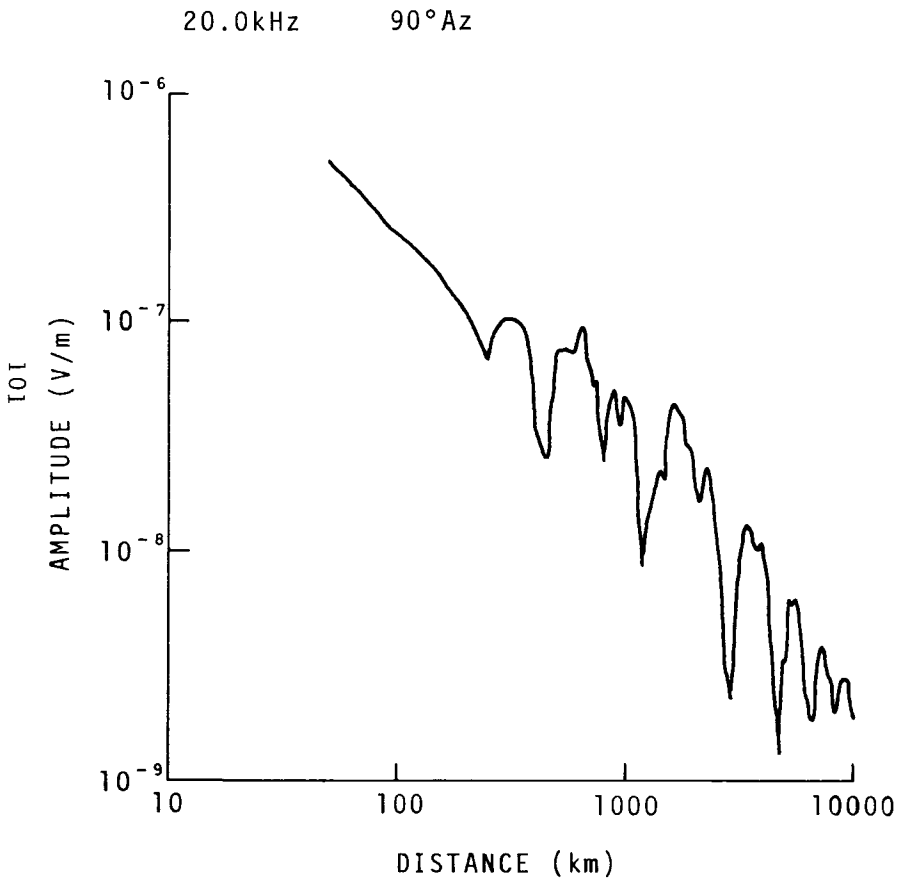

Figure 123.

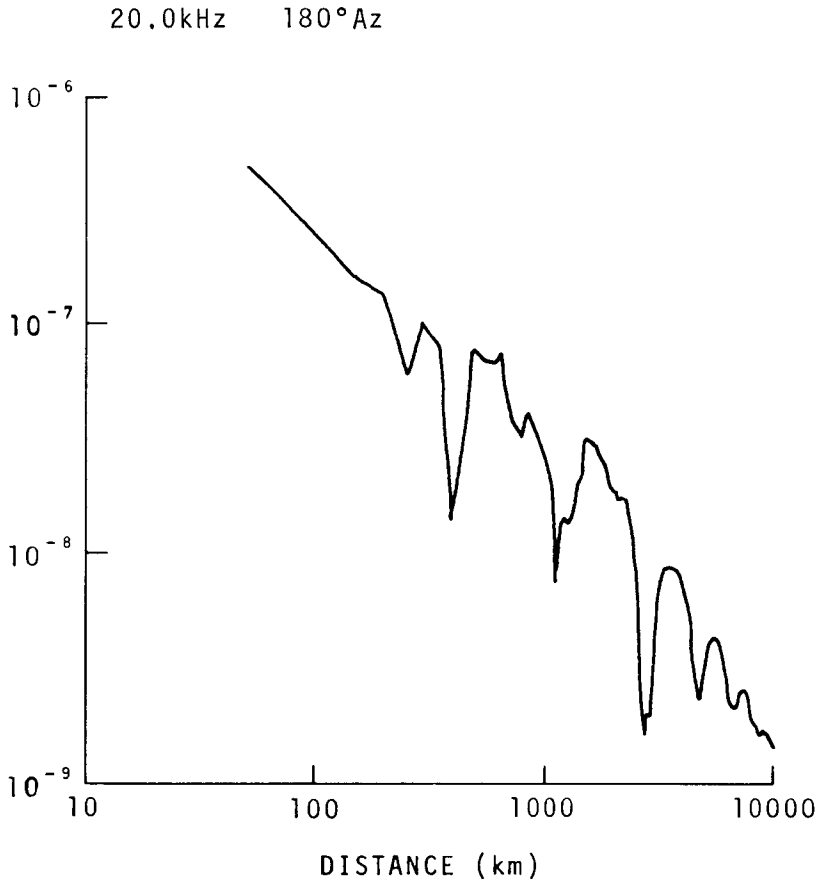

Figure 124.

AMPLITUDE
NORMAL NIGHT

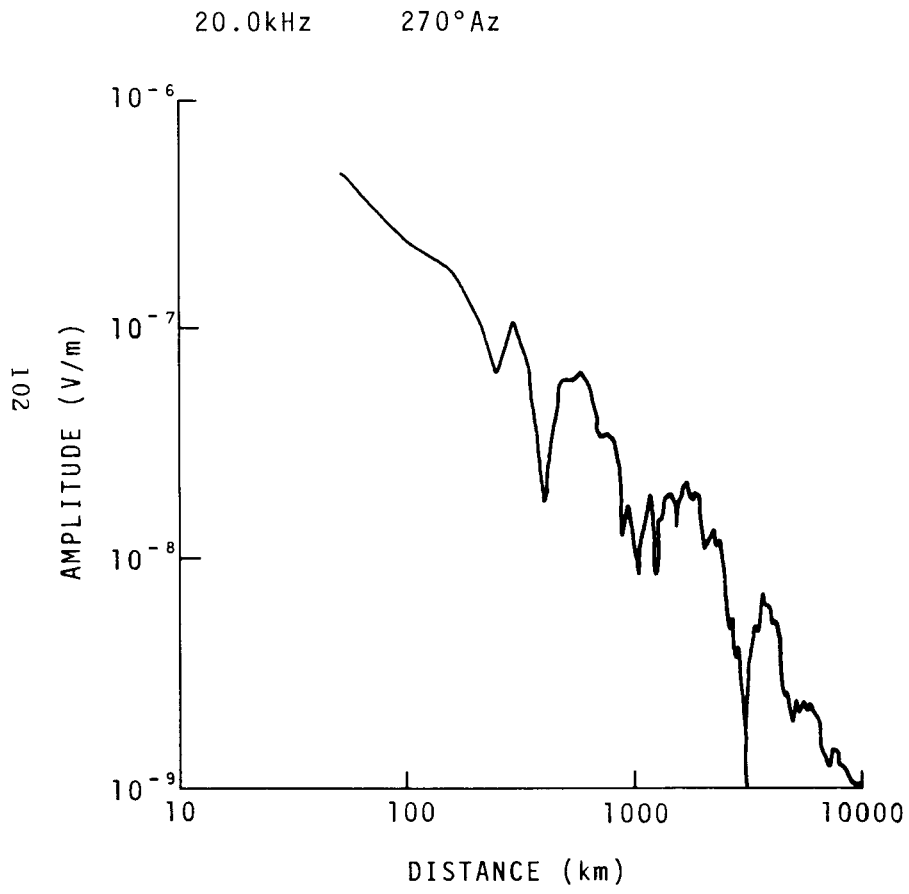

Figure 125.

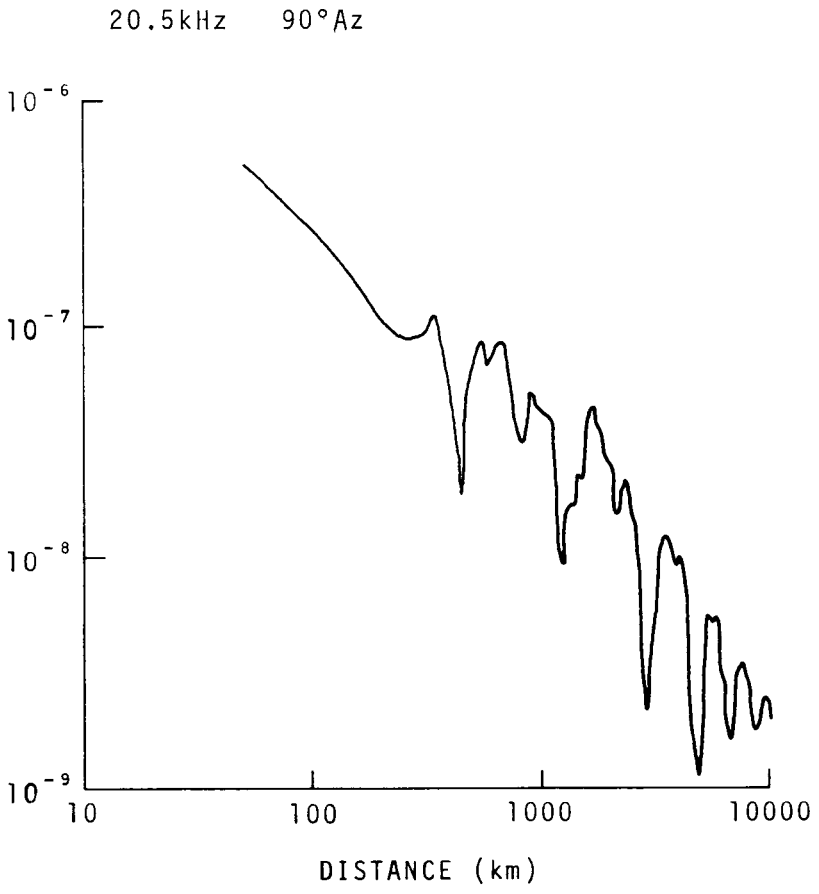

Figure 126.

AMPLITUDE
NORMAL NIGHT

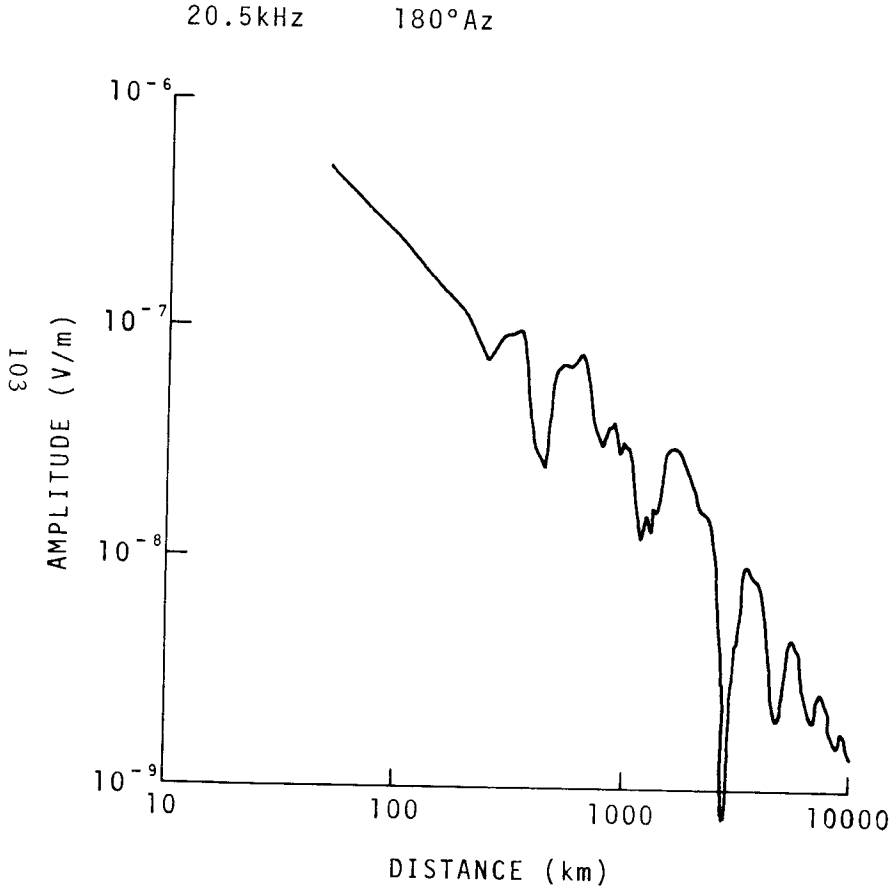

Figure 127.

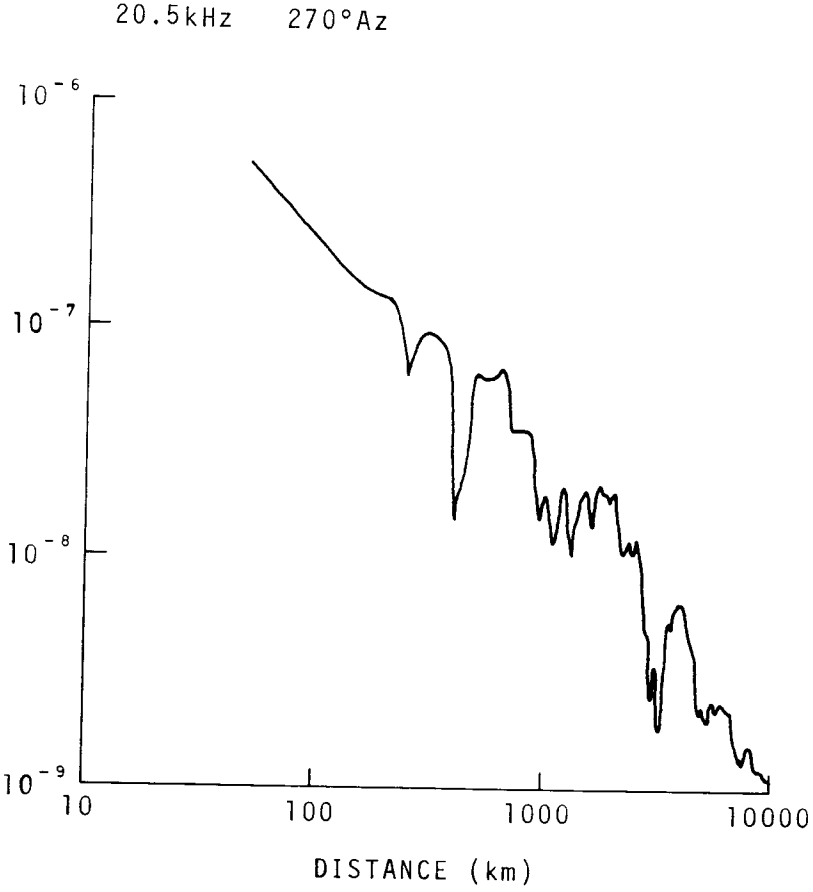

Figure 128.

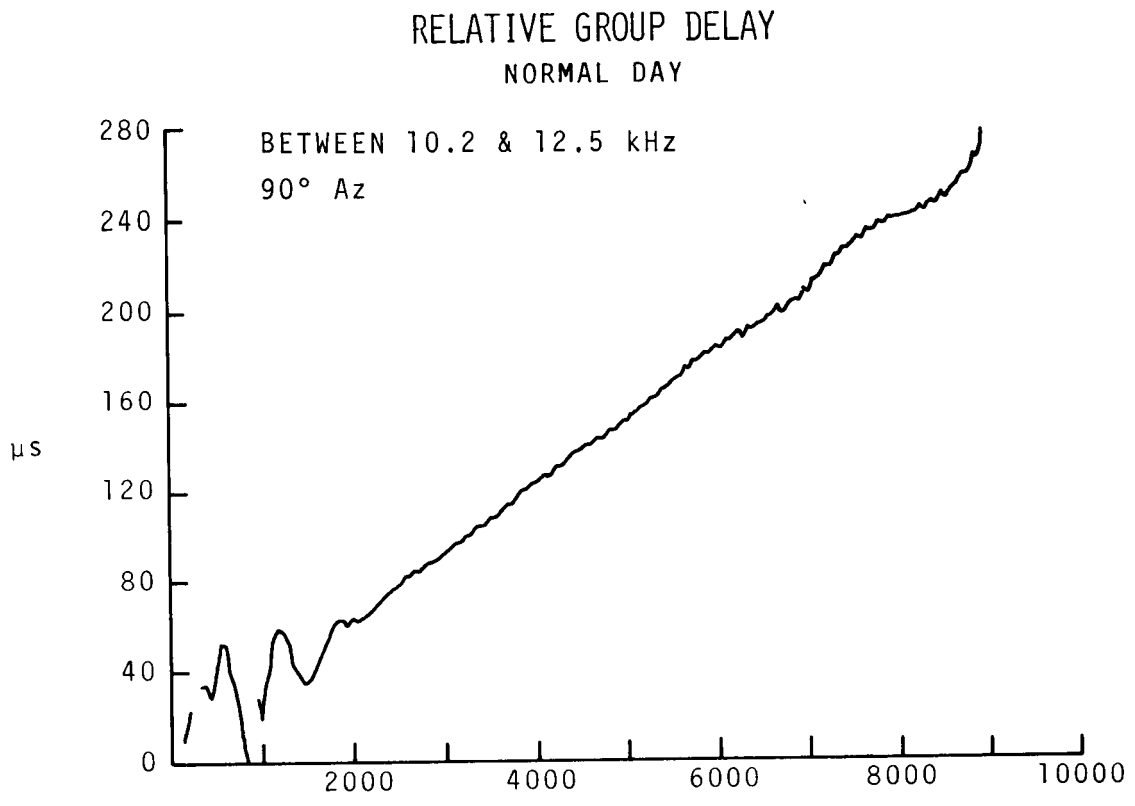

Figure 129.

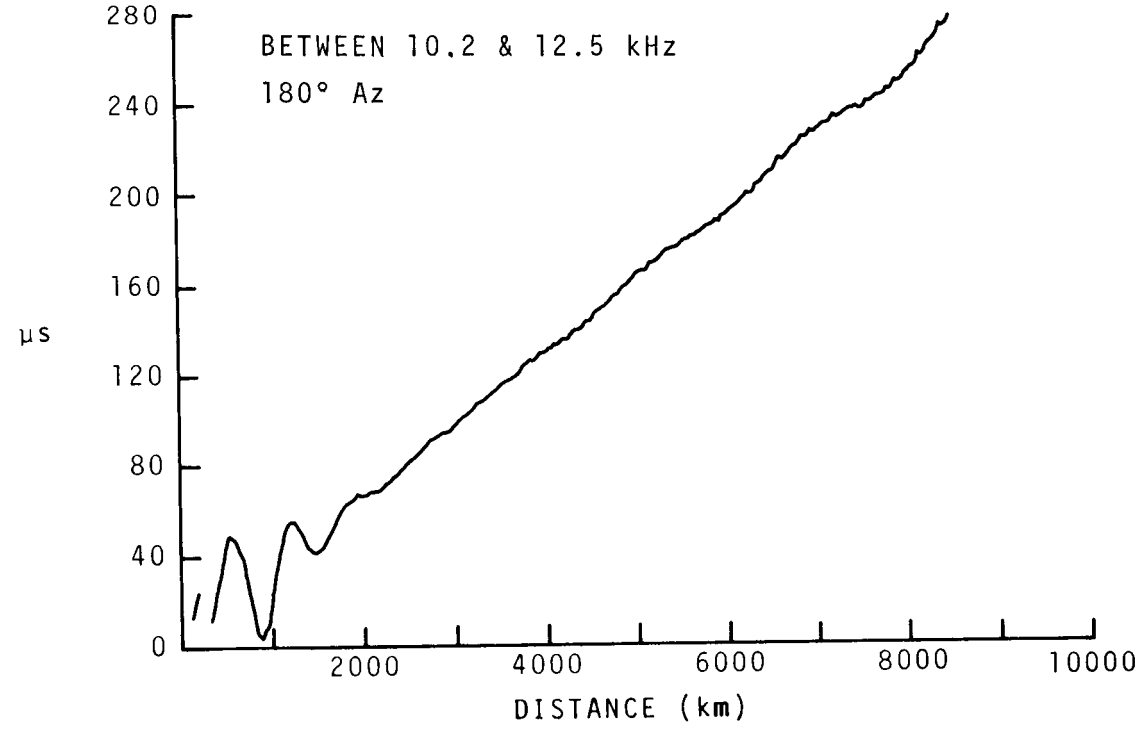

Figure 130.

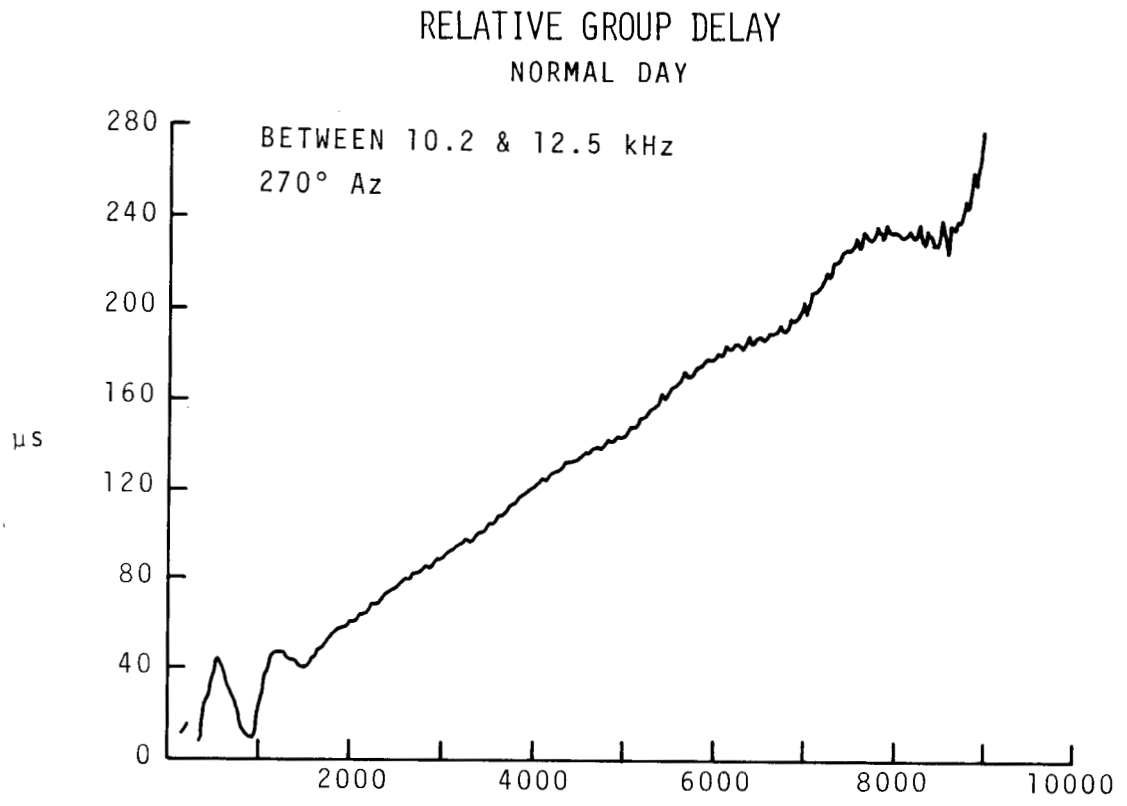

Figure 131.

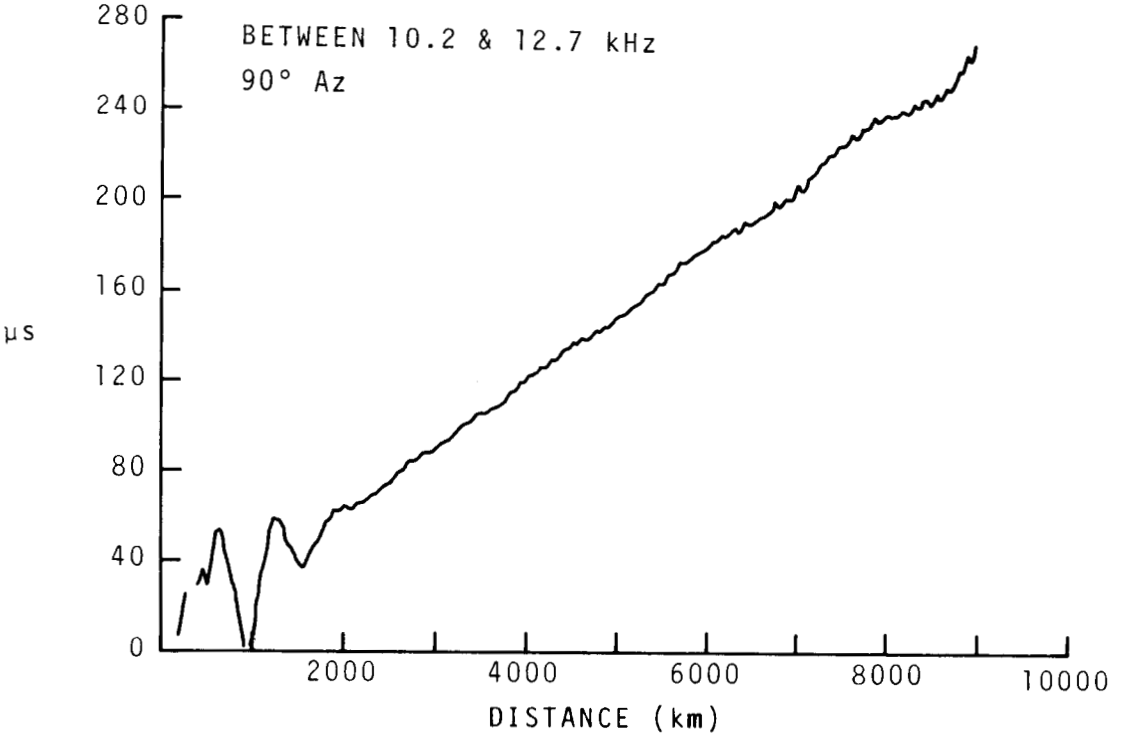

Figure 132.

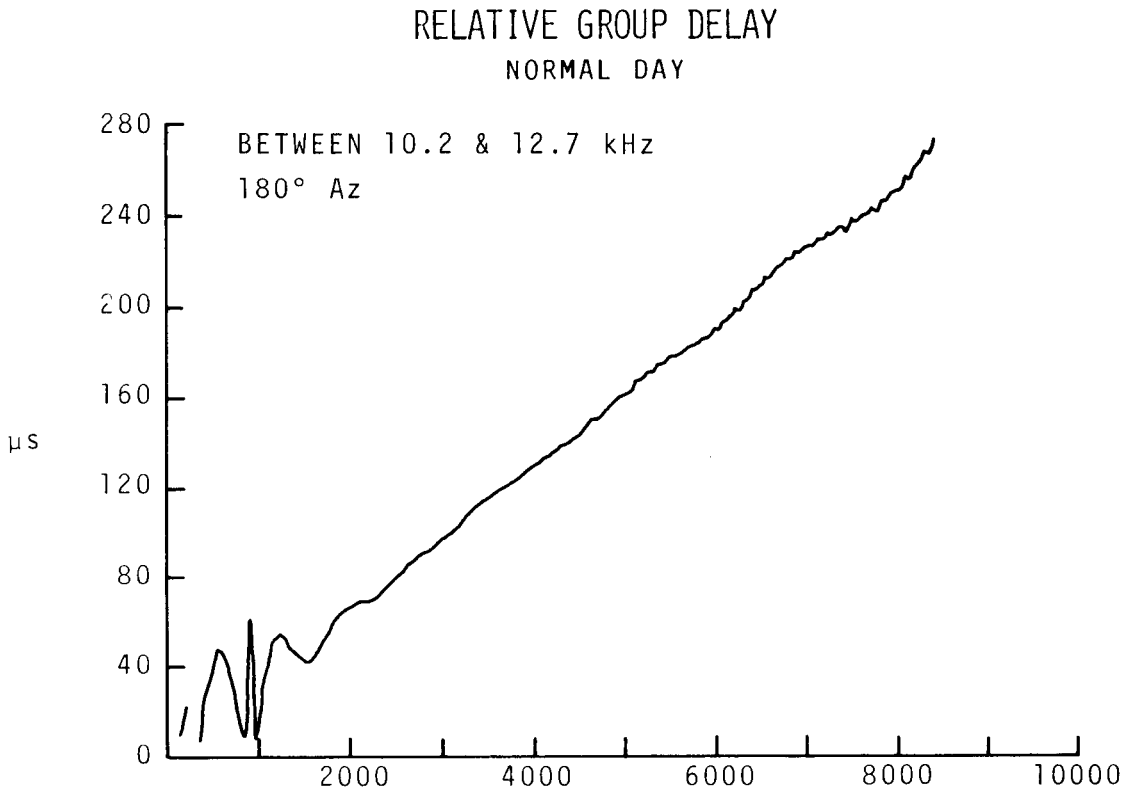

Figure 133.

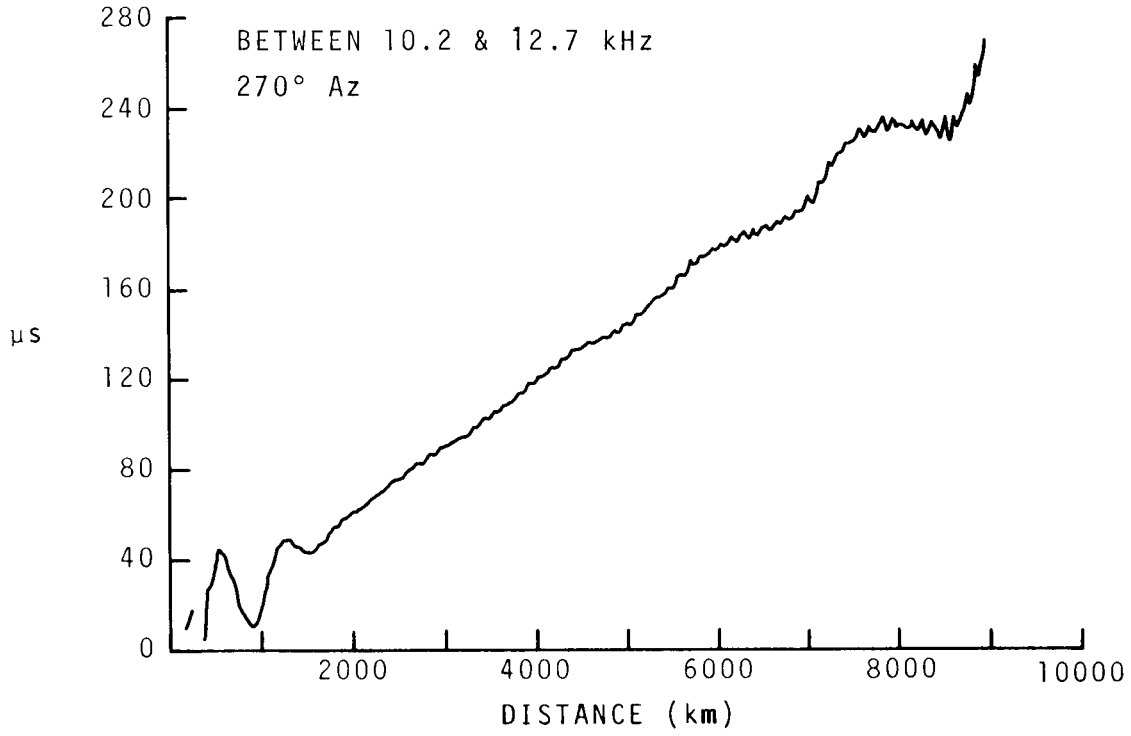

Figure 134.

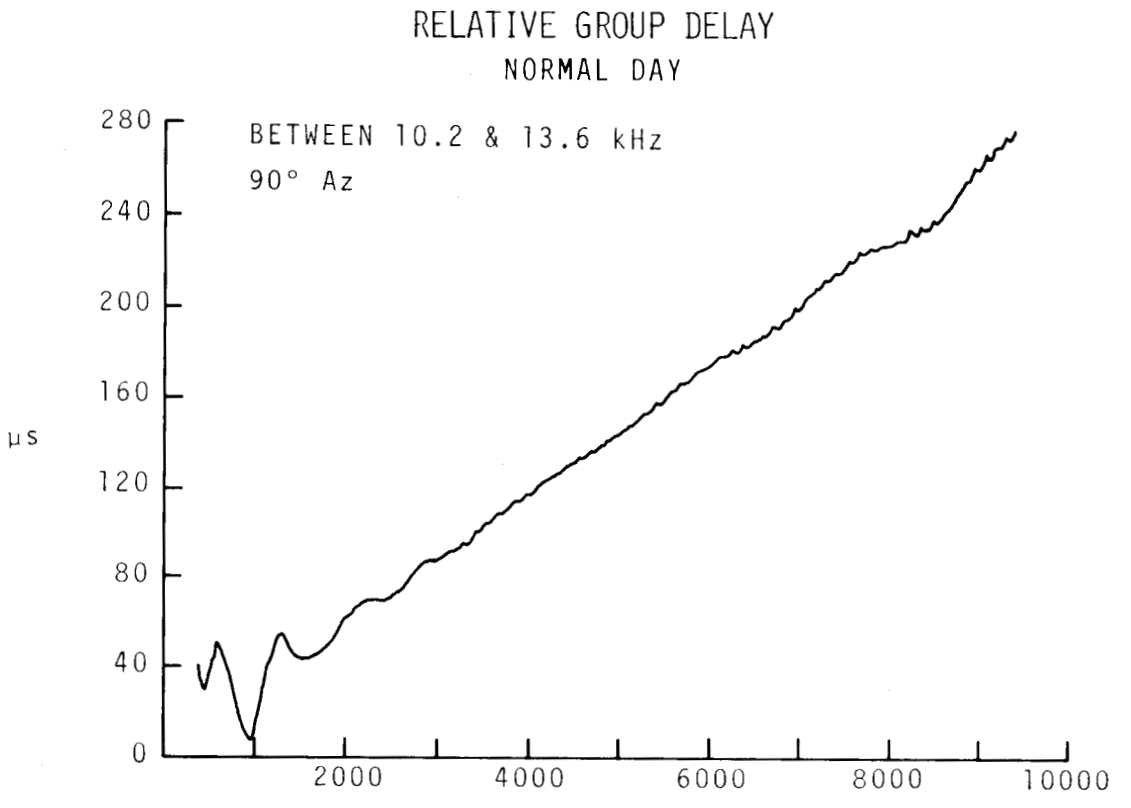

Figure 135.

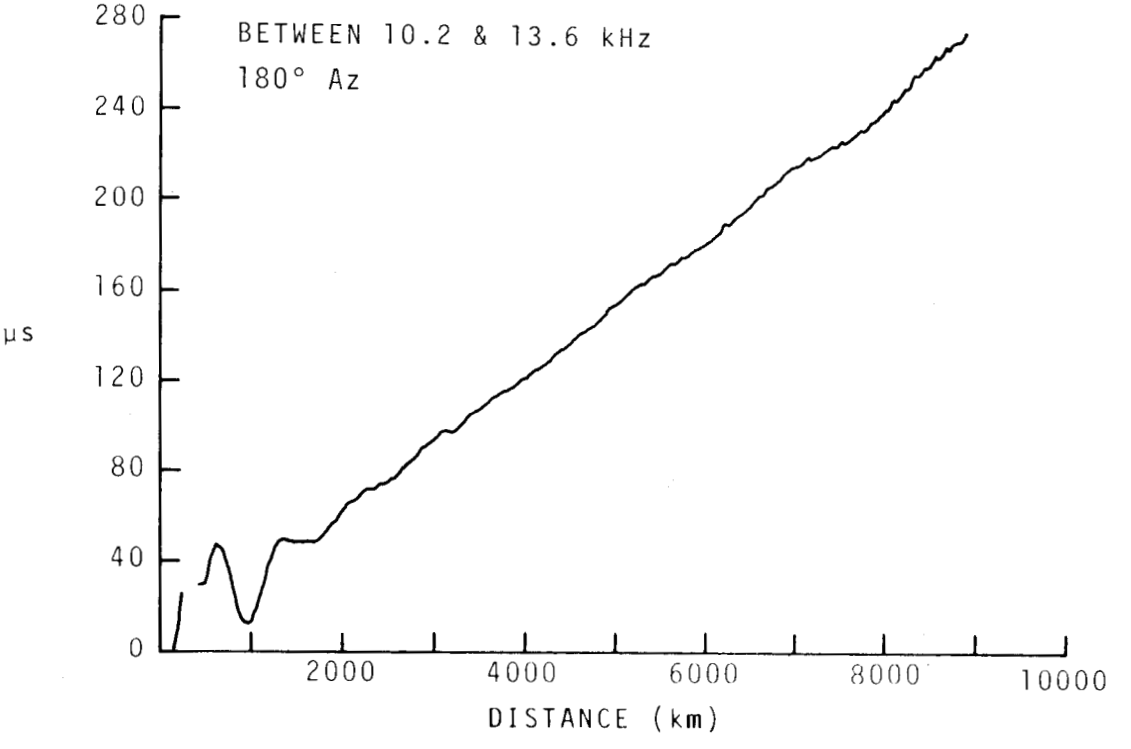

Figure 136.

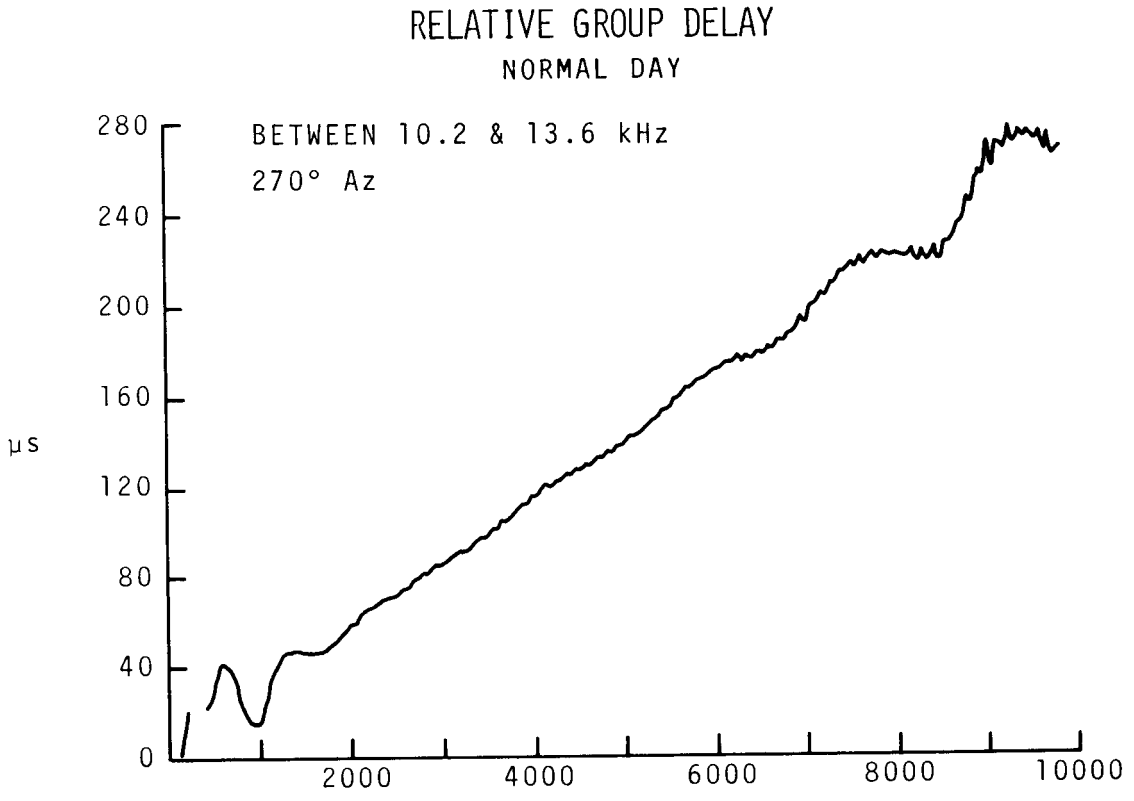

Figure 137.

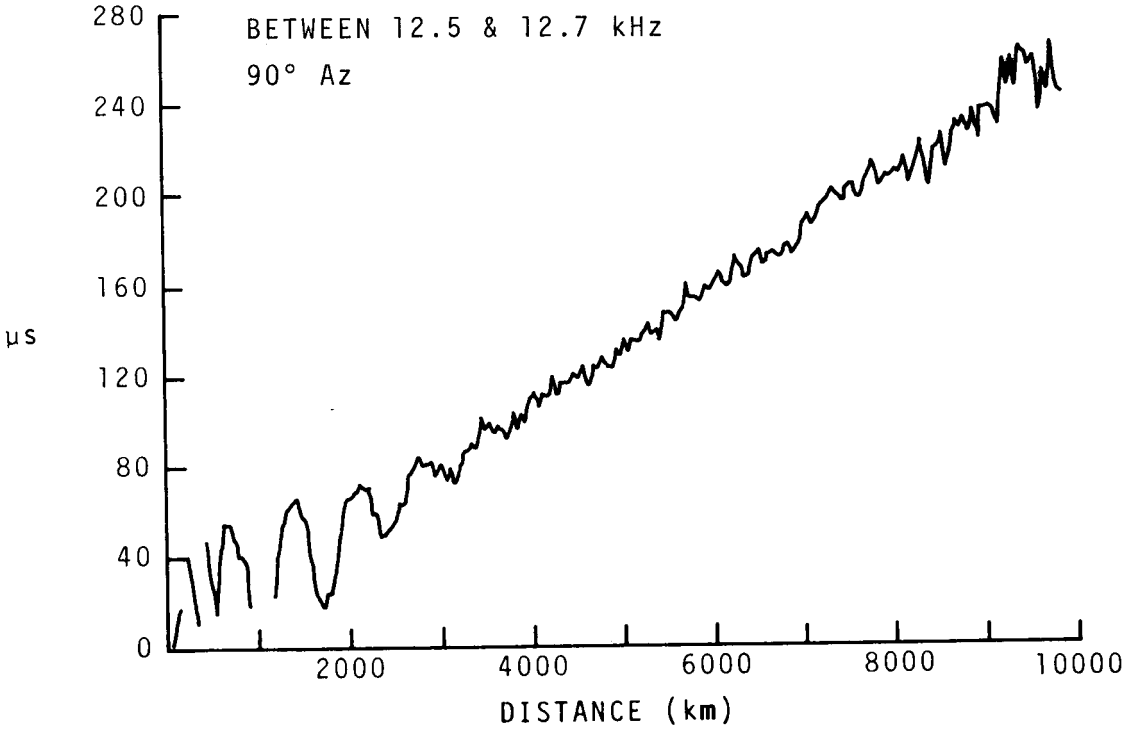

Figure 138.

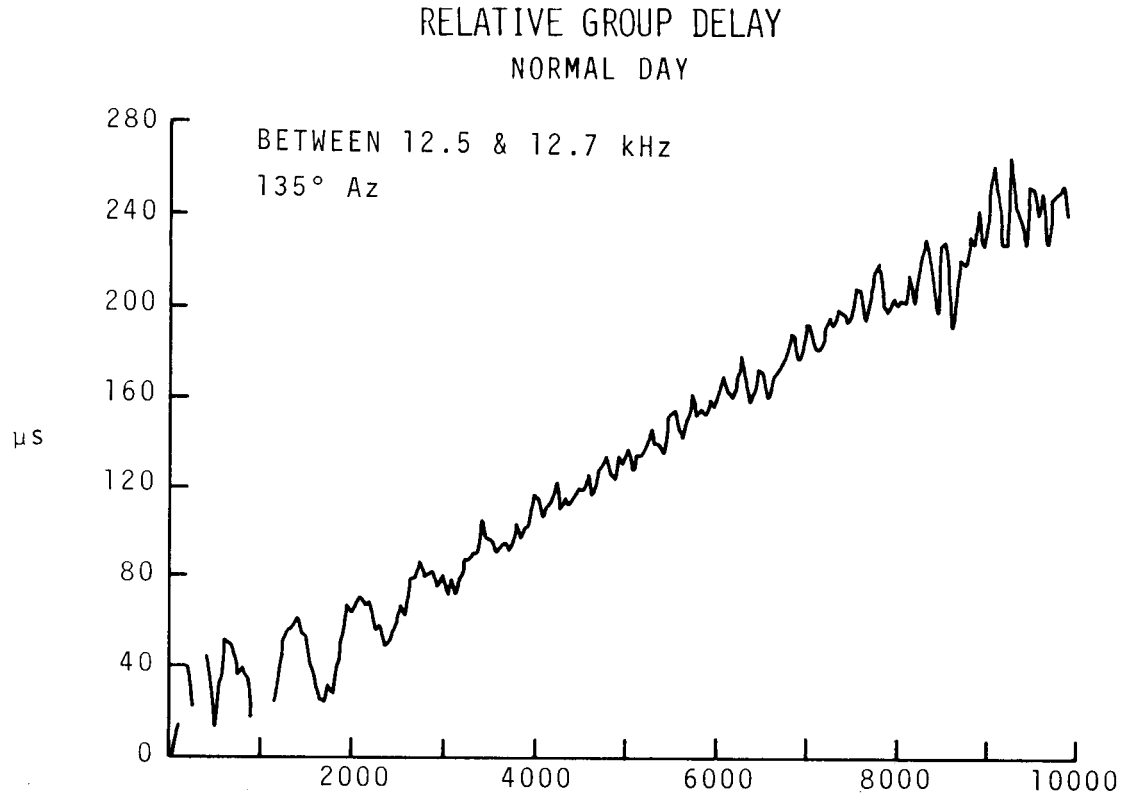

Figure 139.

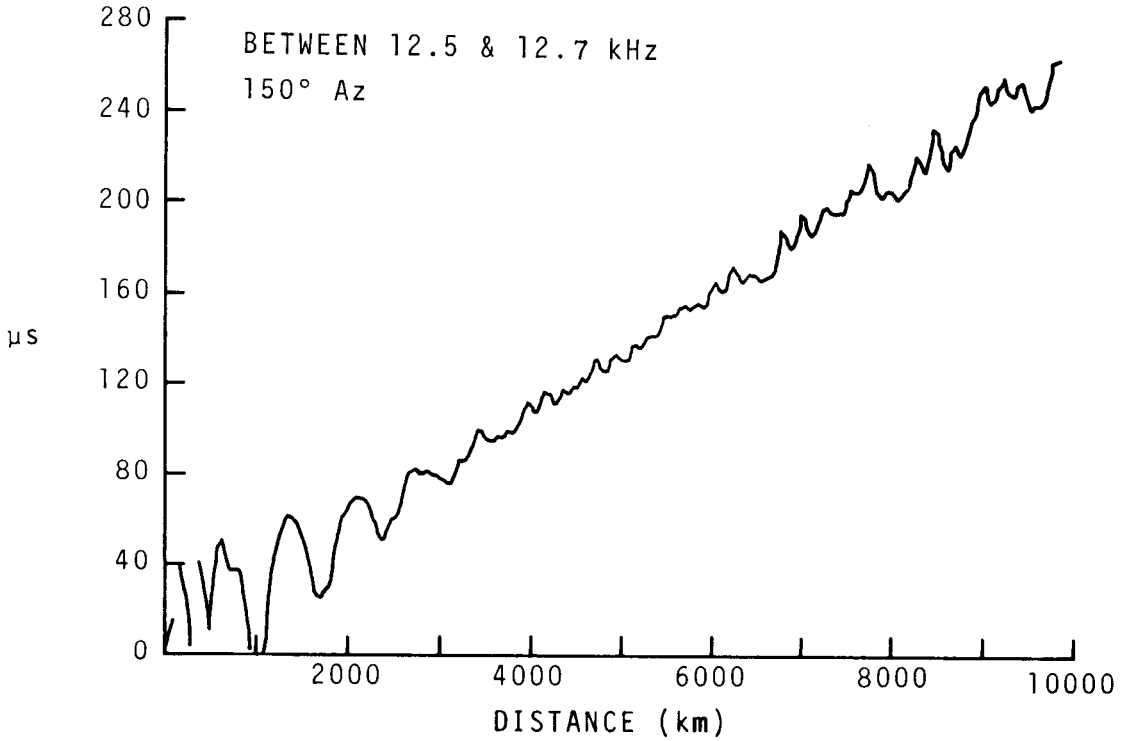

Figure 140.

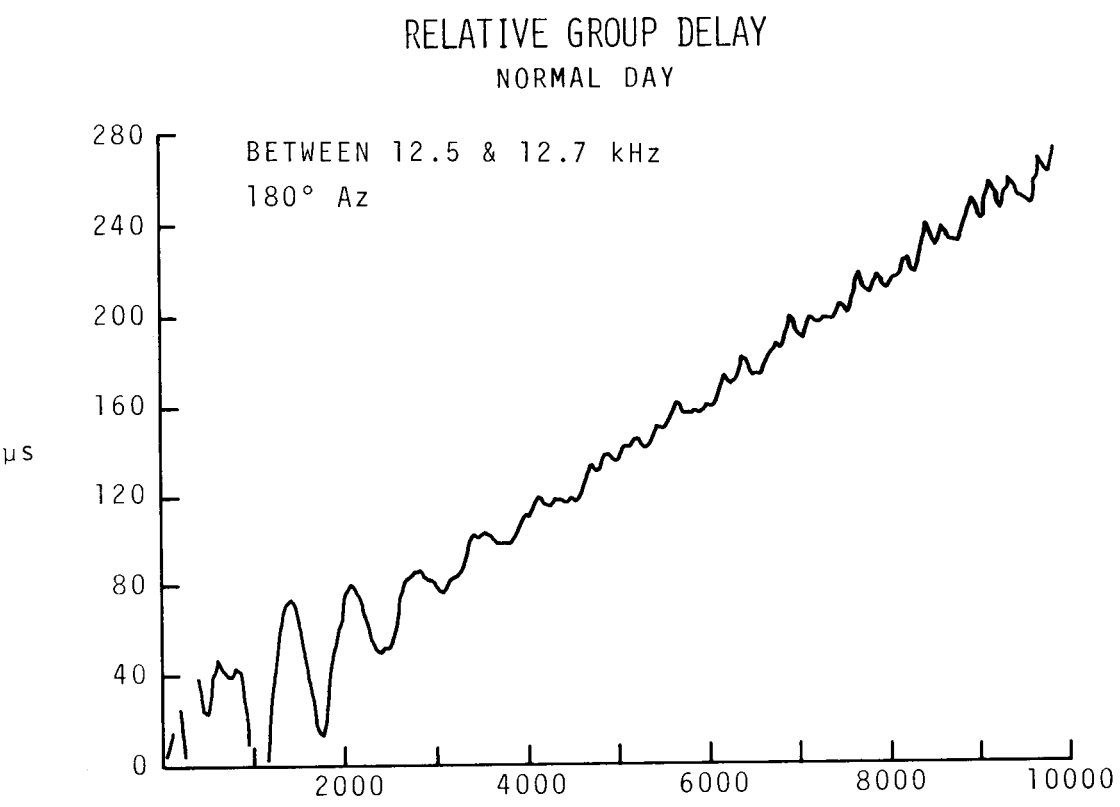

Figure 141.

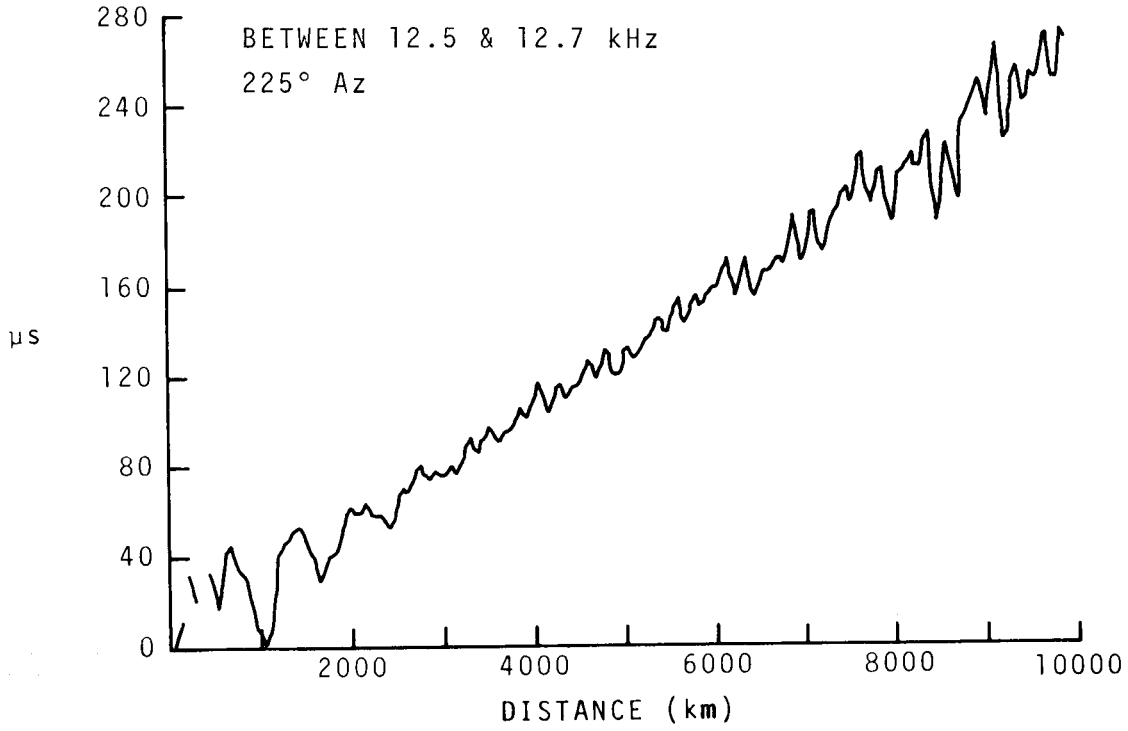

Figure 142.

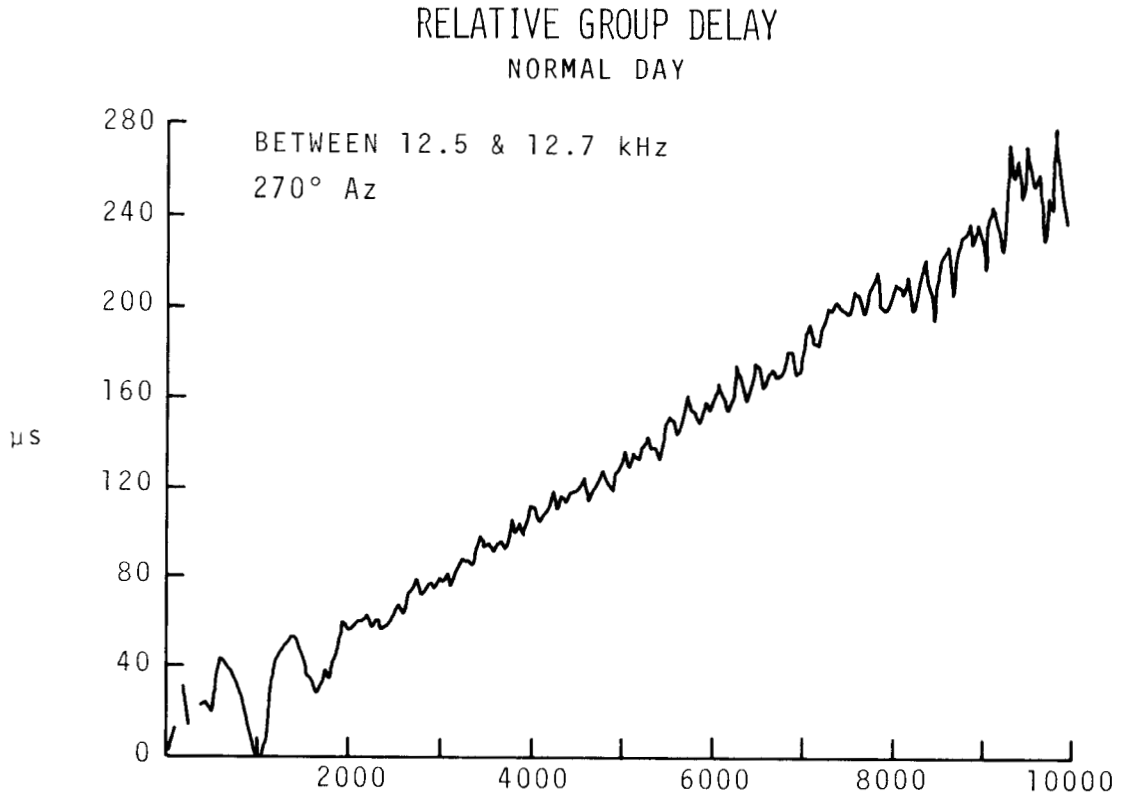

Figure 143.

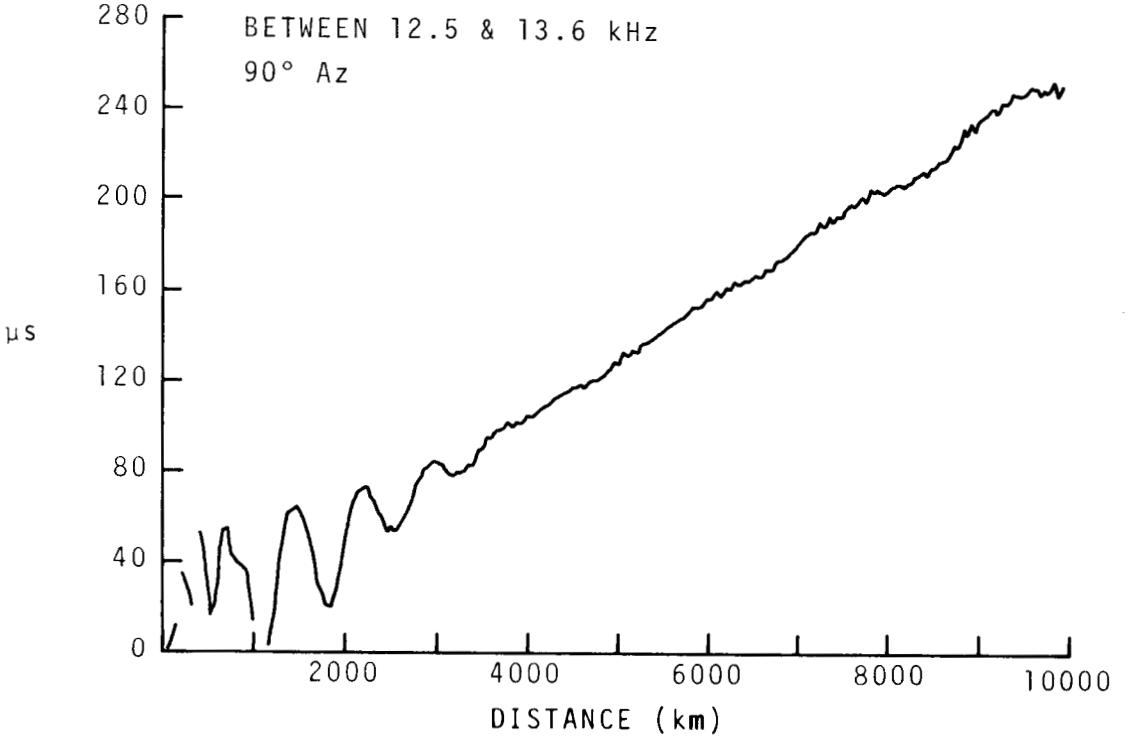

Figure 144.

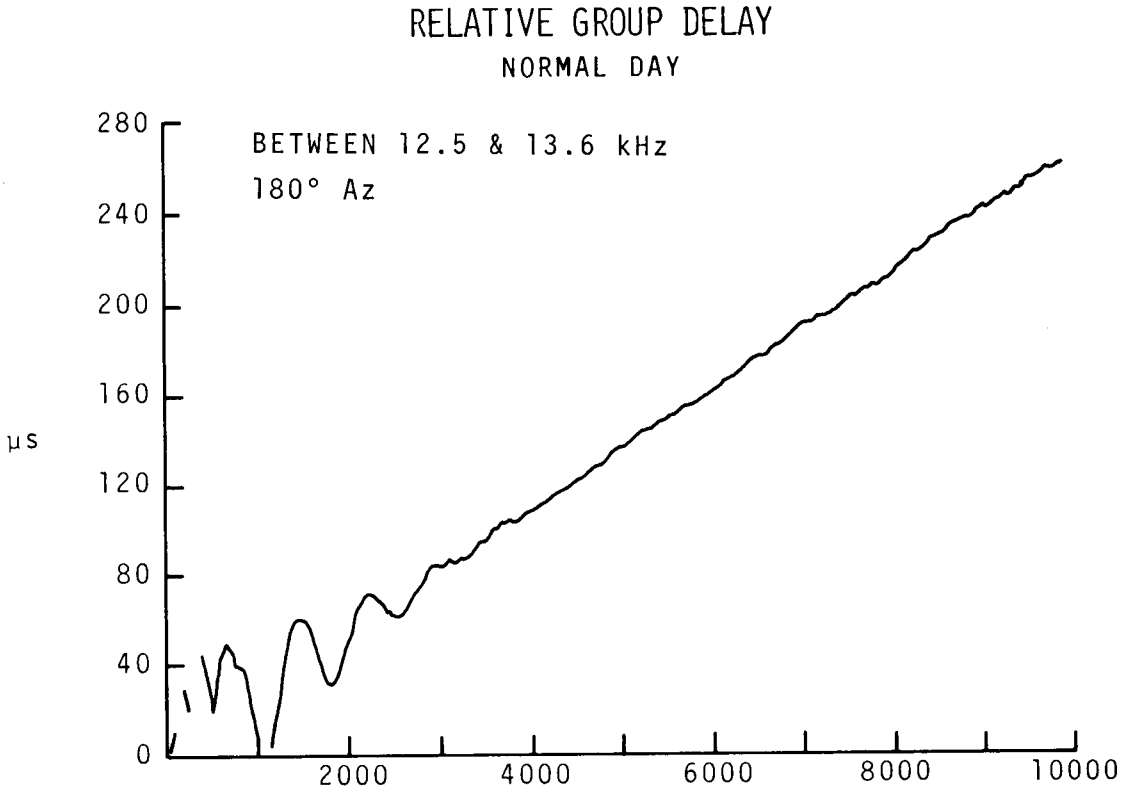

Figure 145.

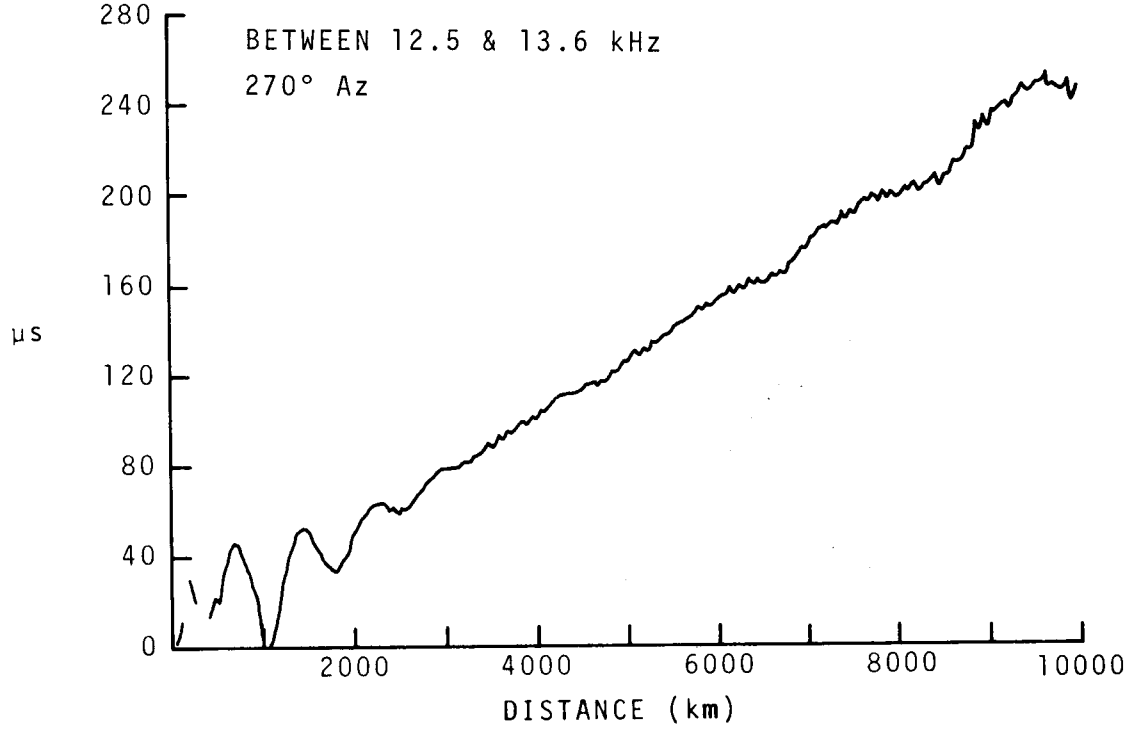

Figure 146.

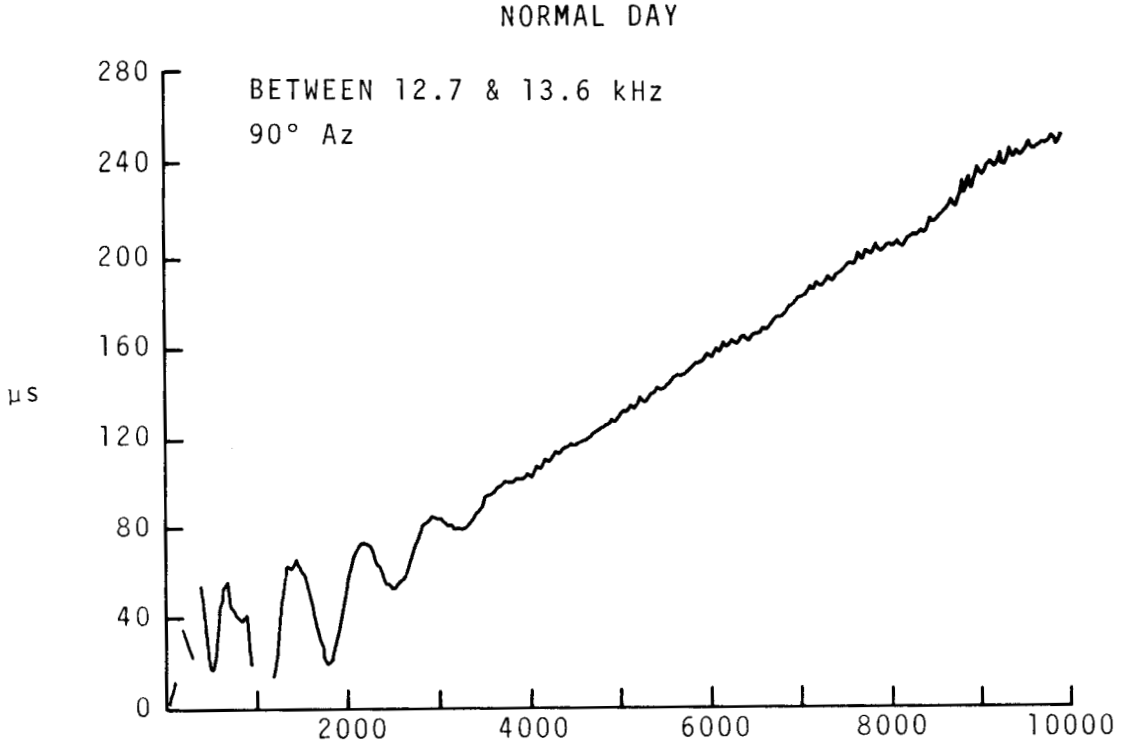

Figure 147.

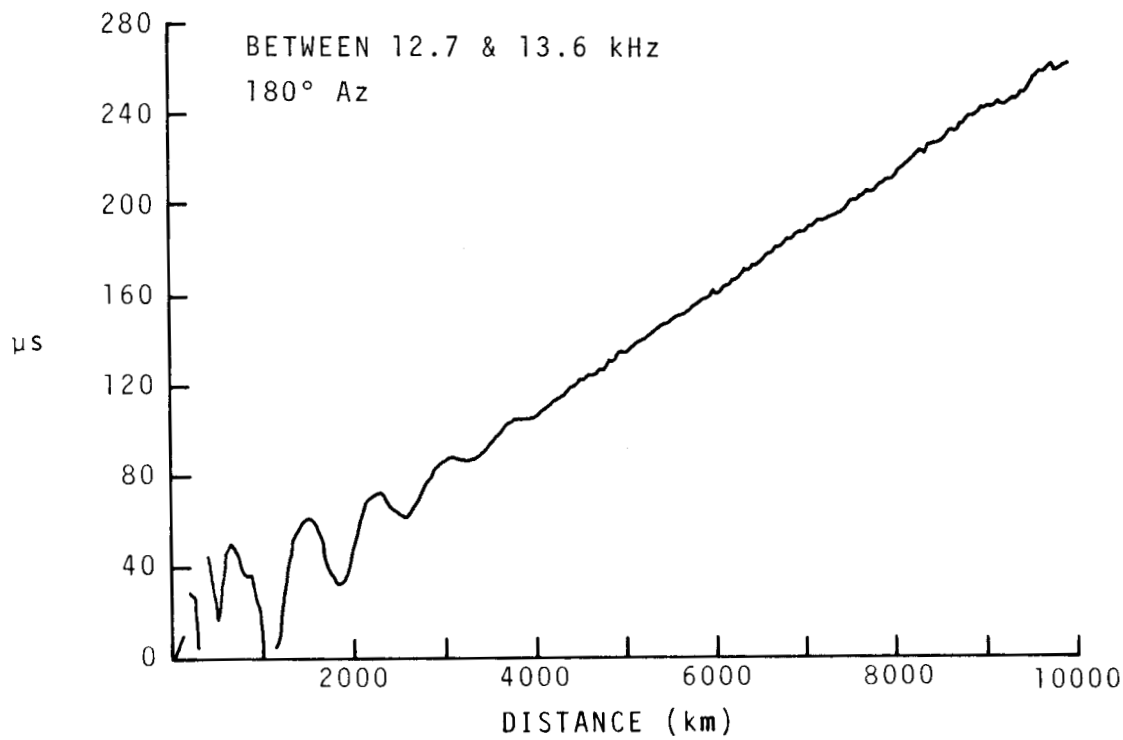

Figure 148.

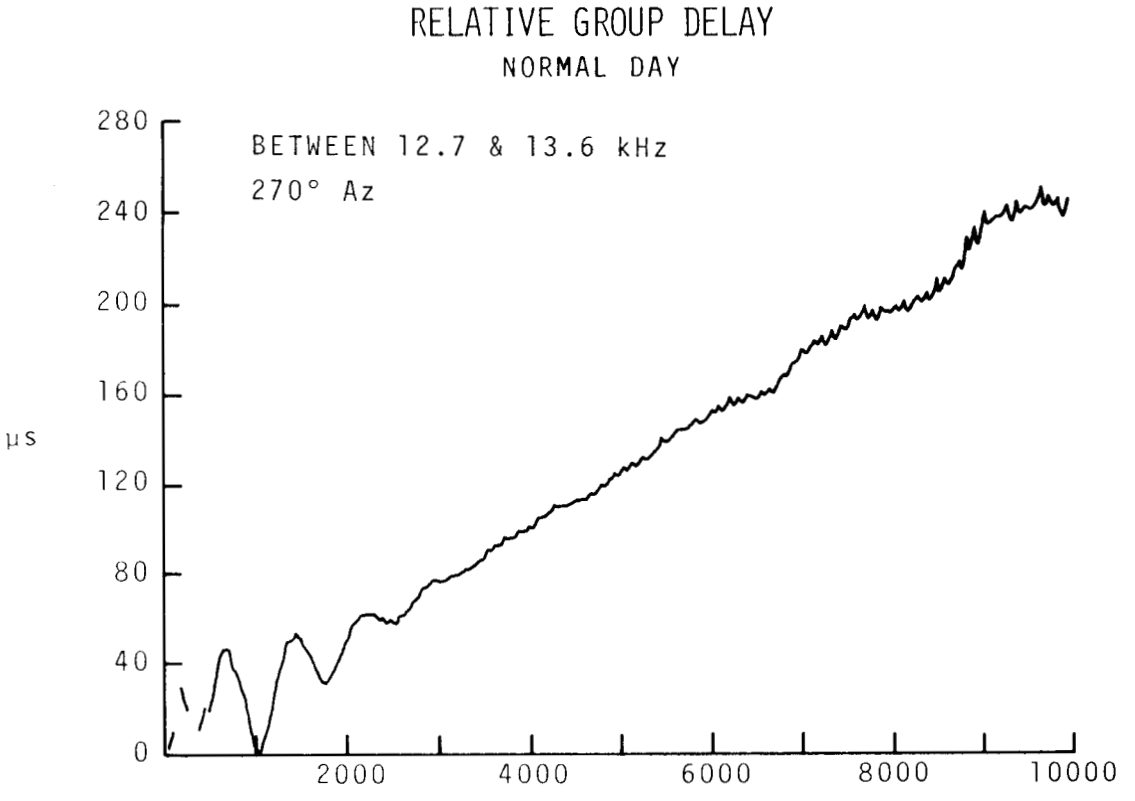

Figure 149.

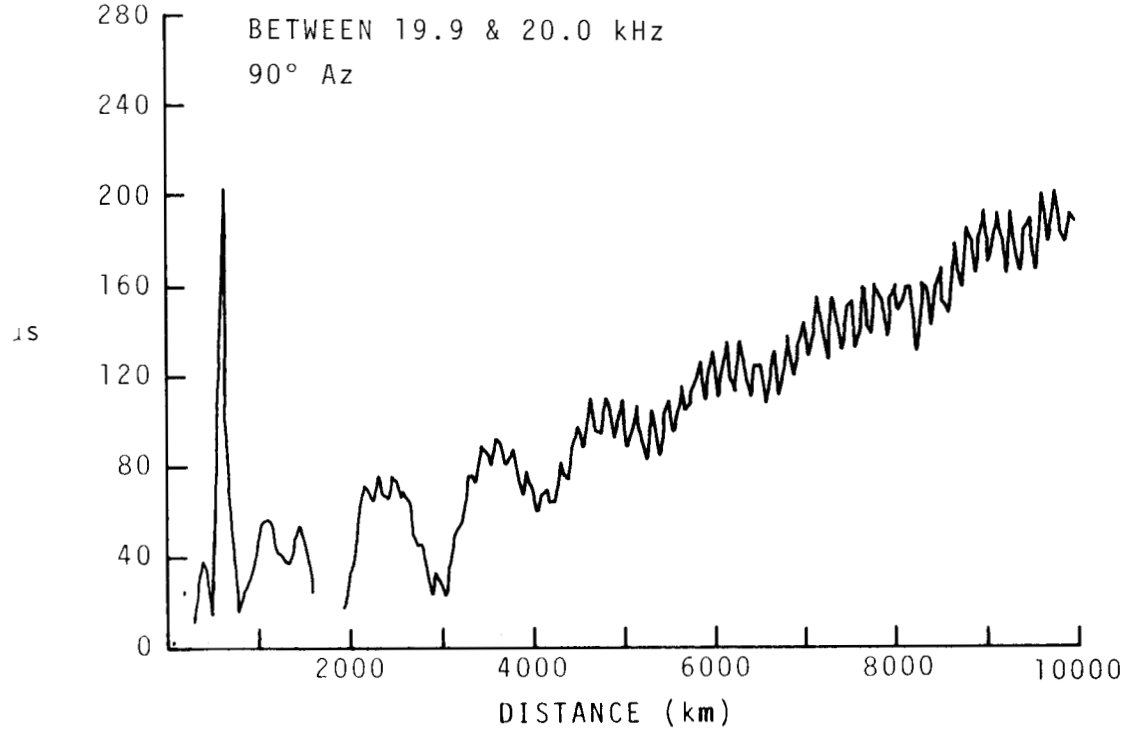

Figure 150.

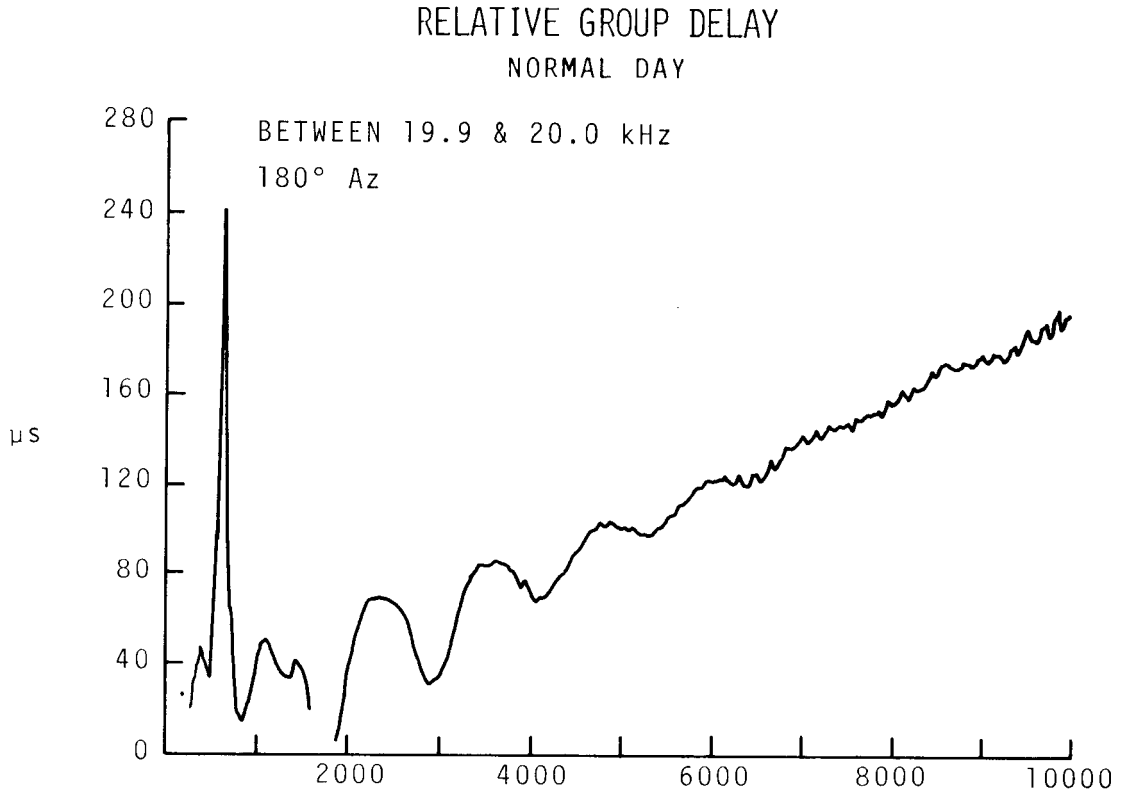

Figure 151.

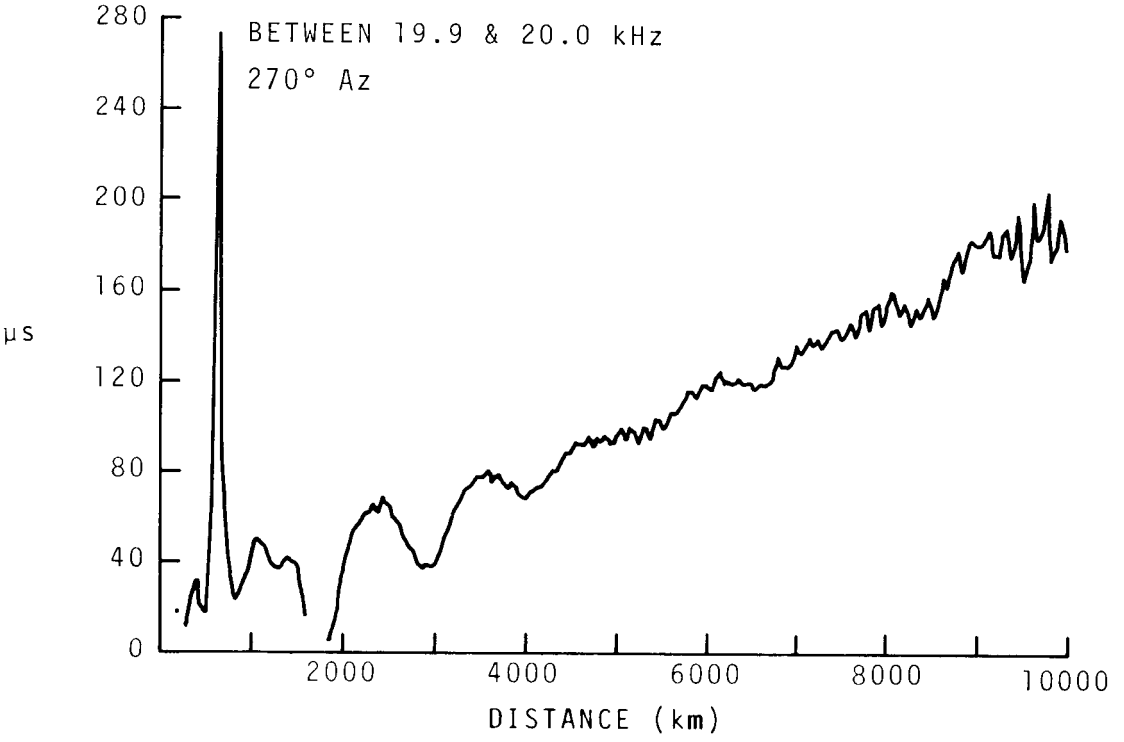

Figure 152.

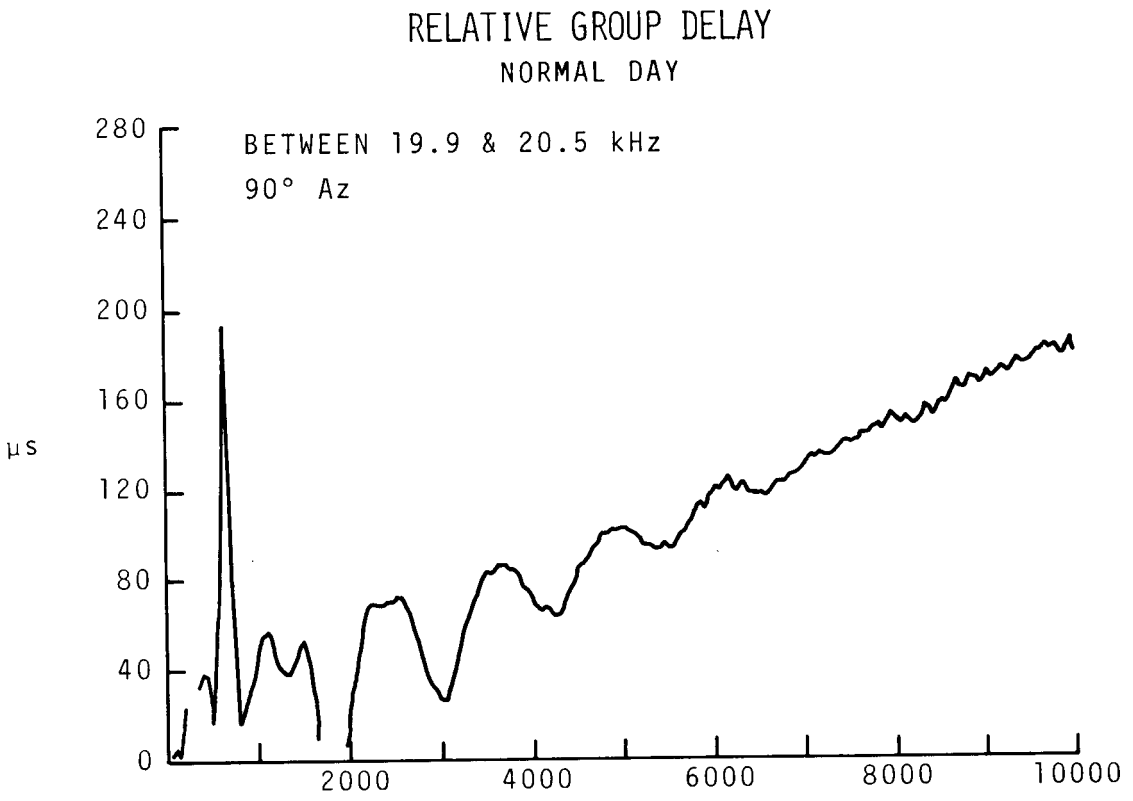

Figure 153.

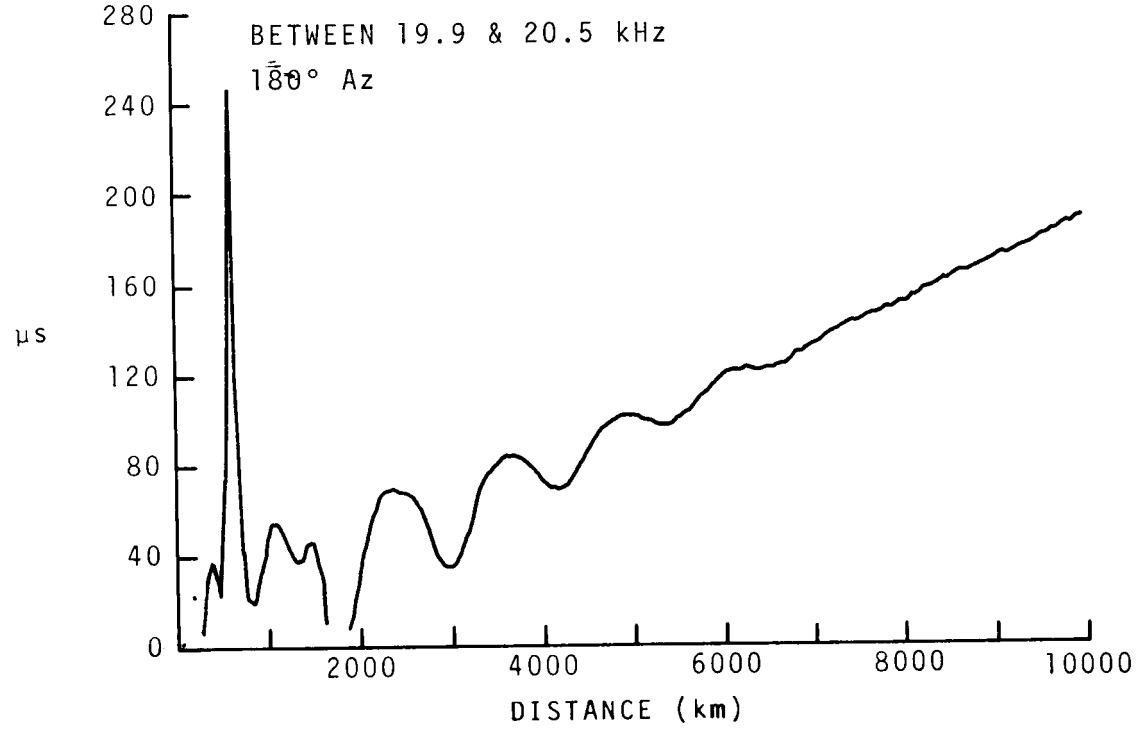

Figure 154.

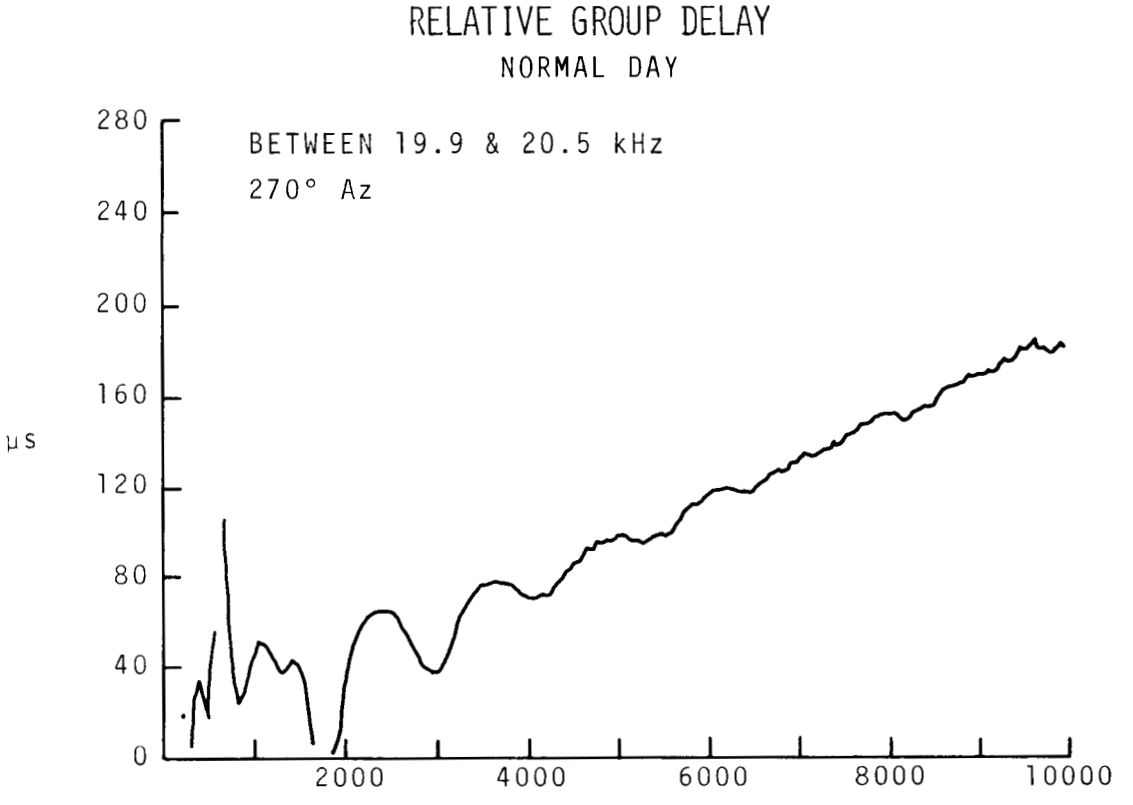

Figure 155.

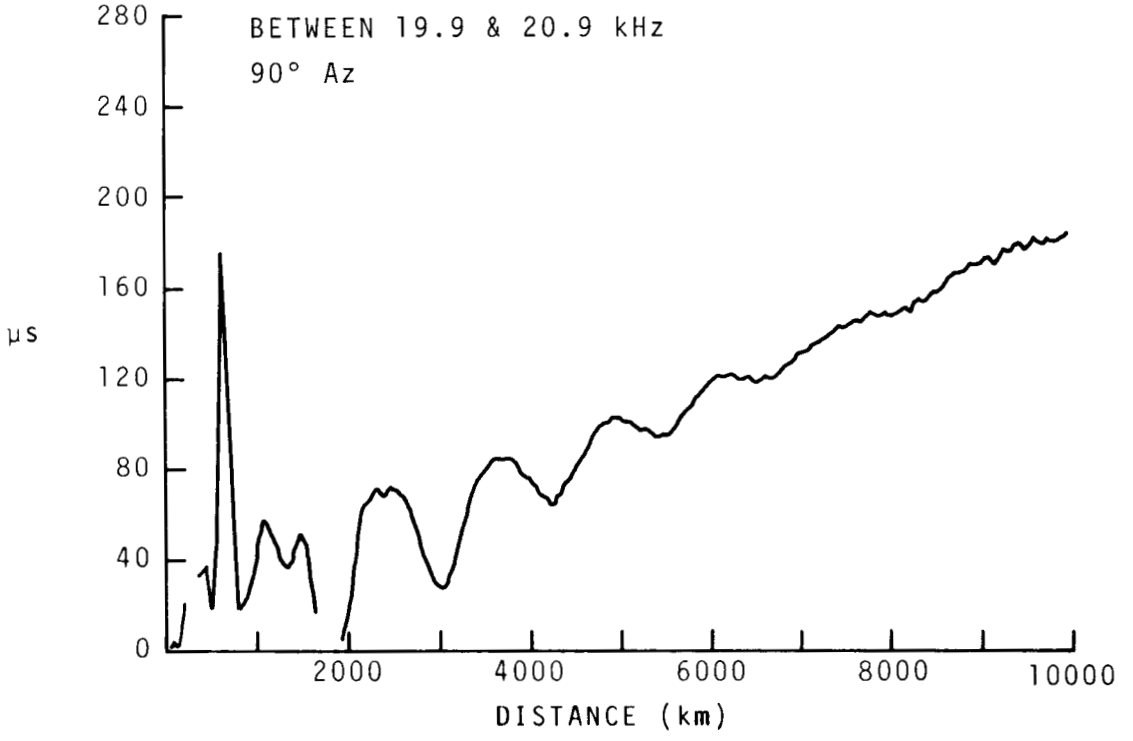

Figure 156.

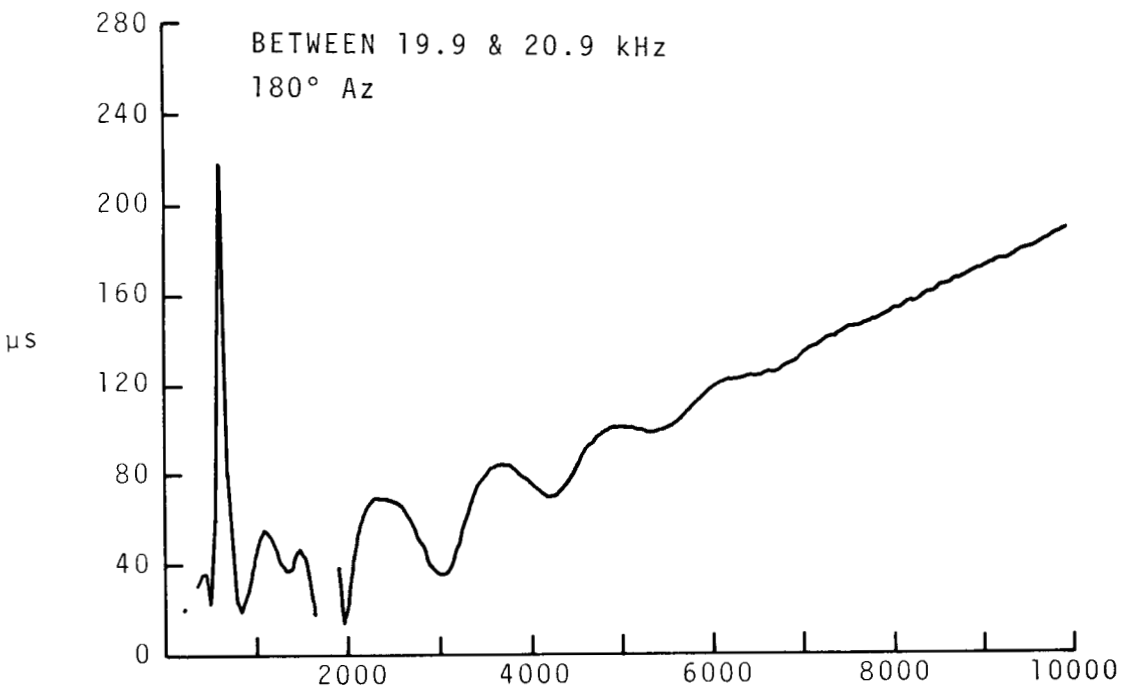

Figure 157.

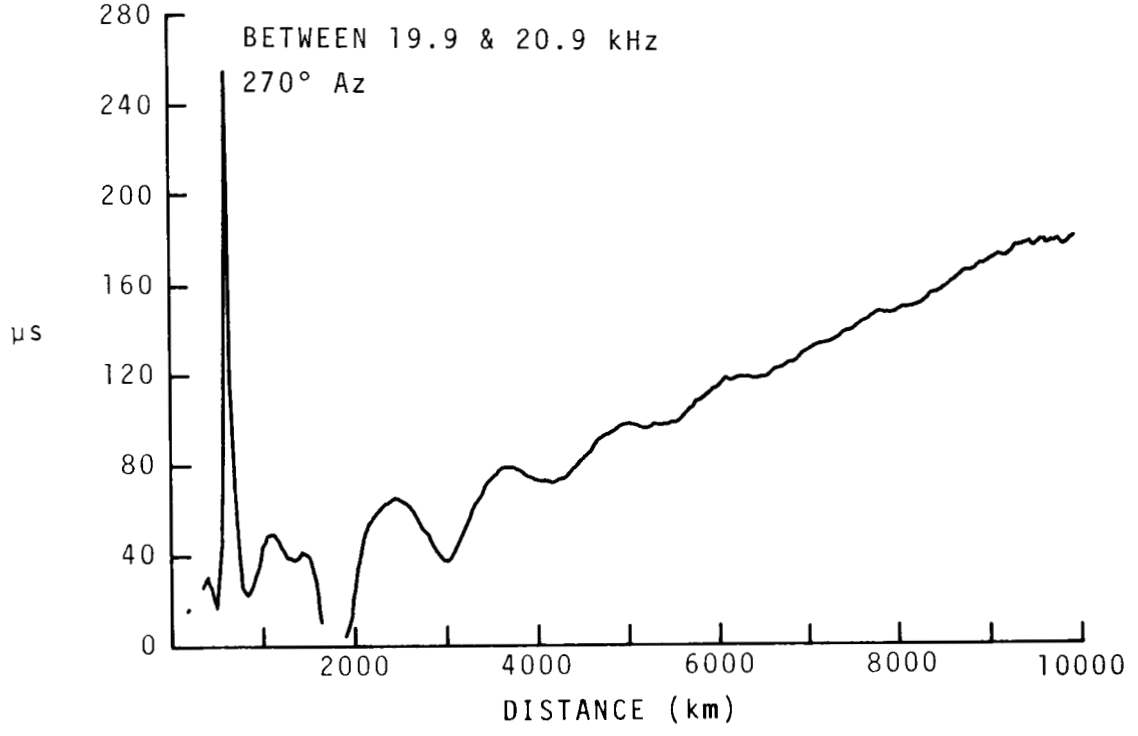

Figure 158.

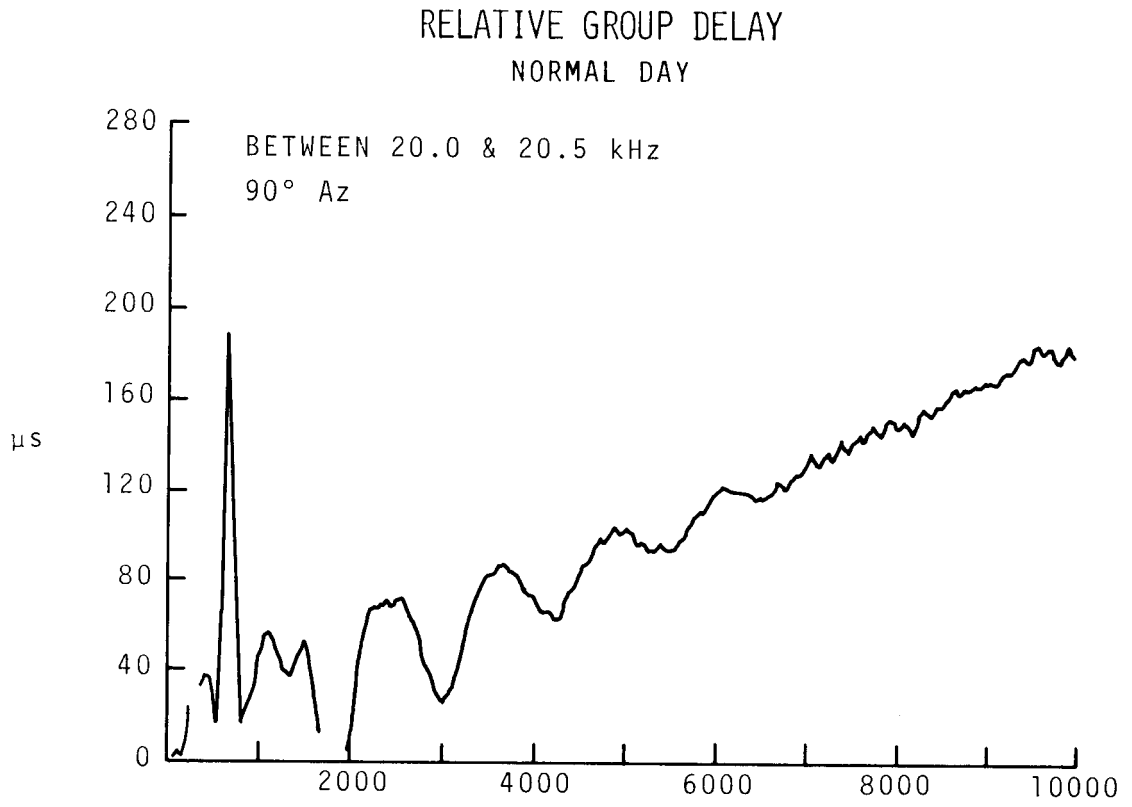

Figure 159.

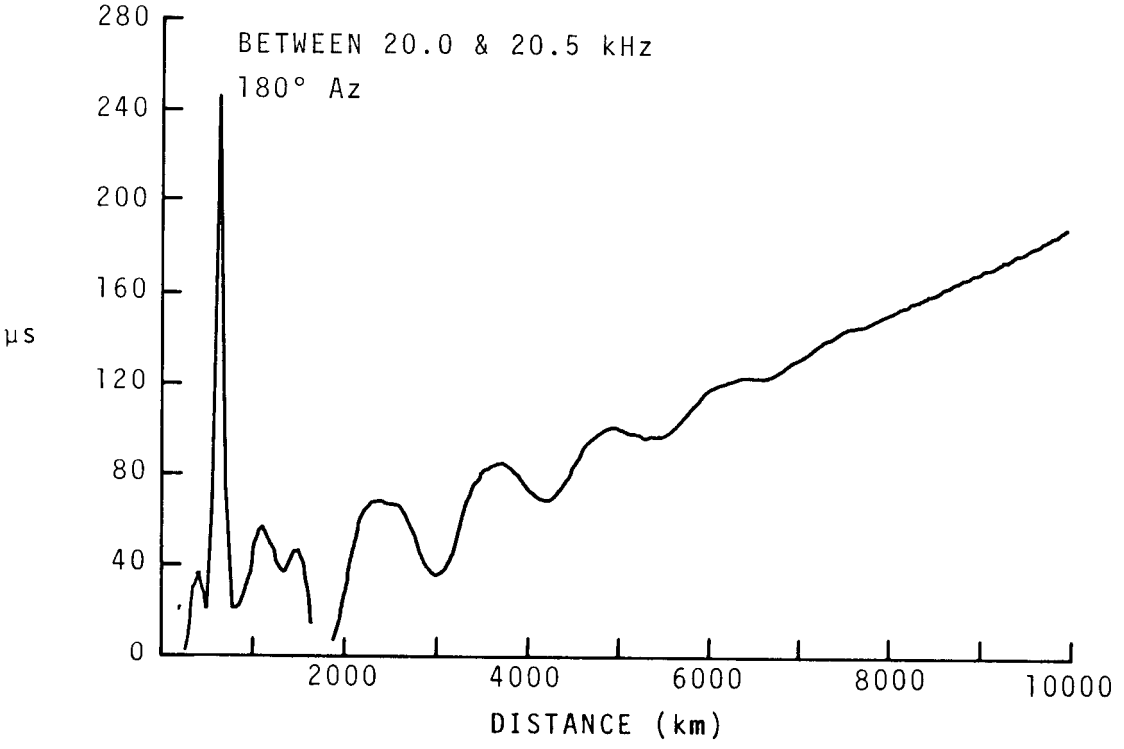

Figure 160.

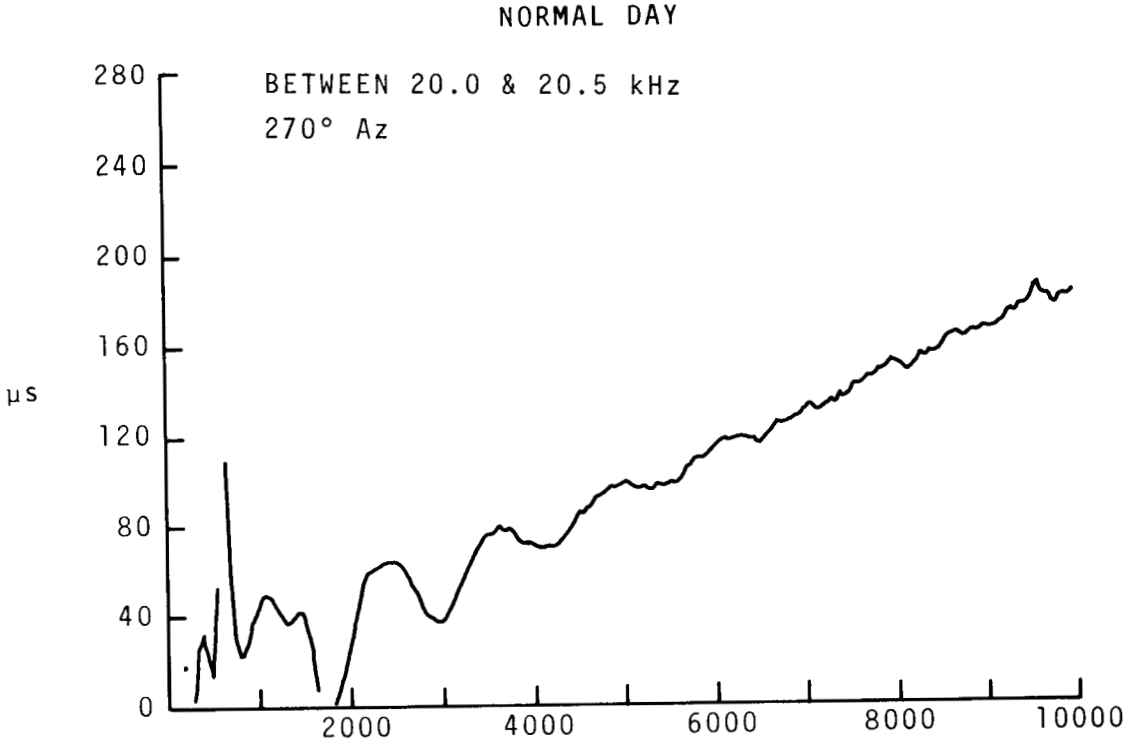

Figure 161.

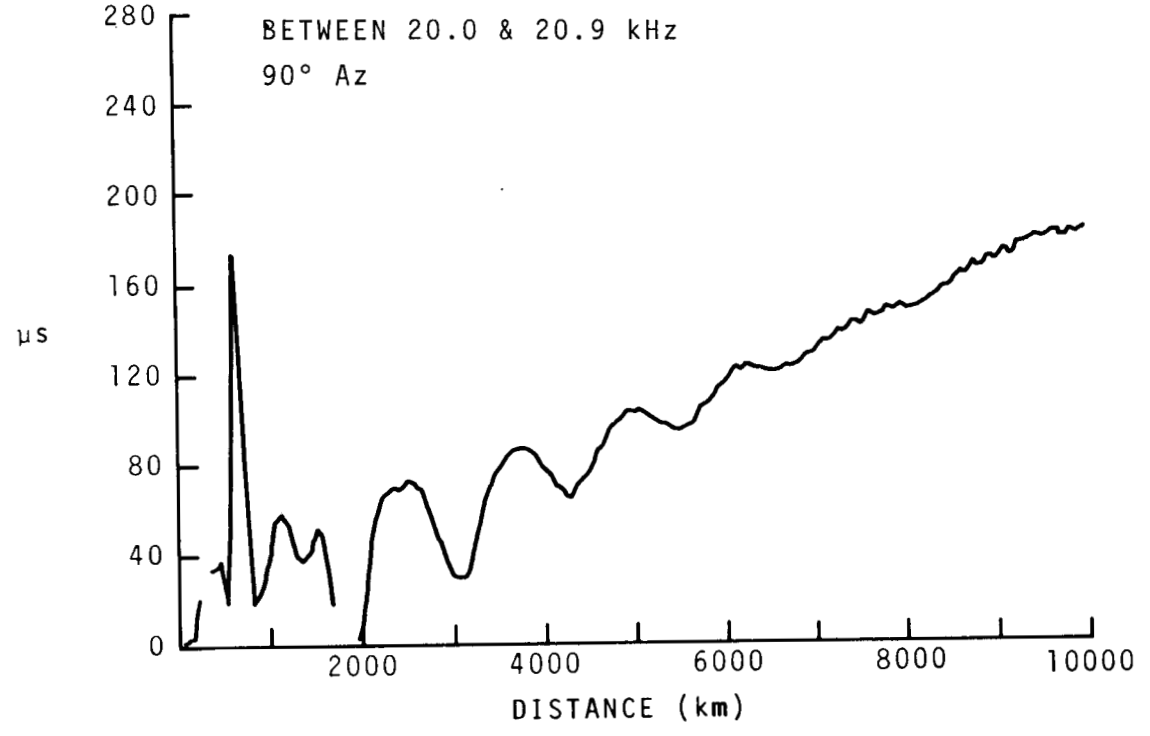

Figure 162.

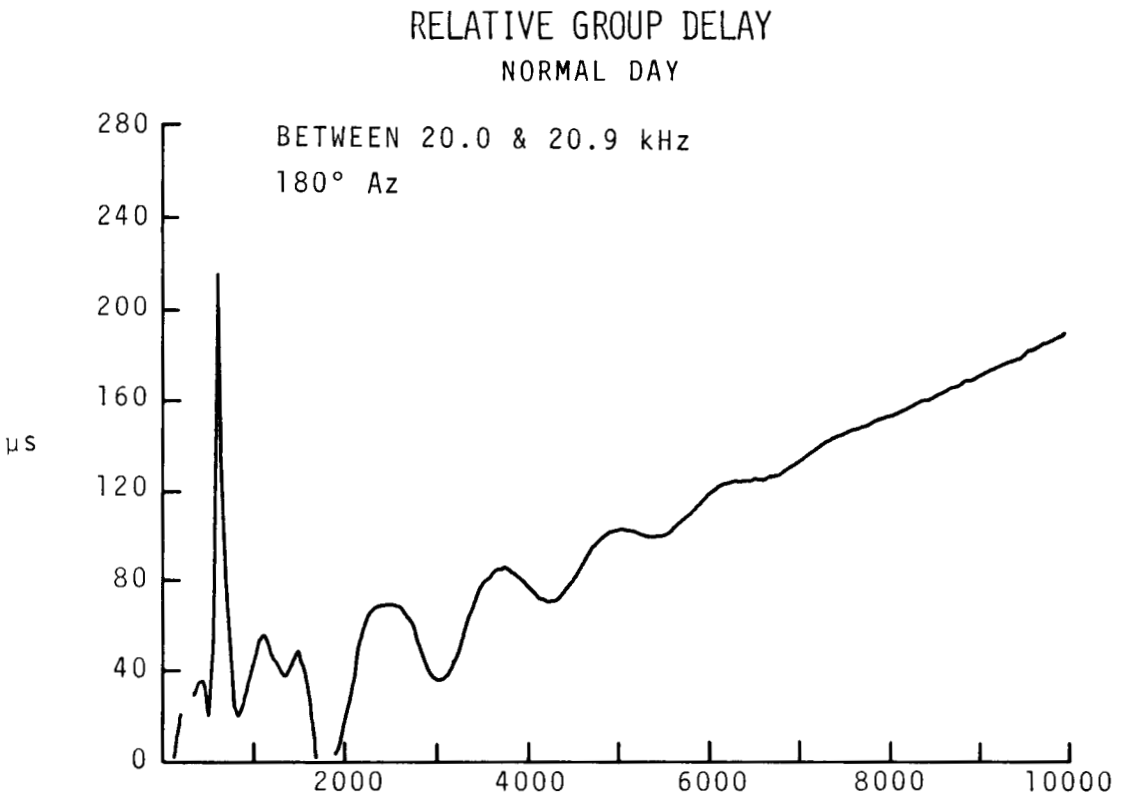

Figure 163.

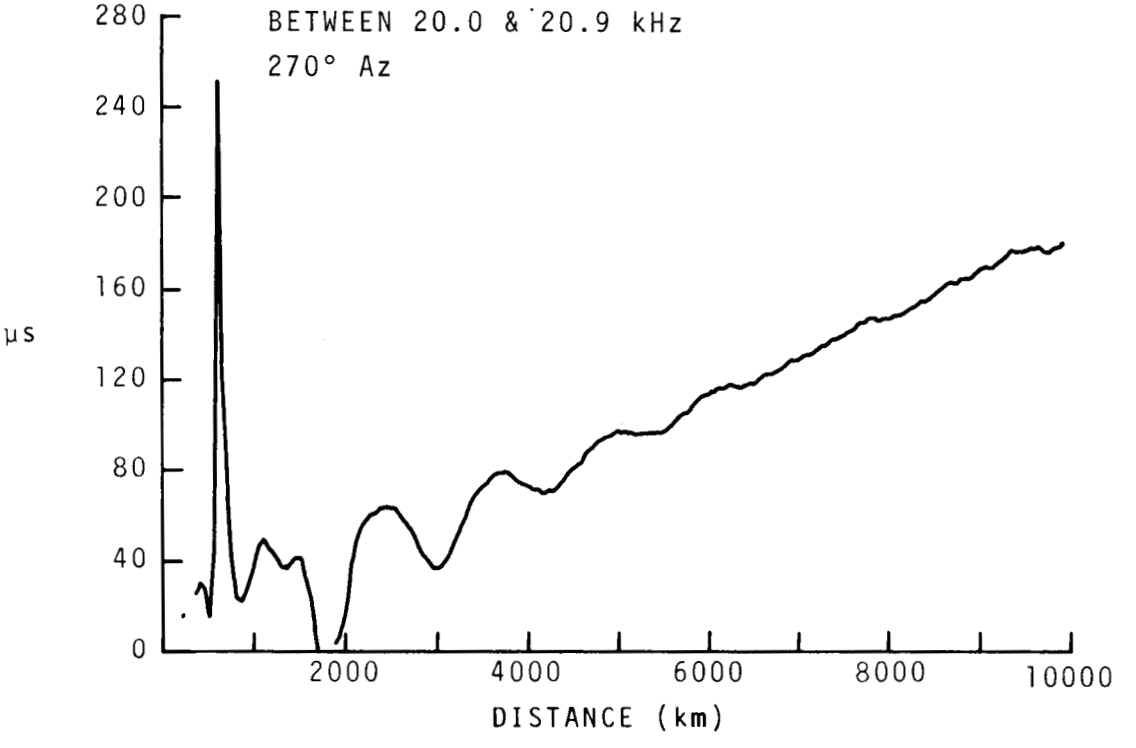

Figure 164.

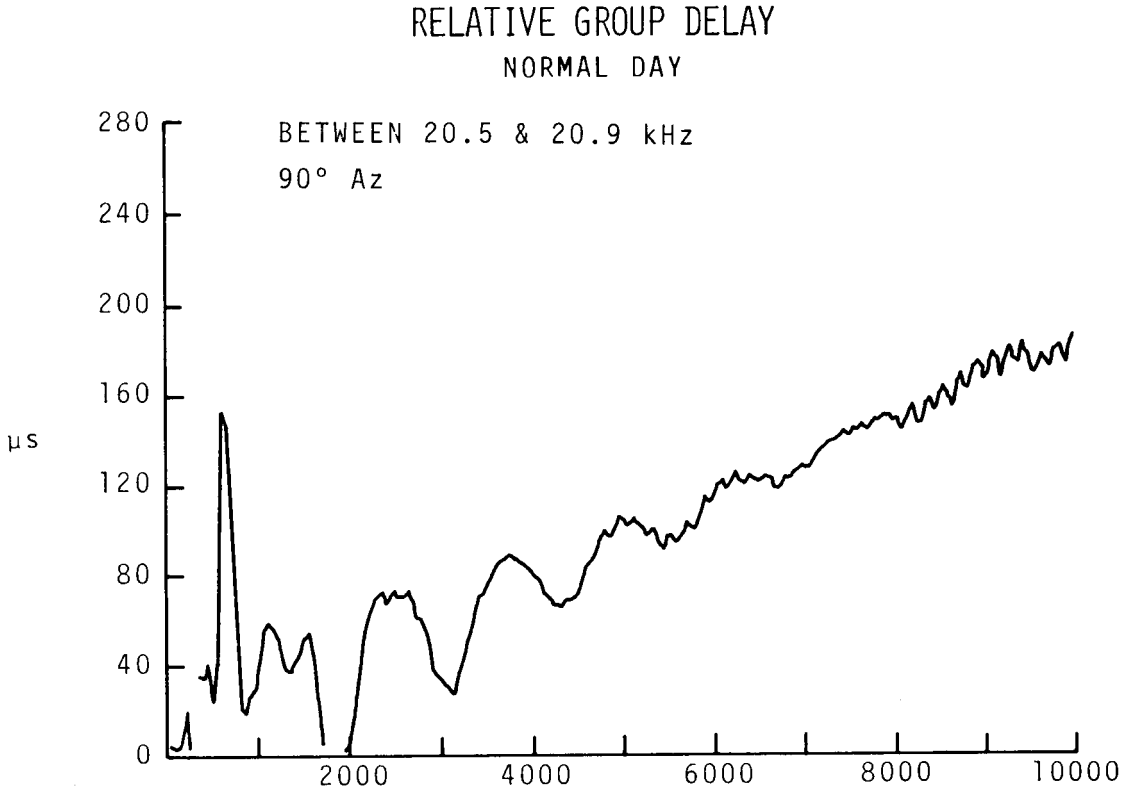

Figure 165.

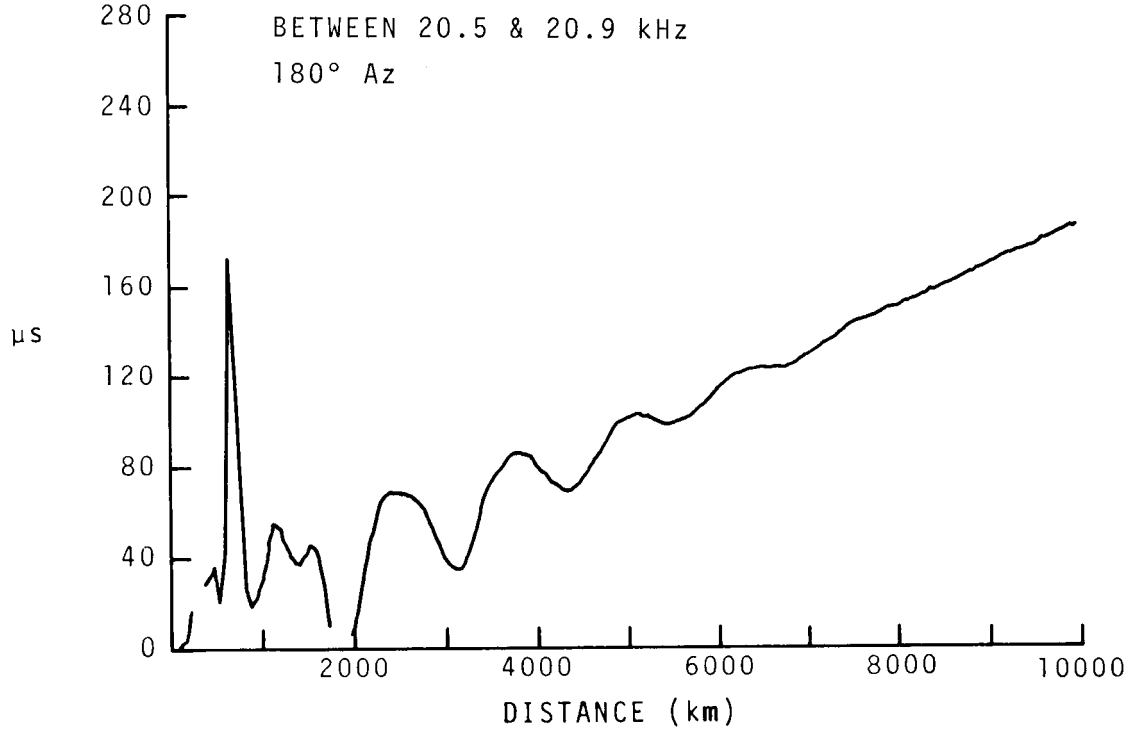

Figure 166.

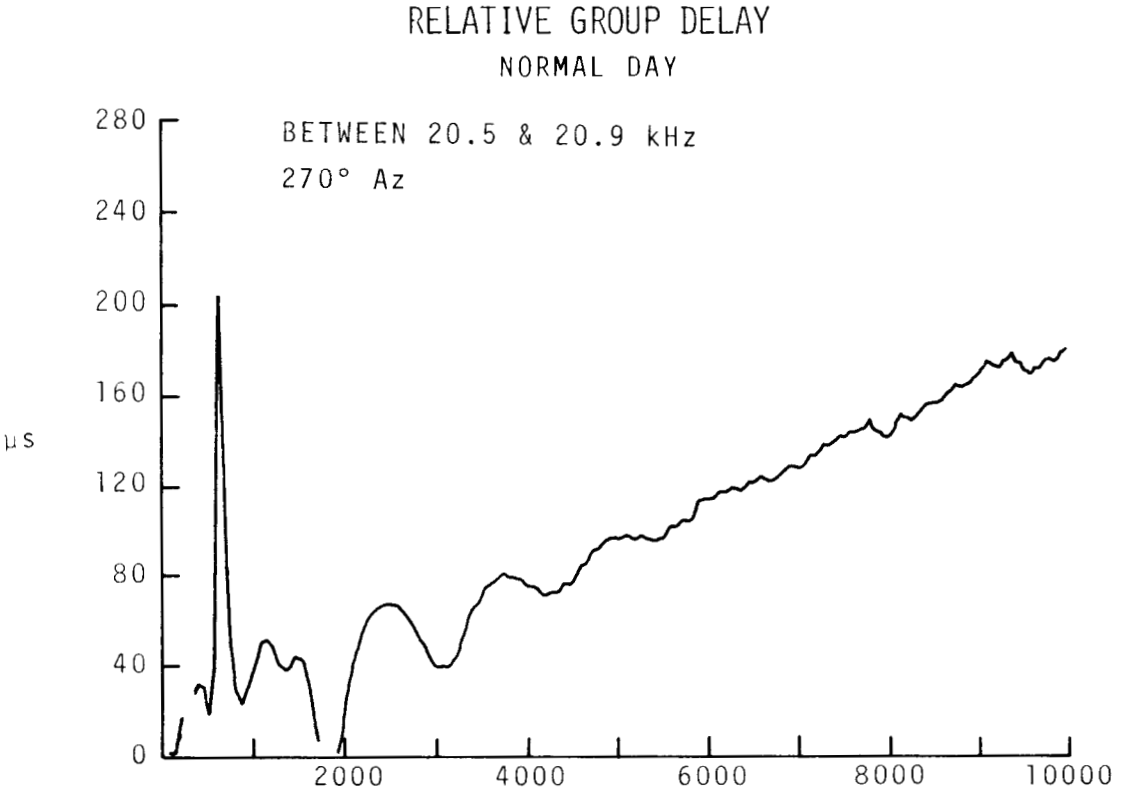
RELATIVE GROUP DELAY
NORMAL DAY
BETWEEN 20.5 & 20.9 kHz
270° Az
280
240
200
160
120
80
40
0
μs
2000
4000
6000
8000
10000

Figure 167.

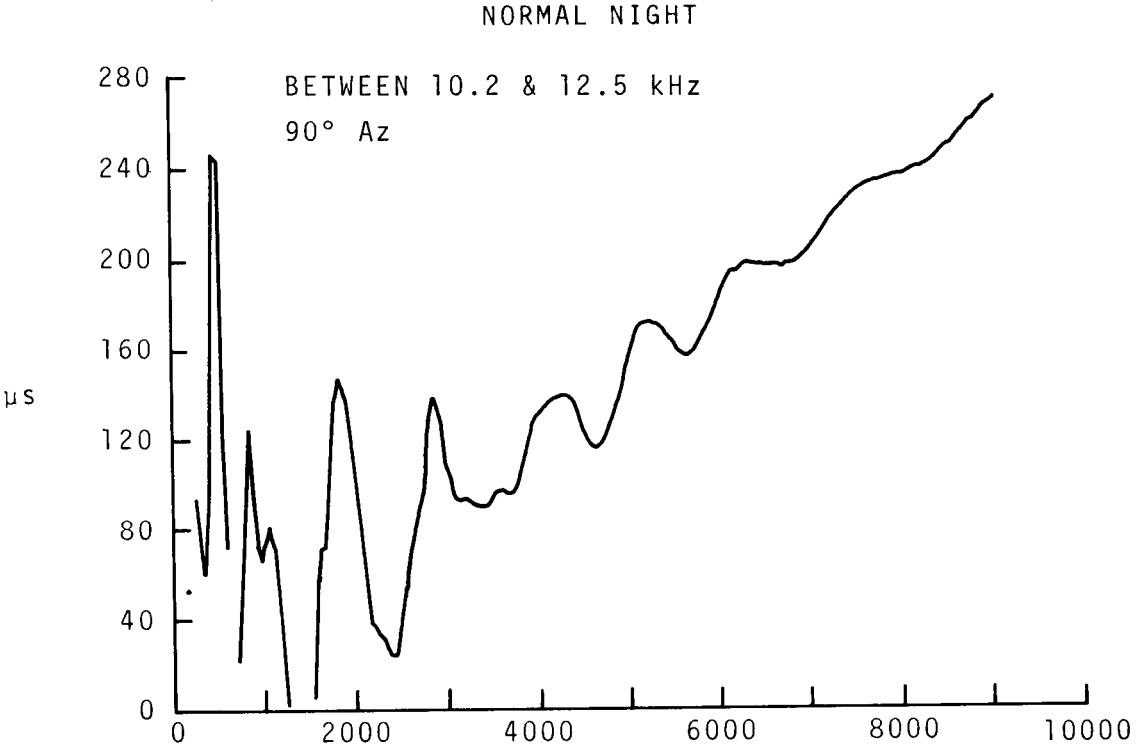

Figure 168.

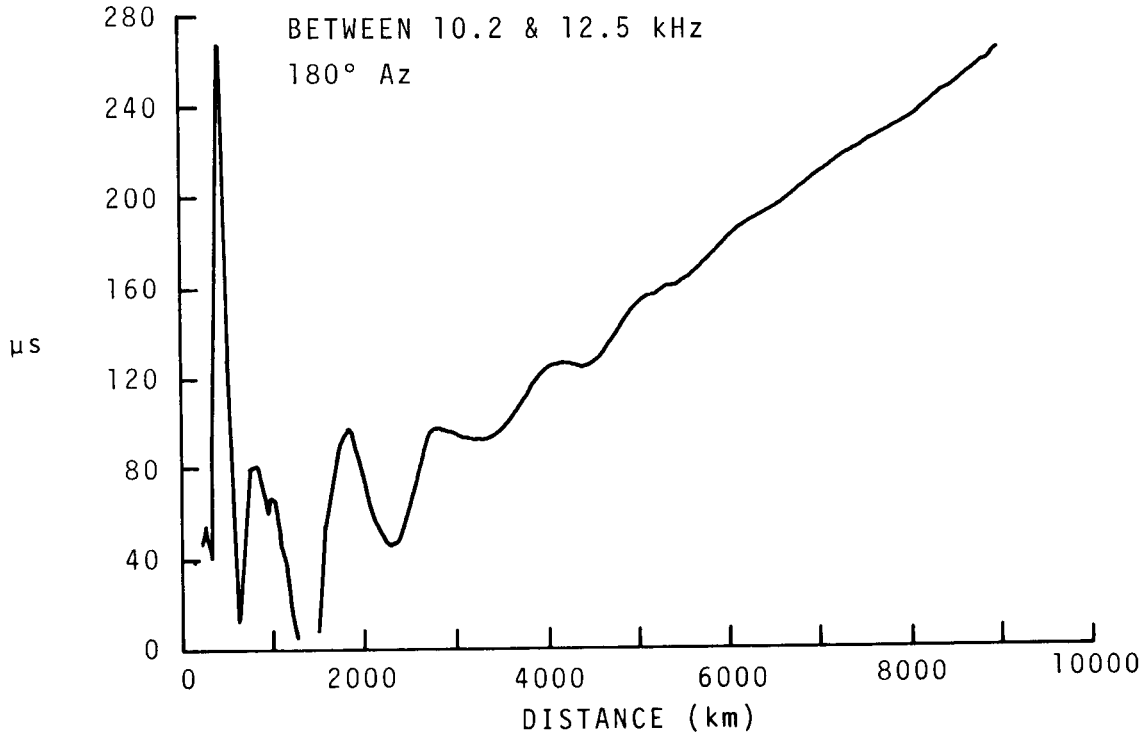

Figure 169.

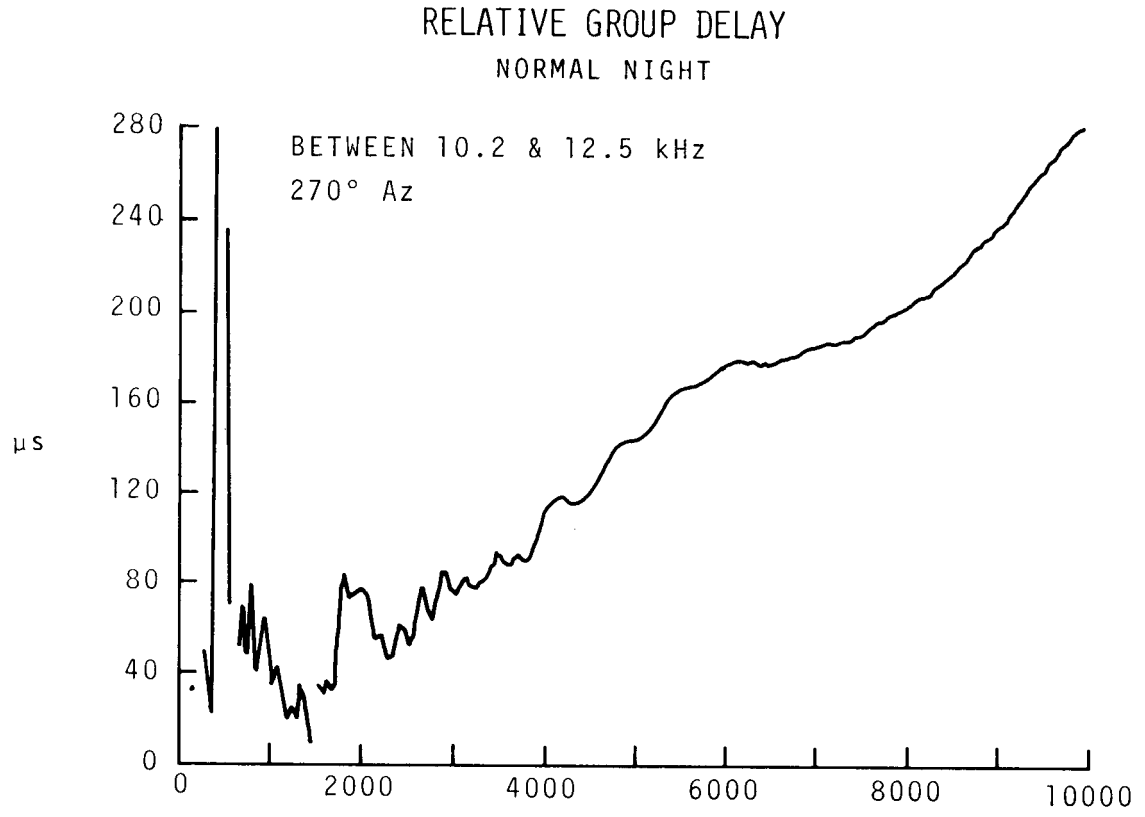

Figure 170.

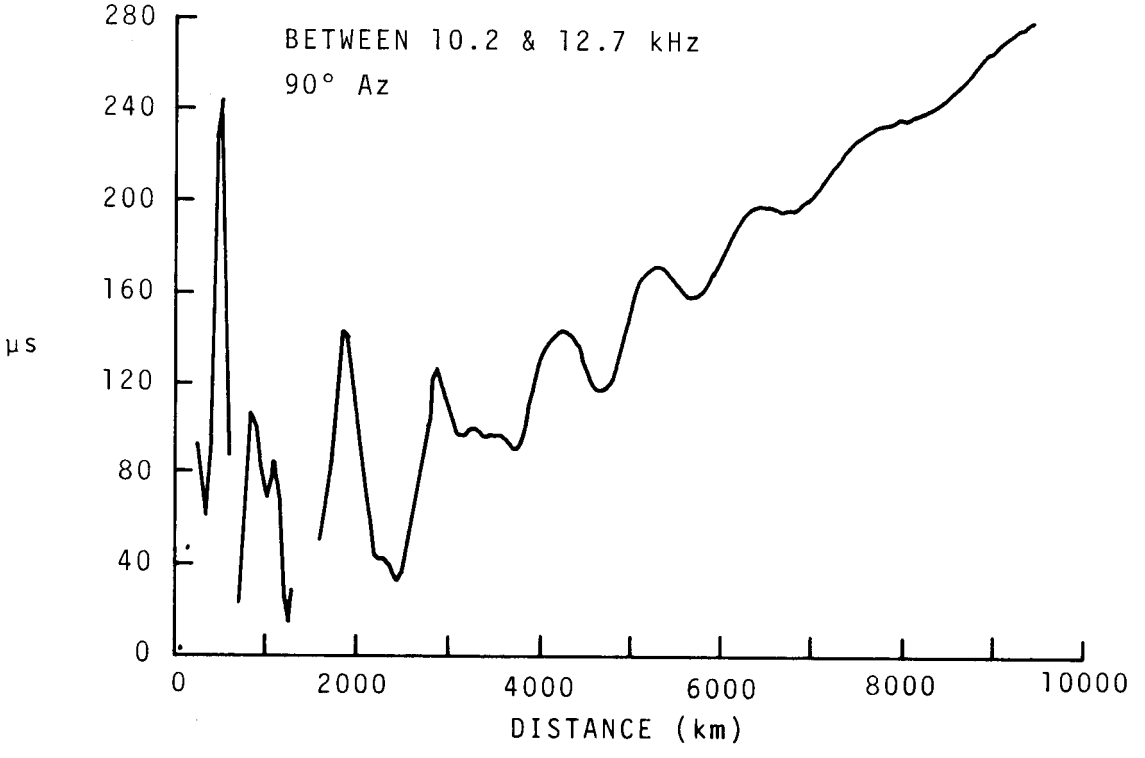

Figure 171.

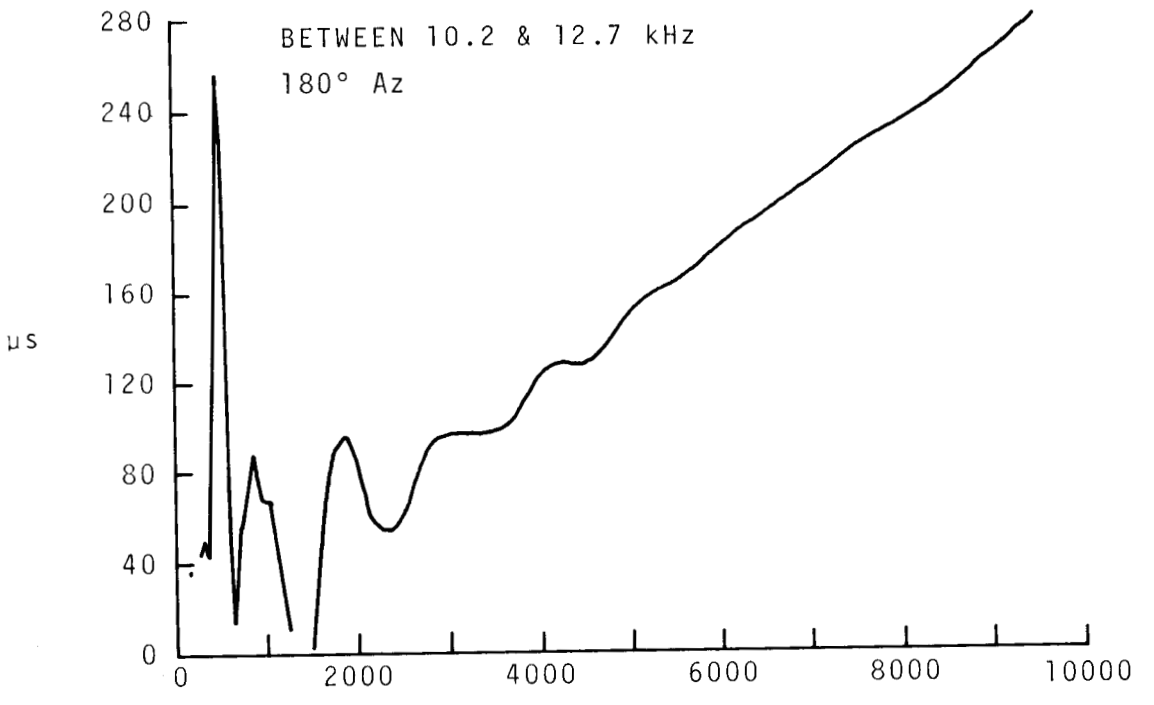

Figure 172.

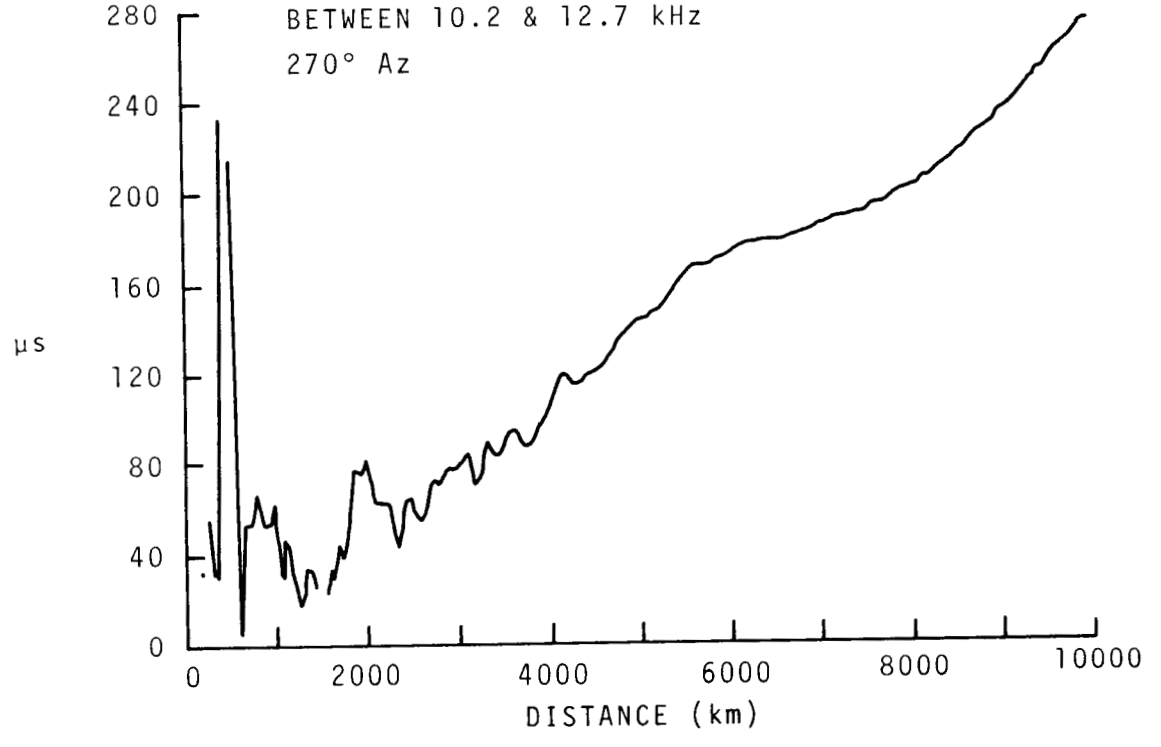

Figure 173.

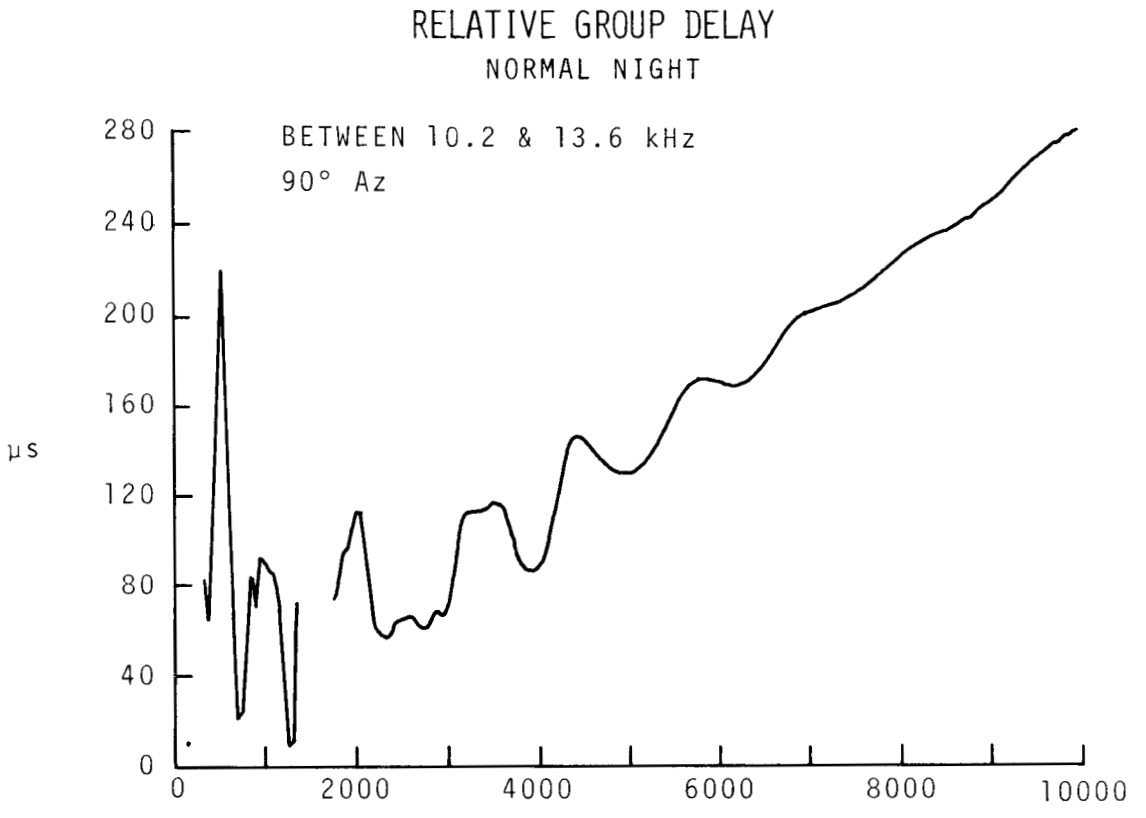

Figure 174.

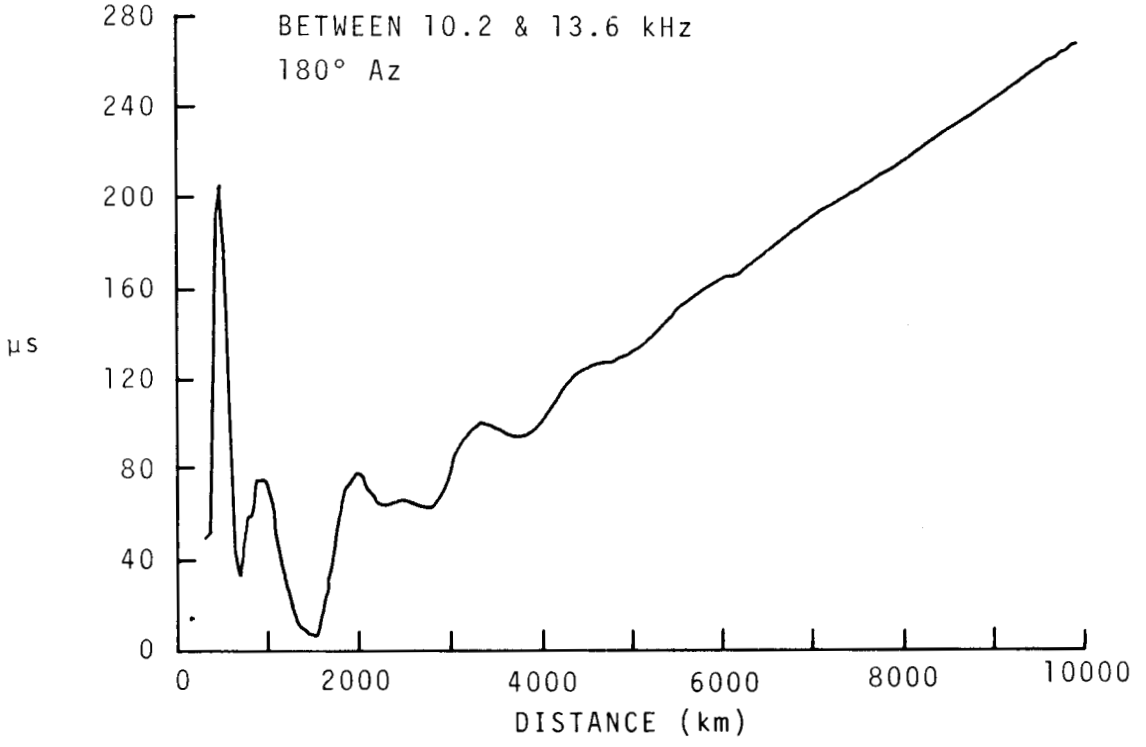

Figure 175.

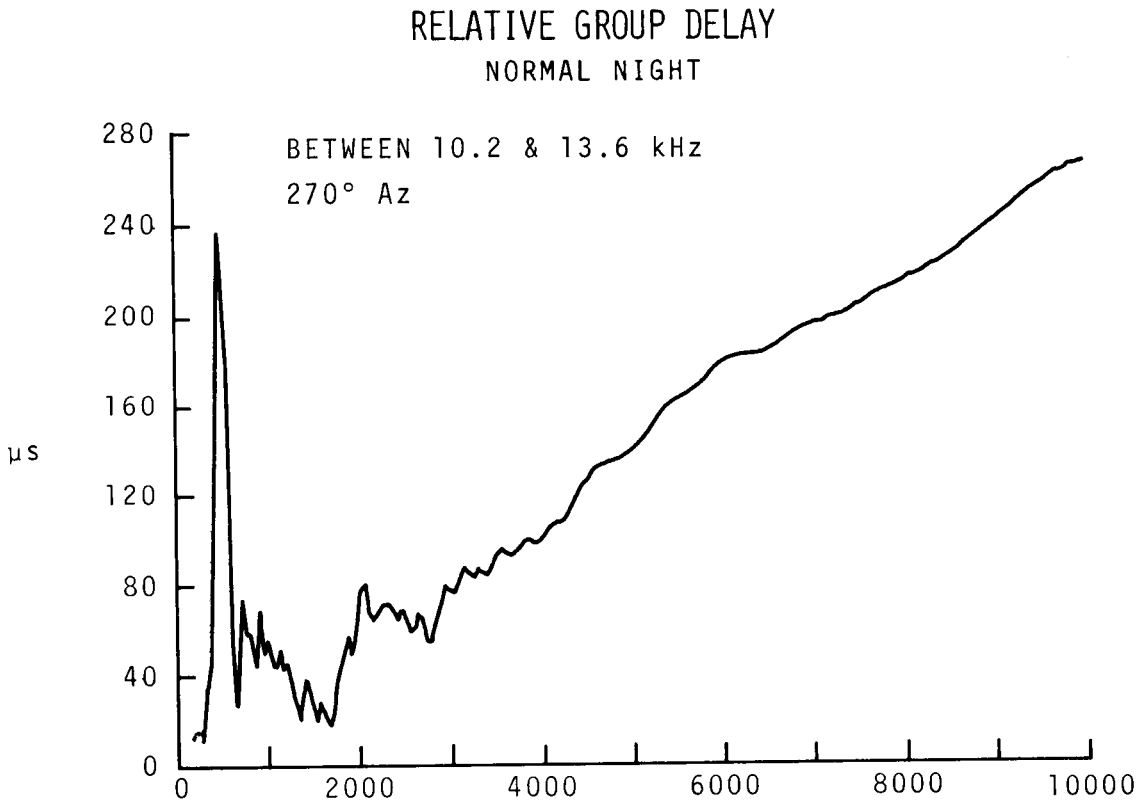

Figure 176.

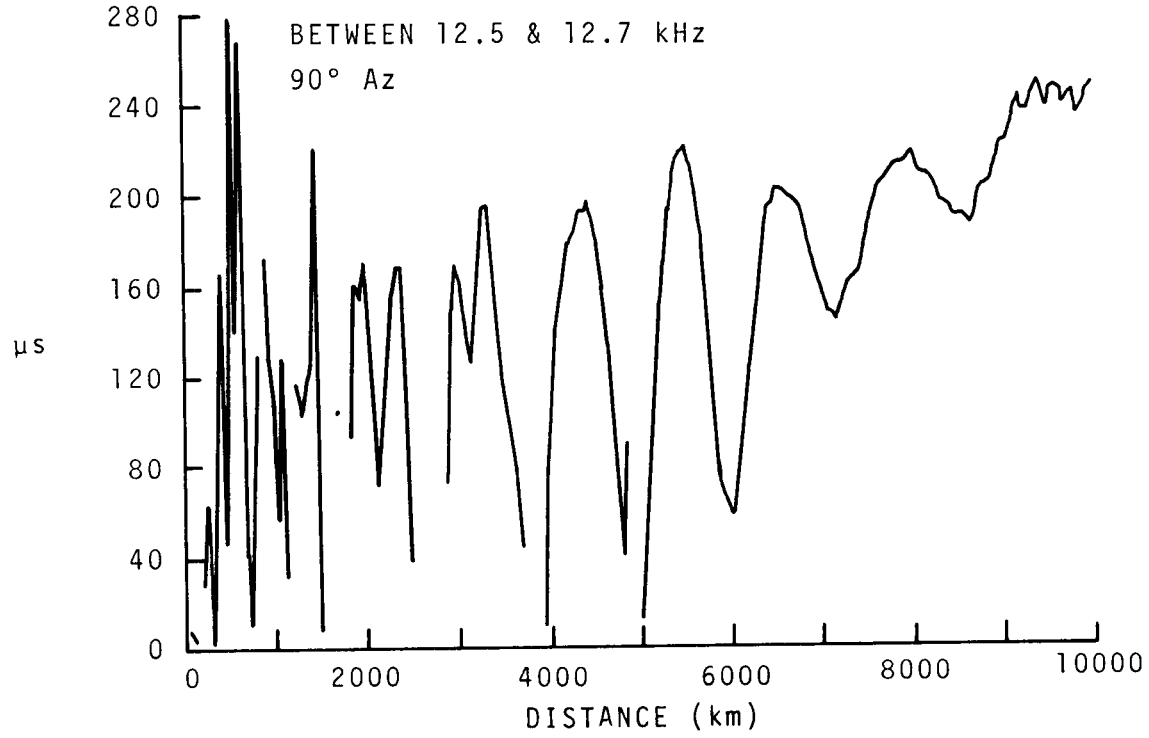

Figure 177.

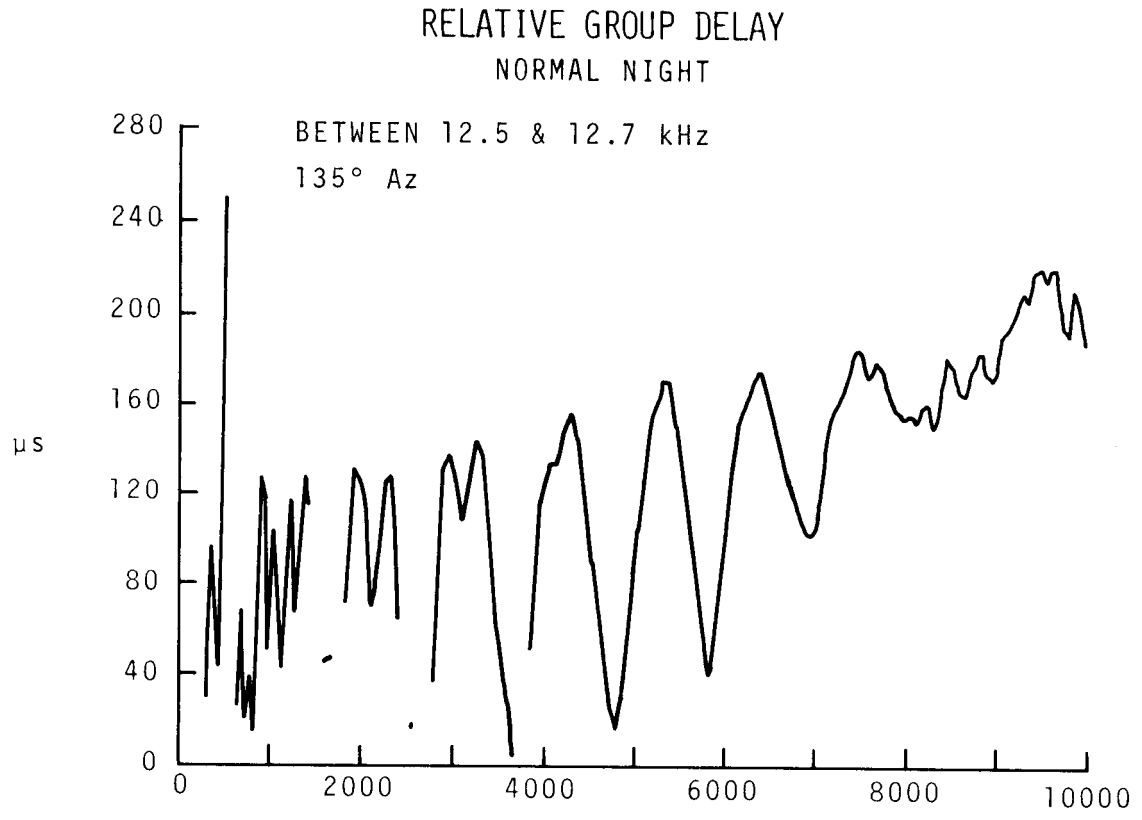

Figure 178.

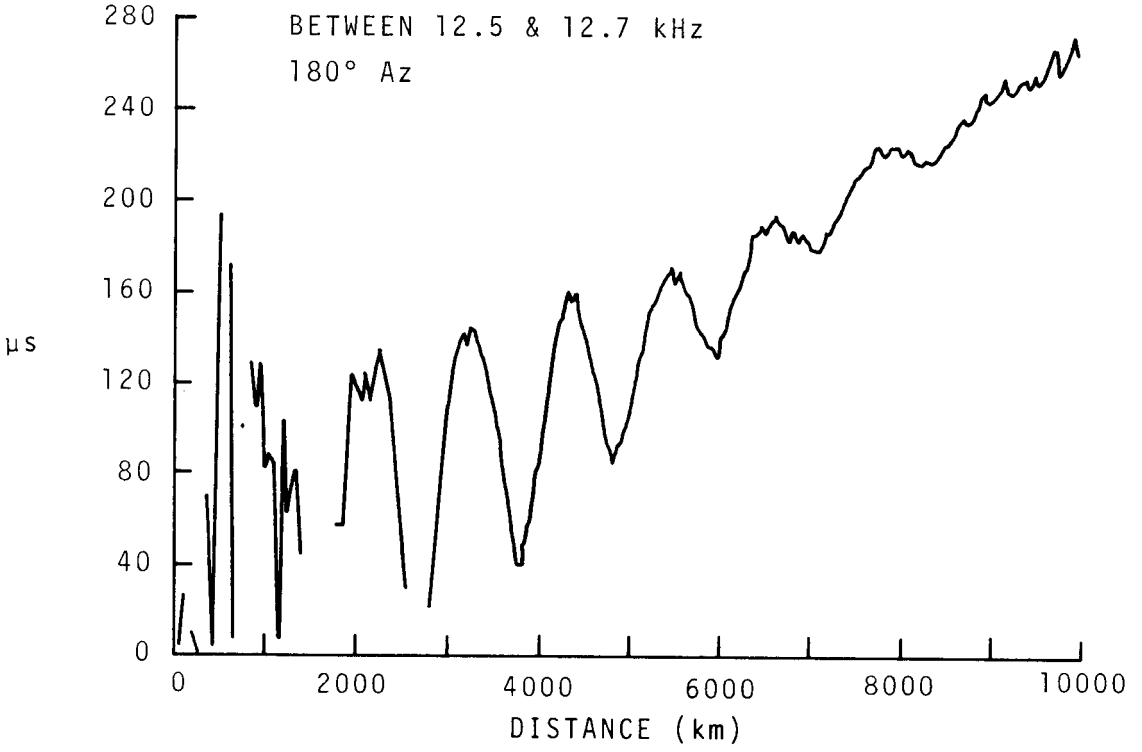

Figure 179.

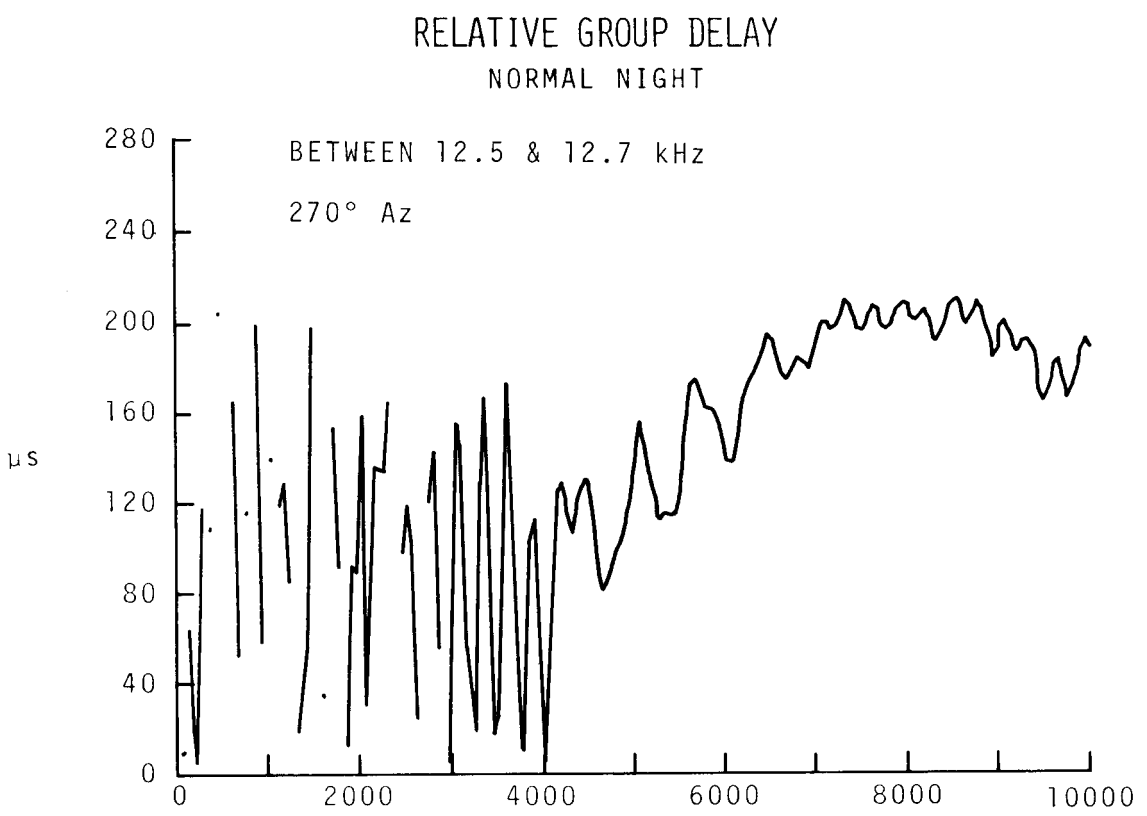

Figure 180.

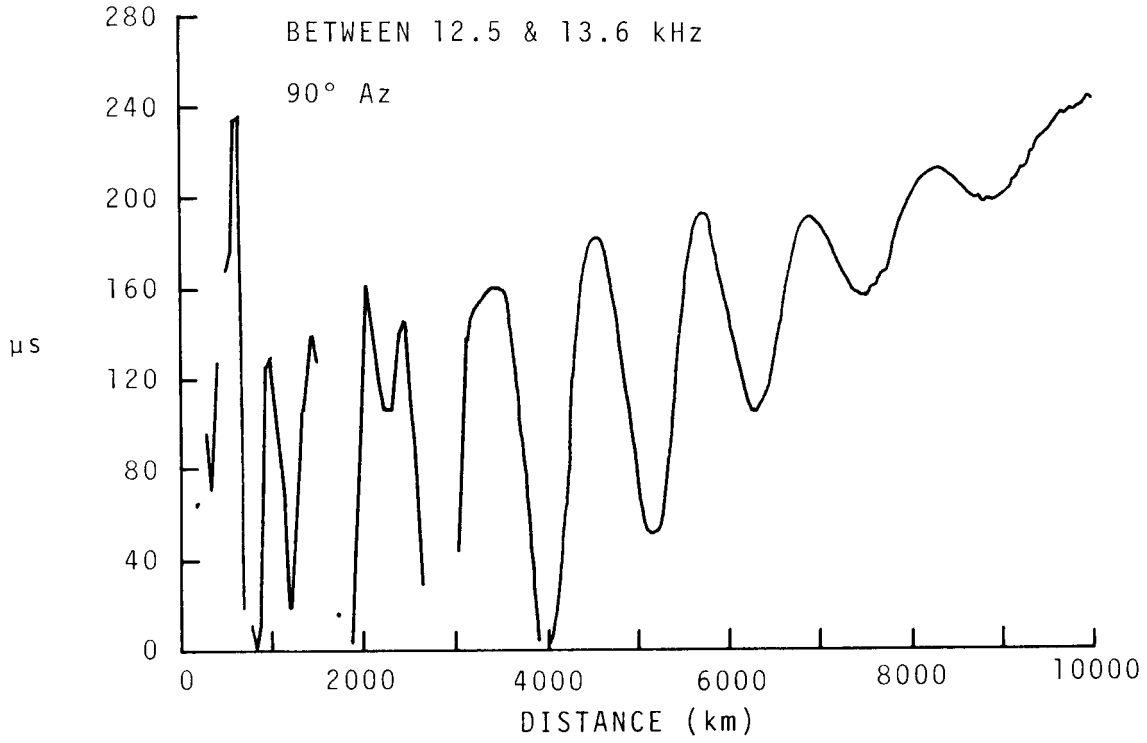

Figure 181.

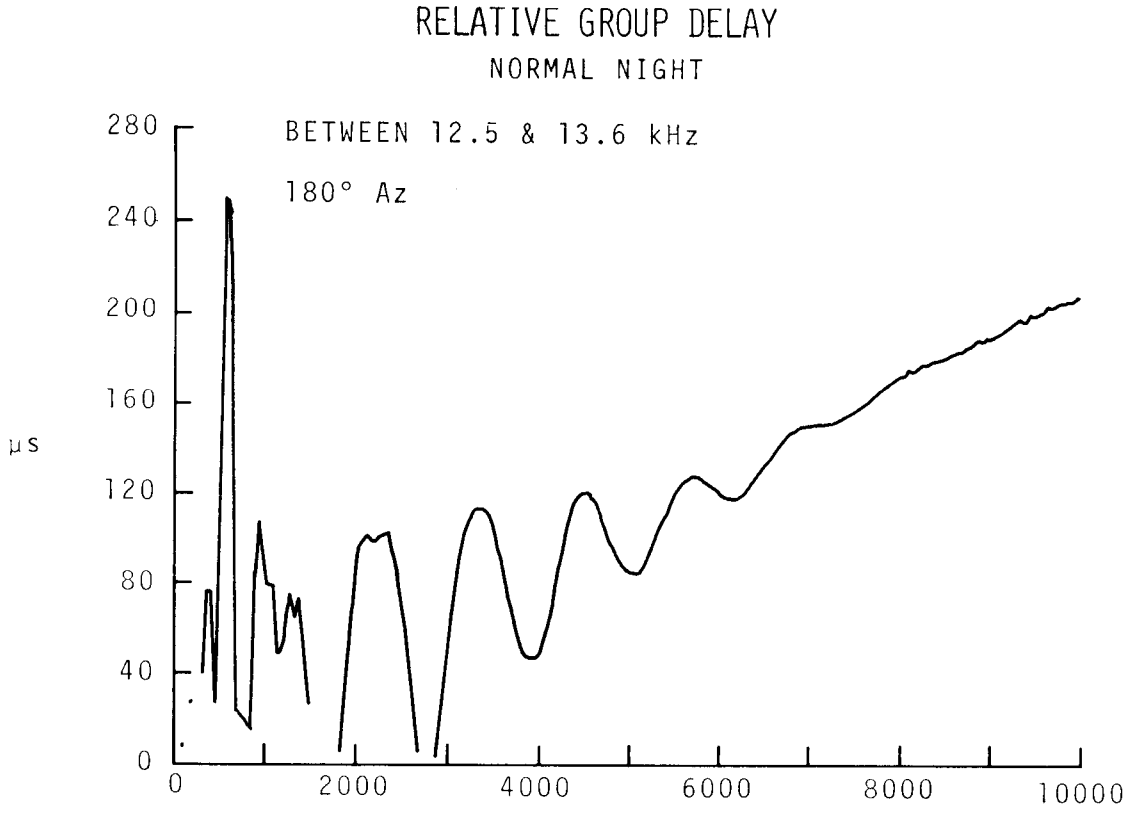

Figure 182.

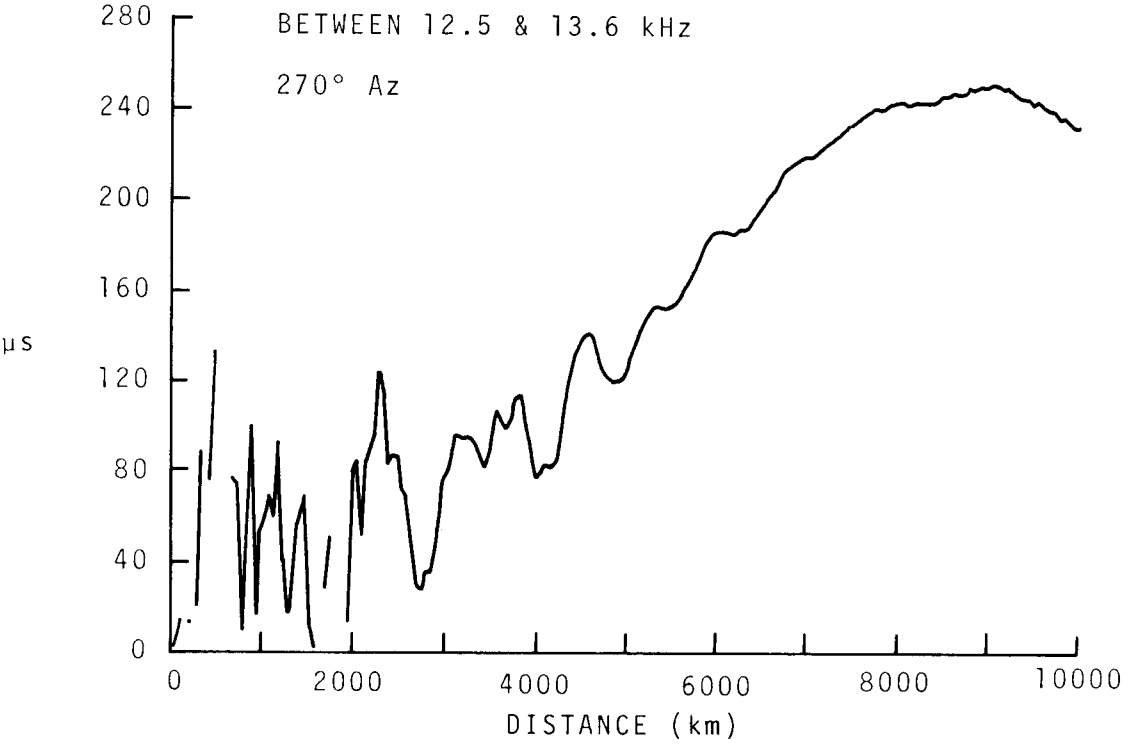

Figure 183.

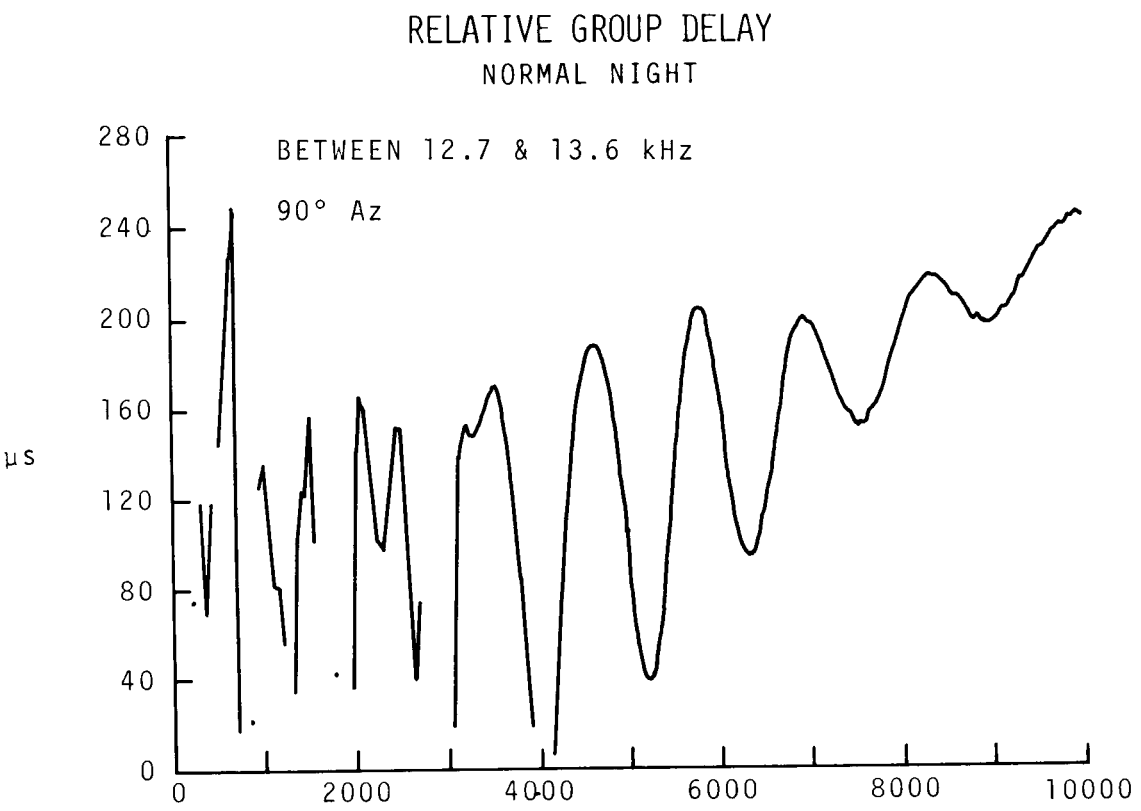

Figure 184.

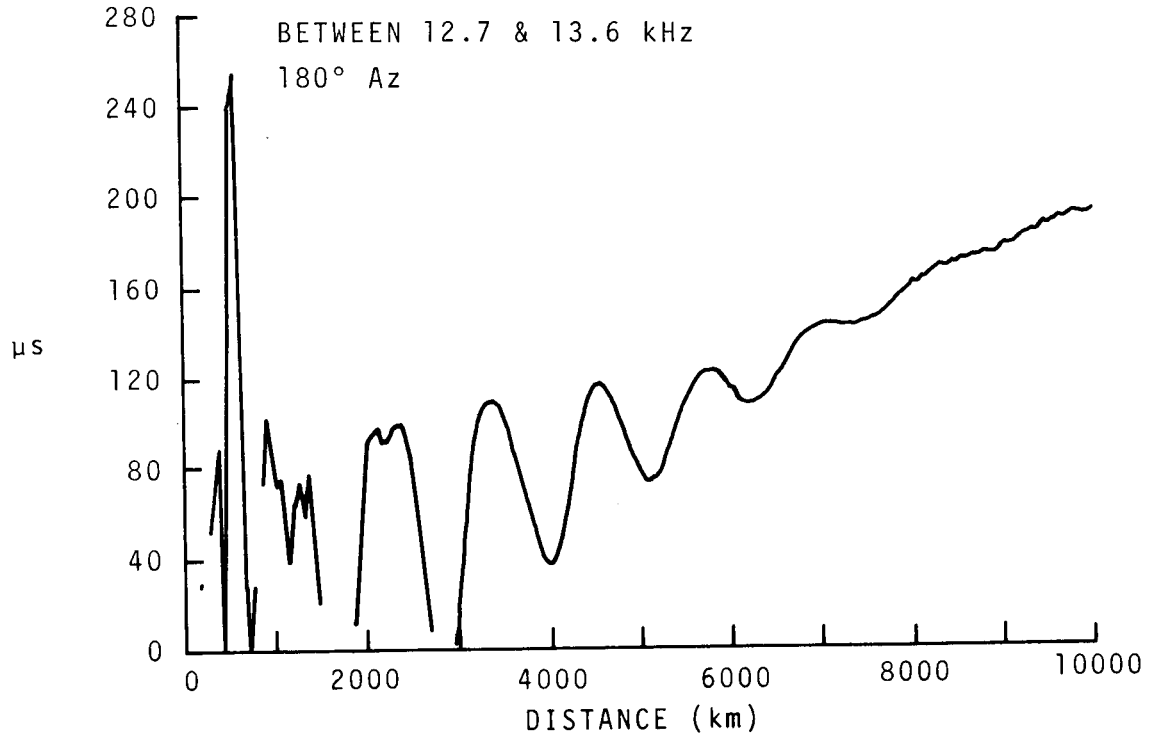

Figure 185.

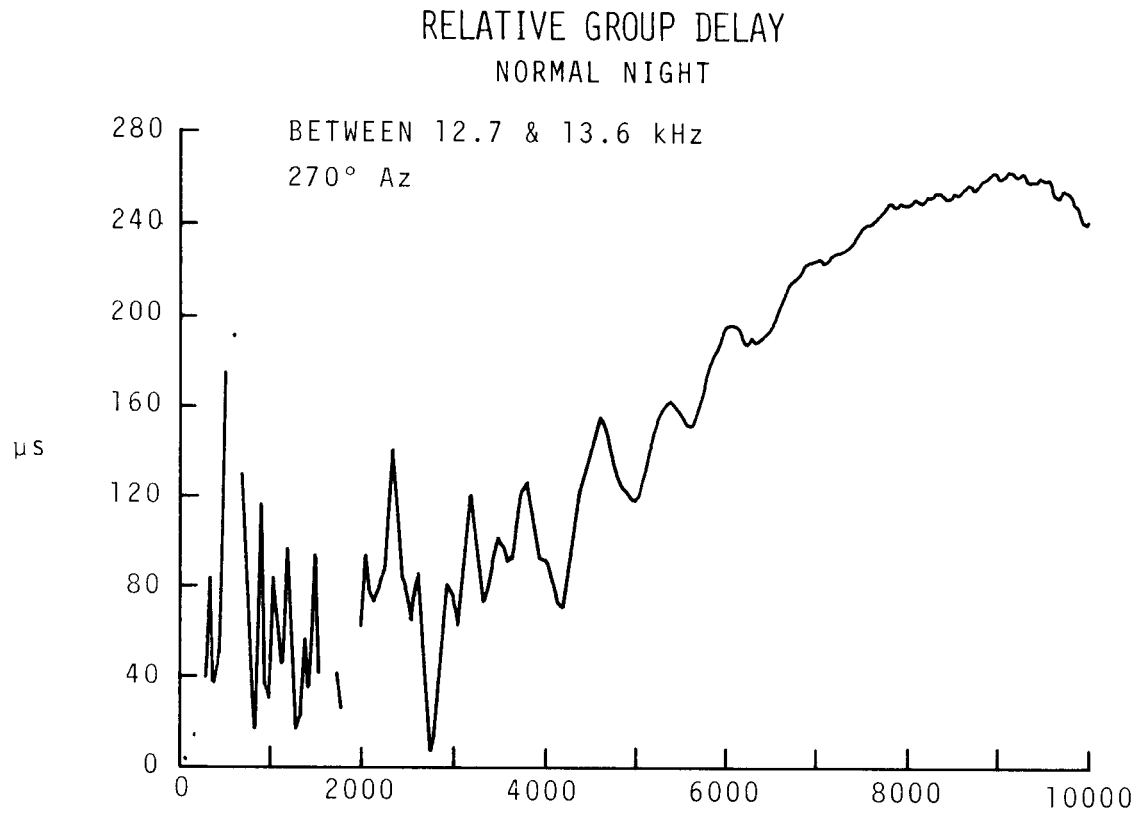

Figure 186.

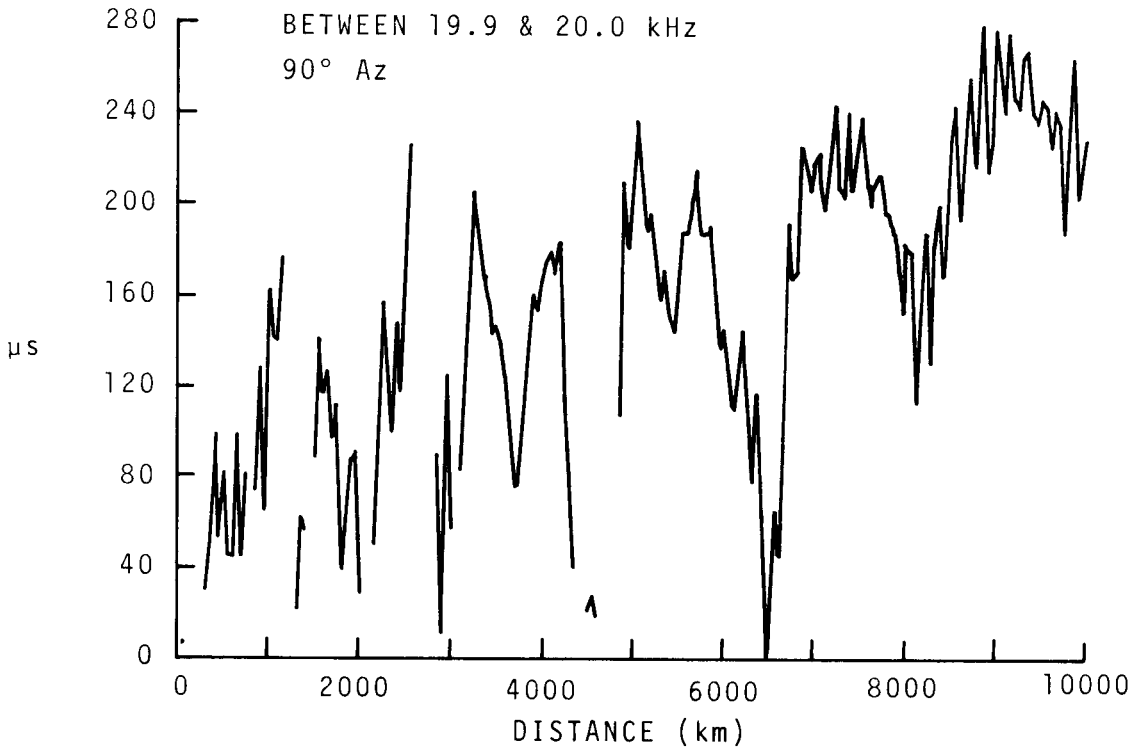

Figure 187.

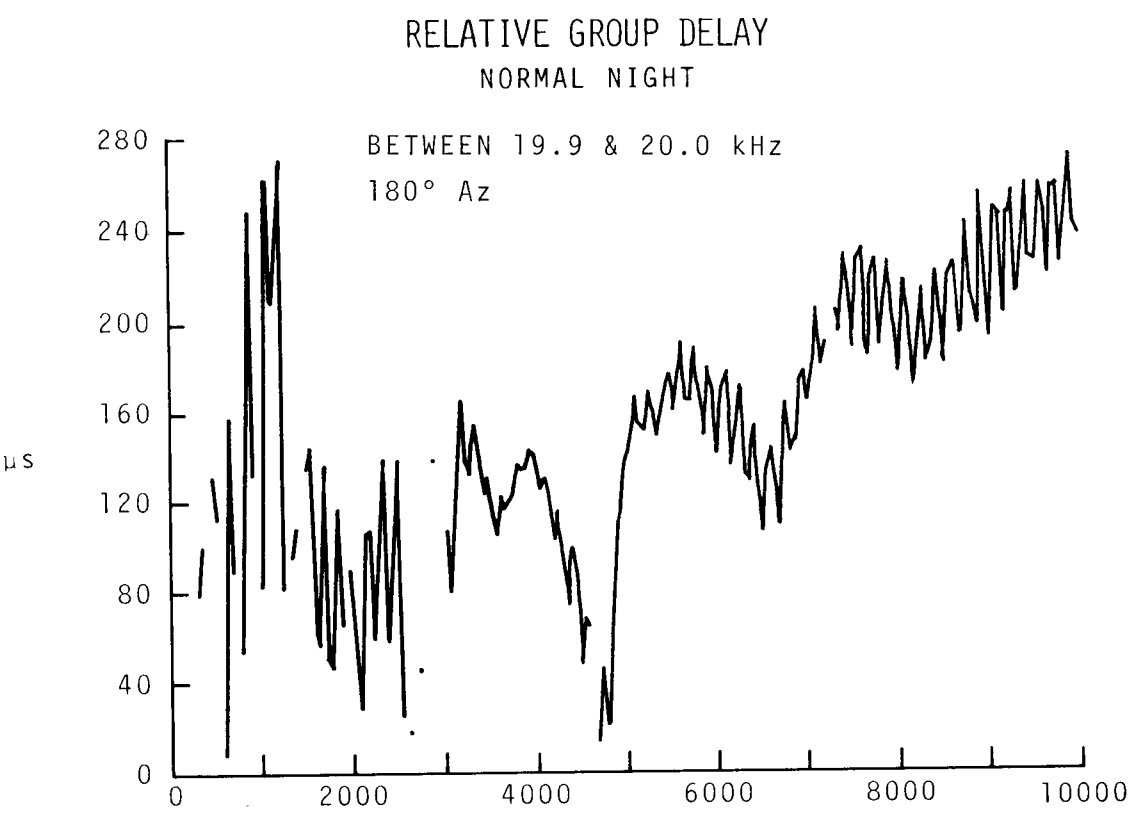

Figure 188.

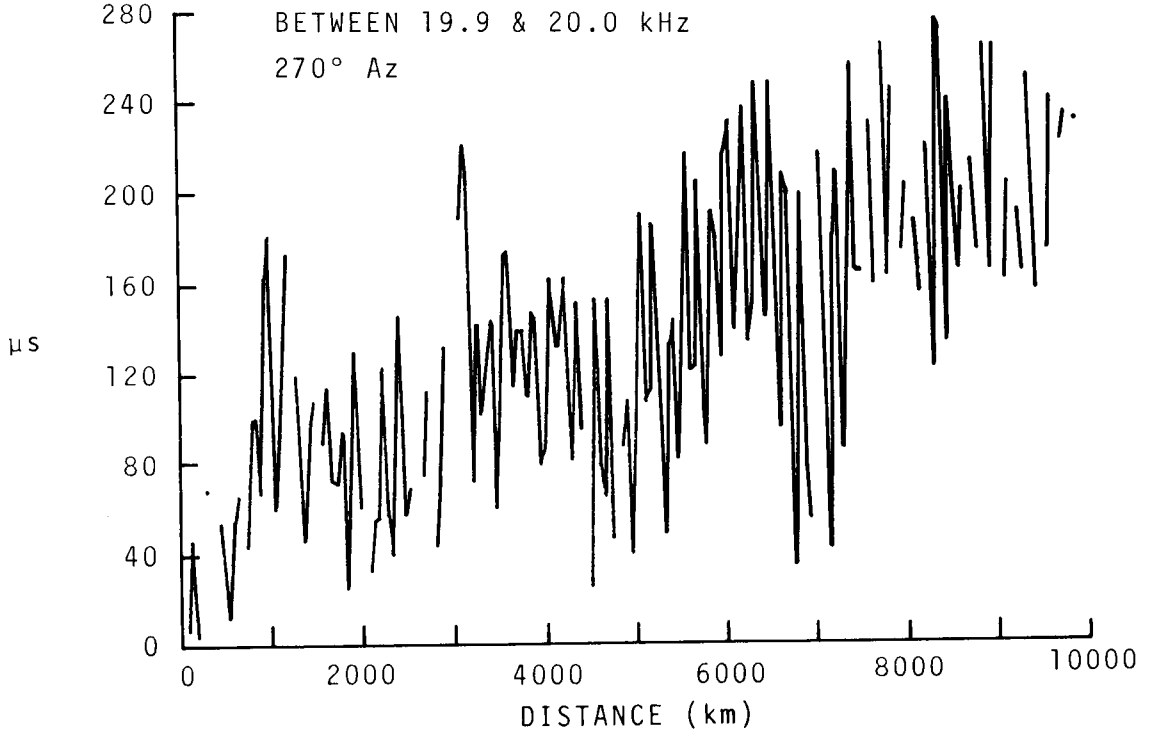

Figure 189.

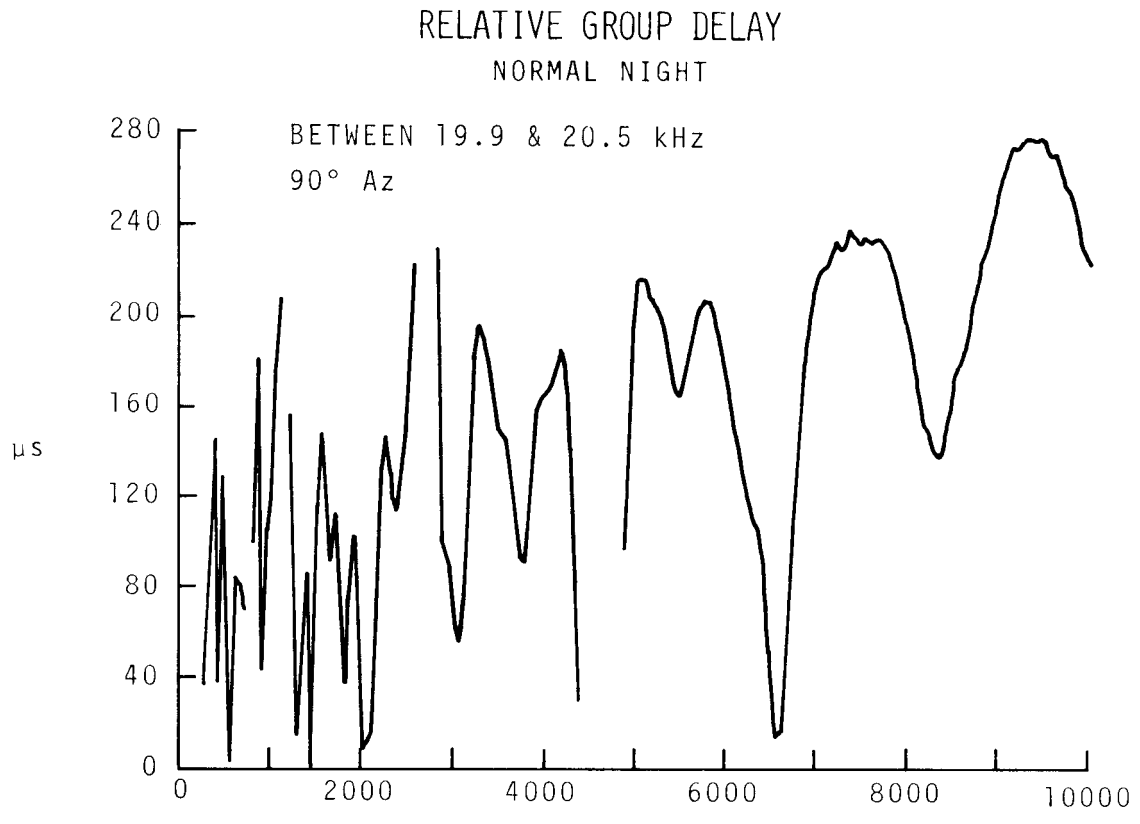

Figure 190.

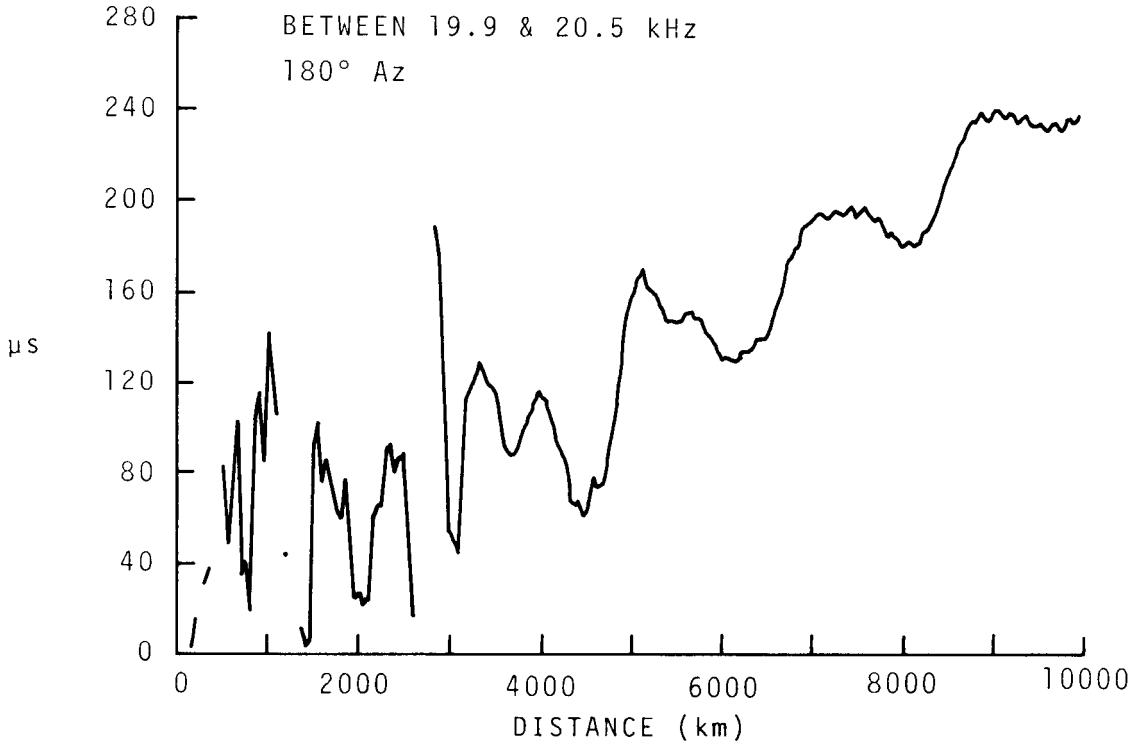

Figure 191.

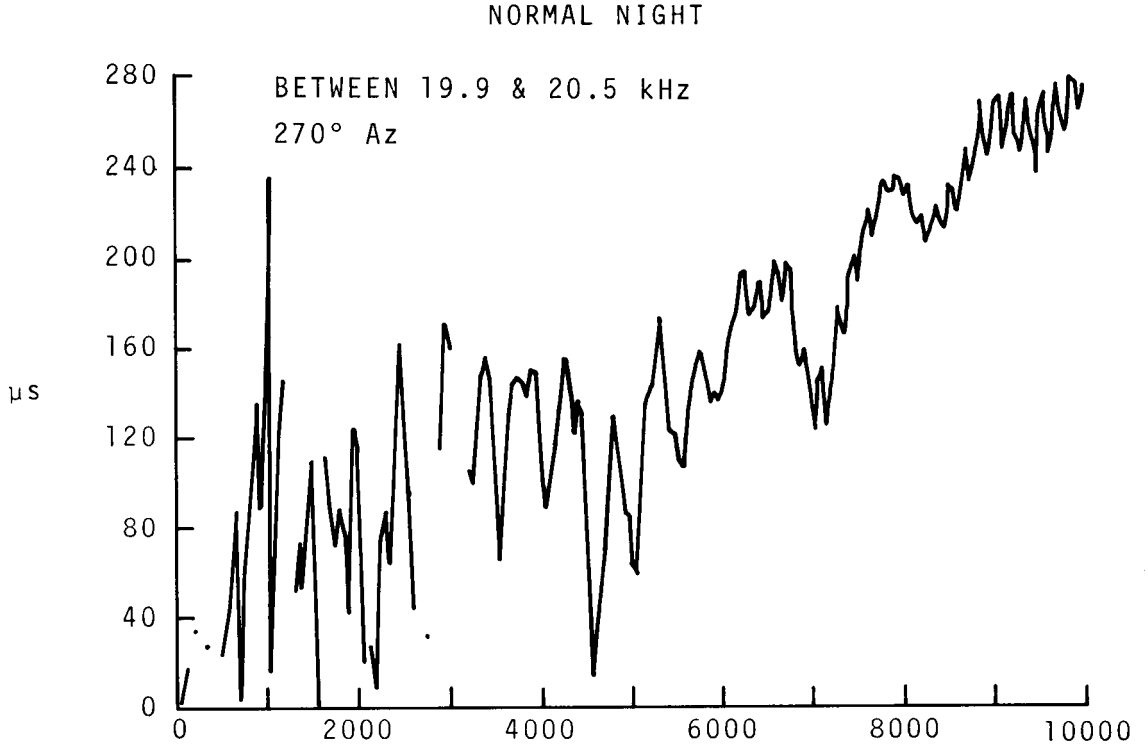

Figure 192.

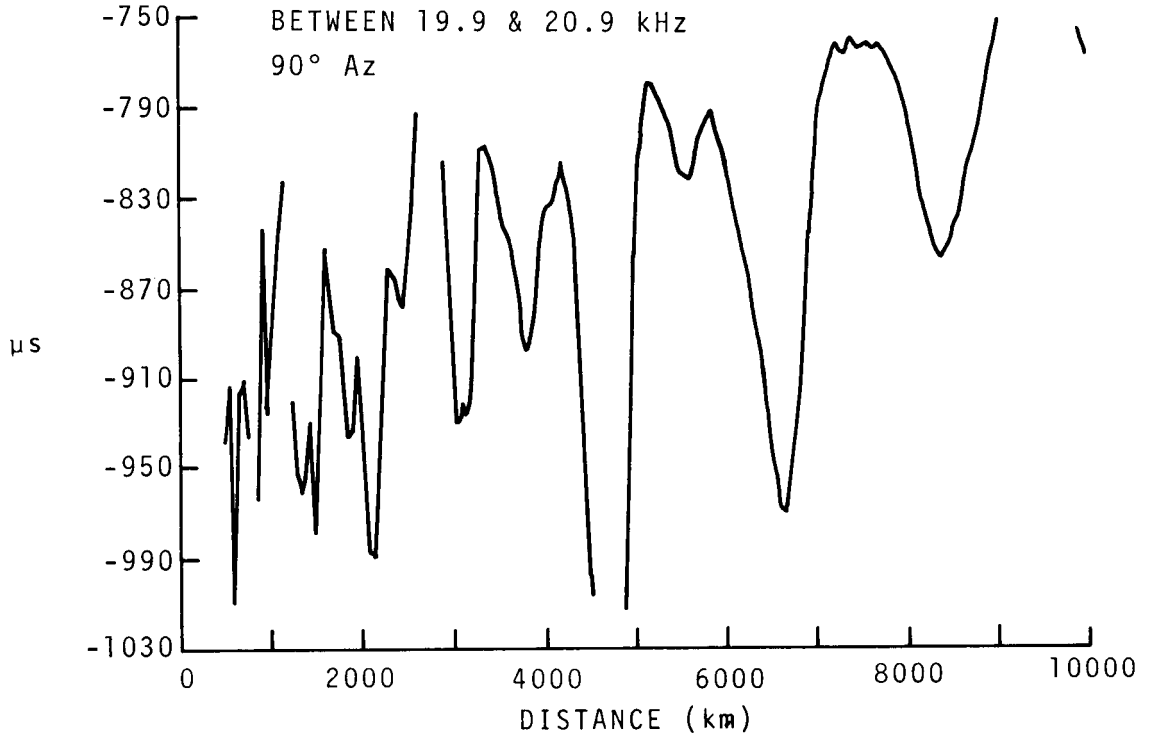

Figure 193.

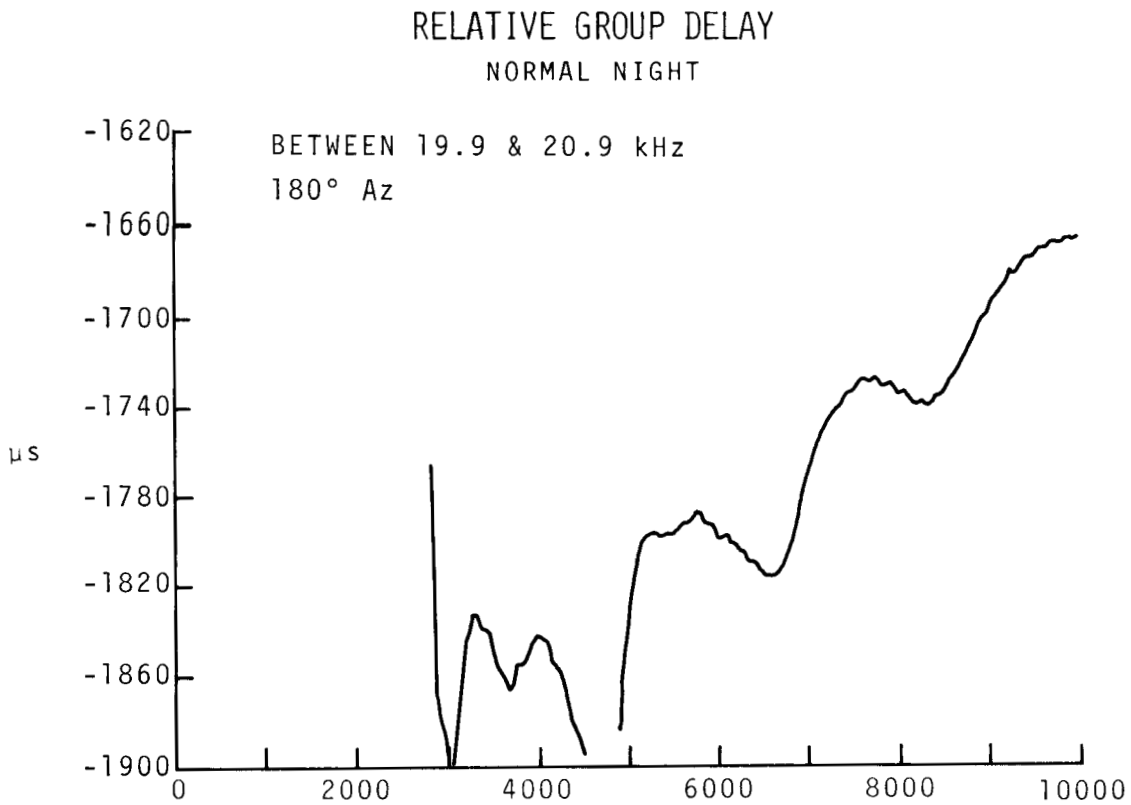

Figure 194.

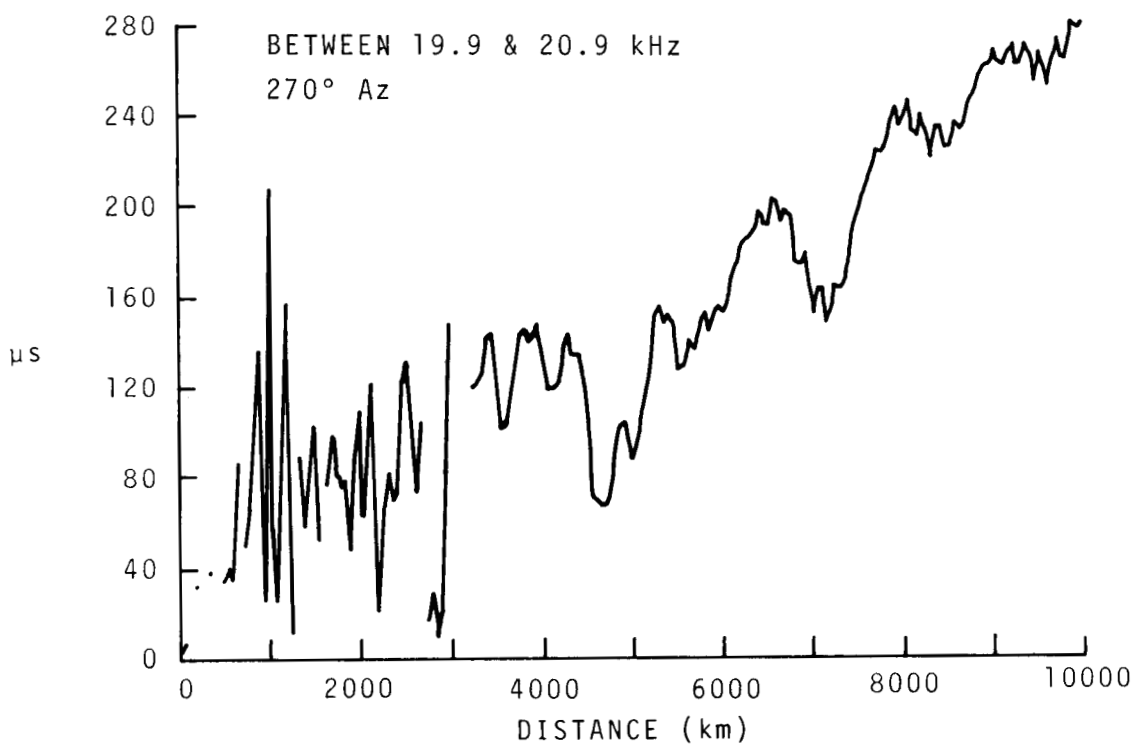

Figure 195.

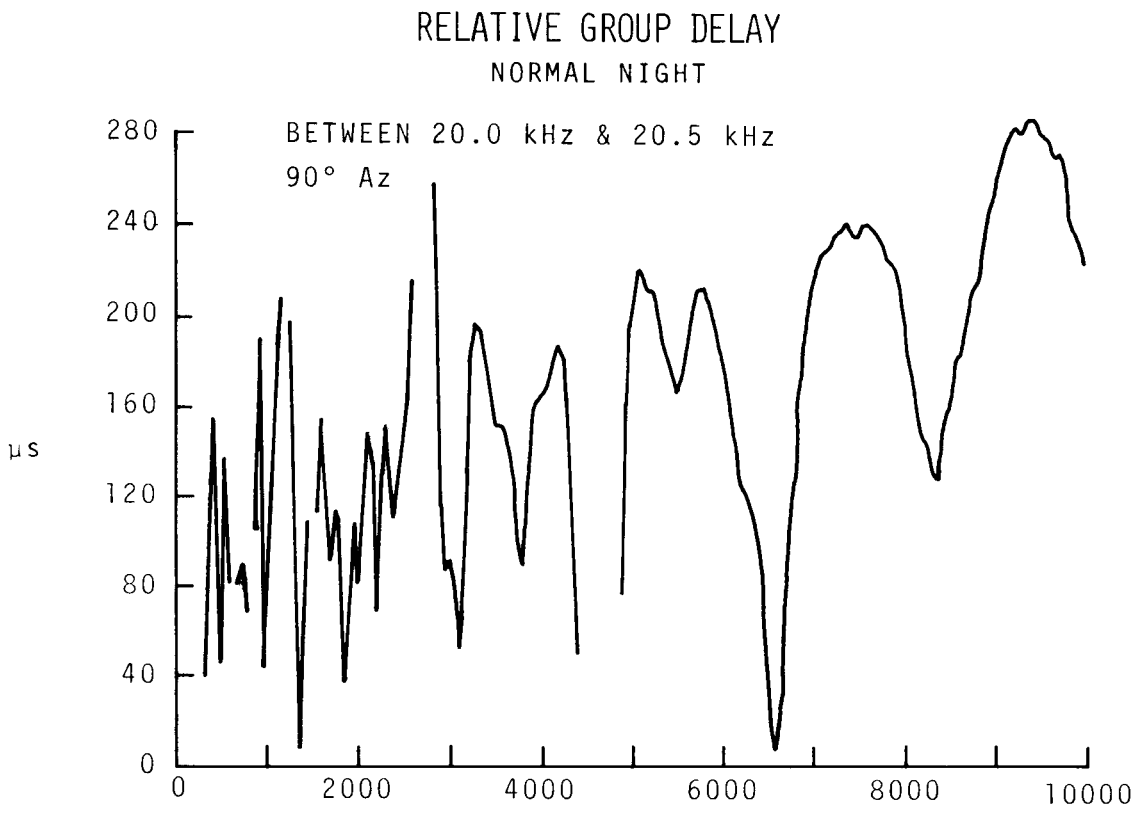

Figure 196.

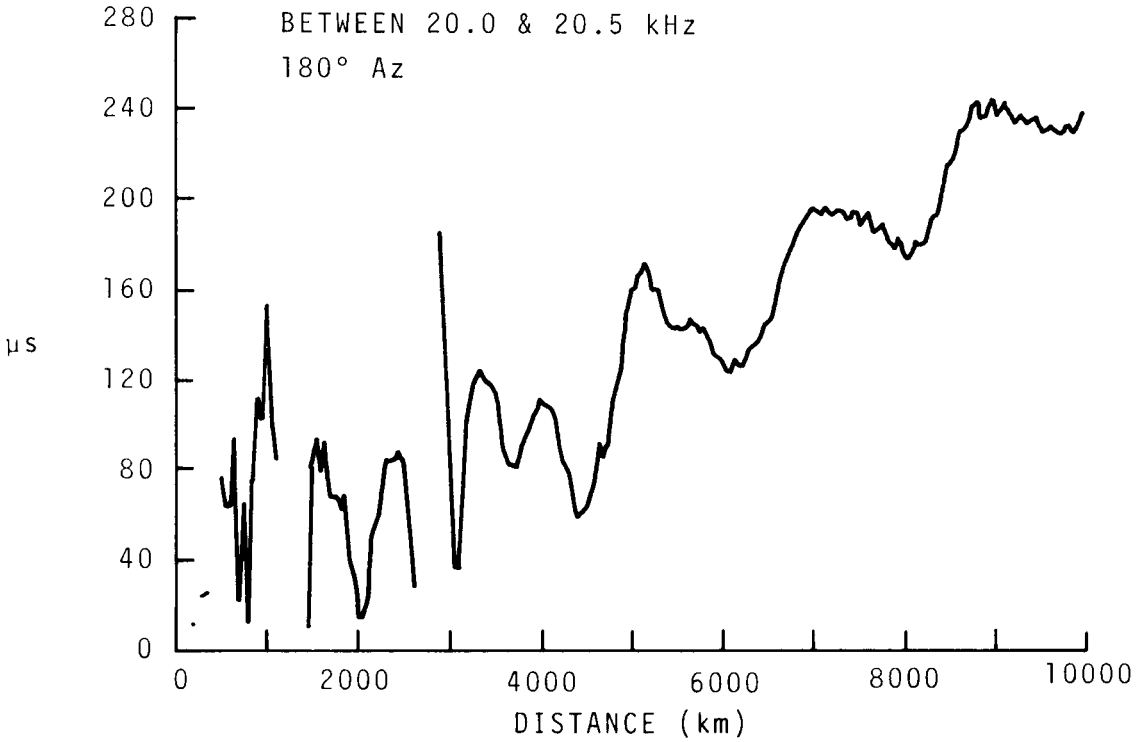

Figure 197.

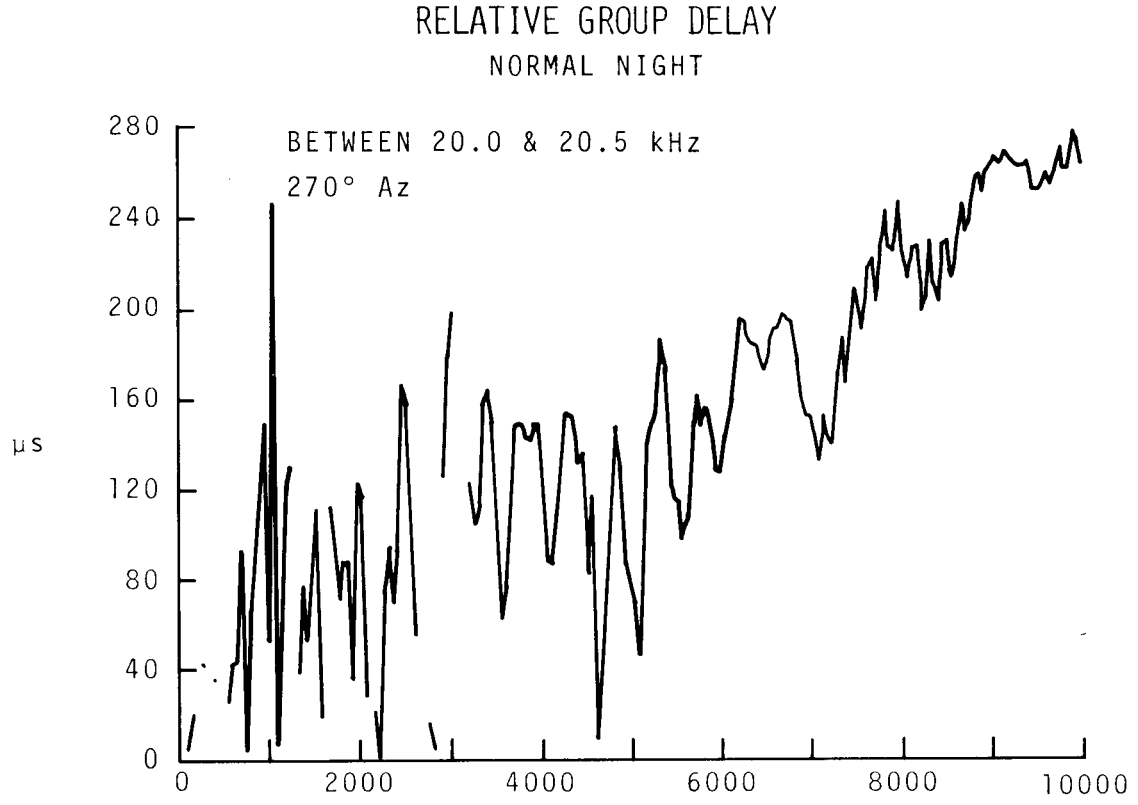

Figure 198.

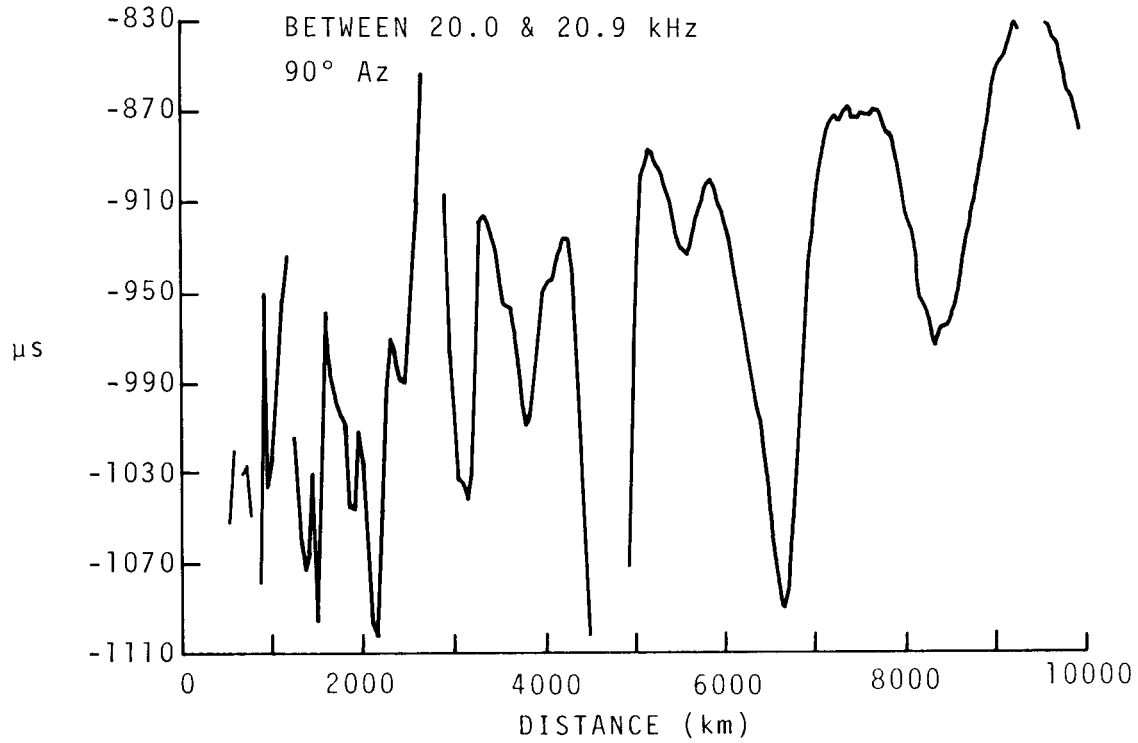

Figure 199.

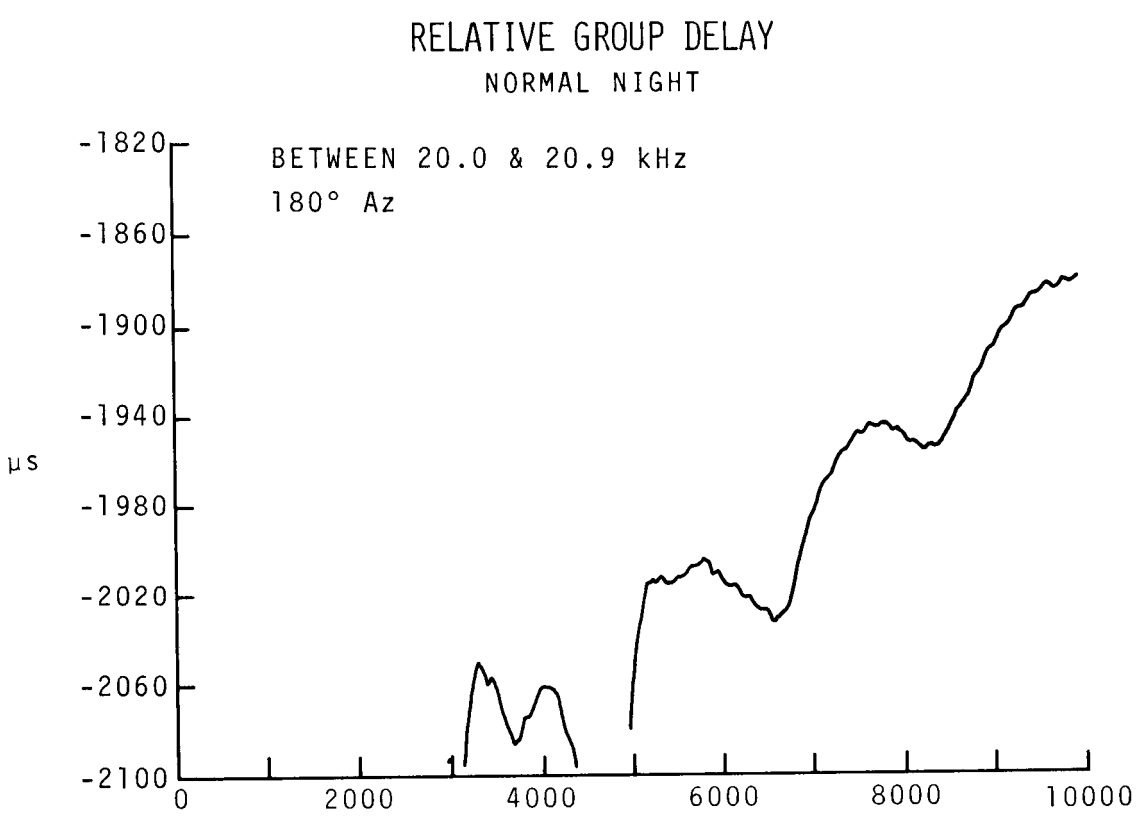

Figure 200.

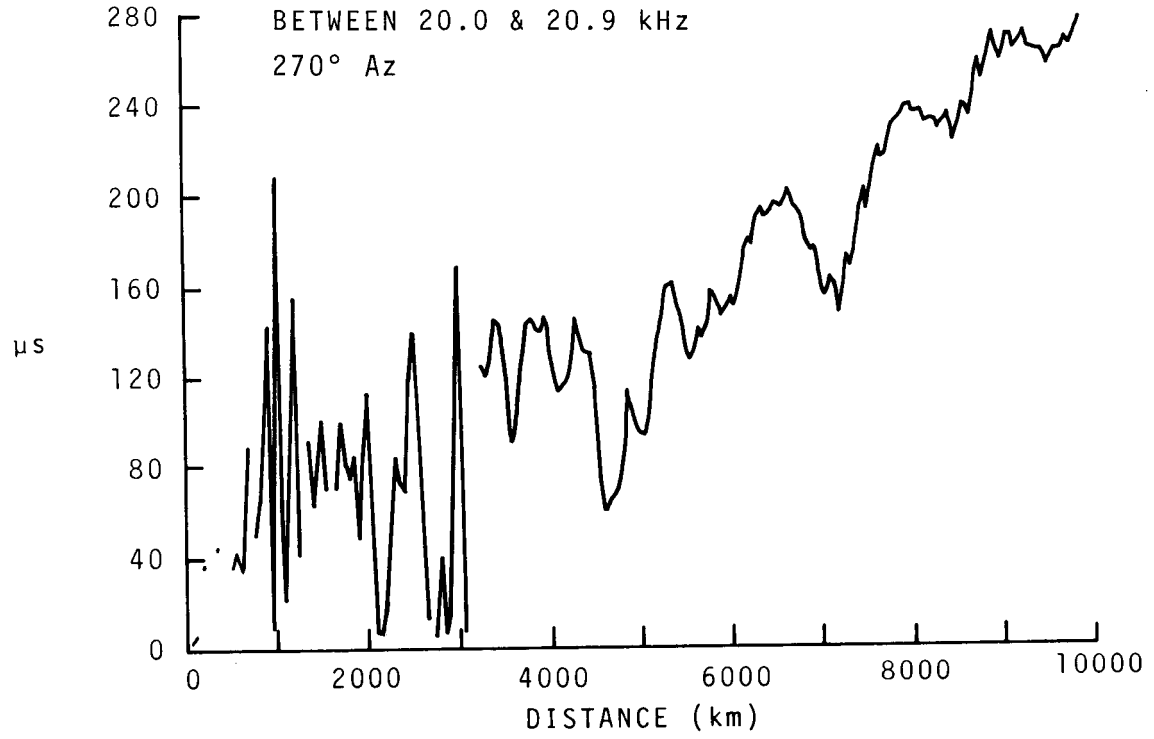

Figure 201.

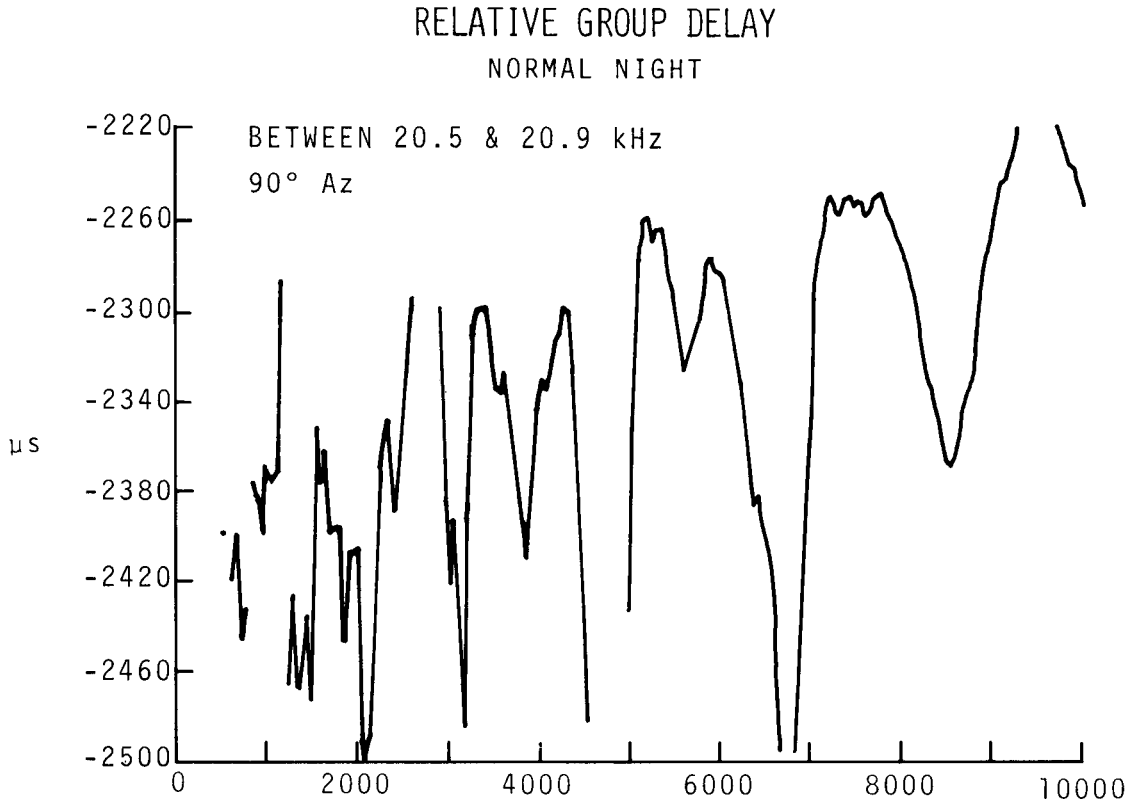

Figure 202.

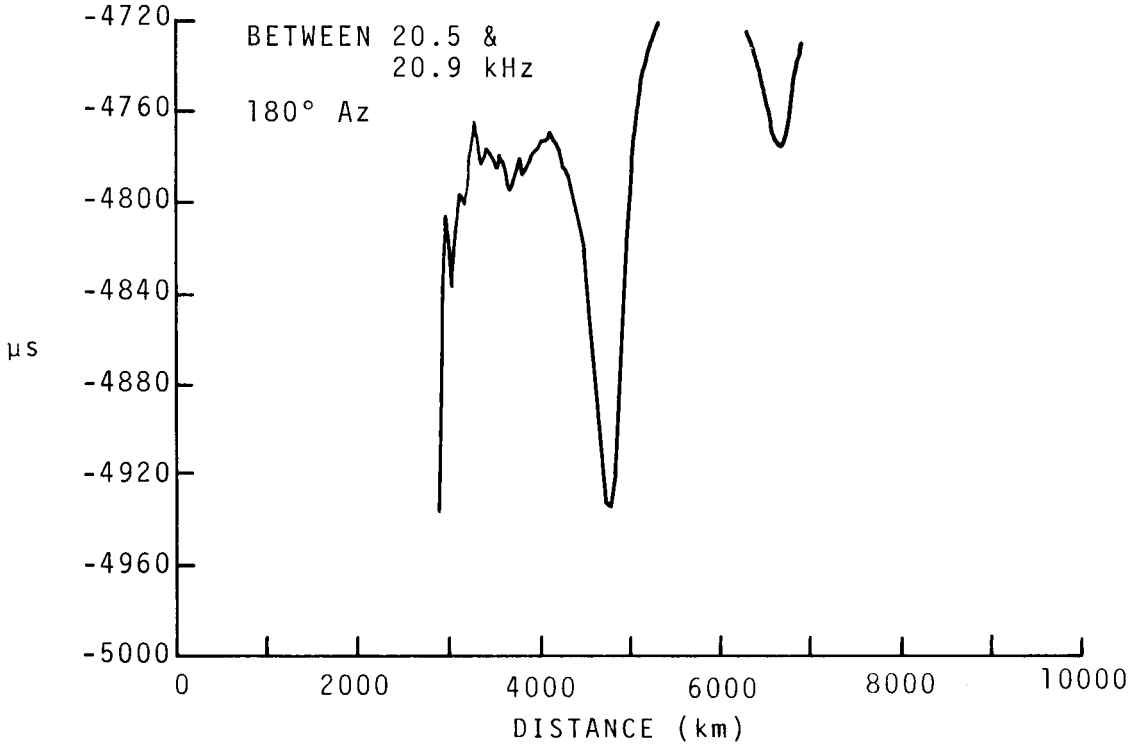

Figure 203.

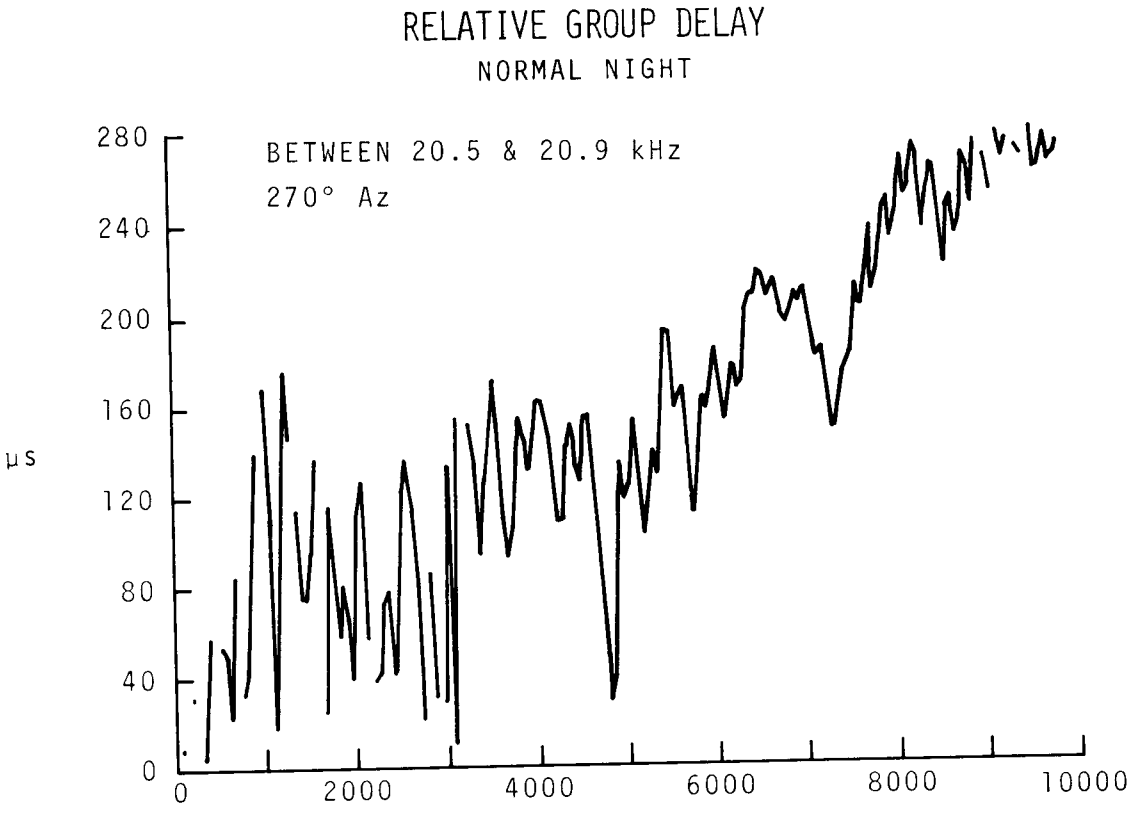
RELATIVE GROUP DELAY
NORMAL NIGHT
BETWEEN 20.5 & 20.9 kHz
270° Az
μs
280
240
200
160
120
80
40
0
0
2000
4000
6000
8000
10000

Figure 204.

DIURNAL PHASE

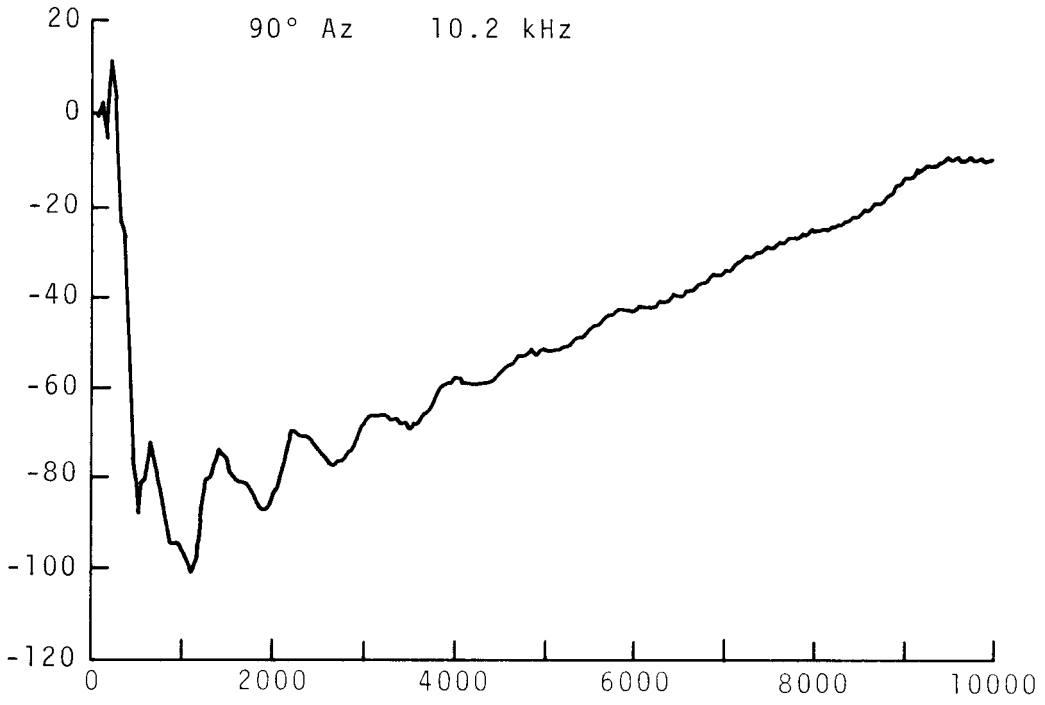

μs

Figure 205.

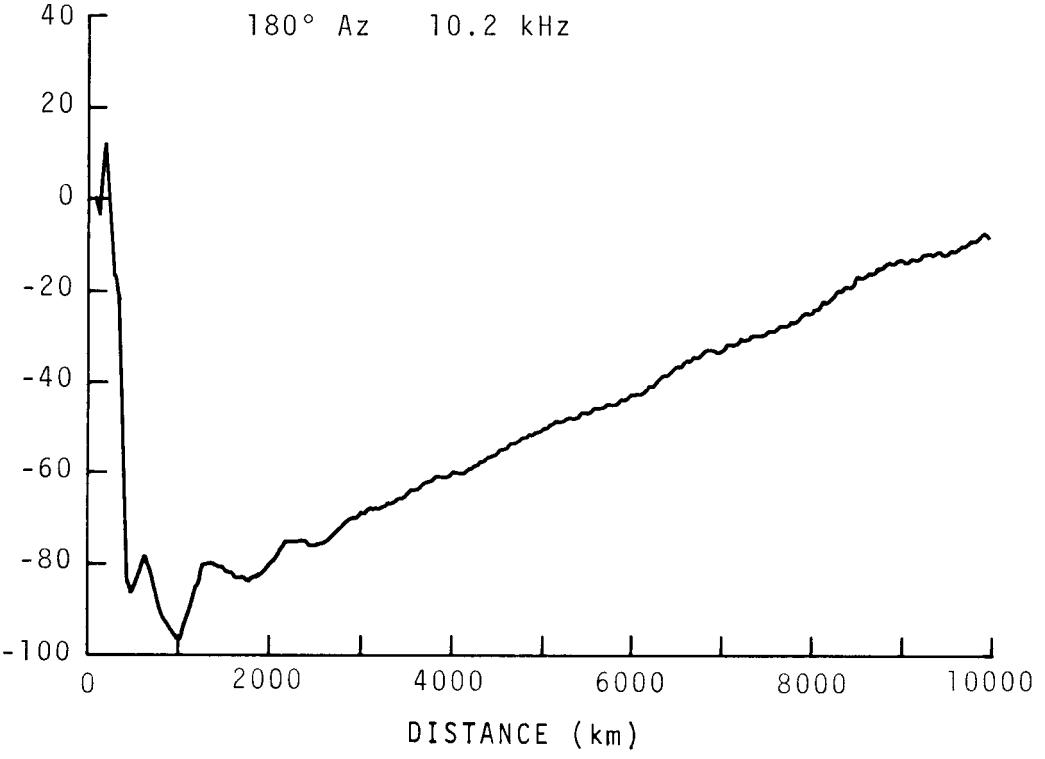

μs

Figure 206.

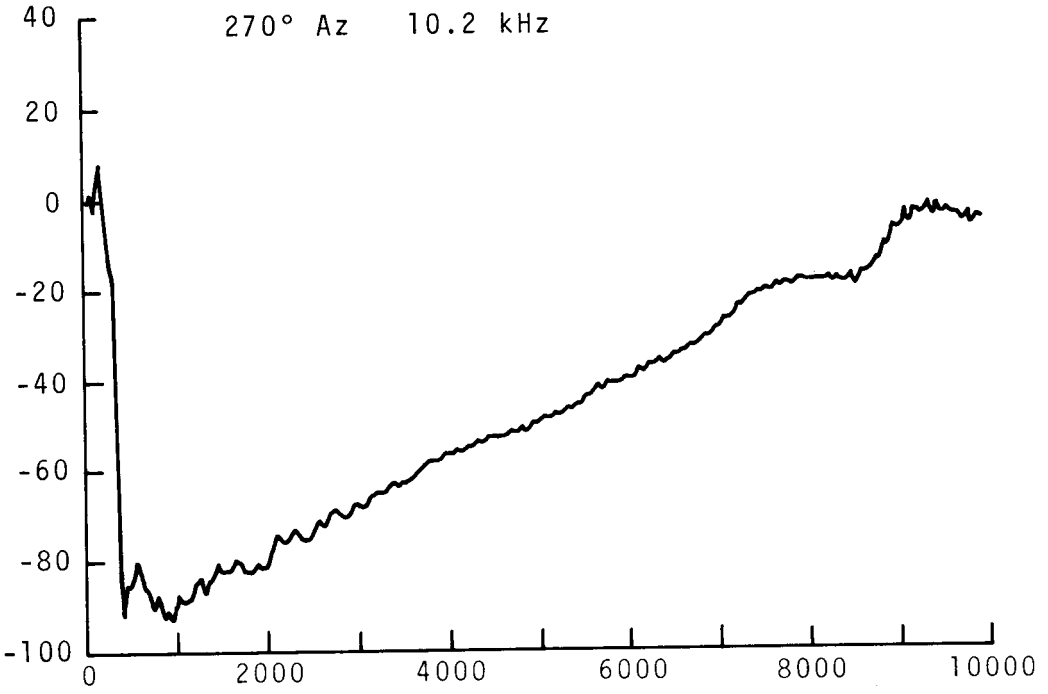

Figure 207.

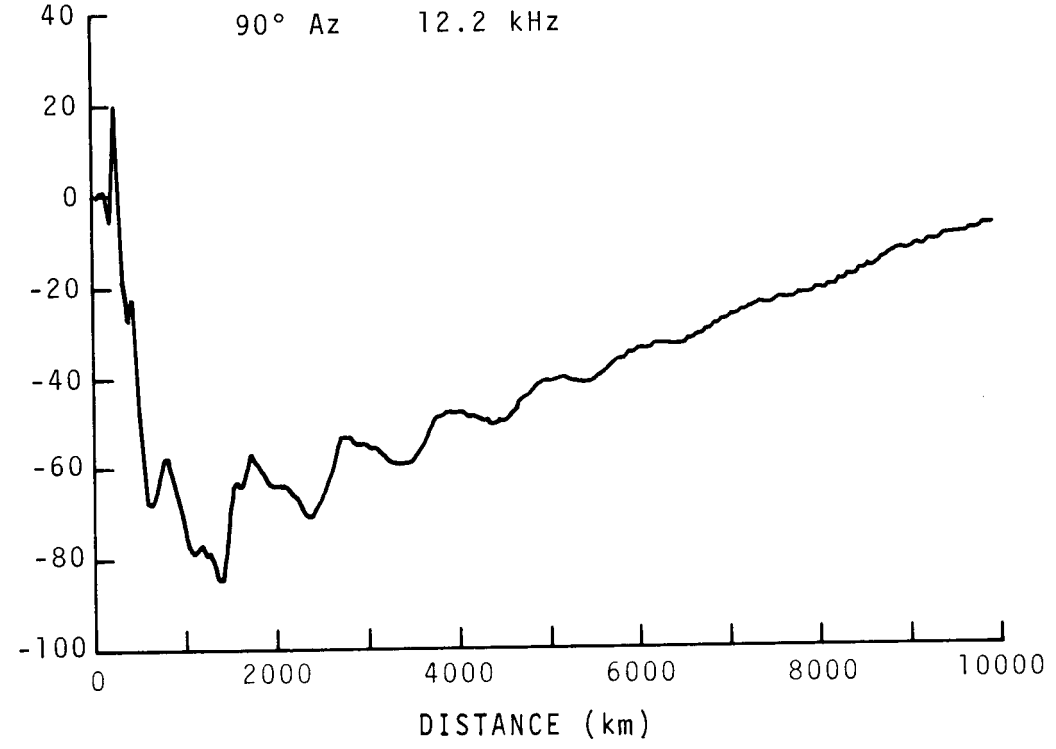

Figure 208.

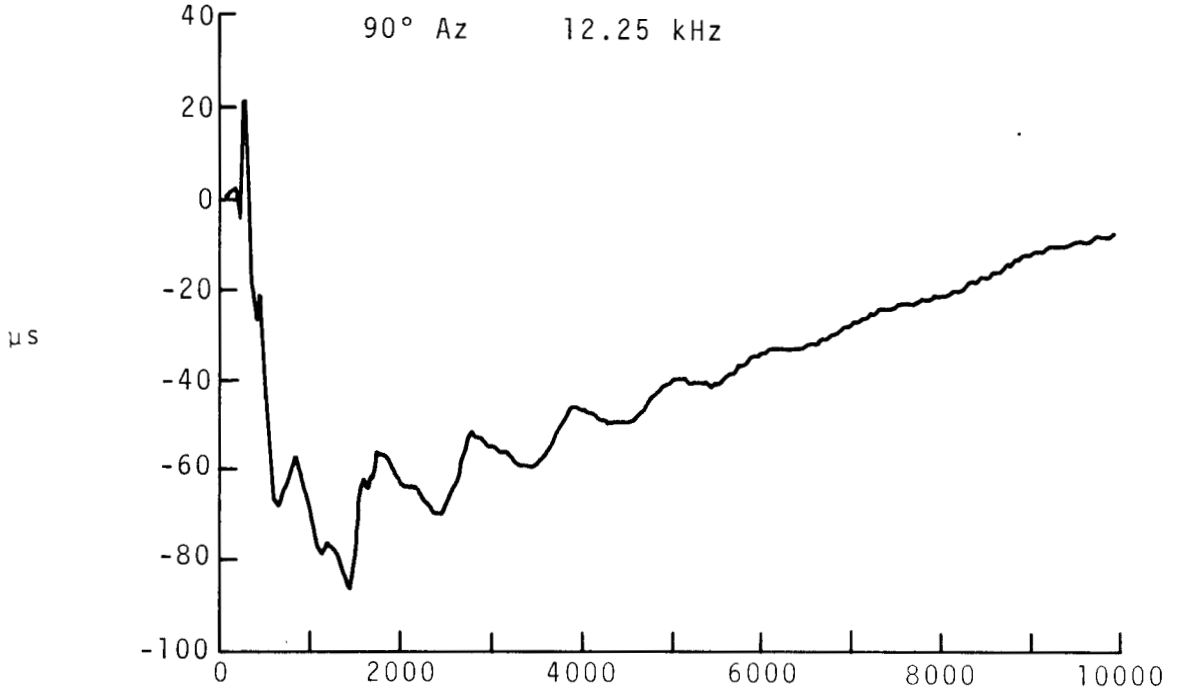

Figure 209.

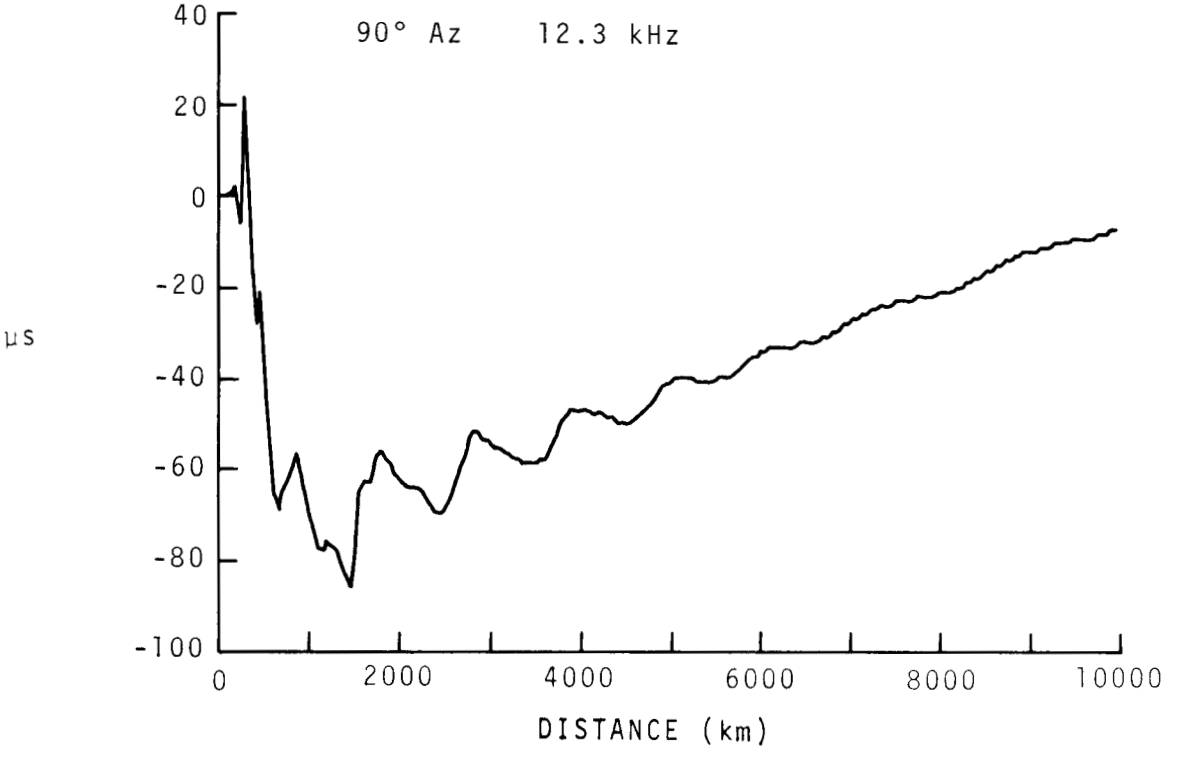

Figure 210.

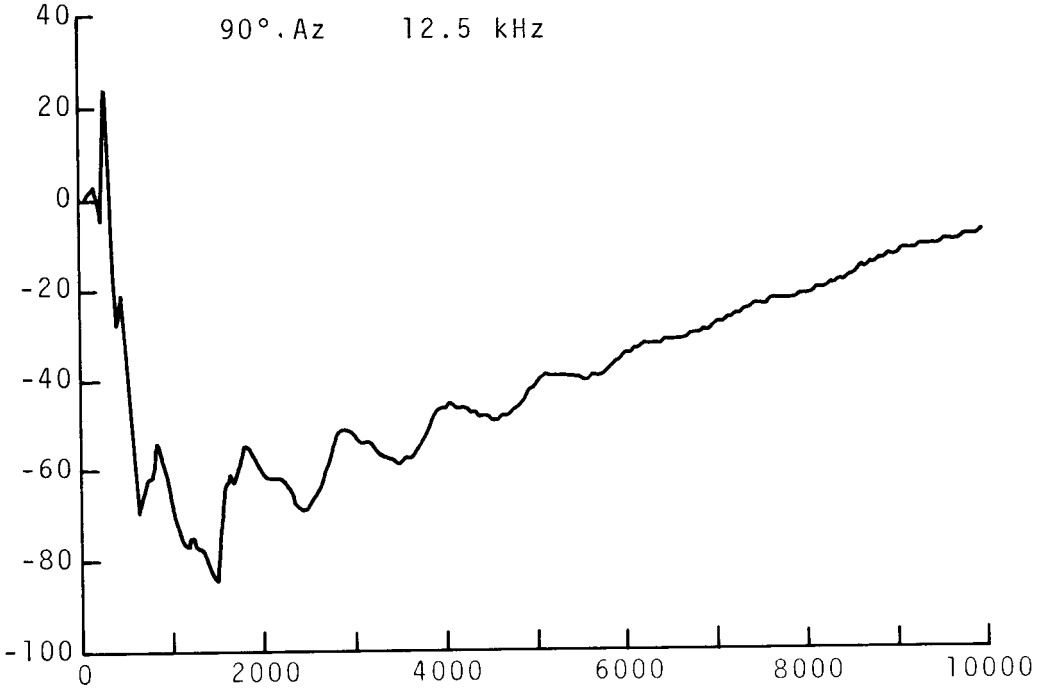

Figure 211.

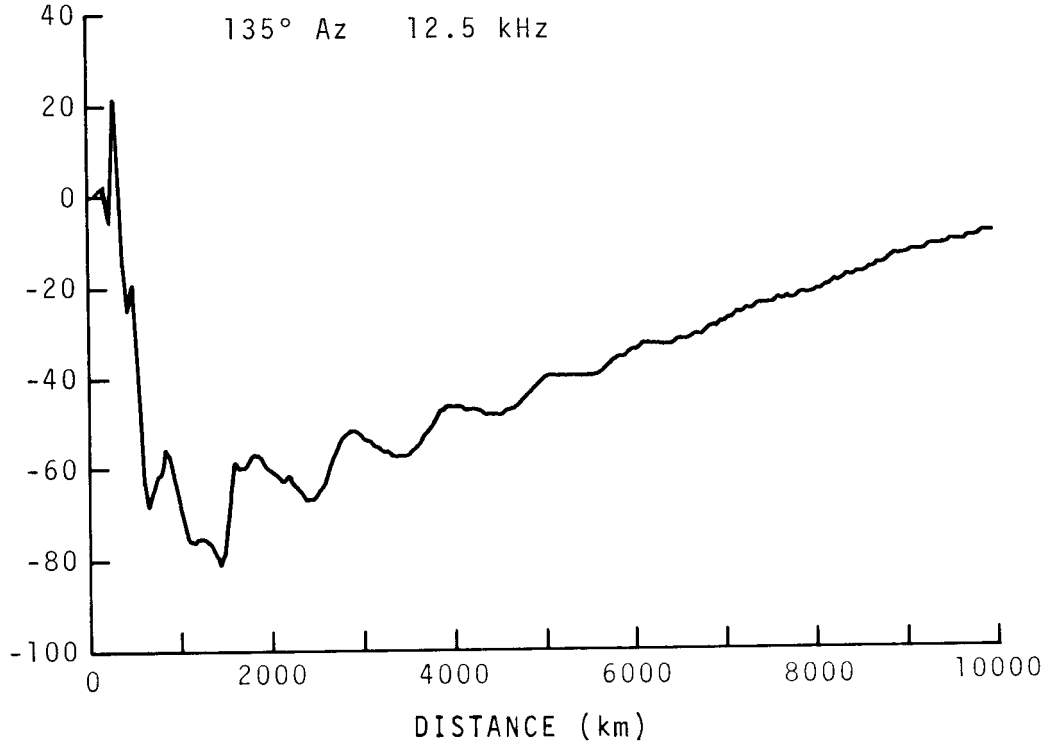

Figure 212.

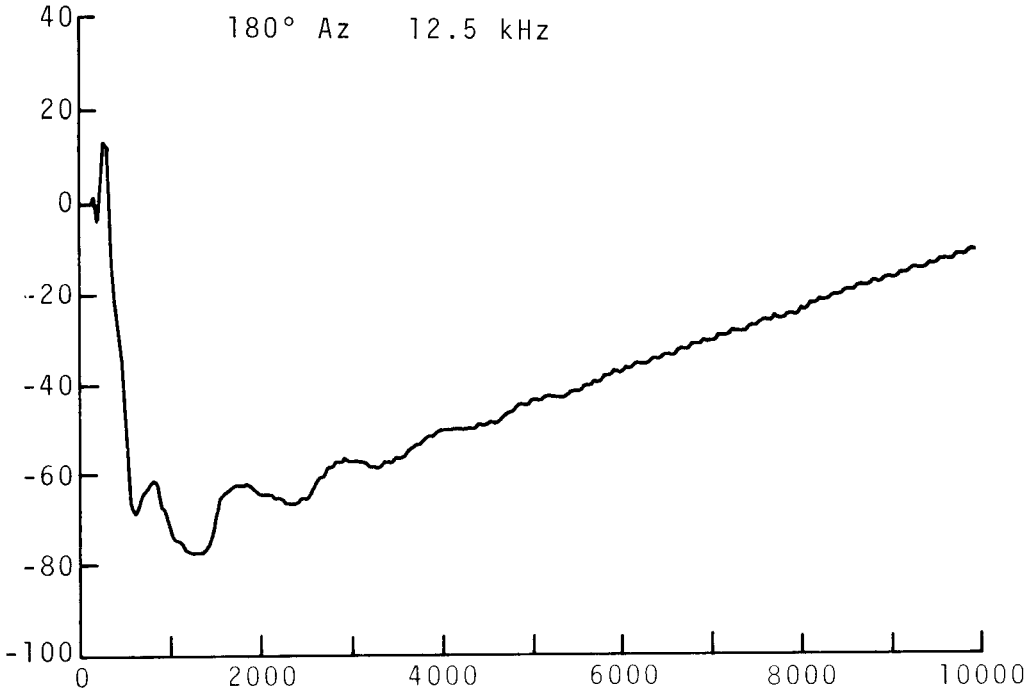

Figure 213.

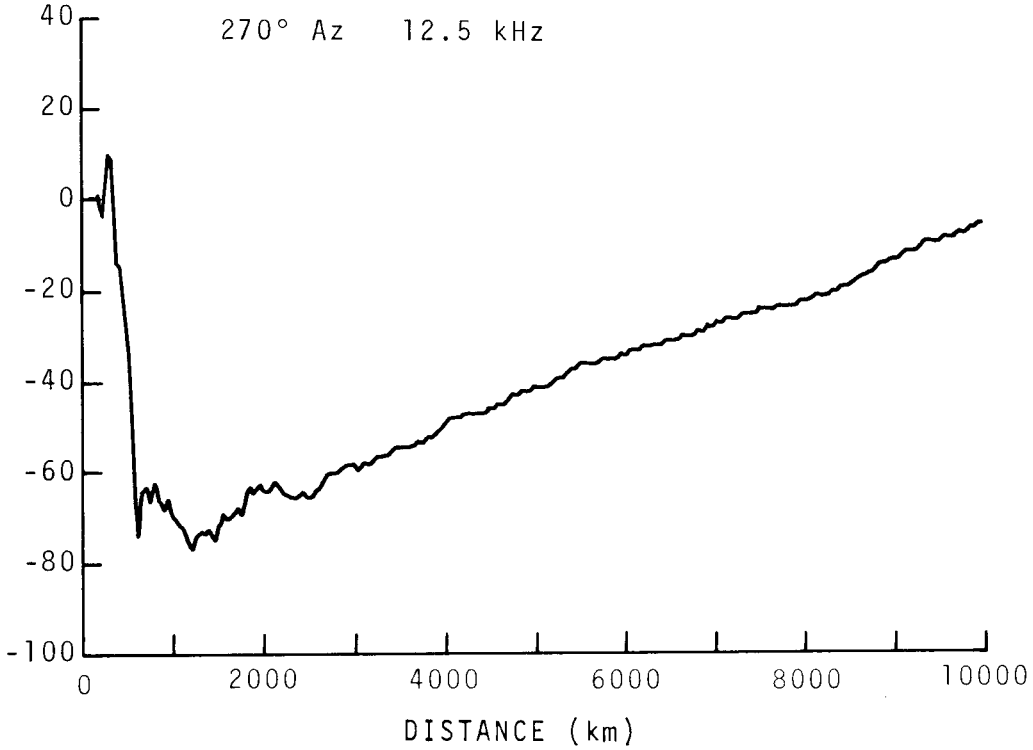

Figure 214.

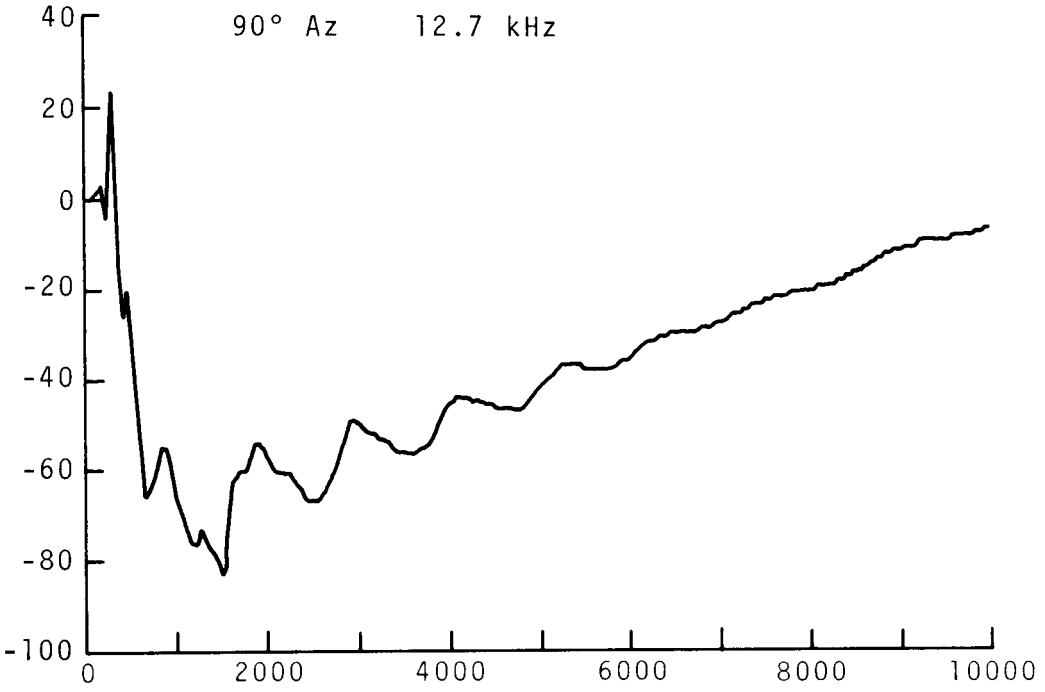

Figure 215.

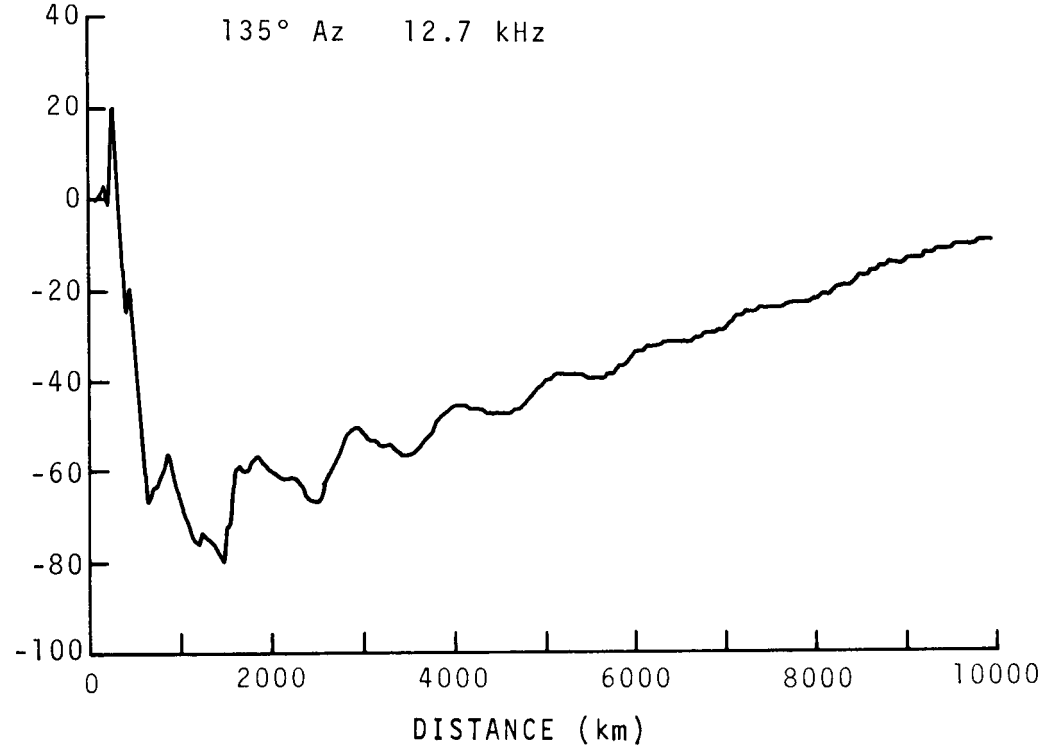

Figure 216.

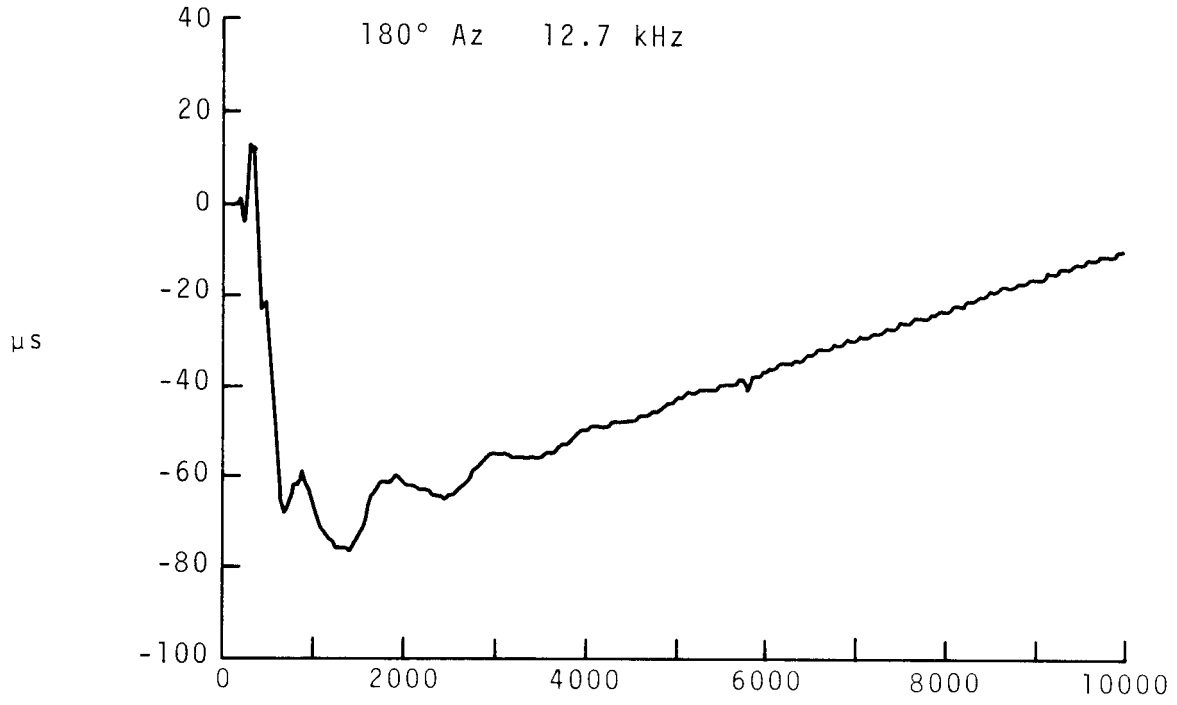

Figure 217.

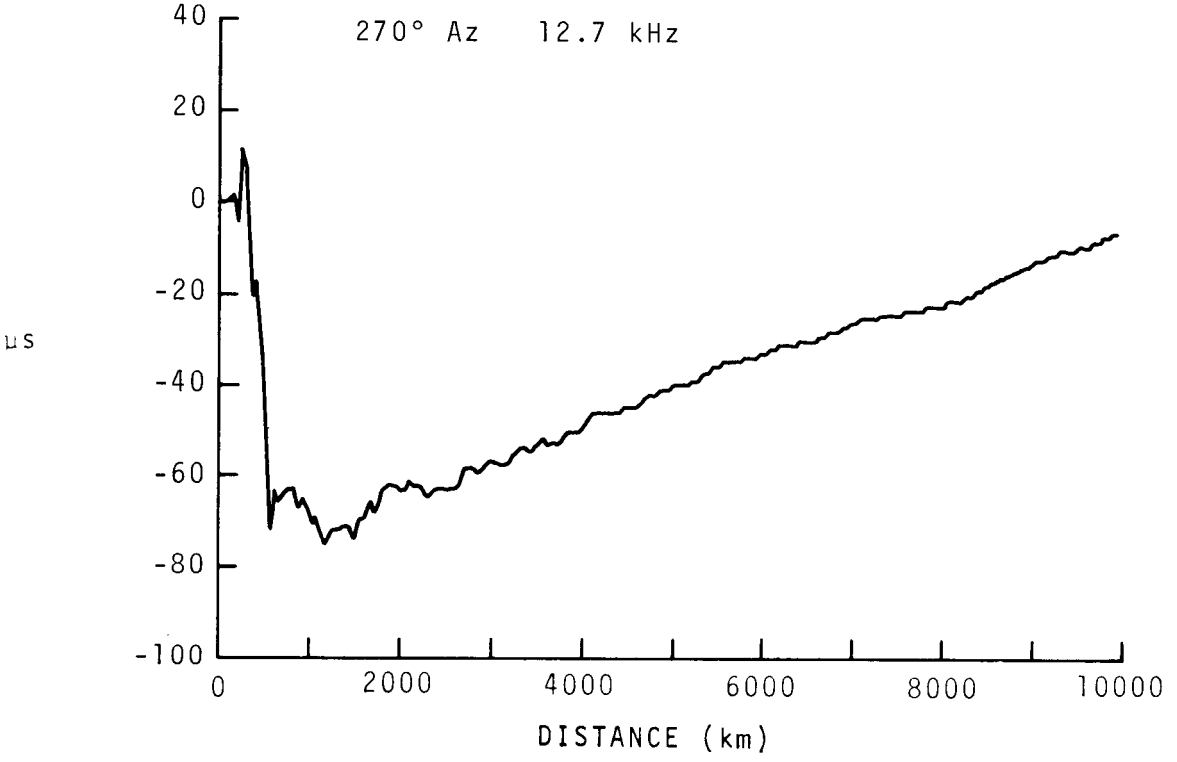

Figure 218.

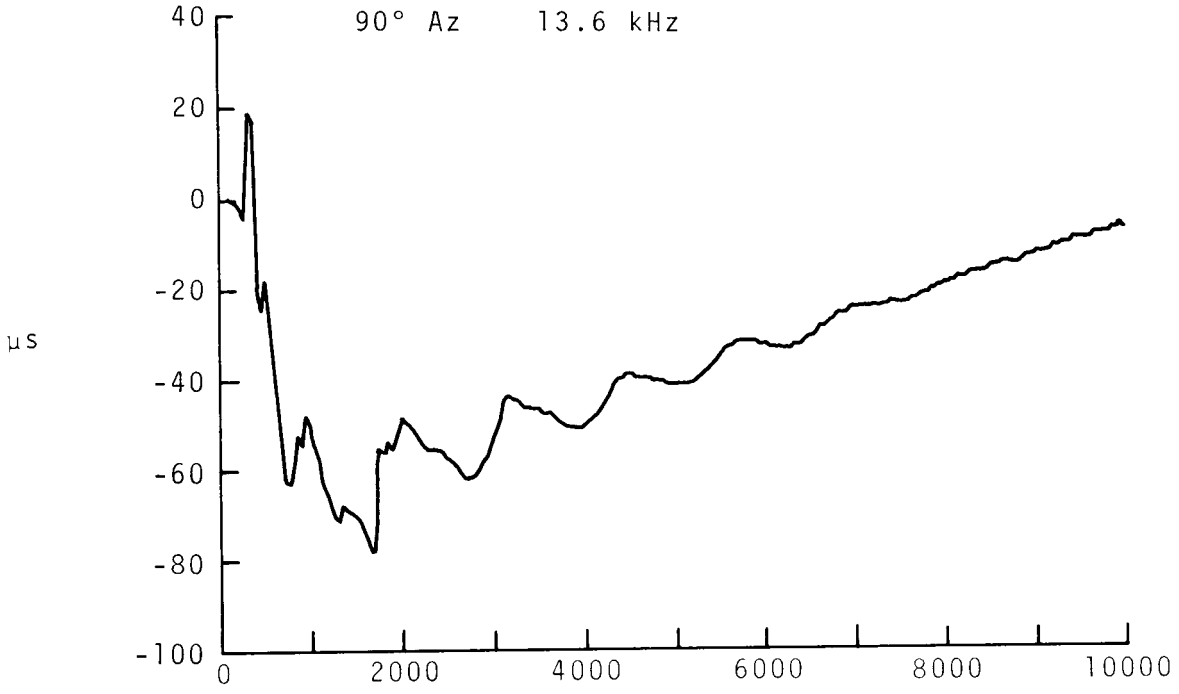

Figure 219.

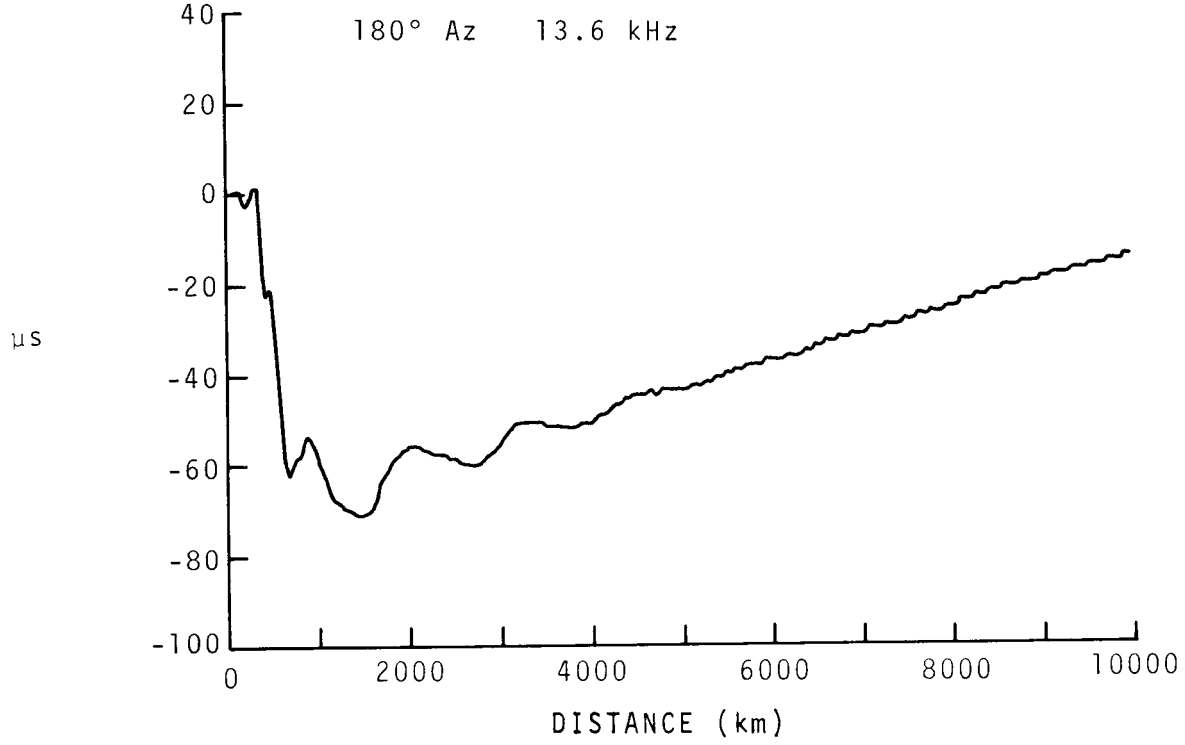

Figure 220.

DIURNAL PHASE

Figure 221.

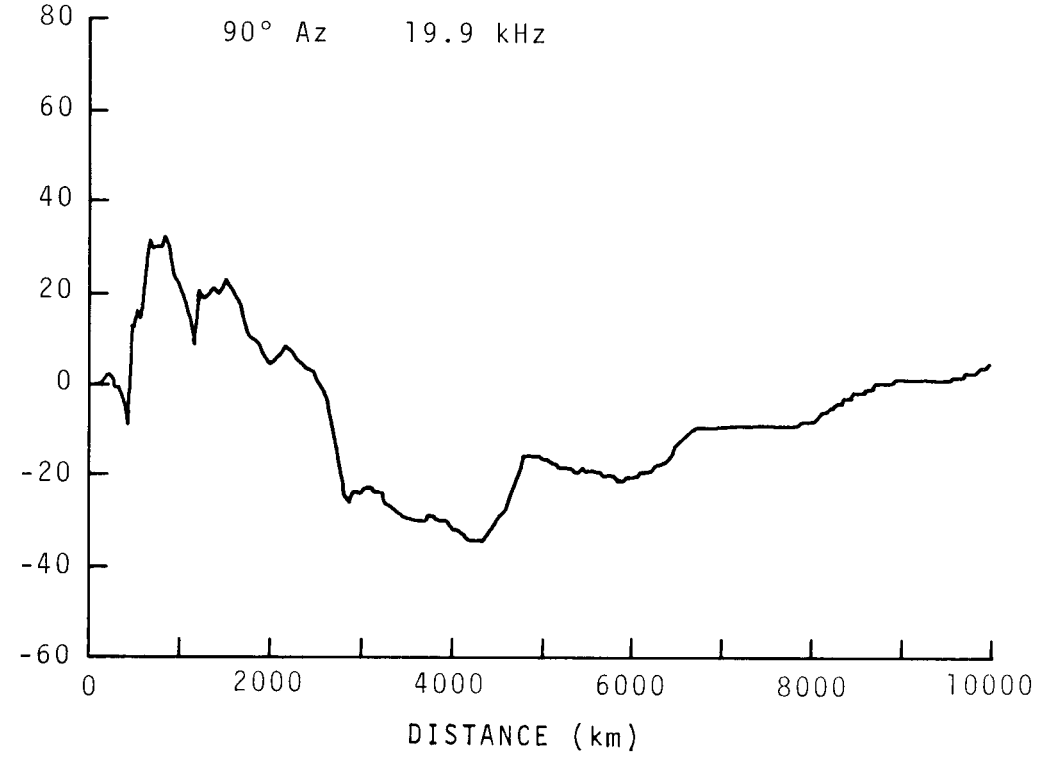

Figure 222.

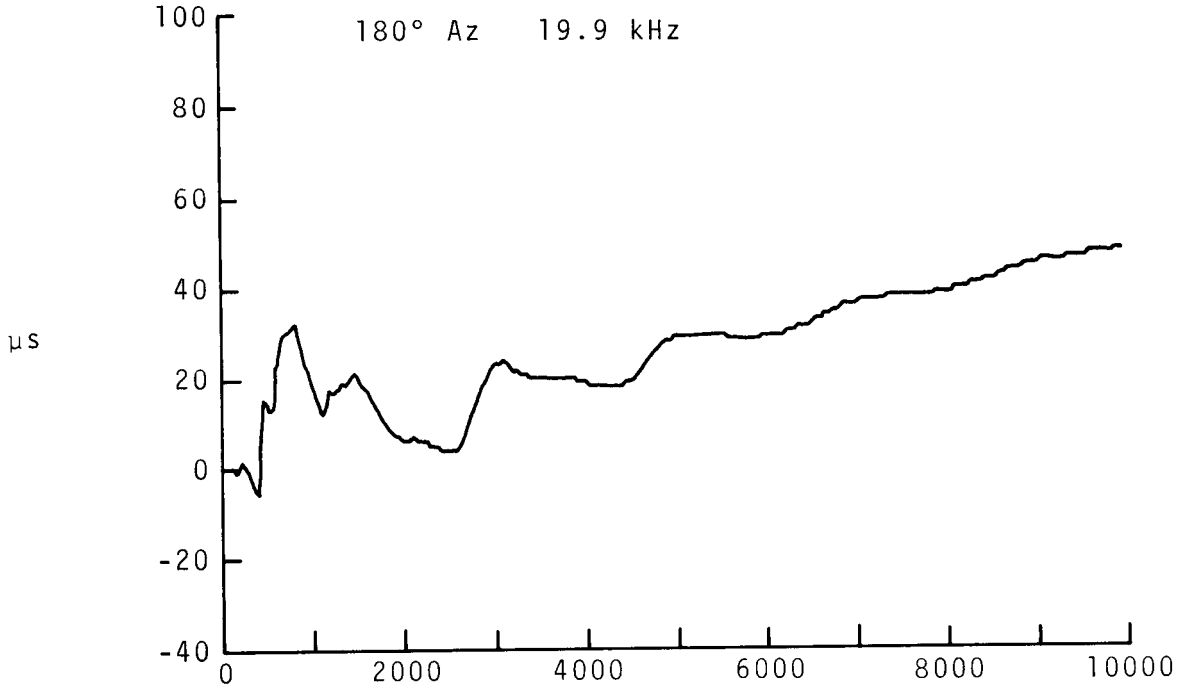

Figure 223.

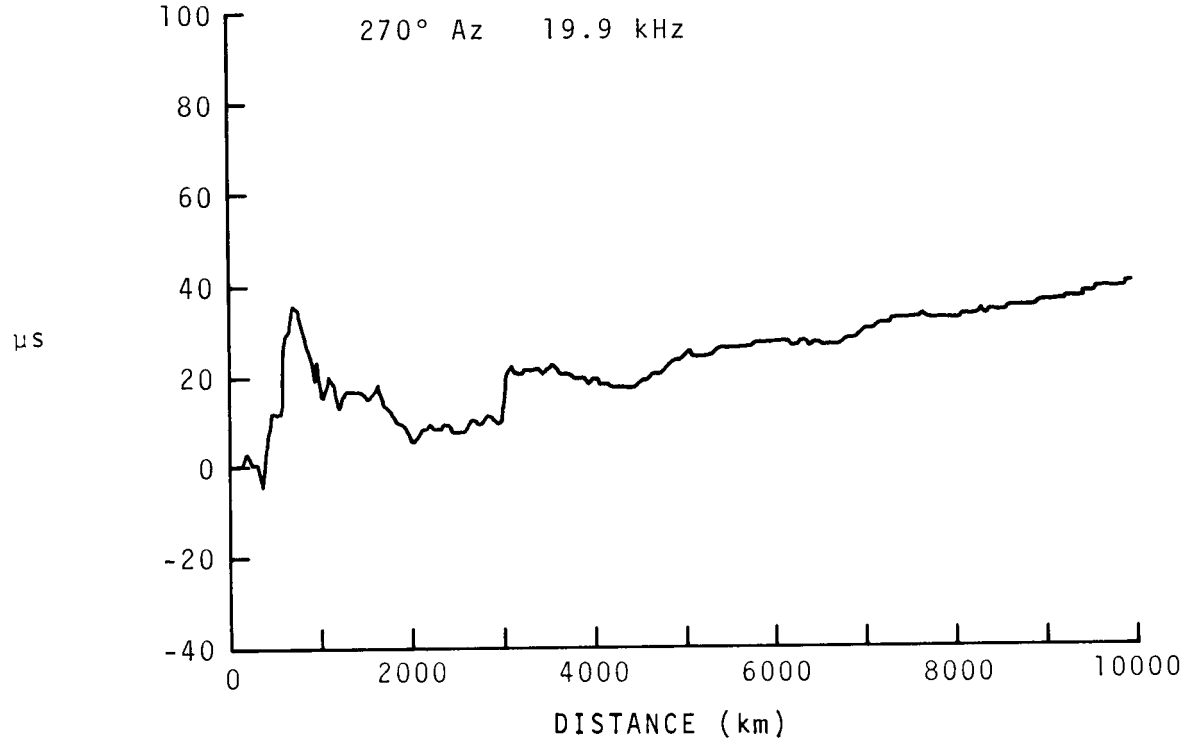

Figure 224.

DIURNAL PHASE

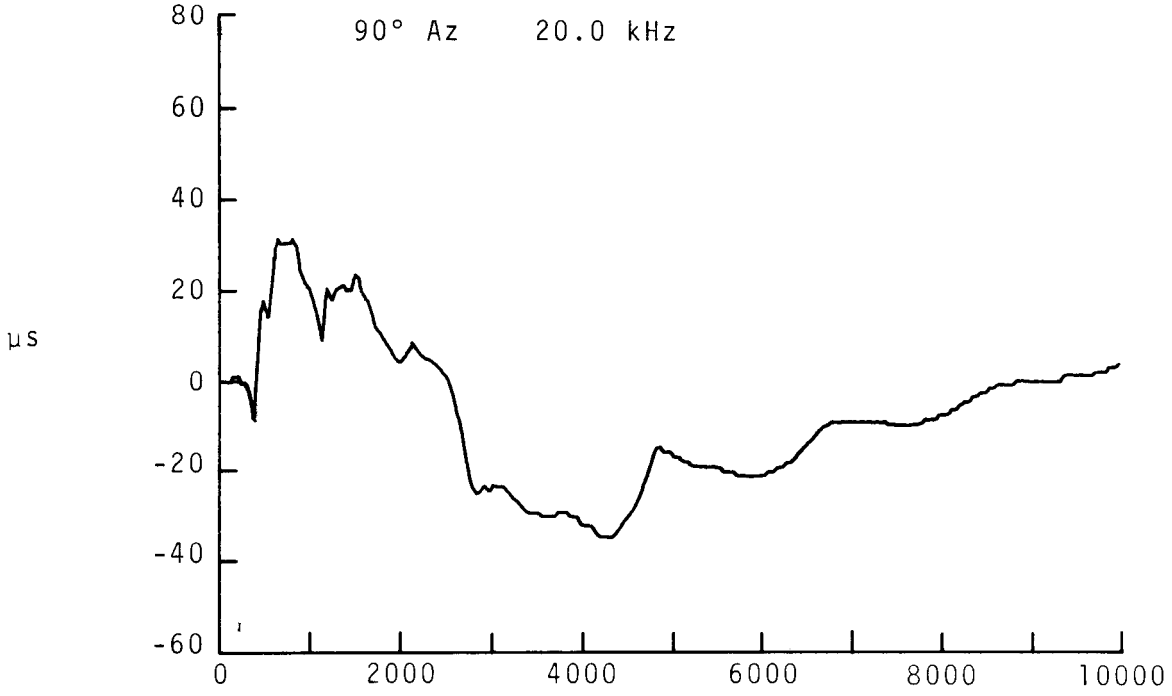

Figure 225.

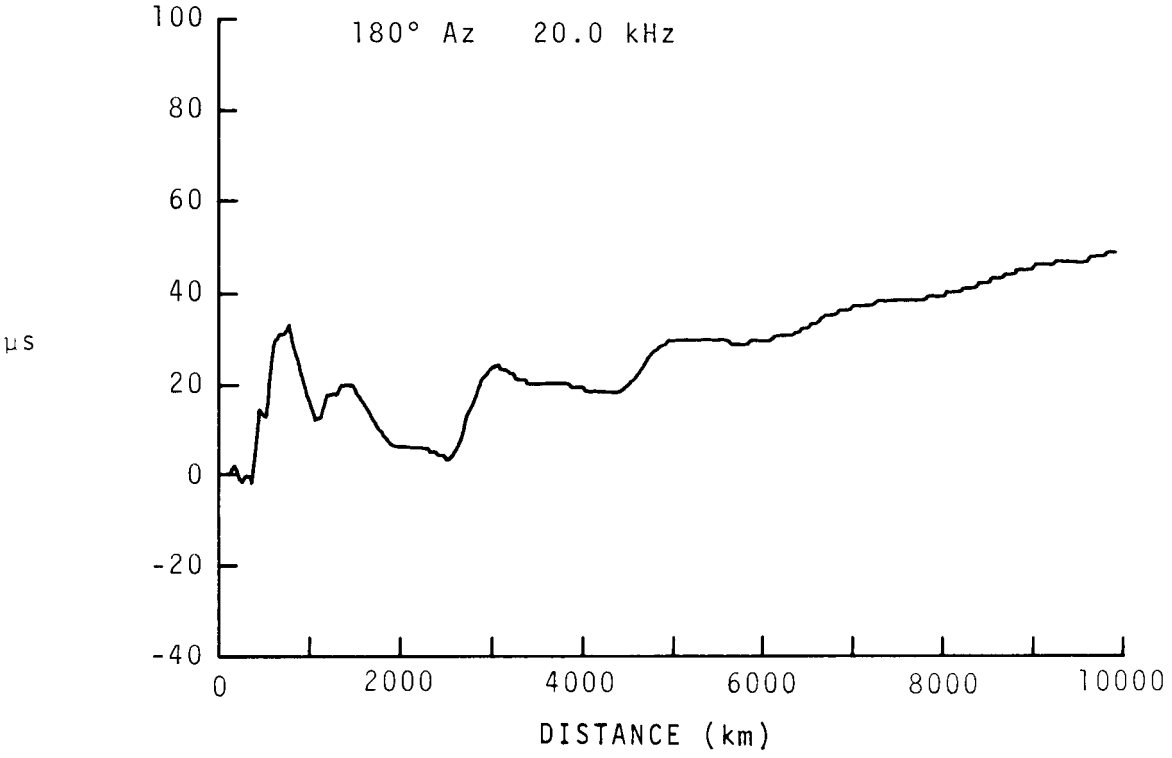

Figure 226.

DIURNAL PHASE

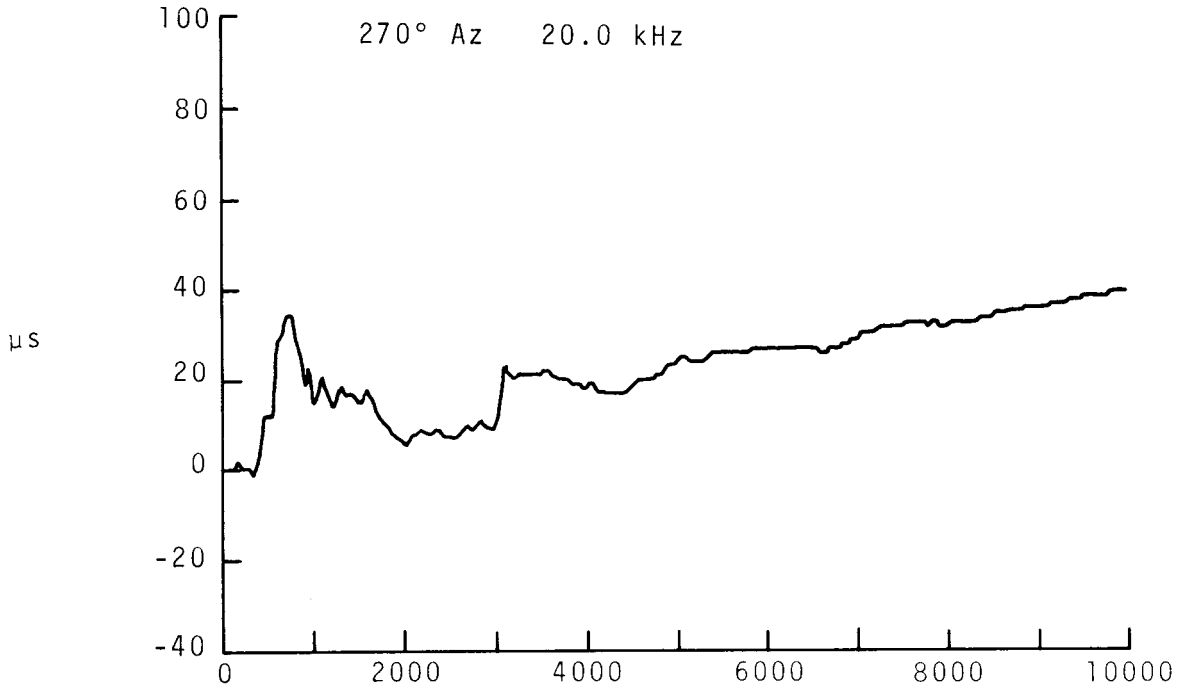

Figure 227.

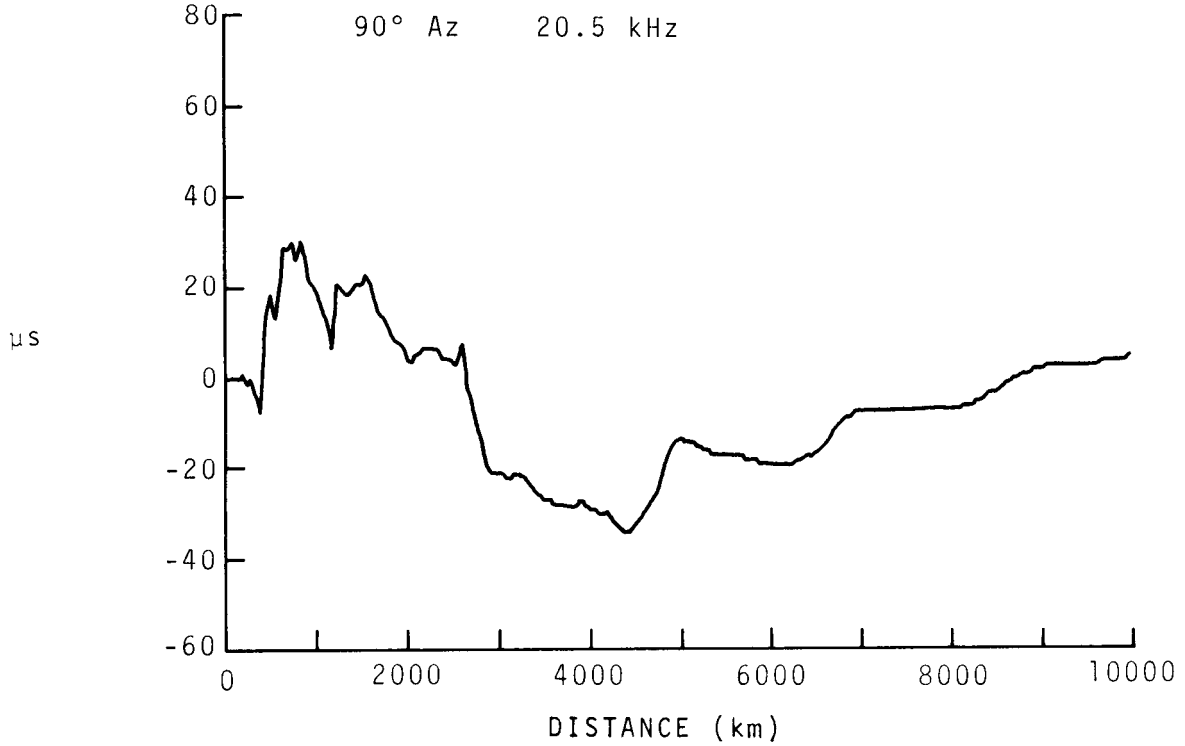

Figure 228.

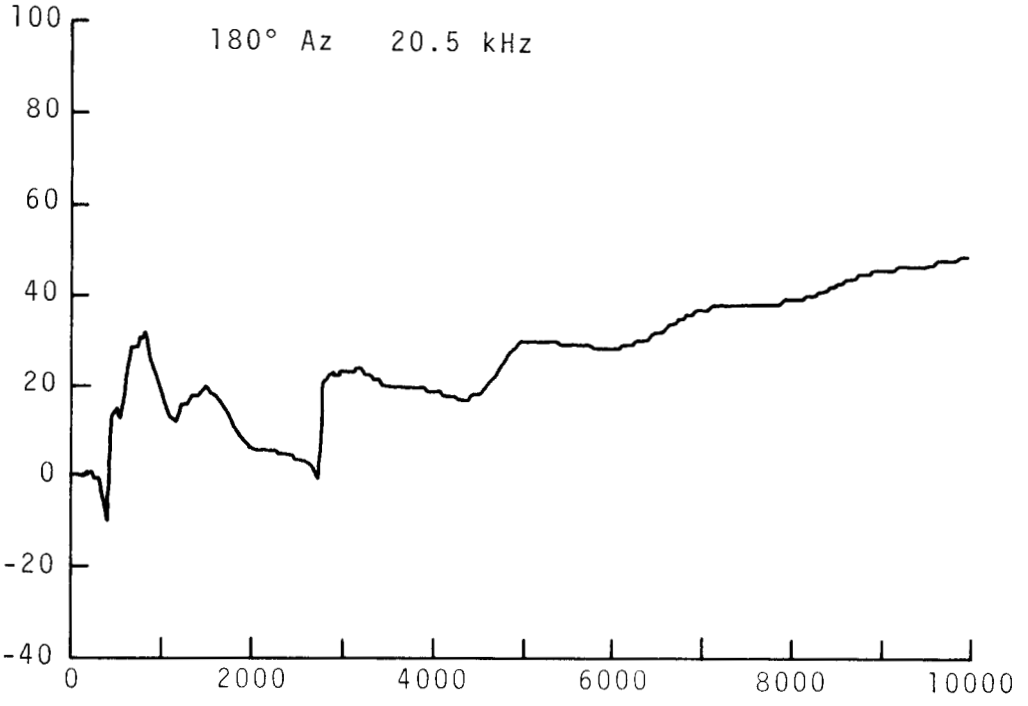

Figure 229.

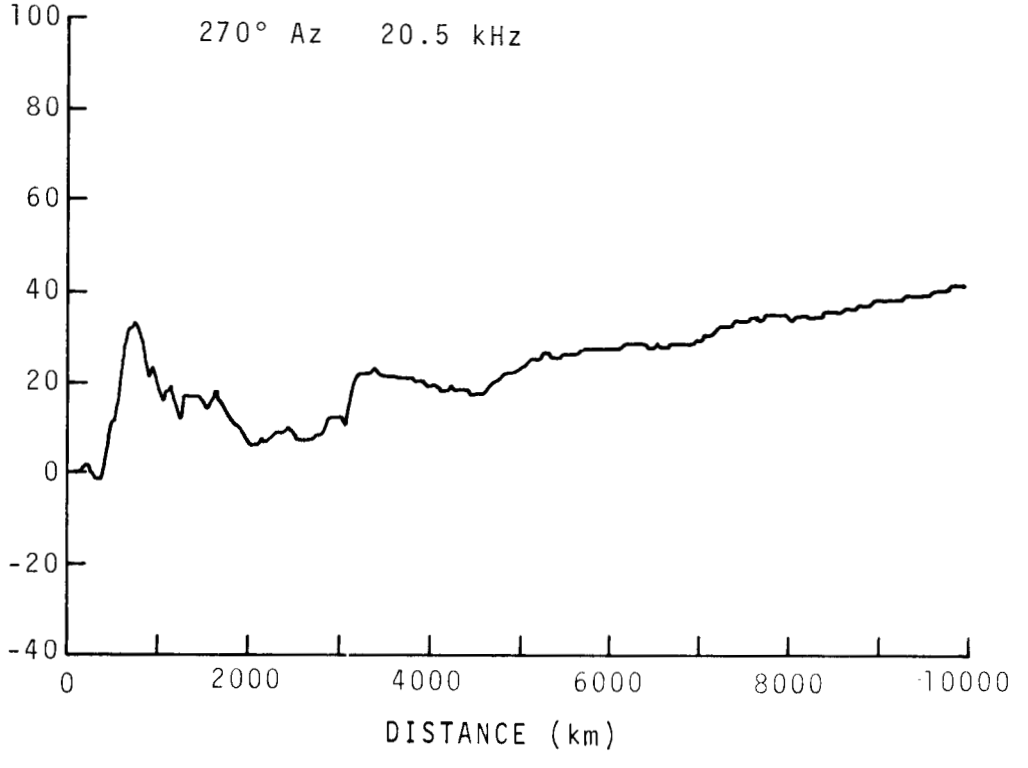

Figure 230.

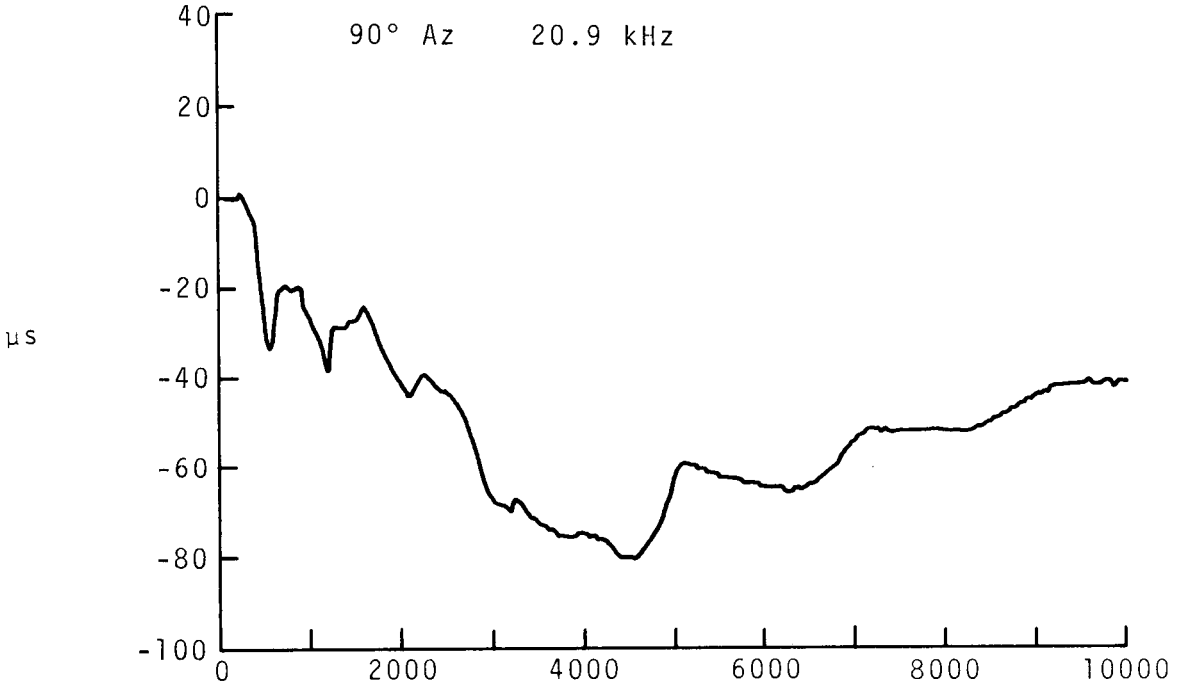

Figure 231.

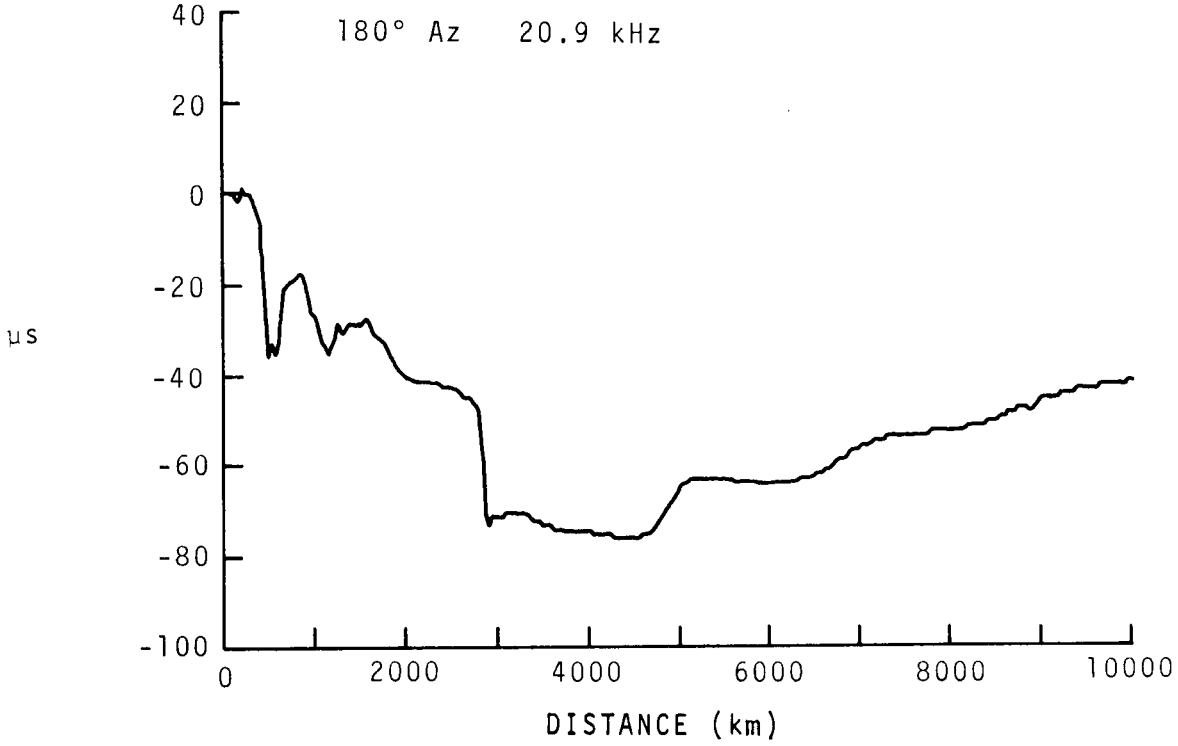

Figure 232.

DIURNAL PHASE

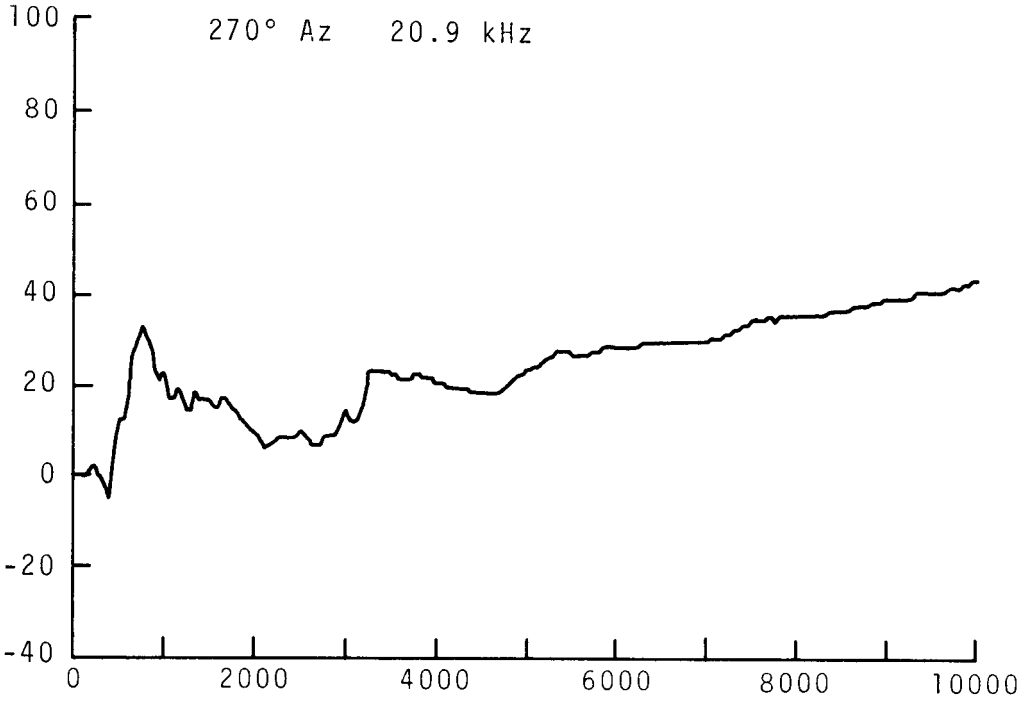

Figure 233.

RELATIVE PHASE
Normal Day (lowered 2.5 km)

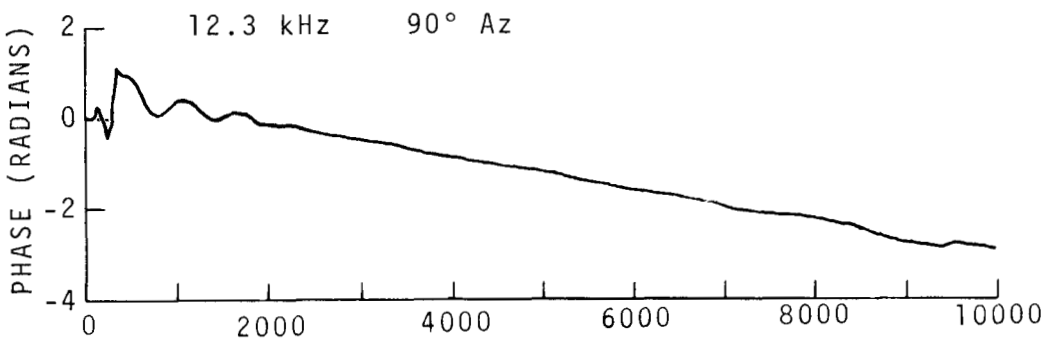

Figure 234.

RELATIVE PHASE
Normal Day (raised 2.5 km)

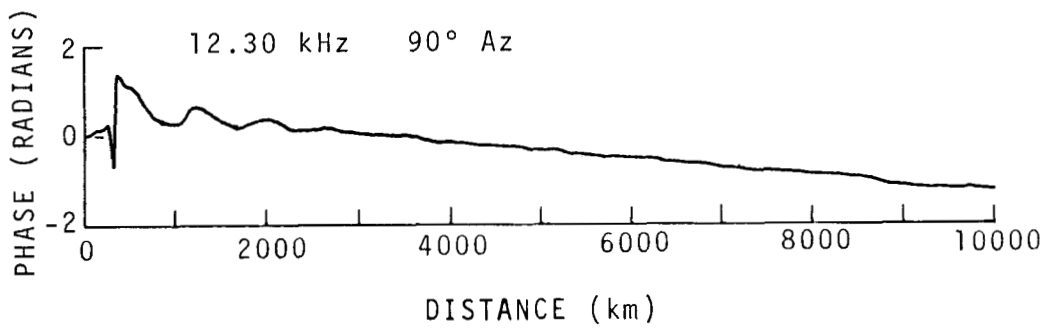

Figure 235.

RELATIVE PHASE
Normal Night (raised 2.5 km)

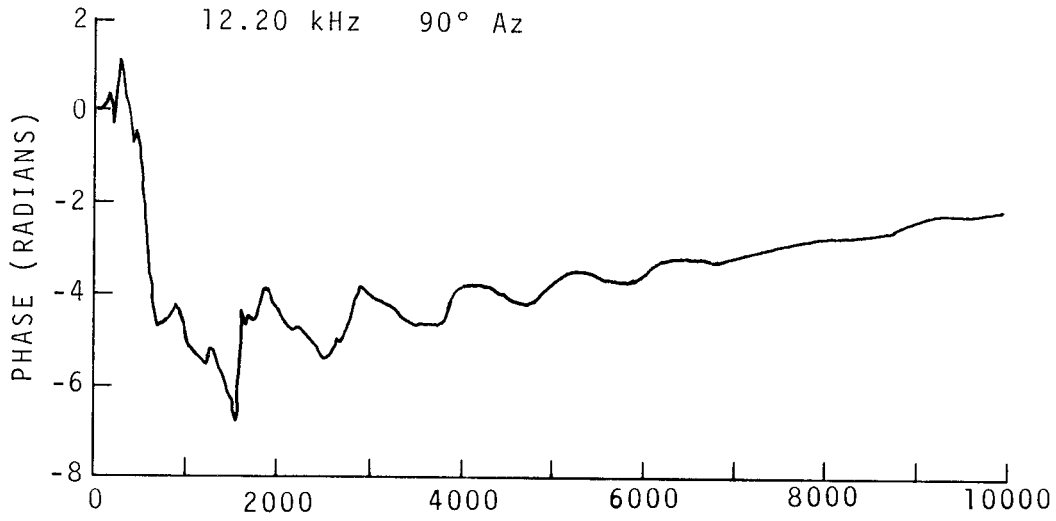

Figure 236.

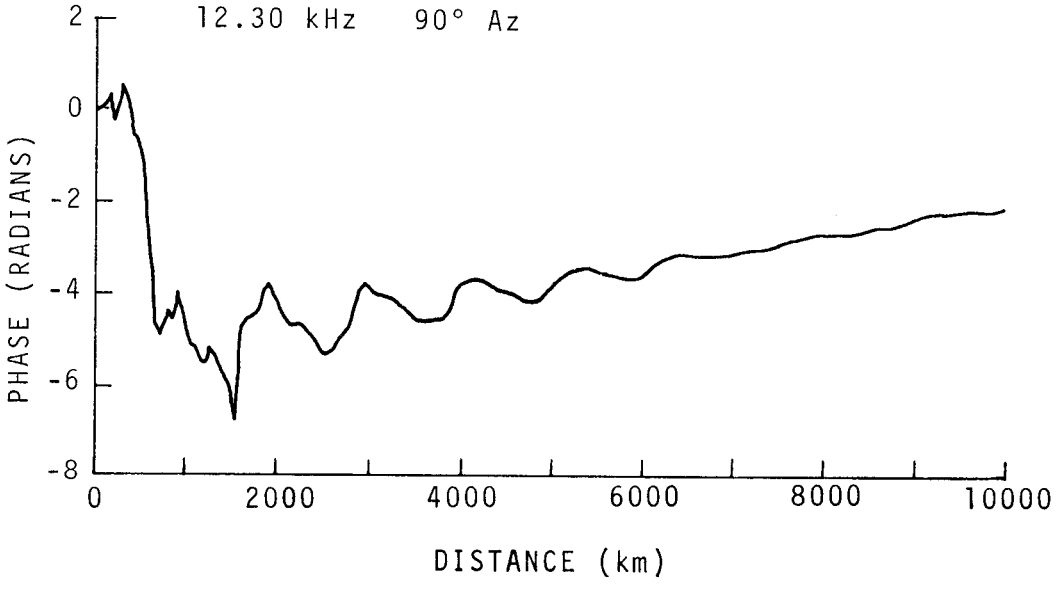

Figure 237.

RELATIVE PHASE
Normal Day (sea water)

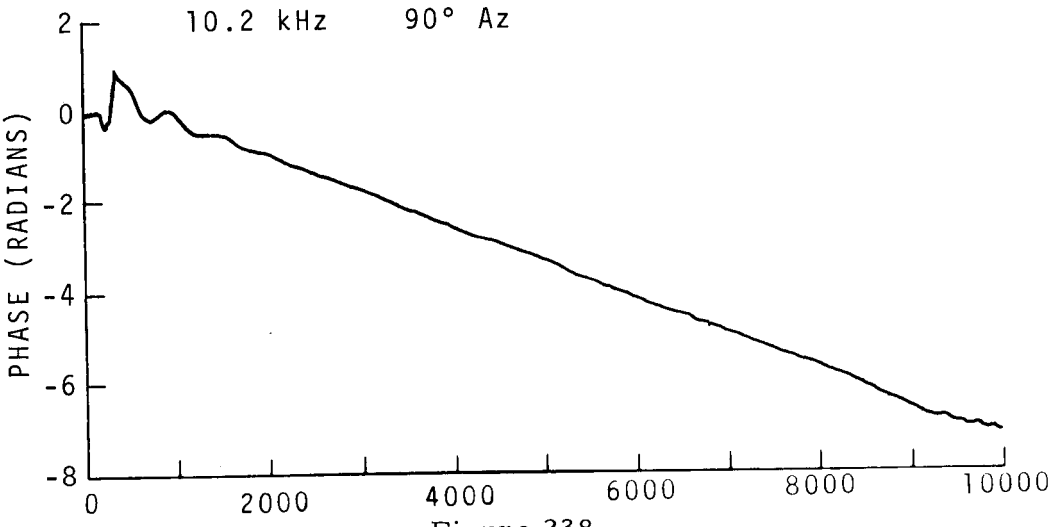

Figure 238.

RELATIVE PHASE
Normal Day (lowered 2.5 km)

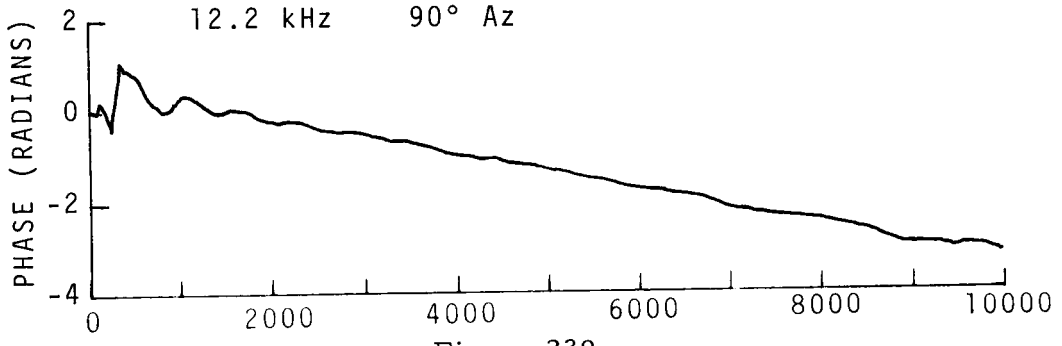

Figure 239.

RELATIVE PHASE
Normal Day (raised 2.5 km)

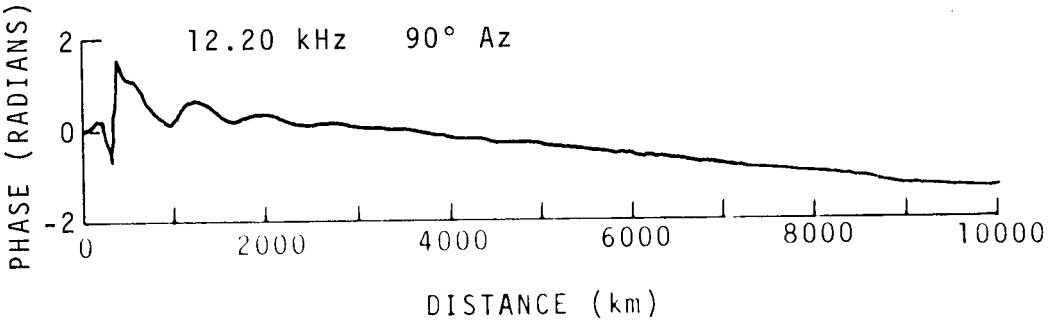

Figure 240.

RELATIVE PHASE
Normal Day (sea water)

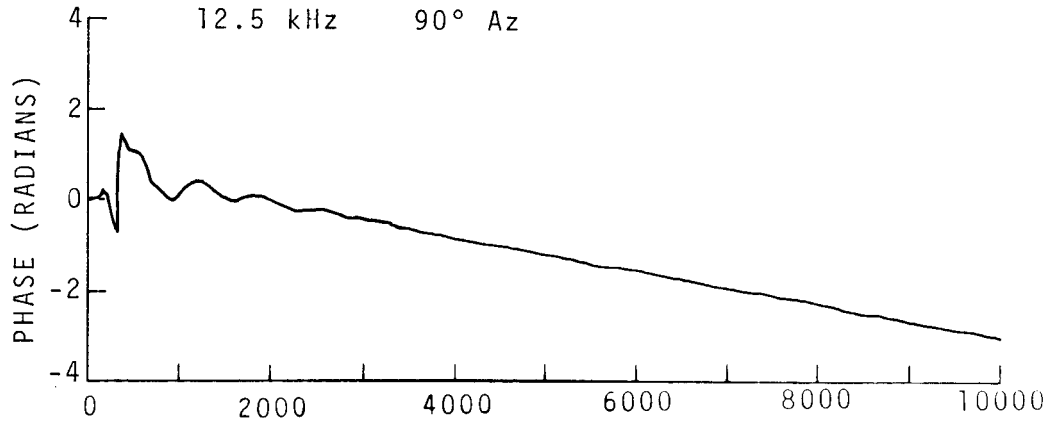

Figure 241.

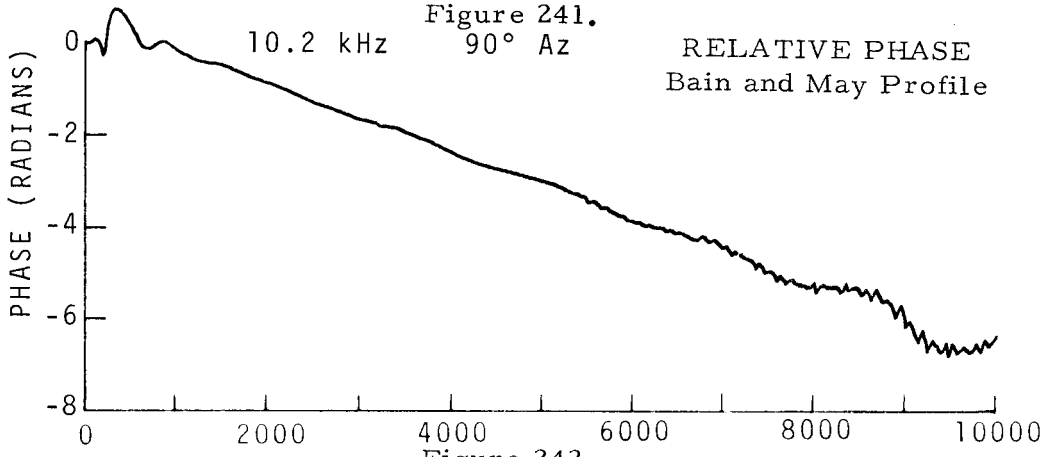

Figure 242.

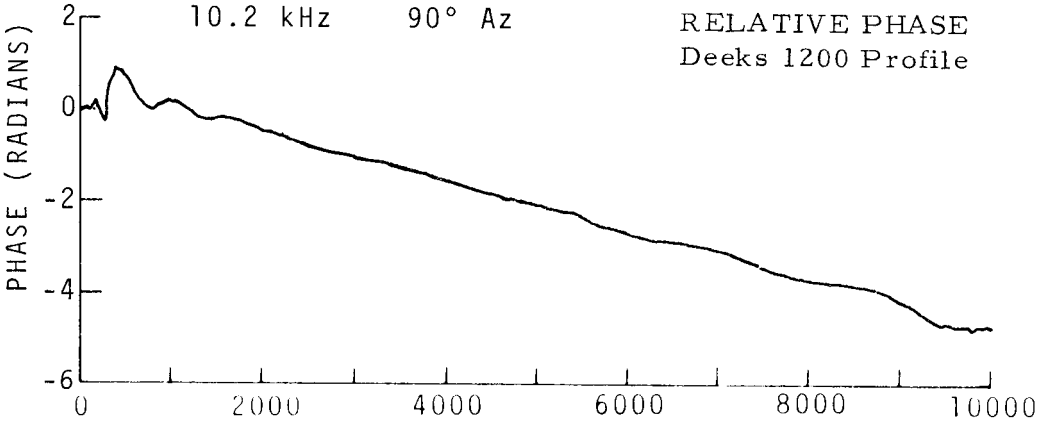

Figure 243.

RELATIVE PHASE
Normal Day (sea water)

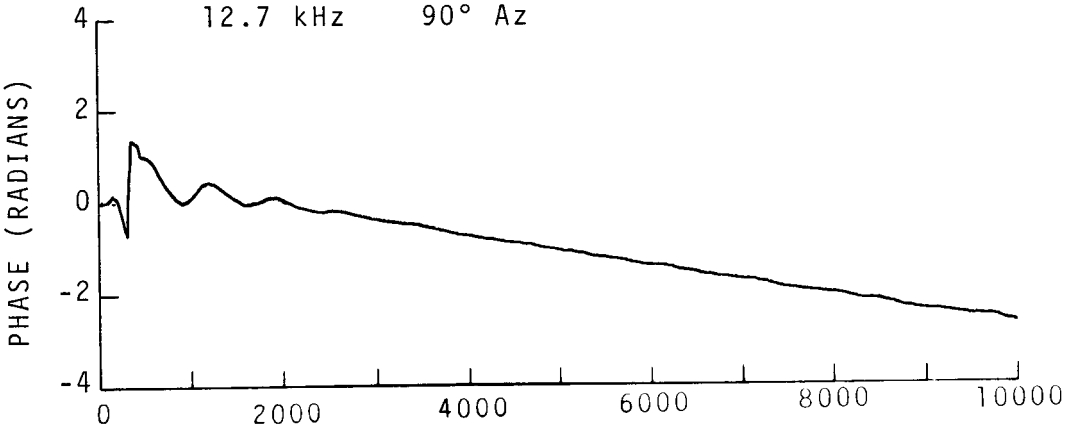

Figure 244.

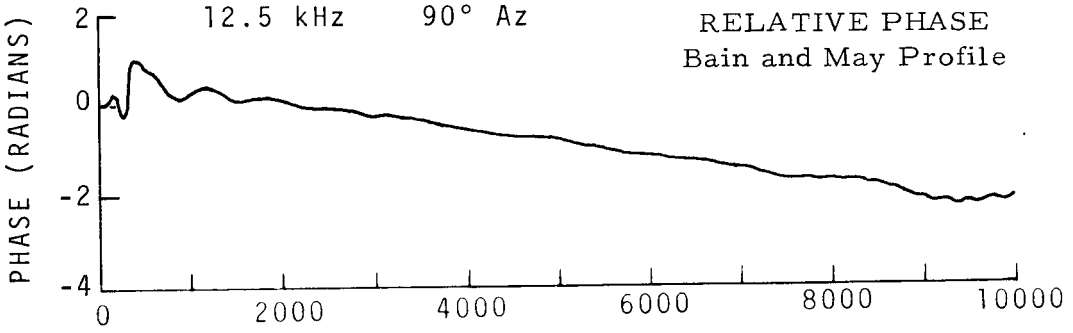

Figure 245.

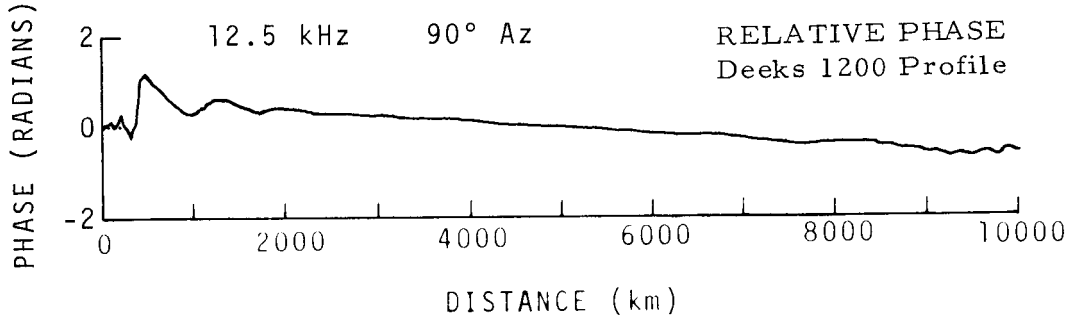

Figure 246.

RELATIVE PHASE
Normal Day (sea water)

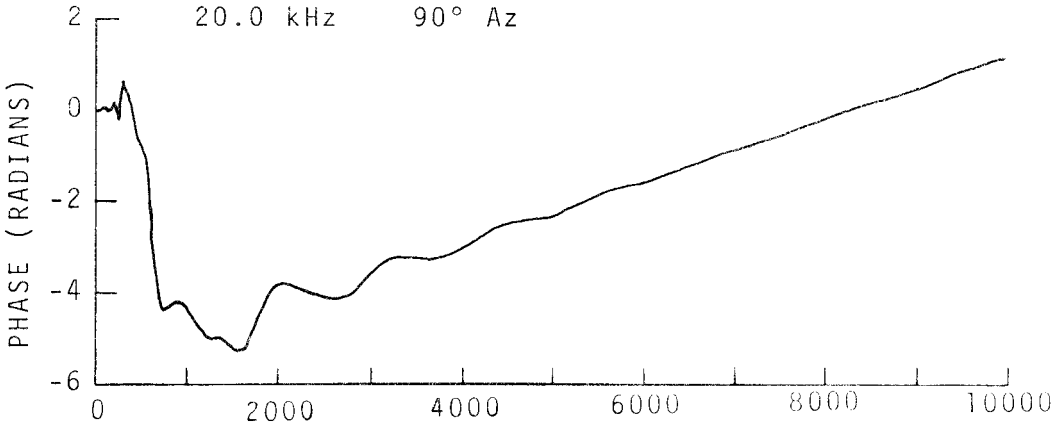

Figure 247.

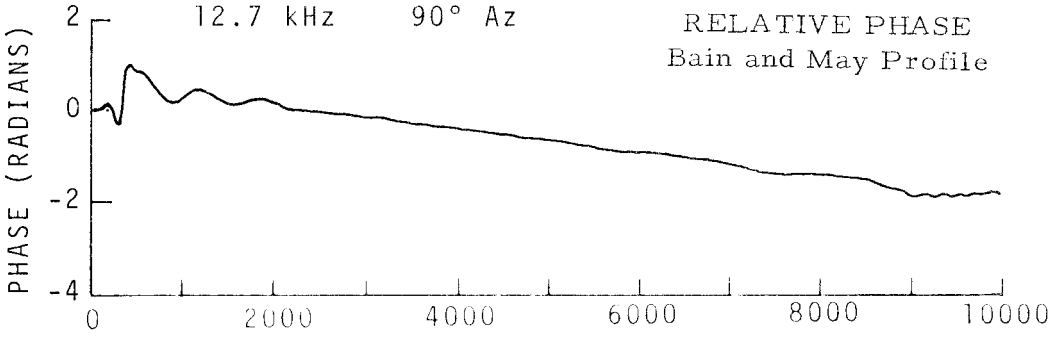

Figure 248.

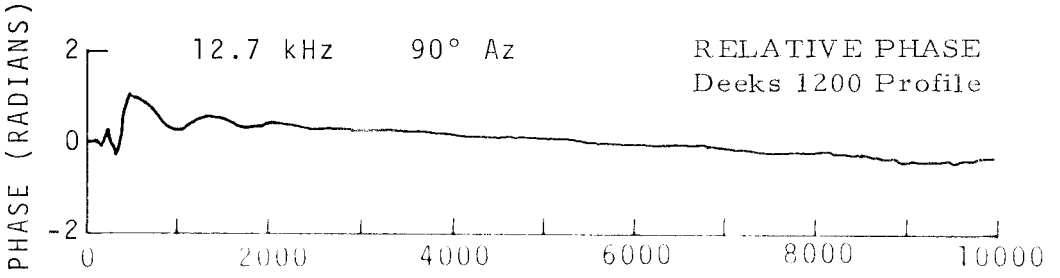

Figure 249.

RELATIVE PHASE
Bain and May Profile

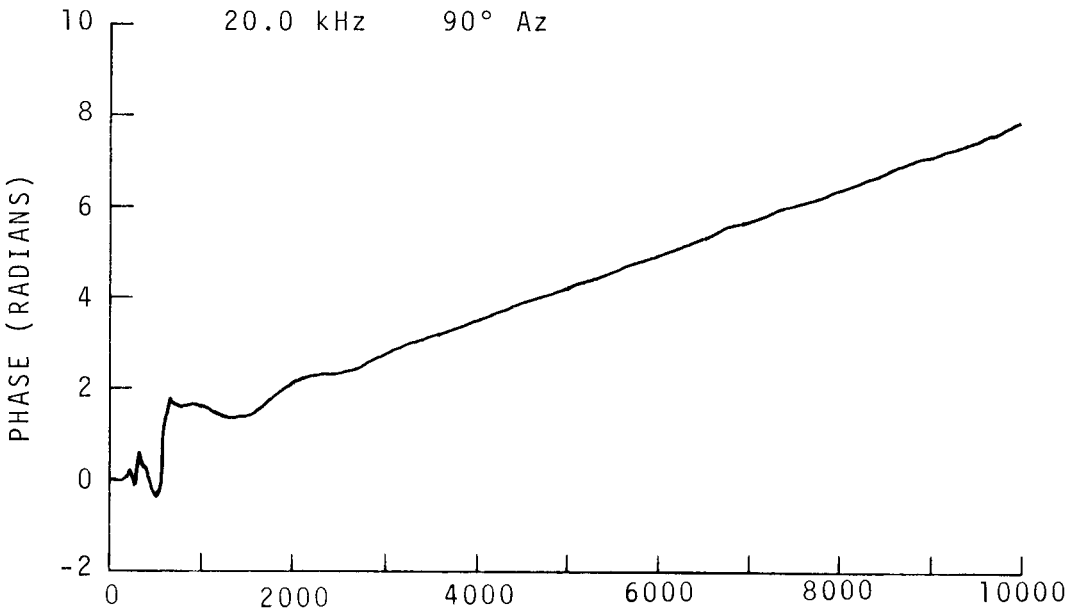

Figure 250.

RELATIVE PHASE
Deeks 1200 Profile

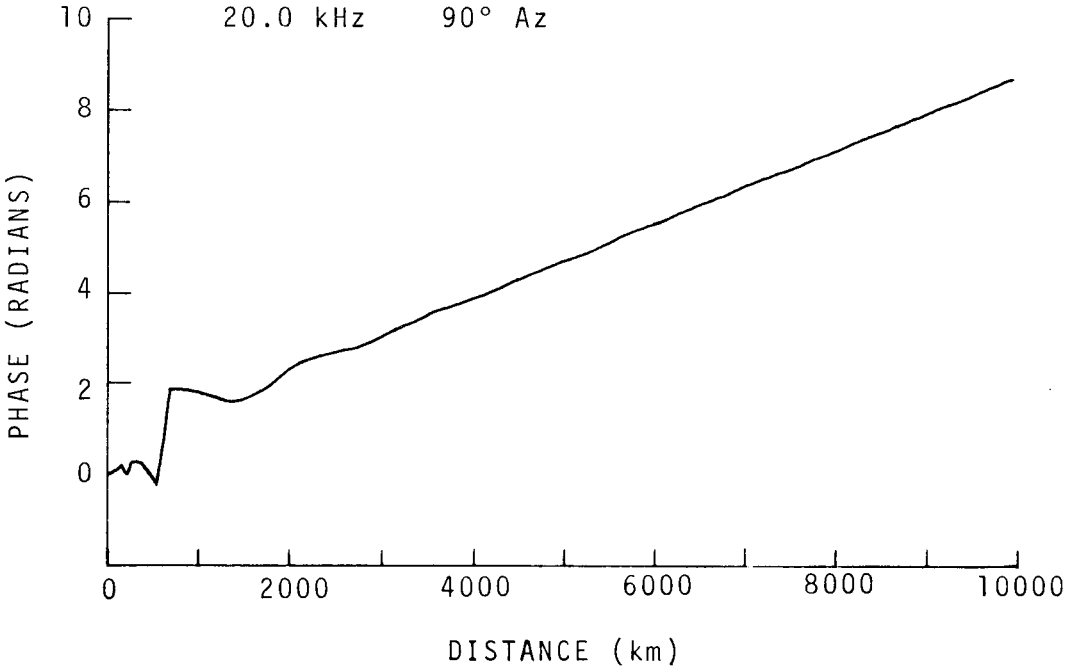

Figure 251.

RELATIVE GROUP DELAY
Normal Day (sea water)

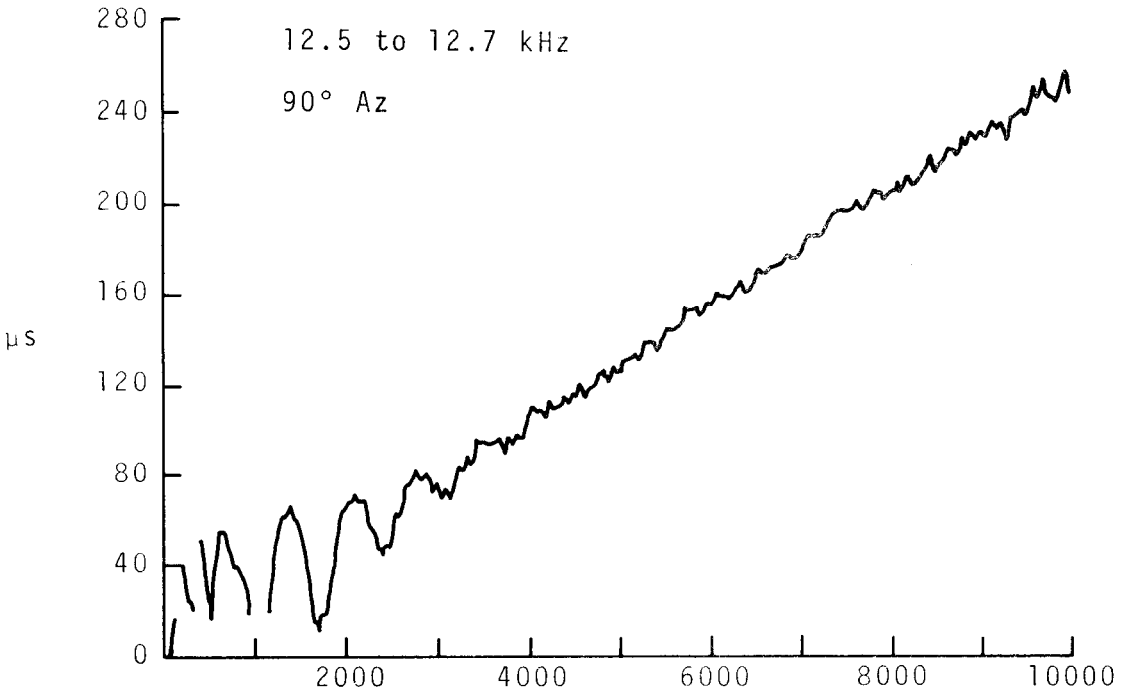

Figure 252.

RELATIVE GROUP DELAY
Deeks 1200 Profile

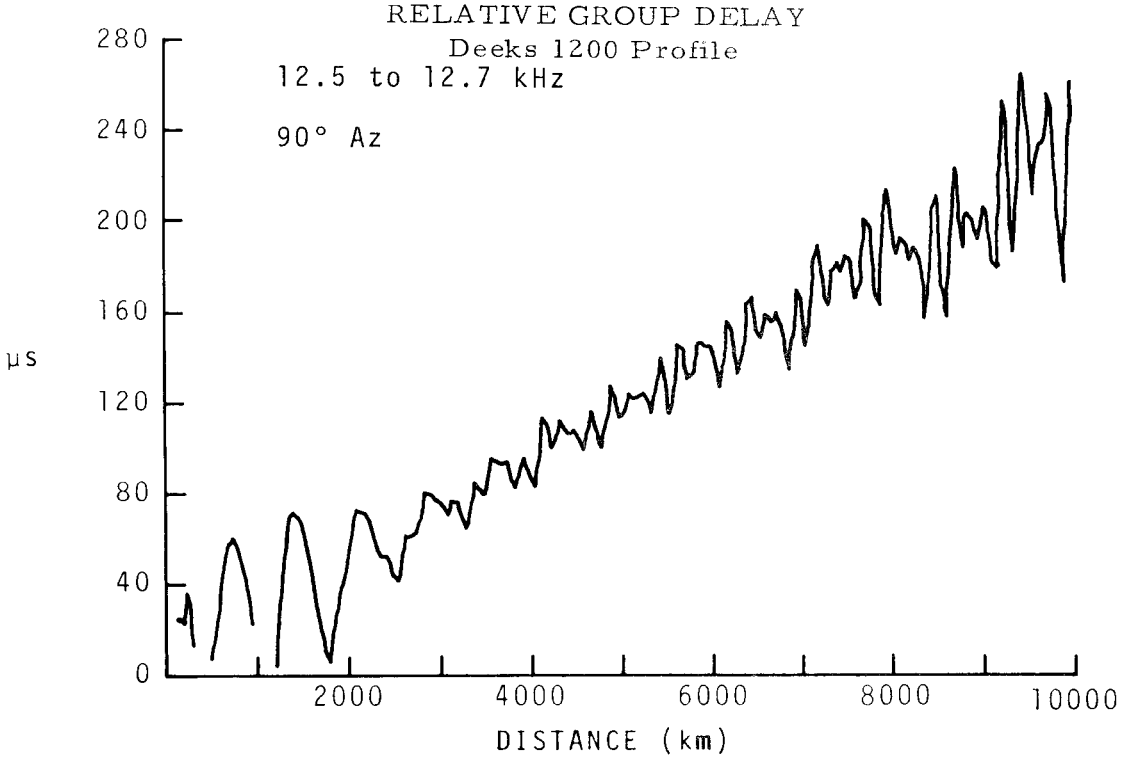

Figure 253.

RELATIVE GROUP DELAY
Bain and May Profile

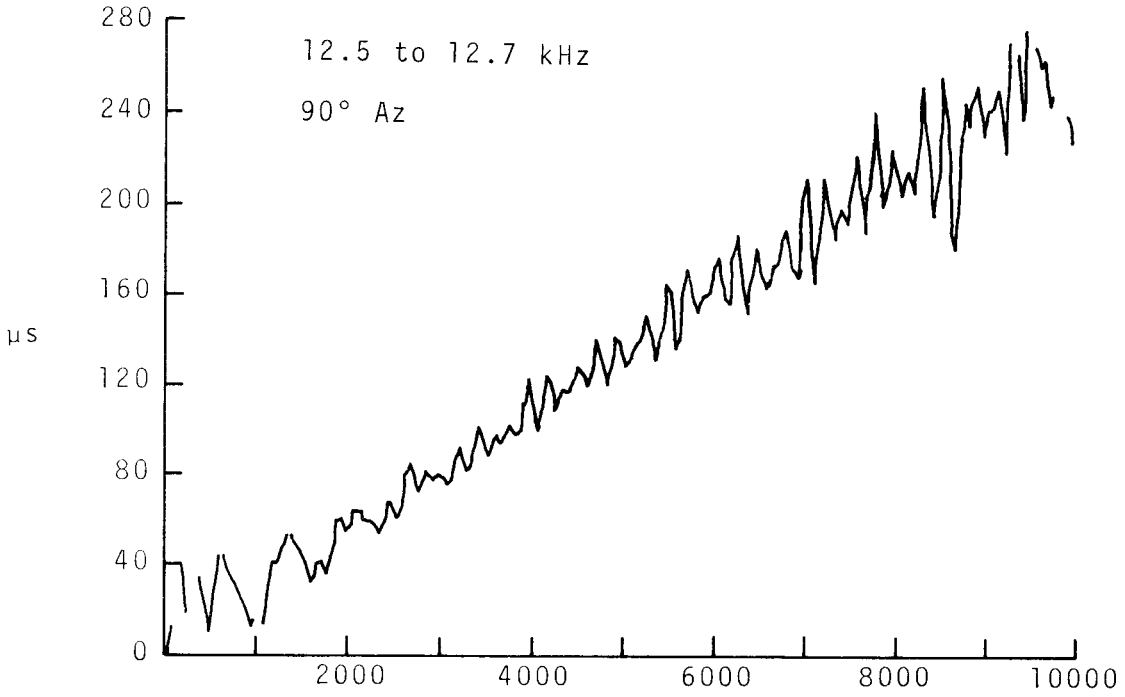

Figure 254.

NBS TECHNICAL PUBLICATIONS

PERIODICALS

JOURNAL OF RESEARCH reports National Bureau of Standards research and development in physics, mathematics, chemistry, and engineering. Comprehensive scientific papers give complete details of the work, including laboratory data, experimental procedures, and theoretical and mathematical analyses. Illustrated with photographs, drawings, and charts.

Published in three sections, available separately:

• Physics and Chemistry

Papers of interest primarily to scientists working in these fields. This section covers a broad range of physical and chemical research, with major emphasis on standards of physical measurement, fundamental constants, and properties of matter. Issued six times a year. Annual subscription: Domestic, $9.50; $2.25 additional for foreign mailing.

• Mathematical Sciences

Studies and compilations designed mainly for the mathematician and theoretical physicist. Topics in mathematical statistics, theory of experiment design, numerical analysis, theoretical physics and chemisty, logical design and programming of computers and computer systems. Short numerical tables. Issued quarterly. Annual subscription: Domestic, $5.00; $1.25 additional for foreign mailing.

• Engineering and Instrumentation

Reporting results of interest chiefly to the engineer and the applied scientist. This section includes many of the new developments in instrumentation resulting from the Bureau's work in physical measurement, data processing, and development of test methods. It will also cover some of the work in acoustics, applied mechanics, building research, and cryogenic engineering. Issued quarterly. Annual subscription: Domestic, $5.00; $1.25 additional for foreign mailing.

TECHNICAL NEWS BULLETIN

The best single source of information concerning the Bureau's research, developmental, cooperative, and publication activities, this monthly publication is designed for the industry-oriented individual whose daily work involves intimate contact with science and technology—*for engineers, chemists, physicists, research managers, product-development managers, and company executives.* Annual subscription: Domestic, $3.00; $1.00 additional for foreign mailing.

NONPERIODICALS

Applied Mathematics Series. Mathematical tables, manuals, and studies.

Building Science Series. Research results, test methods, and performance criteria of building materials, components, systems, and structures.

Handbooks. Recommended codes of engineering and industrial practice (including safety codes) developed in cooperation with interested industries, professional organizations, and regulatory bodies.

Special Publications. Proceedings of NBS conferences, bibliographies, annual reports, wall charts, pamphlets, etc.

Monographs. Major contributions to the technical literature on various subjects related to the Bureau's scientific and technical activities.

National Standard Reference Data Series. NSRDS provides quantitative data on the physical and chemical properties of materials, compiled from the world's literature and critically evaluated.

Product Standards. Provide requirements for sizes, types, quality, and methods for testing various industrial products. These standards are developed cooperatively with interested Government and industry groups and provide the basis for common understanding of product characteristics for both buyers and sellers. Their use is voluntary.

Technical Notes. This series consists of communications and reports (covering both other agency and NBS-sponsored work) of limited or transitory interest.

Federal Information Processing Standards Publications. This series is the official publication within the Federal Government for information on standards adopted and promulgated under the Public Law 89–306, and Bureau of the Budget Circular A–86 entitled, Standardization of Data Elements and Codes in Data Systems.

Consumer Information Series. Practical information, based on NBS research and experience, covering areas of interest to the consumer. Easily understandable language and illustrations provide useful background knowledge for shopping in today's technological marketplace.

NBS Special Publication 305, Supplement 1, Publications of the NBS, 1968-1969. When ordering, include Catalog No. C13.10:305. Price $4.50; $1.25 additional for foreign mailing.

Order NBS publications from:

Superintendent of Documents
Government Printing Office
Washington, D.C. 20402